The Function of Δ40p53 in Breast Cancer

Xiajie Zhang
M. Sc. (Dresden, Germany)
B. Sc. (Beijing China)

Doctor of Philosophy (Medical Genetics)
University of Newcastle
Submitted for examination November 2019

Declarations

STATEMENT OF ORIGINALITY

I hereby certify that the work embodied in the thesis is my own work, conducted under normal supervision. The thesis contains no material which has been accepted, or is being examined, for the award of any other degree or diploma in any university or other tertiary institution and, to the best of my knowledge and belief, contains no material previously published or written by another person, except where due reference has been made. I give consent to the final version of my thesis being made available worldwide when deposited in the University's Digital Repository, subject to the provisions of the Copyright Act 1968 and any approved embargo.

Xiajie Zhang

15/11/2019

STATEMENT OF COLLABORATION

I hereby certify that the work embodied in this thesis has been done in collaboration with other researchers. I have included below a statement outlining the extent of collaboration, with whom and under what auspices.

CONTRIBUTION BY OTHERS TO THE THESIS

There were a number of collaborators who have made important contributions to the unpublished work presented in this thesis as follows:

- Dr Hamish Campbell and Professor Antony Braithwaite generated the MCF-7-LeGO and MCF-7Δ40p53 cell lines.

- Dr Brianna Catherine Morten, being my co-supervisor and lab colleague, helped the work throughout investigation of cell line responses to DNA-damage.

Acknowledgement

This thesis would not have been completed without the help and support of a number of wonderful people. I truly and will forever appreciate the guidance and friendship throughout this PhD journey and would like to acknowledge them for making this milestone possible.

Firstly, I would like to thank my supervisors, Professor Rodney Scott and Kelly Avery-Kiejda, for giving me this chance to come to Australia. Rodney, thank you for your prompt reply to my inquiry and this amazing opportunity to work in the awesome genomic cancer research facility. Kelly, I cannot thank you more for all the guidance and help throughout these four years and the encouraging push for me to be brave and independent. I cannot forget the conference journeys with you, when you were certainly not just a supervisor, but more like a friend I trust and open up to. A special thank-you to my co-supervisor Brianna Morten. You are such a cheerful soul, and best work mate one can ask for, I will always remember our nerdy chat over Δ40p53, thank you for sharing the knowledge with me. Another special thank-you to my co-supervisor Rick Thorne, the inspiration and guidance you have offered are amazingly instructive. Thank you for making yourself always available for me.

To others who have kindly offered help in my data analysis, Carlos, Heather and Sean, thank you for being patient listeners and teachers. Sean, thank you very much as my swimming instructor and also for being such a bright spirit.

To the team of breast cancer research group, present and past, thank you for your help and support in life and at work. Andrea, you were my one and only connection here to my life back in Dresden and I could not forget your generous help. Katherine, Mamta, Maddi, Luiza and Coralie, the friendship with you girls is a treasure for me. To all friendly faces at level 3 west, Ellise, Kira, Samara, Kumar, Dani, Michelle and many many more, thank you for being such understanding and kind friends; Ann, Megan and many many more, thanks for the sympathy and help when I broke my wrist. Your kind words and support are truly a comfort. To my friends out of the lab, Debbie, you are one most stable existence here in Newcastle, I will never ever forget all the time with you, crazy, adventurous and full of joy. Thank you, Shankar, Candy, Aun, Yudi, Kelly and many more, the friendship with you is so important.

To my family, Mum and Dad, without you, none of this would be possible. Thank you for letting your little girl to chase her dream, thank you for being respectful and supportive for my whole life, thank you for simply being there where I call a home!

To my partner Alex, I feel so blessed and lucky to have you as my best friend. We almost go through this whole PhD together and get to know each other a bit more every day and yet I never have felt bored. I really appreciate your accompany, kindness, humour and positivity. I have become stronger

because of you. Thank you very much also for numerous discussion on experiments, bioinformatics and all sorts of scientific topics.

Finally, I would like to acknowledge the University of Newcastle for this fantastic opportunity to do a PhD and for providing me the UNIPRS and UNRSC5050 scholarships. A further acknowledgement goes to the Hunter Medical Research Institute for letting me conduct my research in such fabulous research facility, and to Hunter Cancer Research Alliance for providing incredible opportunities in research support, communication and personal development.

This thesis is dedicated to the most loving, caring and supportive Mom and Dad, and to my wonderful partner Alex. Without your generous devotion, I could not have accomplished this milestone.

Thank you.

List of publications and oral conference presentations

Publication:

Zhang X, Morten BC, Scott RJ, Avery-Kiejda KA. A Simple Migration/Invasion Workflow Using an Automated Live-cell Imager. JoVE. 2019(144):e59042.

Oral presentations:

Zhang X, Möller FJ, Vollmer G: "Impact of a prenatally started and continuously maintained soy-derived isoflavones (sISO) exposure on mammary glands of ovary-intact ACI rats", The 2015 Hunter Cancer Research Symposium, rapid poster session, Newcastle, Australia, 27th November 2016.

-

Zhang X, Morten BC, Campbell H, Braithwaite A, Scott RJ, Avery-Kiejda KA: "Δ40p53 regulates migration in breast cancer cell line MCF-7 cells carrying wild type p53", The 2016 Hunter Cancer Research Symposium, Newcastle, Australia, 25th November 2016.

Zhang X, Morten BC, Campbell H, Braithwaite A, Scott RJ, Avery-Kiejda KA: "Δ40p53 has a potential role in regulating EMT", HCRA, ECR and PhD Students Seminar, Newcastle, Australia, 29th March, 2017.

Zhang X: "Little Bro, Big Role", 3MT Competition, Newcastle, Australia, 31st May 2017.

Zhang X, Morten BC, Campbell H, Braithwaite A, Scott RJ, Avery-Kiejda KA: "Δ40p53 has a potential role in regulating EMT in MCF-7 breast cancer cells", Australian Metastasis Research Society Annual Scientific Meeting, Sydney, Australia, 15th November 2017.

-

Zhang X, Morten BC, Campbell H, Braithwaite A, Scott RJ, Avery-Kiejda KA: "The role of Δ40p53 in EMT in breast cancer", ASMR Hunter Region Satellite Scientific Meeting, Newcastle, Australia, 1st June 2018.

Zhang X, Morten BC, Campbell H, Braithwaite A, Avery-Kiejda KA: "Characterisation of transcriptional targets regulated by Δ40p53 in response to DNA damage in breast cancer cells", 4th International p53 isoform workshop, flash poster session, Dubrovnik, Croatia, 3-6th November, 2019.

Table of Contents

Abstract

Breast cancer is the most commonly diagnosed female malignancy and the second leading cause of cancer-related death. Nearly all deaths from breast cancer are a result of resistance to DNA-damaging therapies and the subsequent development of metastases. The tumour suppressor, p53, is a master regulator of cell fate outcome following DNA damage, by regulating the expression of target genes involved in cell cycle arrest, DNA repair or apoptosis. Mutation of the tumour suppressor gene *TP53* occurs frequently in other solid cancers, but in breast cancer, it is mutated in <25% of all cases, suggesting other mechanisms are accountable for dysregulation of the canonical p53 function. Twelve truncated p53 protein variants (isoforms) are generated from the *TP53* gene. Studies have revealed their regulatory role toward the full-length p53 (p53α) and their prognostic value in cancer. The Δ40p53 isoform has been identified in our previous studies to be the mostly highly expressed p53 isoform in breast cancer and a high Δ40p53:p53 ratio is associated with worse-disease survival. This has led to the hypothesis that that high levels of Δ40p53 (as observed in breast cancer) will have a negative impact on p53 functional activities resulting in increased proliferation, migration and invasion, contributing to p53-mediated DNA methylation, as well as inhibition of apoptosis in response to DNA damaging therapies; and that this is responsible for the association of worse outcomes in breast cancer patients with high Δ40p53/p53 ratios. However, the endogenous role of Δ40p53 in the acquisition of an aggressive breast cancer phenotype and in the response to DNA damage is unclear. The overall aim of the studies described in this thesis is to investigate the molecular and functional consequences of a high Δ40p53/p53α ratio in regulating breast cancer growth, metastasis-related processes and in the response to DNA-damaging therapies.

Gene expression analysis performed on breast cancer specimens with high or low Δ40p53 expression level highlighted a role for Δ40p53 in epithelial-mesenchymal transition, extracellular matrix communication and immune responses. Breast cancer cell line models derived from MCF-7 and ZR751 cells (with wild-type p53) were established using shRNA-transduction to generate stable and specific Δ40p53 or p53α knockdown, simulating the naturally occurring isoform-imbalance in breast cancers. A series of functional assays investigating the role of Δ40p53 in EMT, cell proliferation/migration/ invasion at the basal level were performed on these sublines as well as on previously established Δ40p53-overexpressing MCF-7 cell models. Results showed p53α-knockdown fundamentally contributed to increased cancer cell mobility and invasiveness, while Δ40p53-knockdown had limited and cell-dependent impact. Molecular characterisation by RNA-seq analysis further confirmed a link between Δ40p53 and immunity, and showed that Δ40p53 was an influencing factor in cell differentiation and tissue development.

Following this, DNA methylation signatures were obtained by performing Illumina EPIC 850k methylation arrays. Differentially methylated probes (DMPs) and differentially methylated regions (DMRs) were identified comparing to the respective controls. An isoform-associated cytoband region containing pro-inflammatory factors and regulating extracellular components was shown to be differentially methylated following p53 isoform alteration. In addition, multiple transcription factor binding sites, micro-RNAs and cancer-associated genes were differentially affected depending on which p53 isoform was knocked down. These results imply that p53 isoforms are capable of regulating gene expression through both transcriptional and epigenetic means and this has not been demonstrated previously.

In addition to the intrinsic differences caused by isoform-alteration, DNA-damaging treatment triggered similar responses across all cell lines. A high ratio of Δ40p53/p53α was associated with enhanced G2 arrest and attenuated apoptosis. These results were confirmed by RNA-seq analysis comparing doxorubicin-treated cells to untreated cells, identifying critical molecular markers such as *CCNB1* and *GADD45* that were altered by the p53 isoforms and that govern cell cycle progression.

The comprehensive characterisation of these cell lines provides novel insights and potential biomarkers for further investigation of Δ40p53 in breast cancer as well as other cancers. The novel finding of Δ40p53 regulation of genes involved in immune responses contributes to the current knowledge of p53 isoform research and provides a new perspective accounting for breast cancer heterogeneity and treatment possibilities. Importantly, the finding that the Δ40p53/p53α ratio was a causative factor in the decreased response to DNA-damaging therapies may contribute to the discovery of novel treatment strategies with decreased toxicity and increased efficacy in breast cancers.

List of Figures

List of Tables

List of Abbreviations

Abbreviation	Full description
AML	acute myeloid leukemia
ANOVA	analysis of variance
ARF	alternative reading frame
ATM	ataxia telangiectasia mutated
bHLH	basic helix-loop-helix family
BRCA1/2	breast cancer susceptibility gene 1/2
CDDP	cisplatin
ChAMP	Chip analysis methylation pipeline
CTC	circulating tumour cells
DBD	DNA binding domain
DCIS	Ductal carcinoma *in situ*
DEG	differentially expressed genes
DMEM	dulbecco's modified eagle medium
DMG	DMR-associated genes
DMP	differentially methylated probes
DMR	differentially methylated regions
DMSO	dimethyl sulfoxide
DNA	deoxyribonucleic acid
DNMT	DNA methyltransferase
DOX	doxorubicin
ECM	extracellular matrix
EGF	epidermal growth factor
eIF	eukaryotic initiation factors
EMT	epithelial-mesenchymal transition
ER	estrogen receptor
ERE	estrogen response element
ESR1/Erα	estrogen receptor 1

ESR2/ERβ	estrogen receptor 2
FBS	fetal bovine serum
FFPE	formalin-fixed paraffin-embedded
G4	g-quadruplex structure
GATA3	GATA binding protein 3
GSEA	gene set enrichment analysis
HDAC	histone deacetylase
HER2	human epidermal growth factor receptor 2
IDC	invasive ductal carcinoma
IGF-1	insulin-like growth factor 1
iPS	induced pluripotent stem cell
IRES	internal ribosome entry site
kDa	kilodalton
LCIS	lobular carcinoma *in situ*
MAPK	mitogen-activated protein kinase
HDM2	human double minute 2
miR	micro-RNA
MMP	matrix metalloproteinase
mRNA	messenger RNA
MSigDB	the Molecular Signatures Database
mTOR	mechanistic target of rapamycin,aserine/threonine kinase
NANOG	Nanog homeobox
NES	nuclear export signal
NGF	neuron growth factor
NLS	nuclear localisation signal
NT	non-targeting control
PCR	polymerase chain reaction
PI	propidium iodide
PIN2/3	polymorphism in intron 2/3 of p53
PR	progesterone receptor
PTEN	phosphatase and tensin homolog
PUMA	p53 up-regulated modulator of apoptosis

RIN	RNA integrity number
RNA	ribonucleic acid
RNAi	RNA inteference
RNA-seq	RNA sequencing
RT	room temperature
RWD	relative wound density
SDS-PAGE	sodium dodecyl sulphate polyacrylamide gel electrophoresis
shRNA	short-hairpin RNA
siRNA	small interference RNA
SRSF	serine and arginine rich splicing factor family
TAD	Transactivation domain
TDLU	terminal ductal and lobular unit
TGFβ	transforming growth factor beta
TNBC	triple negative breast cancer
TP53	tumour suppressor gene TP53
VEGF	vascular endothelial growth factor
wt p53	wild-type p53

Chapter 1
Introduction

Chapter 1 Introduction

1.1 Overview

Breast cancer is the most commonly diagnosed cancer and the second-leading cause of cancer-related deaths among women worldwide (1). It is a heterogeneous disease that can be subdivided into distinct molecular subtypes primarily based on the differential expression of estrogen receptor (ER), progesterone receptor (PR) and human epidermal growth factor receptor 2 (HER2) (2). The majority of breast cancers (60-80%) are ER-positive and have the best prognosis and outcomes (3), while breast cancers negative for all three receptors are called triple-negative breast cancers (TNBCs) and have very poor prognosis (4). The major challenges in curing breast cancer involve the estimated 20-30% of cases which become resistant to treatment along with their metastatic ability (5), which describes the process of breast cancer cells losing cell-cell connections, spreading to distant tissues and initiating secondary cancer growth (6, 7).

The tumour suppressor gene *TP53* is essential for genomic stability and therefore is called the guardian of the genome (8). *TP53* encodes a transcription factor that regulates an extensive gene network. Importantly, it is the most commonly mutated gene in sporadic human cancers, but its mutation is comparatively rare in breast cancers, with a frequency of lower than 25% and with a dominant occurrence in TNBC cases but not ER-positive cases (9, 10). p53 dysregulated genes are a better predictor of outcome and therapeutic responses in breast cancers than *TP53* mutations (11, 12), implying that p53 function is compromised by mechanisms other than mutation.

Twelve protein variants (isoforms) can be produced by the *TP53* gene by alternative usage of an internal promoter, alternative splicing and alternative initiation of translation, and these isoforms are reported to have a regulatory role toward full-length p53 (13-16). Studies from our laboratory have reported a link between breast cancer and the N-terminally truncated p53 isoform, Δ40p53. Specifically, these studies showed that (1) Δ40p53 expression is higher than the other p53 isoforms in breast cancer, that it is higher in breast cancer cells lines as well as breast cancer specimens when compared to the normal adjacent tissue (17), and (2) a high ratio of Δ40p53/p53 is associated with worse disease-free survival (18). This has led to our interest in studying Δ40p53 in breast cancer progression and response to chemotherapy. However, functional analyses are needed to better understand the role of Δ40p53 in breast cancer.

The focus of this thesis is to investigate the function of Δ40p53 in regulating breast cancer growth, metastasis and response to therapy. This Chapter will provide an outline of the current challenges in breast cancer treatment; as well as the role of p53 in cancer, its regulation and how it promotes its tumour suppressor functions. Finally, this chapter will describe what is known about the p53 isoforms, with a specific emphasis on Δ40p53.

1.2 Breast cancer

Breast cancer is the most common cancer in women and the major cause of cancer-related deaths among women worldwide irrespective of regional differences (1). In Australia, it was the most commonly diagnosed cancer in 2015 among women (19) and is estimated to affect 19,371 Australian women and cause 3058 deaths by the end of 2019. Although the incidence of breast cancer is increasing, the mortality rate of breast cancer is relatively steady and 5-year relative survival is over 80% and continuously increasing due to advancements in treatments and early detection (20-22).

Tumours are a result of excessive cell growth in the human body. A benign tumour is commonly confined within a sac created by the immune system and usually not life-threatening. It can become harmful when pressing against a nerve or an artery. A malignant tumour (or cancer), on the other hand, contains uncontrolled highly proliferative cells which have the potential to invade the adjacent tissue, spread to distant tissues and initiate secondary growth (23).

The human breast consists of lobules (milk production) and ducts (milk transport), fatty and connective tissue, blood vessels and lymph vessels. Each breast has 15-20 lobes, and each lobe has 20-40 terminal ductal and lobular units (TDLU), which are the functional milk production source. TDLUs harbour two

layers of epithelial cells: the luminal epithelium and the myoepithelium, the latter providing contractile force to expel milk produced by the luminal cells (24) (Figure 1.1A).

Unlike most of the other organs, the breast has unique developmental stages which correlate with the female reproductive cycle. The development of the human mammary glands remains slow until the onset of puberty. The development of ducts and lobules accelerates, and further differentiates during pregnancy. During lactation, the epithelial cells lining the lobules can undergo further differentiation into lactocytes (24).

Breast cancer originates in the ducts or the lobules and is called ductal carcinoma *in situ* (DCIS) or lobular carcinoma *in situ* (LCIS) respectively if the abnormal cell growth remains within these two tissue compartments (20). *In situ* carcinomas are mostly curable (20, 25). Invasive cancer is where the cancer has spread into the surrounding tissue and includes infiltrating/invasive lobular (ILC) or ductal (IDC) carcinoma (20, 25). IDC is the most common breast tumour (c.a. 80%). Secondary breast cancer (metastatic or advanced breast cancer) is a term used to describe the stage when cancer cells spread to other body parts through the blood or lymphatic system, and initiate secondary growth elsewhere. Once metastasized, cancers are considered incurable and this is the major cause of cancer-related death (6, 7).

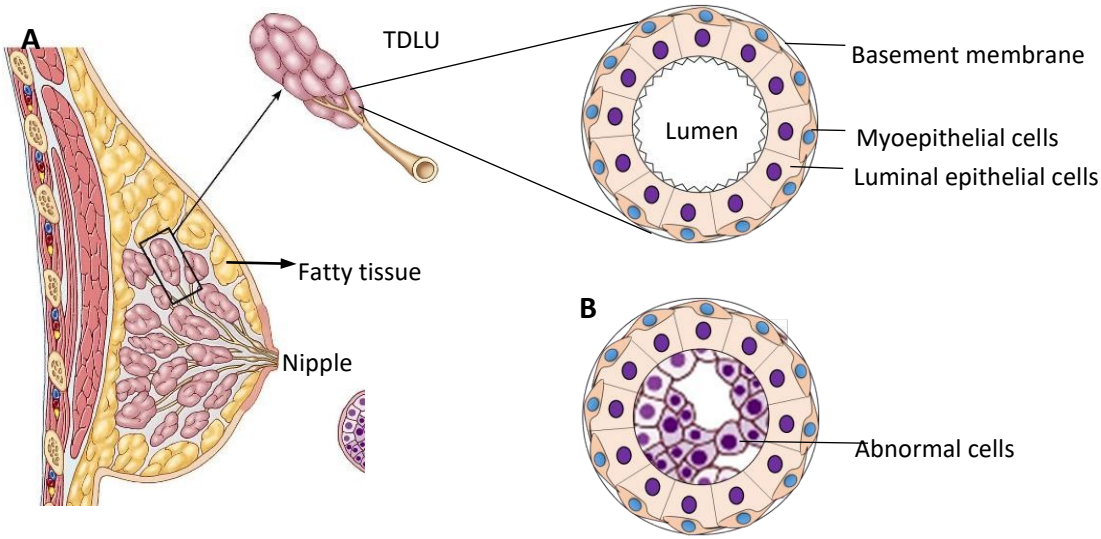

Figure 1.1 Illustration of normal breast microanatomy and breast carcinoma. A, A normal breast is comprised of a ductlobule system and fatty tissue, and the fundamental unit is the TDLU. A normal TDLU has myoepithelial and luminal epithelial cells surrounding a basement membrane, forming a hollow lumen. B, Abnormal cells commonly originate from the luminal epithelium and fill the lumen. Adapted from (26).

1.2.1 Breast cancer and its risk factors

The risk factors for breast cancer can be divided into two major categories: heritable and environmental/lifestyle factors.

Hereditary breast cancer accounts for only 5-10% of all breast cancer incidences, among which germline mutation of either one of the BReast CAncer susceptibility genes 1 or 2 (*BRCA1* and *BRCA2)* is well-established (27). Germline mutations in the tumour suppressor gene p53 are often associated with Li-Fraumeni Syndrome and females with a germline p53 mutation are estimated to have a 50% chance of developing breast cancer (28). Other genes involved in the p53 pathway such as *ATM* (ataxia telangiectasia mutated) and *PTEN* (Phosphatase and tensin homolog) may play a role in breast cancer development, with mutations in these genes accounting for less than 1% of hereditary breast cancers (29).

Environmental factors such as exposure to radiation can lead to carcinogenesis including breast cancer. Lifestyle factors including alcohol consumption, lack of exercise and diet containing poor/high fatty acids, can lead to an altered risk of developing breast cancer (20, 23). More importantly, other physiological events, such as early onset of menarche, late pregnancy, deficient breastfeeding, as well as late menopause and hormone replacement therapy, are potential breast cancer risk factors (20, 23). These endocrine and age-related factors render females at an increasing risk of breast tumorigenesis given that the mammary gland has a postnatal phase of further growth and differentiation (30, 31).

1.2.2 Hormones and their receptors

Breast morphogenesis is mediated through corresponding hormone receptors, in which estrogen receptor (ER), progesterone receptor (PR) and the human epidermal growth factor receptor 2 (HER2) (2) are the most important. They are also of great significance in breast cancer diagnosis and treatment.

Estrogen is an undisputed breast mitogen. Derived from cholesterol and able to diffuse across membranes, estrogen binds to its receptors (ER) and forms a dimer, which enters the nucleus and binds to estrogen response elements (ERE) within target genes to initiate downstream transcriptional activities (32). ER can also trigger a fast biological response through a non-genomic mechanism by binding to other membrane receptors such as HER2 (33, 34). ER has two isoforms, expressed at different amounts in different tissues. ERα, encoded by the ESR1 gene, is found predominantly in the mammary gland and ovarian theca (endocrine) cells; whereas ERβ, encoded by the ESR2 gene, appears mainly in brain, lung and ovarian granulosa (follicular) cells (35), therefore estrogen as a breast mitogen is primarily executed by ERα (36).

Progesterone, another steroid hormone, is involved in pubertal breast development and pregnancyrelated processes, thus it is also known as a pregnancy hormone (2, 37). Progesterone receptors are nuclear receptors as well, and similar to ER, in the presence of the ligand, they homo- or heterodimerize and bind to progesterone response element (PREs) within target genes to activate

or repress their transcription (37, 38). The two PR isoforms PR-A and PR-B have estrogen-inducible promoters, hence it is difficult to isolate the effect of progesterone from estrogen (39, 40).

HER2 is a transmembrane receptor that forms a heterodimer with the other three HER family members, with however, a higher proliferation-inducing ability (41). The signal is then transmitted to the nucleus through signalling cascades such as the MAPK (mitogen-activated protein kinase) cascade, which can drive cellular processes including proliferation and migration (41, 42). It has been reported that in the absence of epidermal growth factor, PR expression cannot be induced by estrogen, indicating a crosstalk among these three receptors (40).

The three receptors have differential expression in different breast cancer subtypes (Table 1.1). ER and PR are expressed in about 70% of all breast cancer cases, HER2 overexpression or geneamplification is found in about 15% of all breast cancer cases, among which ~20-25% cases are ERpositive (40, 43, 44). Breast cancers negative for ER, PR or HER2 are termed triple-negative breast cancers (TNBC) and those tumours are associated with the worst prognosis when compared to receptor-positive subtypes and account for approximately 15% of all breast cancer cases (4, 45).

1.2.3 Classification of breast cancer

The treatment of breast cancer is determined by the disease stage (0-4), and may include surgery, radiation therapy, hormone therapy and targeted therapy. In the clinic, testing for the presence of ER, PR and HER2 is used to determine which treatment a patient should receive. Hormone receptorpositive breast cancer is normally treated with a targeted therapy either to decrease the level of estrogen or to block its function by interfering with ER, such as Tamoxifen (46). Alternatively Herceptin or trastuzumab is used to treat HER2-positive breast cancers and its binding to HER2 receptors prolongs their half-life, therefore inhibiting cell growth by blocking the HER2 receptor and flagging the cancer cell for destruction by the immune system. TNBC cases are receptor negative, and are more challenging to treat due to a lack of targets for currently available treatments. Metastatic breast cancer (stage 4) is considered incurable and thus the goal of treatment is to slow down the growth and spread of the cancer cells and increase or stabilize the quality of life for breast cancer patients (47).

Breast cancer is a heterogeneous disease with a number of different subtypes, prognoses and treatment responses (46). In an effort to better characterise this disease, many studies have further classified breast cancer at the transcriptomic level and this has been shown to correlate with patient outcomes (46). Based on gene expression profiling, 6 molecular subtypes have been defined: luminal A, luminal B, HER2-enriched, basal-like, normal breast-like, the claudin-low or mesenchymal-like subtype (48) (Table 1.1). ER positive breast cancers have been divided into luminal A and B, which

have the best prognosis (46). Triple-negative tumours (ER-/PR-/HER2-) are mainly found in the basallike and claudin-low subtypes (9). However, it is worth noting that the receptor phenotype does not completely match the gene expression profiles, for example, 15-25% of breast cancers with positive ER/PR are classified as claudin-low (49). Recently, Lehmann *et al* suggested a further division of triple negative tumours, but these subtypes have not been validated for clinical use (50).

Table 1.1 Molecular subtypes of breast cancer and p53 mutation profile (3).

Molecular subtype	Frequency	Receptor status	Histological Grade	TP53 mutations	Prognosis
Basal-like	10-20%	ER-/PR-/HER2-	High	High	Poor
HER2-enriched	10-15%	ER-/PR-/HER2+	High	High	Poor
Normal breast-like	5-10%	ER-/+ HER2-	Low	Low	Intermediate
Luminal A	50-60%	ER+/PR+/HER2-	Low	Low	Good
Luminal B	10-20%	ER+/- PR+/- HER2-/+	Intermediate/High	Intermediate	Intermediate/Poor
Claudin-Low	12-14%	ER-/PR-/HER2-	High	High	Poor

1.2.4 Breast cancer initiation and metastasis

The human body has very precise machinery for regulating a very complex system of biological processes, with strict control of the fate of each cell in the body. When this control is lost or the mechanisms controlling cell fate are not functioning properly, the body fails to regulate itself and one possible consequence of this is cancer development. Figure 1.2 summarizes tumour initiation and the metastatic process.

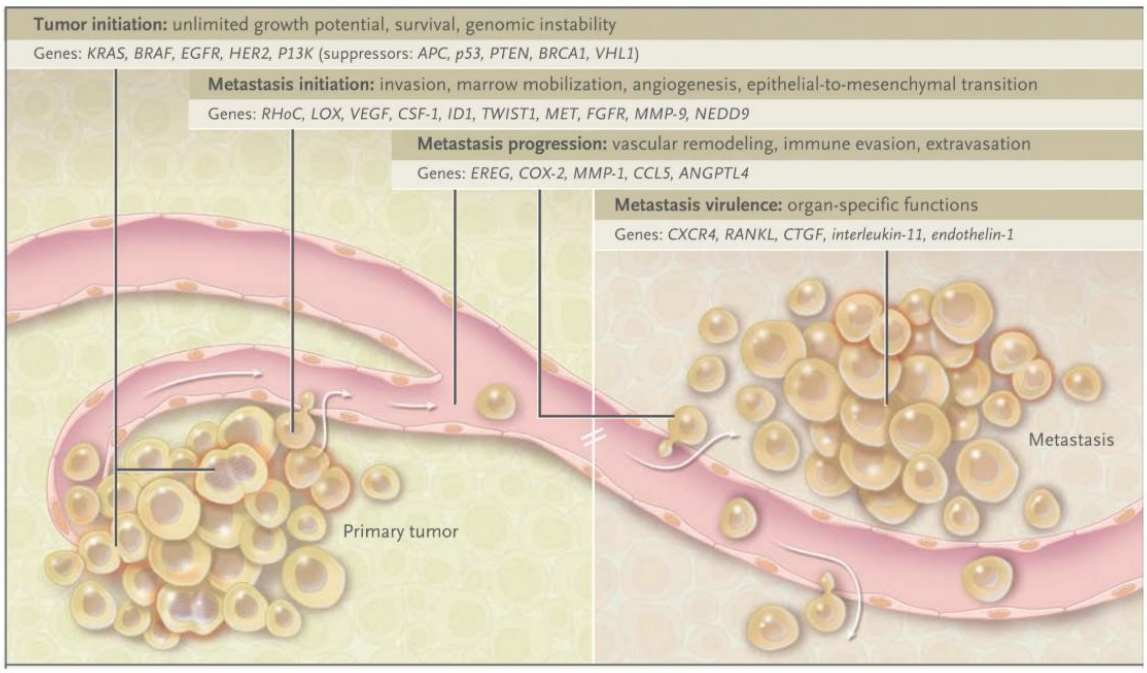

Figure 1.2 Overview of tumour initiation, the metastatic processes and relevant molecular markers. Tumour initiation is commonly associated with oncogenic mutations and inactivation of tumour-suppressor genes. Metastasis initiation includes EMT, local invasion and associated angiogenesis before extravasation and further tumour progression. Secondary growth of the tumour are organ-specific (51).

Cancer cells have infinite proliferative potential and increased input of growth stimulation leads to their increased cell proliferation. As mentioned above, estrogen is the main breast mitogen; it is not surprising that postmenopausal females receiving hormonal therapy or with obesity (as adipocytes serve as a main source of estrogen) have a worse prognosis and worse response to treatment (3, 23). Growth signals can be secreted through autocrine or paracrine mechanisms, and an increased expression of membrane receptors for these growth signals generally leads to increased cellular growth. A clear example is the HER2 pathway, which sequentially activates Ras/Raf/MAPK, JAK/Stat and PIK3/AKT/mTOR pathways, leading to cancer cell proliferation, survival and even migration capabilities (3). Uncontrolled proliferation is further facilitated by compromised tumor suppressor genes. As mentioned earlier, germline mutations of *BRCA1/2* and *TP53* are well-established predisposition factors in breast and ovarian cancer (27). Additionally, a study profiling somatic mutations in 2433 breast cancer patients showed that mutant PIK3CA and TP53 cancers dominate the mutation landscape in ER positive and ER negative breast cancers respectively (52). Hence, mutation of key genes involved in regulating cell fate leads to further uncontrolled growth and further genetic instability.

In the normal breast, epithelial cells adhere to one another and to the basement membrane through membrane proteins such as E-cadherin and integrins (53). However, breast cancer cells that become invasive have lost their polarity and cell-cell adhesion, and classically undergo epithelial mesenchymal transition (EMT) and gain the ability to move, invading adjacent or distant tissues. The EMT is believed to be important for critical steps in the invasion-metastasis cascade which involves: (1) local invasion, where cancer cells penetrate through surrounding extracellular matrix, (2) intravasation, where they enter blood vessels or the lymphatic system, (3) survival while being transported, (4) attaching at distant tropistic sites, (5) extravasation, (6) survival at a foreign environment, and (7) secondary growth (54, 55).

Local invasion is the very first step of metastasis. Luminal epithelial cells are believed to be the main origin of carcinomas, whereas myoepithelial cells serve not only as a physical barrier between the luminal cells and the extra cellular matrix (ECM), but also as a paracrine source inhibiting luminal cell proliferation and invasion. Abnormal myoepithelia have been found to lose these features and facilitate tumour cell contact with the basement membrane (56). When cancer cells contact the basement membrane, they release proteases such as matrix metalloproteinases (MMPs) (57, 58). Compromised basement membrane allows cancer cells to further penetrate into stroma. Cleavage of

the ECM may generate growth factors and chemokines (59), which can further alter tumour immunogenesis and thus lead to progression (60).

The way that cells penetrate the adjacent tissue can be grouped (collective migration/invasion) or as a single cell through the “protease-, stress-fiber-, and integrin-dependent mesenchymal invasion” or “protease-, stress-fiber-, and Rho/ROCK-dependent amoeboid invasion” (61). Amoeboid migration uses a less adhesive manner, physically protruding or squeezing through the ECM (62, 63), and is commonly seen in small-cell lung cancer, small-cell prostate cancer and lymphoma (64, 65). Mesenchymal migration, on the other hand, uses a more adhesive manner in which interaction with integrin is needed and cells exhibit a more fibroblast-like morphology, such as fibrosarcomas (66, 67). Cancers with increased dedifferentiated epithelium, such as IDC, can utilize mesenchymal migration as they lose the epithelial phenotype. Nevertheless, epithelial cancers mostly migrate in a collective manner in a cluster or cell sheets, because they maintain their epithelial characteristics with the presence of cell-cell connections (68, 69). The leading front can be one or more highly migrative cells, passively dragging the following cells through cell-cell adhesion (70). These units of cells can remain or lose their connection to the primary tumor sites, and therefore may not be as efficient as single cell migration (71, 72). However, collective migration is a much more resistant unit compared to single cells. For example, single cells are more predisposed to immunological reactions, given that the core of a migration unit is protected (61).

However, these events are not fully independent, but rather interchangeable. Most cancers originating from the epithelial cells, are prone to collectively move as they have strong cell-cell connections. But as the cancer progresses, dedifferentiation occurs leading to dissemination of single cells, where epithelial-mesenchymal transition (EMT) takes place, typically characterized by loss of Ecadherin with expression gains of EMT markers including but not limited to N-cadherin, vimentin and snail/slug. Amoeboid-like cells can be transformed from mesenchymal-like cells when treated with a protease inhibitor, or from collectively migrating cells when treated with integrin inhibitors (61, 67). This drug-induced plasticity is particularly challenging in clinical aspects (73).

The spreading of tumor cells is carried out by the blood or lymphatic vessels. Epidermal growth factor (EGF) and cytokine transforming growth factor β (TGFβ) are reported to stimulate penetration of tumour cells (74, 75). In addition, tumours can stimulate angiogenesis as well as neurogenesis in the surrounding microenvironment through factors such as vascular endothelial growth factor (VEGF) and neuron growth factor (NGF) (76, 77). The tumour-associated vasculature is not as well-structured as the normal blood vessel, as such, both the endothelia and pericytes are prone to be reconstructed to facilitate penetration. Cancer cells which have penetrated through the blood vessels can survive

through different strategies. Multi-cell units, as discussed above, may sacrifice the outer layer cells and manage to deliver the core cells to the secondary site. Single circulating tumour cells (CTCs) may cling to the platelets thus escaping from immune cells (78).

It has been reported that CTCs have proclivity regarding choice of distant metastasis sites. In breast cancer, tumour cells favor bone marrow metastasis, followed by lung, brain and liver (79-82). Metastatic breast cancer cells disrupt the balance of bone formation and degradation by increasing the amount of parathyroid hormone-related peptide (PTHrP) in the bone marrow, which can be secreted by the breast cancer cells or osteoclasts. Upregulated PTHrP increases expression of the ligand for receptor activator nuclear factor-κB (RANK), which in turn stimulates the differentiation of osteoclasts, introducing osteoclastic lesions (83). Patients can suffer from severe fatigue, sudden pain and even an inability to move (84).

Although micrometastases in the bone marrow are associated with worse prognosis, relapse and mortality (85, 86), metastasis appears to be a very inefficient process and detected CTC dissemination may not necessarily be associated with metastatic ability. This is particularly important when it comes to aggressive treatments (87).

As discussed in the above paragraphs, initiation and progression of breast cancers is very complex and dysregulation of tumour suppressor genes such as *TP53* can be a contributing factor.

1.3 The p53 tumour suppressor protein

DNA integrity is essential for sustaining cellular functions, hence any mutations or alterations in genes critical for the maintenance of genomic stability increase the susceptibility to diseases, such as cancer (88). p53 is a tumour suppressor protein encoded by the *TP53* gene (OMIM 191170) that plays a critical role in DNA repair and apoptosis and is well-known as the guardian of the genome (89, 90).

1.3.1 The p53 pathway

p53 is a transcription factor that regulates the expression of multiple genes that have a complex network of cellular functions. Figure 1.3 illustrates the detailed p53 pathway showing the core regulation, the upstream stress input and the downstream transcriptional targets as well as biological responses.

1.3.1.1 Core regulation

Generally, the p53 protein, with a short life span of 5-20 minutes, remains at extremely low expression levels in cells through regulatory control conferred by a ring finger type E3 ubiqutin ligase named Mouse Double Minute-2 (HDM2), which binds specifically to TAD1 of the p53 protein. HDM2 can

ubiquitinate itself as well as the substrate it binds to, depending on its post-translational modifications: phosphorylation leads to p53 degradation while sumoylation leads to self-degradation (91). Upon cellular stress, HDM2 becomes sumoylated facilitating self-degradation; p53 therefore becomes stabilized and accumulates in the nucleus. The interaction between p53 and HDM2 is a negativefeedback loop as p53 transactivates HDM2, which in return leads to a lower level of the p53 protein
(92).

The ARF tumour suppressor (alternative reading frame, protein product of *INK4a* locus, $p14^{ARF}$ in human and $p19^{ARF}$ in mice) is specifically activated by oncogenic signals other than normal mitogenic signals or DNA damage (93). It binds directly to HDM2, inhibiting p53 degradation, therefore it's not surprising that mutation or loss of $p14^{ARF}$ is found in many cancer types (94, 95).

1.3.1.2 Upstream and downstream mediators of p53 function

The p53 protein forms a tetramer and undergoes several modifications following activation by cellular stress including phosphorylation and acetylation, this leads to DNA-binding and transcriptional activation of downstream target genes, respectively (96). As shown in Figure 1.3, the tetrameric p53 complex can activate a number of transcriptional targets and induce a range of biological responses depending on the cellular context including the cell type, growth conditions and the nature and level of stress involved (96, 97). The primary function of p53 is to maintain genomic stability within the cell in response to cellular stress and this can be achieved through the p53 pathway in multiple ways.

Importantly, p53 mediates cell-cycle arrest and induces apoptosis under internal or external stress stimuli such as DNA damage and hypoxia (98). It allows DNA repair by halting the cell cycle, where various types of DNA abnormalities such as DNA double strand breaks or bulky DNA lesions can be recognised and repaired through various mechanisms including nucleotide excision repair, base excision repair, mismatch repair, non-homologous end joining and homologous recombination (99). For example, under low stress conditions, p53 activates the cyclin-dependent kinase inhibitor $p21^{WAF1}$ and Reprimo, which further regulate the G1/S and G2/M checkpoints (91, 100); while under severe stress, p53 activates an apoptotic cascade by activating several pro-apoptotic proteins such as Bax, BID and Puma (98). p53 can also induce apoptosis through transcription-independent mechanisms from the mitrochondria or the cytosol (101).

P53 also has well known roles in regulating cell metabolism and survival through inhibition of the IGF1/AKT and mTOR pathway, which are conserved pathways through evolution, through which cells sense nutrition and growth factors (102). Stress-activated p53 suppresses these two pathways by activating IGF-BP3, PTEN and Tsc2 genes, allowing replication errors to be corrected. Mutation of PTEN

therefore is an indicator of ongoing nutrient uptake, hence an indication of highly proliferative tumour cells (102).

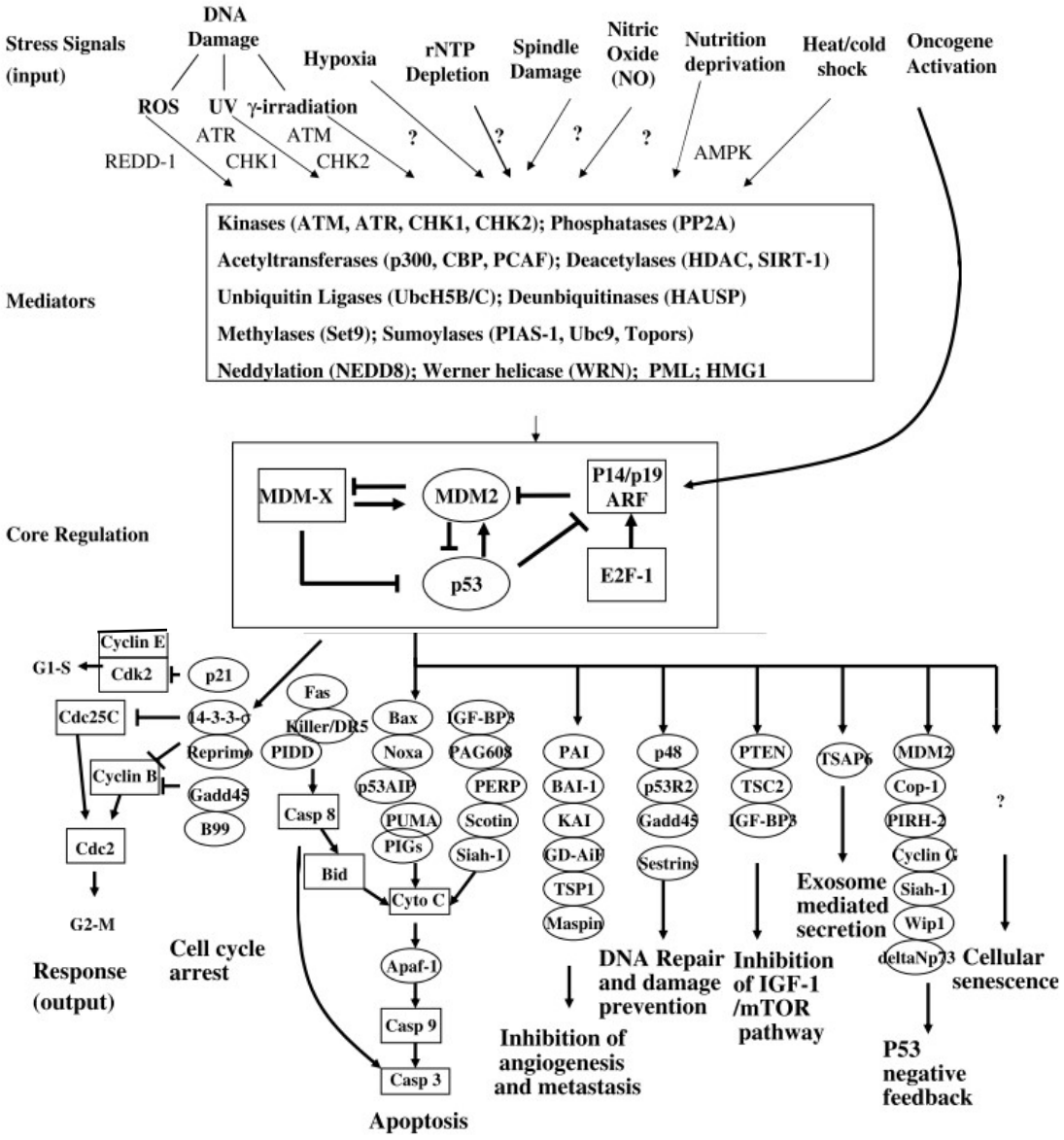

Figure 1.3 The p53 pathway. Various stress stimuli are detected by the cell and communicated to the p53 protein by multiple mediators, resulting in HDM2 degradation and p53 activation. The p53 protein regulates HDM2 expression in a negative feedback manner. Activated p53 is a transcription factor, which mediates the transactivation of downstream genes leading to a range of cellular functions that are important for maintain genomic stability. **Adapted from (103).**

1.3.1.3 The role of p53 in cancer metastasis

Recent studies add new perspectives to the role of p53 in inhibiting cancer other than its primary functions in suppressing proliferation and inducing cell death. Metastasis-associated processes, including loss of tissue integrity, EMT and cancer cell stemness are also under direct or indirect p53

modulation. Loss of p53, for instance, has been reported to lead to increased migration in fibroblasts, keratinocytes, as well as breast cancer cell lines (104-107). Additionally, MCF-7 cells that have been xenografted into nude mice showed increased distant metastasis to the lung when p53 function was impaired, compared to those with wt p53 (105), further supporting an *in vivo* role for p53 in metastasis suppression. Figure 1.4 shows the target genes regulated by p53 that are involved in metastasis, including EMT, cell mobility and cell-microenvironment interaction which includes a number of key metastatic markers introduced in the previous section (Section 1.2.4).

Cells that detach from the primary tumour intrude the ECM, and this has been reported to be regulated by p53. For instance, overexpression of wtp53 in melanoma cells with mutant p53 reduced the secretion of metalloproteinase 2 (MMP2) (108). The Rho family, including Rho, Rac, cdc42, is a well-established intracellular GTPase signal transducer involved in the regulation of cytoskeletal dynamics (109, 110). In primary mouse embryonic fibroblast cells, p53 loss coincides with increased Rho expression, leading to up-regulation of ECM proteins, associated with the mesenchymal phenotype (such as fibronectin and collagens), resulting in increased invasion (111). In addition, p53 has been reported to suppress the stimulation of Rho through Ras, leading to decreased motility through matrigel in human colon cancer cells HCT116 (107) and immortalized mouse colonic epithelial YAMC cells (106).

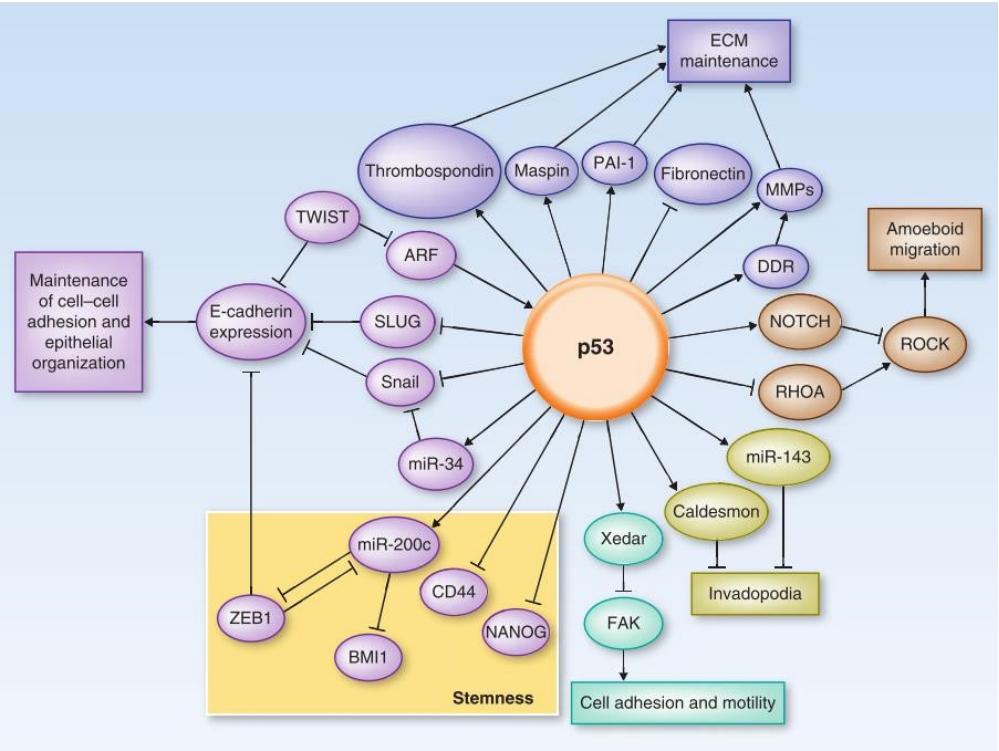

Figure 1.4 Metastasis related events that affect or are affected by p53. The p53 protein suppresses genes involved in cancer metastasis. Different pathways and the relevant component regulated by p53 are grouped in different colors **(54).**

1.3.1.4 The regulation of E-cadherin by p53 in epithelial-mesenchymal transition

As stated previously in Section 1.2.4, E-cadherin plays a key role in maintaining tissue integrity and loss of this protein has been recognized as a hallmark of EMT and an indicator of metastasis. In fact, EMT is a critical biological process in normal cells. To date, three types of EMT have been proposed according to the biological events: Type I related to implantation, embryogenesis and organ development; Type 2 related to tissue regeneration and organ fibrosis; and Type 3 associated with tumour progression and metastasis accompanied by genetic or epigenetic changes (53, 112). As illustrated in Figure 1.5, the E-cadherin protein has intracellular, transmembrane and extracellular domains, through which it links the actin cytoskeleton in the cell through its interaction with α, β and γ-catenin in a zipper manner as homodimers, thus linking adjacent cells (113). β -catenin is involved in the WNT signaling pathway, promoting cell proliferation. Crosstalk of the WNT signaling-pathway with the TGFβ signaling pathway, allows β-catenin and Smad proteins to form a transcriptional complex, and repress E-cadherin expression and thus inducing EMT (114-116).

p53 is reported to maintain E-cadherin expression through directly or indirectly opposing its negative transcription factors. These repressive regulators include Snail, ZEB and bHLH (basic helix-loop-helix) families (112, 117). p53 indirectly regulates Snail/Slug through HDM2 or miR-34 (micro RNA-34) (118). Interestingly, HDM2 regulation of Slug can be both negative (via p53) (104) and positive (119). In 2013, Jung *et al* (119) found that in the absence of p53, HDM2 up-regulates Slug by stabilising Slug mRNA, but the interaction between HDM2 and Slug mRNA is not affected by p53. p53 also indirectly represses ZEB by inducing miR-200c (118), as well as functioning as an antagonist to TWIST1 on target genes such as p21 (120). Through direct interaction, Twist and p53 negatively regulate the expression of target genes such as p21 (120). In addition, the histone deacetylase SIRT1 (HDAC family) can deacetylate p53 when p53 becomes inactive (121); miR-34a suppresses SIRT1 thus stabilizing p53 and is a direct target of p53, featuring a positive feedback loop between p53 and miR-34a and a negative association between p53 and SIRT1 (122). E-cadherin expression can be reduced directly by a complex of SIRT1, MBD1 (Methyl-CpG binding domain protein 1) and TWIST1 (bHLH family) (123). Hence, in the absence or malfunction of p53, the absence of E-cadherin can arise through multiple mechanisms and is likely to be associated with altered tissue integrity leading to cancer cell invasion.

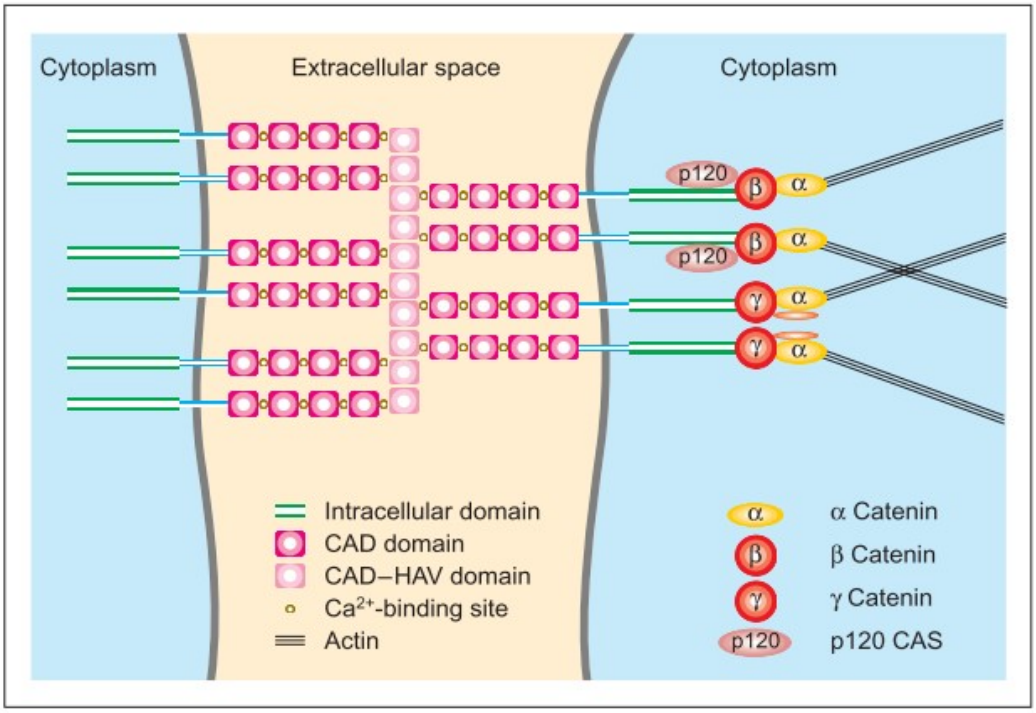

Figure 1.5 E-cadherin-mediated cell-cell connection. The most distant extracellular domain of E-cadherin (the CAD domain, shown by the bright pink squares) has a HAV motif (light pink squares), which interacts with the E-cadherin molecule of the adjacent cell. The intracellular cadherin complex includes α, β and γ catenins and p120 CAS, linking E-cadherin to the actin cytoskeleton (shown by the black lines) (103).

1.3.1.5 p53 and epigenetics

Epigenetics describes any changes of a gene product without altered genomic sequence, and consists of DNA methylation, histone methylation, altered chromatin packaging and any other posttranslational modifications (124).

Epigenetic factors can modify the p53 protein and lead to suppression of its canonical function. For instance, Aurora A kinase and histone deacetylase (HDAC) can lead to p53 inactivation by removal of the acetyl groups; methylation of p53 C-terminal lysines, especially at K370 and K382, are found to be associated with p53 repression (125, 126), but little is known of p53 methylation in the cancer context. Teratocarcinoma is a type of germline cancer consisting of the embryonal carcinoma stem cells and the differentiated benign cells. A high level of wild-type, yet inactive p53 is expressed in embryonal carcinoma stem cells, but expression of HDM2 and p21 are not detected, both of which are transactivated by functional p53. In the differentiated cells, p53 is functional, leading to expression of HDM2 and p21. It has been found that p53 can be activated once the histone methyltransferases such as SMYD2 and Set8 are down-regulated in embryonal carcinoma stem cells, illustrating a role of methylation in modulating the activity of p53 (125, 126).

However, the relationship between p53 and epigenetics is bi-directional, i.e., p53 can also affect epigenetic modifications. This can be seen in the example of induced pluripotent stem cells (iPS). iPS can be produced in mouse or human fibroblasts by adding reprogramming factors such as Sox2 and Oct4, which are critical for the removal of pre-established epigenetic modifications (127); and p53 inhibits differentiated cells from being reprogrammed. Hence, shortened inducing time and increased iPS induction were seen in the absence of p53 (128). In the field of acute myelogenous leukaemia, drugs blocking epigenetic changes, such as decitabine, have been used to treat patients and have been successful in some but not all patients. A study in 2016 on patients treated with decitabine showed that all patients with p53 mutations responded very well with a reduction of tumour cells (21 out of 21, 100%), while worse responses were observed in comparable patients with wt p53 tumours (32 out of 78, 41%) (129). These findings suggest a surveillance over epigenetic stability by p53. In addition, multiple studies have demonstrated a link between p53 and methylation of promotor regions of DNMT1 (DNA methyltransferase), which re-establishes the methylation status in the newly synthesized DNA instantly after replication (130). DNMT1 has increased expression in a colon cancer cell line upon p53 deletion (131), and *TP53* mutation was associated with overexpression of DNMT1 in lung cancers (132). A study looking at long-interspersed nuclear element 1 (LINE-1), which is demethylated during tumorigenesis in gastric cancer, has found *TP53* mutation is associated with LINE-1 methylation and patient survival. This further suggests an association of p53 in regulating epigenetics.

1.4 Malfunction of p53

The canonical human TP53 gene has 11 exons and 10 introns and the fully-spliced transcript is translated into a 53 kDa (393 aa) protein product, namely the full-length p53 (p53α). p53α has three functional domains: the transactivation domain (TAD I and II), the DNA-binding domain (DBD) and the oligomerization domain (OD), which are critical for p53 to form a functional tetramer, accurately recognize its DNA binding sequence (DBD) and successfully initiate transcription of the target gene at the transcription activation domain (TAD) (Figure 1.6). Since the p53 protein is crucial for normal control of cell growth through DNA repair or the induction of apoptosis, aberrant p53 function leads to aberrant cell proliferation and oncogene activation (133), which results in cancer formation. The apoptotic function of the p53 protein draws much interest due to the fact that functionally-impaired p53 caused by, for example, mutation or the generation of certain p53 isoforms results in oncogenicity (134, 135).

Figure 1.6 Structure of the FLp53 protein: transactivation domain I (TAD I); transactivation domain II (TAD II); proline rich domain (PRD); DNA-binding domain; hinge domain (HD) oligomerization domain (OD) C-terminal domain (CTD) (136).

1.4.1 Mutant p53

The International Agency for Research on Cancer (IARC) TP53 Database shows that p53 mutations are present in about 80% of all human cancers, though the percentages vary among different tumour types (Figure 1.7A). In breast cancer, less than 25% of breast cancer cases exhibit mutant p53, and the proportion of mutations is different between the breast cancer subtypes (Figure 1.7A and Table 1.1). The majority of mutations are missense mutations (Figure 1.7B), present between exon 4 and exon 8, which mainly encode the DNA-binding domain (Figure 1.7C). Mutant p53 has a prolonged half life of up to 24 hours and mutations in p53 can inactivate the wild-type protein by a number of mechanisms including, the mutant p53 protein being: (1) unable to bind to consensus DNA sequences of target genes, (2) unable to form a tetramer and/or (3) unable to recruit cofactors necessary to activate target gene transcription. Together, functional inactivation of p53 through these mechanisms results in an inability to induce cell-cycle arrest or apoptosis, and this can result in increased chemoresistance in cancer cells (134).

Additionally, p53 mutations may result in a gain of function. The gain-of-function hypothesis states that mutant p53 becomes oncogenic, rather than a dysfunctional protein (137). Several mechanisms are proposed: (1) mutant p53 interacts with its family members, p63 and p73, inhibiting their ability to induce apoptosis; (2) it binds to its specific transcription factors, for example NF-Y (nuclear factor Y) and ETS-2, which are not specific for wtp53, and triggers the transcription of downstream genes such as cyclin A and Cdk1, leading to increased cell proliferation; (3) it binds directly to specific promoters and regulates their gene expression, for example nuclear MARs (the matrix attachment regions), which are related to DNA replication but not yet confirmed to have an oncogenic potential *in vivo* (134, 137-139).

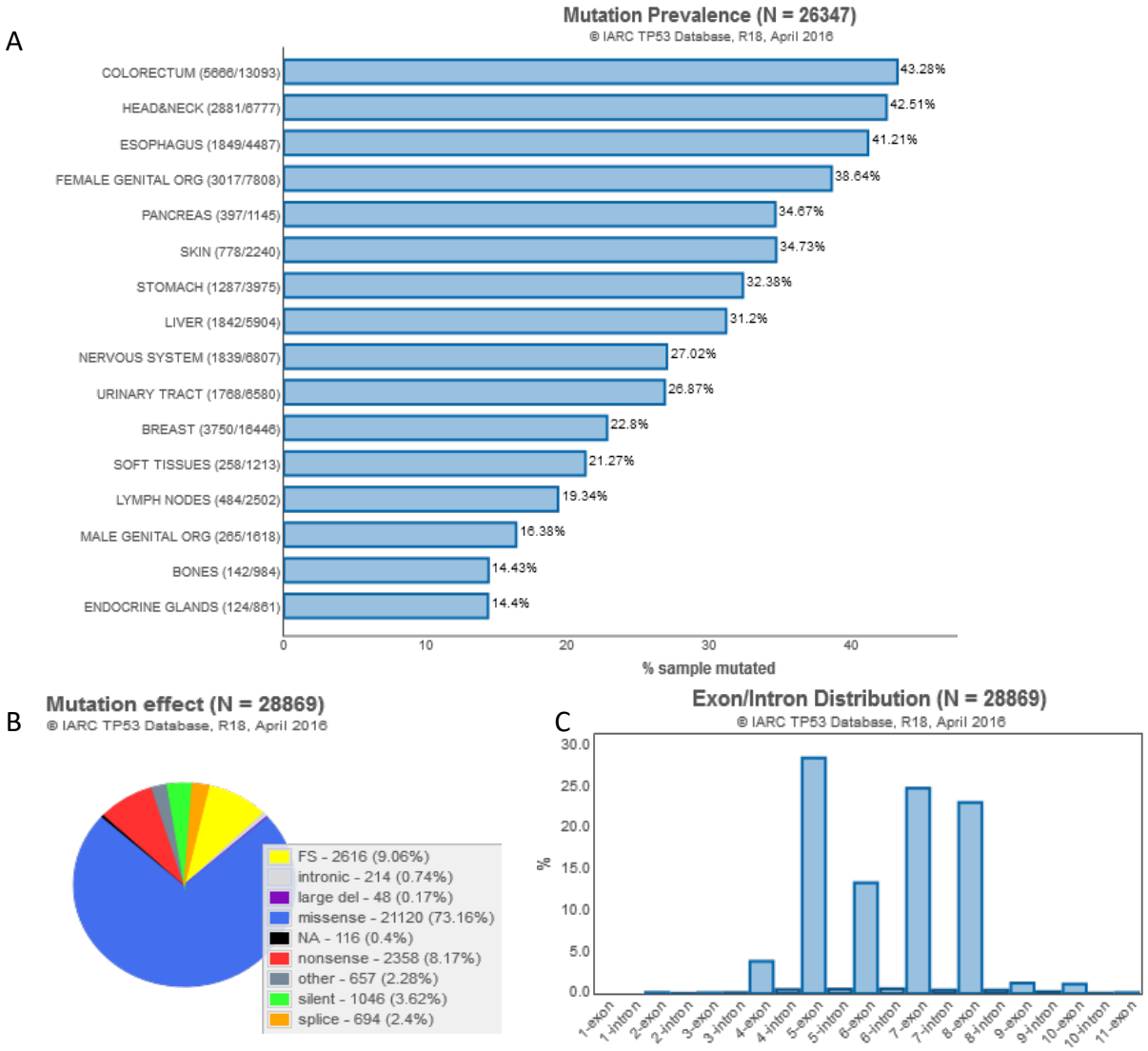

Figure 1.7 *TP53* mutation. A, Tissue-specific mutation prevalence. B, Proportion of different types of p53 mutations (FSframe shift), illustrating that missense mutation are the most common p53 mutation. C, Mutations mostly occur within DBD domain (exons 4-8) (140).

1.4.2 Other mechanisms of p53 inactivation

Since the p53 protein induces its functions through the transcriptional activation of downstream genes, inactivation of p53 commonly results in a failure to activate these downstream target genes. A typical example is the post-translational interaction with the SV40 viral protein, which dates from the very first publication of p53 in 1979 (141). It has been shown that this large T antigen inhibits the transactivation function of wtp53 by blocking its DNA-binding ability, leading to the stabilization and accumulation of inactivated p53 (142, 143). Several other mechanisms for p53 inactivation have also been proposed.

Degradation of p53, on the other hand, directly results in a lower level of p53. Overexpression of HDM2 (144) and enhanced HDM2 activity has been found in brain tumours due to the overexpression of a ubiquitination factor UBE4B (145), which facilitates the elimination of p53. Other negative regulating events in the core regulation of p53 by HDM2 include *PTEN* gene mutation and continuous AKT (Protein kinase B) activation (146). Methylation by the Lysine Methyl Transferases (KMTs) has also been shown to be related to p53 repression or activation depending on the location and number of methyl groups (147).

As a nuclear transcription factor, the cellular localisation of p53 is essential, and the nuclear localisation signal (NLS) and the nuclear export signal (NES) are tightly involved in the regulation of p53 localisation (148). It has been reported that colorectal adenocarcinomas displayed nuclear accumulation of mutant p53 and cytoplasmic accumulation of wt p53, indicating a role for compartmentalization in regulating the function of wt p53 (149).

In breast cancer, p53-dysregulated gene expression signatures are better at predicting outcome and chemotherapy responses than p53 mutation (11, 12), suggesting that wt p53 function is compromised by mechanisms other than mutation. The Cancer Genome Atlas Network presented a comprehensive analysis based on multiple platforms including next generation sequencing and array profiling of 825 patients, where it showed non-silent p53 mutation types being predominantly missense or truncation in basal-like and HER2-enriched cases but not in luminal A and B subtypes (Figure 1.8). They also showed that p53 signalling can be disrupted by various mechanisms including HDM2/4 amplification and ATM loss, and when these are taken into account, a higher proportion of breast cancers are predicted to have functional inactivation of the p53 pathway (150), but a large percentage (51%) still remain unaccounted for.

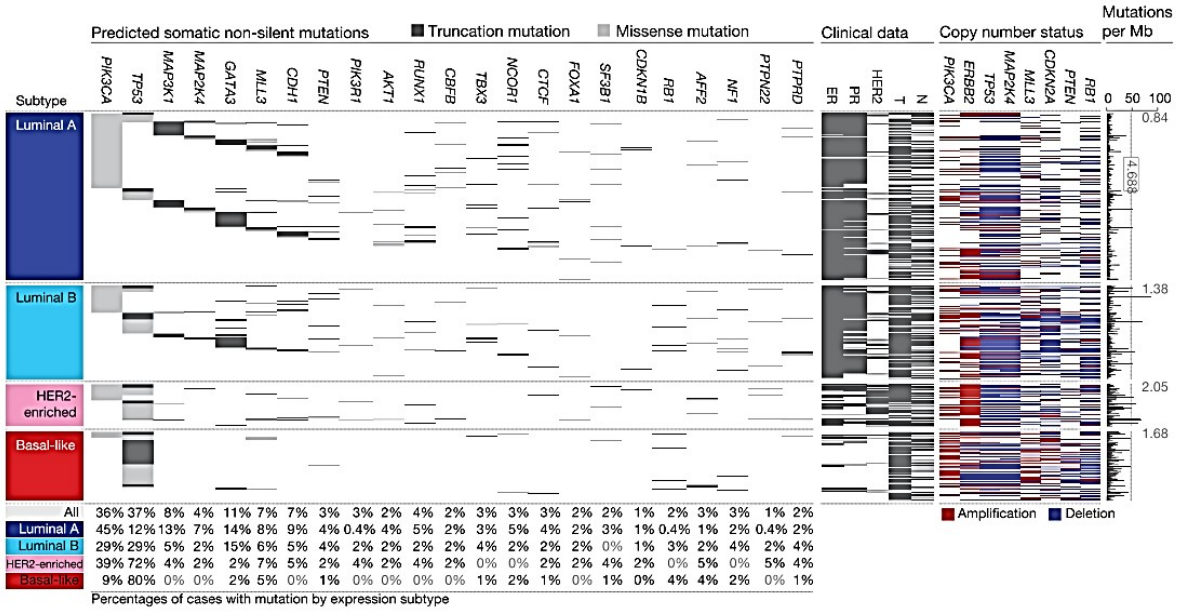

Figure 1.8 Significantly mutated genes in four major molecular subtypes of breast cancers of TCGA data (150).

1.5 Interaction between p53 and its isoforms

1.5.1 The p53 isoforms

The TP53 gene has been reported to generate 8 transcript variants in total (151), as shown in Figure 1.9A, due to alternative usage of an internal promoter in intron 4 (P2), in addition to the proximal promoter upstream of exon 1 (P1) (88, 98) and alternative splicing of intron 9. Transcripts t1-t4 are initiated by P1 (t2 includes a 3 nucleotides deletion at the beginning of exon 2) and can be translated from codon 1 (N-terminal intact) or codon 40 (N-terminally truncated Δ40p53); whereas transcripts t5 - t7 are initiated by P2, and can be translated from codon 133 (Δ133p53) or codon 160 (Δ160p53). The alternative splicing of intron 9 gives rise to C-terminally truncated isoforms (β and γ) lacking portions of the OD, but with substitution of short peptide sequences as shown in Figure 1.9B. Notably, t8 retains intron 2, which includes several stop codons preventing translation of full-length p53 and thus mainly produces Δ40p53 (17, 151). The N-terminal truncations can co-exist with the C-terminal variants and therefore, 12 protein isoforms have been described (13): p53, p53β, p53γ, Δ40p53α, Δ40p53β, Δ40p53γ, Δ133p53α, Δ133p53β, Δ133p53γ, Δ160p53α, Δ160p53β, and Δ160p53γ (15, 16, 88, 133, 152, 153).

Another two isoforms, Δp53 and p53ψ, have been described recently. Δp53 is generated by alternative splicing, eliminating parts of exon 7 and 9 and the whole exon 8 with a substitution of a splice cassette (CA CTG GA) (154). p53ψ retains only a limited part of the DBD (155). However, these two isoforms haven't been fully validated.

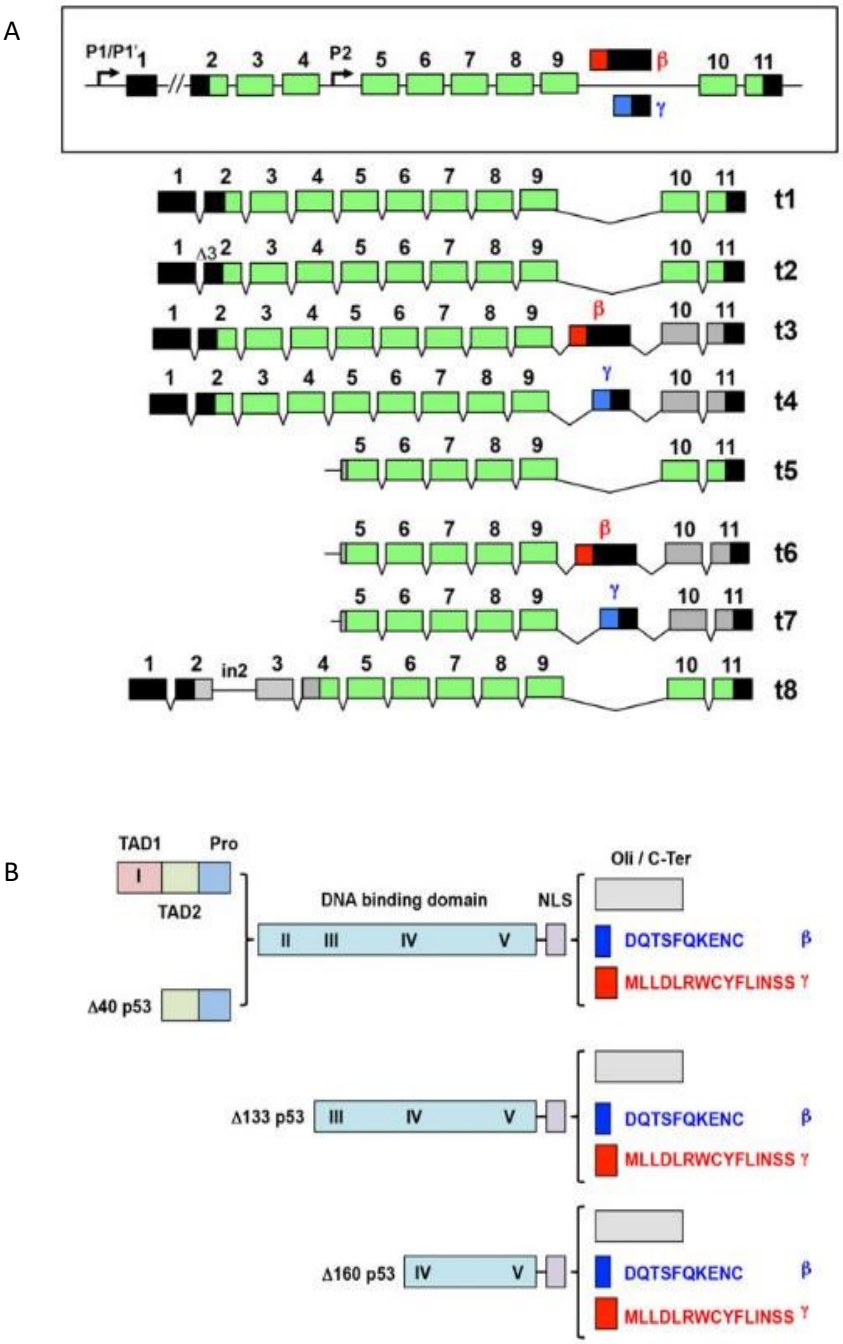

Figure 1.9 The TP53 gene transcripts and protein products. A, the canonical p53 gene (within the black rectangle) has 11 exons and two promoters, the proximal P1 and internal P2**.** Untranslated and translated regions are depicted in black and green. The p53 gene can generate 8 transcripts listed below the gene structure. B, The protein variants produced by the p53 transcripts, including N-terminal variants lacking 40, 133 and 160 amino acids (Δ40, Δ133 and Δ160 variants) as well as Cterminal variants α, β and γ, together generating 12 protein variants (isoforms) (Image source: The TP53 Website).

The above C-/N- truncated isoforms retain different proportions of the functional domains, thus it is inferable that their function is compromised when compared to the full-length protein, but may partially be maintained. A model of one p53 dimer binding to a half-site on the consensus DNA sequence and then further stablized through binding of a second dimer has been proposed (156),

indicating the transactivation function of p53 is executed through the correct formation of a tetramer. Given that the N-terminal TAD I is required for HDM2-mediated degradation and the C-terminal is responsible for NLS, tetramerization and is critical for HDM2-proteasome-mediated degradation (135, 156, 157); it can be presumed that p53 isoforms which lack these domains cannot be regulated in the same manner as p53. For example, the N-terminal isoforms such as Δ40p53 can escape HDM2mediated degradation and are more stable than the full-length protein, while the β and γ isoforms can't form stable tetramers (13, 158). However, Δ40p53 has been reported to form homo- or heterotetramers with p53, while p53β can interact with p53, and Δp53 is also able to oligomerise to itself (Table 1.2), therefore suggesting that the p53 isoforms are able to influence p53 function or may even have their own independent functions. Additionally, p53 isoforms have been reported to have distinct subcellular localisations (Table 1.3), compared to full-length p53, which may in part, explain their altered functional activities (13). For these reasons, the third mechanism for p53 inactivation or modulation of its function could be through the expression of p53 isoforms.

Table 1.2 Oligomerization capability of p53 isoforms

	Heterotetramer with p53	Homotetramer	Ref.
Δ40p53	Yes	Yes	(14, 16, 159, 160)
Δp53	No	Yes	(154, 161)
p53β/γ	interactive, but not fully validated	No	(13, 158)
Δ133p53	not available	Yes	(162)

Table 1.3 Subcellular localisation of p53 isoforms.

	Subcellular localisation	Ref.
p53	Nucleus	(13, 17)
p53β	Mainly in nucleus	(13, 17)
p53γ	Nucleus and cytoplasm	(13, 17)
Δ40p53	Mainly in nucleus	(17, 135)
Δ40p53β	Nucleus and cytoplasm	(17)
Δ133p53	Mainly in Nucleus	(13)
Δ133p53β	Mainly in Nucleus	(13, 163)
Δ133p53γ	Cytoplasm	(13)
Δ160p53	Perinucleolar	(15)
Δ160p53β	Foci pattern	(15)
Δp53	Cytoplasm	(161)
P53ψ	Cytoplasm	(164)

1.5.2 The mechanisms of p53 isoform generation

1.5.2.1 N-terminally truncated isoforms

Δ40p53 can be produced by alternative translation from the start codon at AUG40 of P1-initiated transcripts (14, 16). The life span of full-length p53 is very short in normal cells and is prolonged under stress (165). Normally, most proteins are translated from mRNA in a cap-dependent manner in eukaryotes, but this is different when it comes to p53. The eukaryotic initiation factors (eIFs) are decreased under cellular stresses, affecting the formation of translation-initiation complex at the cap site, thus affecting global protein synthesis (160, 166). P53 mRNA, on the other hand, includes two internal ribosome entry sites (IRESs), and has been found to be critical in regulating p53α and Δ40p53 translation respectively in response to stress (167, 168); however, different drug treatments selectively favour one or the other IRES. A study looking at the cap-independent mechanism of Δ40p53/p53 protein synthesis has found that endoplasmic reticulum stress using tunicamycin and thapsigargin induced both Δ40p53 and p53 protein levels, with the former to the same extent by both drugs and the latter less induced by thapsigargin than by tunicamycin, but doxorubicin had no effect on either isoform protein expression (169).

Δ40p53 can also arise from the alternatively spliced t8 (Figure 1.9A), which retains intron 2 including three in-frame stop codons. This prevents t8 from translating p53α and the main protein product generated is Δ40p53 (14). This mechanism of Δ40p53 production has been reported to be present in the breast cancer cell line MCF-7 for example (14). The shift from fully-spliced mRNA to t8 mRNA is associated with guanine-rich sequences in intron 3 in p53 pre-mRNA. Four 5'-monophosphates (GMPs) are prone to form a G-tract via Hoogsteen hydrogen-bonds with the help of monovalent cations such as K^+ or Na^+. G-tracts stack on each other and form 4-stranded DNA or RNA structures called Gquadruplex (G4) structures, which are highly stable. G4 affects splicing when present in introns or translation when present in mRNA. It has been reported that the G4 in intron 3 can regulate the splicing of intron 2 given the fact that exon 3 is very short (170). In addition, a polymorphism rs17878362 (TP53 PIN3) in intron 3, overlapping with the region in the close vicinity of G4, whose duplication increased the distance between G4 and intron 2, is associated with cancer risk (171, 172), and penetrance of germline mutations in p53 (173). The PIN3 wild-type allele results in a fully-spliced p53 mRNA, subsequently altering the ratio of p53α/Δ40p53; and homozygotes with the PIN3 wildtype allele have lower cancer risk than homozygotes with the polymorphic allele (18, 170, 172, 174). The relationship between PIN3 and another polymorphism rs1642785 (PIN2) located in intron 2 is still elusive, but it has been experimentally proven that the combination of homozygous WT PIN2 and WT PIN3 is optimal for the production of p53α (174). More recently, post-translational degradation of

p53α protein via the 20S proteasome was shown to generate Δ40p53 under oxidative stress (175), adding to the above mechanisms generating Δ40p53.

Δ133p53 and Δ160p53 are translated from P2-initiated transcripts at AUG133 and AUG160 respectively, resulting in protein products that are completely lacking the whole TAD domain and containing part of the DNA binding domain (15). Researchers have reported transactivation of Δ133p53 by p53α due to a p53 response element in P2 in zebrafish and human cell lines (176, 177).
At least four of the p63/p73 (p53 family) isoforms bind to P2 and have been shown to regulate Δ133p53 expression (178). Moore *et al* also reported a p53-dependent increase in Δ133p53 mRNA/protein level following knockdown of RNA helicase p68 (binds to the C-terminus of p53α) (179). In zebrafish, Δ113p53 (counterpart of Δ133p53 in human) but not wild type p53 was significantly upregulated when *def* (digestive-organ expansion factor) was mutated, indicating tissue-specific regulation (180). In zebrafish, a naturally occurring 4bp deletion in p53 intron 1 (counterpart of intron 4 in human) contributes to Δ113p53 production by creating a start codon, but this has not been validated in the human p53 gene (181). *Helicobacter pylori* infection may introduce various cellular stresses and has been reported to induce Δ133p53 and Δ160p53 (182). The mechanisms by which the expression of the Δ160p53 isoform is regulated have not been investigated, the level of which, however, was reported to be associated with p53 mutation at amino acid 273 (183).

1.5.2.2 C-terminally truncated isoforms

The β/γ isoforms are generated by alternative splicing, and the inclusion of intron 9 results in stop codons that prevent the translation of the OD domain, which is replaced with short substitution peptides translated from alternative exon 9β/γ. Interestingly, despite an intact TAD domain, p53β/γ cannot be targeted by HDM2, because several lysine residues at the C-terminus are responsible for ubiquitin ligation in HDM2-mediated proteasome degradation (157, 158). It has been found that SRSF3, a member of serine/arginine-rich splicing factor family, binds to p53β specific sequences and prevents its inclusion when pre-mRNA is undergoing splicing (184). Another SRSF factor SFRS1 regulates splicing balance between α and β/γ isoforms (185). Sequentially, SRSF7 was identified to induce p53β following ionizing irradiation (186). These findings suggest the significance of SRSFs in regulating alternative splicing of the C-terminus of p53 pre-mRNA. Following this, disruption of nonsensemediated mRNA decay (NMD) pathway was hypothesized to synergistically regulate the generation of C-terminally truncated p53 isoforms (187).

As illustrated by the preceding sections, p53 is subject to extensive alternative splicing resulting in the generation of multiple p53 isoforms. There is growing appreciation that their expression is induced under specific cell contexts through tightly regulated mechanisms. In the following section the function of these p53 isoforms is examined, where there is an equally diverse and intriguing

contribution of p53 isoforms to the regulation of p53 downstream targets and cellular functions. Moreover, in specific instances, p53 isoforms have been shown to be directly responsible for functions traditionally associated with the canonical p53 form. Neverthless, understanding the roles of the p53 isoforms probably remains the greatest challenge in the field of p53 research.

1.5.3 The function of p53 isoforms

p53 isoforms have been demonstrated to regulate the function of the full-length protein. Most of what is known regarding the functions of the p53 isoforms has been demonstrated through the use of overexpression models. The p53 isoforms are also differentially expressed in a range of cancers and their elevated level is associated with different clinical outcomes (188).

1.5.3.1 The function of C-terminally truncated isoforms p53β and p53γ

Generally speaking, p53β is thought to act as an enhancer of p53 function. It binds better to the BAX and p21 promoter than to HDM2 and can enhance p53-mediated transactivation of BAX, which leads to apoptosis (13, 189). It has also been shown to induce senescence in normal fibroblasts (190). In acute myeloid leukaemia, p53β/γ expression has been reported to be positively correlated with survival and negatively correlated with chemoresistance (191); meanwhile, previous studies from our laboratory have shown that the p53β isoform was up-regulated by cisplatin in melanoma (192). In contrast, studies on the p53-null cell line H1299 (lung carcinoma) injected subcutaneously in NSG mice have shown that expression of p53β or p53γ accelerated early tumour growth (193). High p53β mRNA expression in ovarian and renal tumours was associated with worse prognosis and tumour grade respectively (17, 194, 195). P53β expression has also been observed in head and neck squamous cell carcinoma (196) and glioblastoma (197), but with reduced expression in breast cancer (13). These results indicate that p53β can modulate p53 function in a context specific manner and that it may also have independent functions from p53. The expression of p53γ has been found to be an overall good prognostic marker, as it is positively related to favourable prognosis in breast cancer (198) and with responsiveness to chemotherapy in acute myeloid leukemia (199).

1.5.3.2 The function of N-terminally truncated isoform Δ133p53 and Δ160p53

P53 isoforms lacking the transactivation domain and containing a partial DNA binding domain are generally believed to behave in a dominant negative manner on p53 function due to unstable tetramer formation (136). Several studies have shown that Δ133p53 can act as an inhibitor of p53. Δ133p53 has been shown to impair the apoptosis-inducing function of p53 in the H1299 lung cancer cell line following co-transfection due to a missing TAD and partial DNA binding domain at N-terminal (13). In human glioblastoma U87 cells containing wt p53, Δ133p53 knockdown induced p53 expression, but

not vice versa (200). The same study showed that Δ133p53 represses p53, but under stress, p53 can transactivate Δ133p53 through the second promoter (200), indicating a negative feedback loop.

Recently, it has been proposed that aggregations of p53 protein variants may play a role in regulating the function of p53. Δ133p53 and Δ160p53, particularly, lack the full DBD domain including the βsheet, which renders the tetramer unstable and leads to aggregates (136). This coincides with the phenomenon of mutant p53 aggregates in cancer (201), indicating a mutant p53-like function of these isoforms. Indeed, overexpression of Δ160p53 induced mutant-like gain-of-function in tumorigenesis, and can be generated by mutant p53 mRNA (183). With this concept, it is not surprising that Δ133p53 and Δ160p53 are associated with inhibited apoptosis, delayed senescence, EMT and oncogenic functions (183, 200, 202-204). Δ133p53 appears in multiple cancers such as colorectal cancer, primary breast cancer, ovarian cancer and glioblastoma (17, 200, 205); in addition, Δ133p53β, which also lacks the OD domain, is found in breast cancers and melanoma cells, and can enhance cancer stem cell potential as shown by Arsic *et al* (205).

1.5.3.3 The function of the N-terminally truncated p53 isoform Δ40p53

Δ40p53 was initially believed to be a dominant negative regulator of p53. Early studies showed that Δ40p53 can form a heterotetramer which resulted in elevated nuclear export of p53, a reduction in the transactivation of certain p53 target genes and inhibition of p53-mediated apoptosis (14, 16). On the other hand, a study of melanoma using lentivirus-transduced cell lines overexpressing Δ40p53 showed that Δ40p53 causes apoptosis (206).

Δ40p53 has also been shown to function independently from p53 and it has become clear that the functional attribution of p53 control over the cell cycle is actually regulated by p53α and Δ40p53. Earlier work from Courtois *et al* showed high Δ40p53 expression at the onset of S phase (16), and Ray *et al* showed that Δ40p53 translation is most active at G1-S transition (167). A study later in 2010 found that in response to endoplasmic reticulum stress, p53α induces G1 arrest, while Δ40p53 induces G2 arrest by inducing 14-3-3σ (160). This agrees with the fact that Δ40p53 cannot transactivate p21 due to lack of TAD1 (16), therefore the regulation of p21 over G1 phase is lost. The p21 transactivation may be compromised by the p53/Δ40p53 heterotetramer or the Δ40p53 homotetramer, however the mechanism is not fully understood.

In addition, a study attempting to reveal the function of TAD domains using the Saos2 cell line combined with microarray gene expression analysis showed that different gene expression profiles were induced when p53 lacked TAD1, contained a non-functional TAD (point mutation of all serine residues) and/or was present in its full-length form; this led to the researchers proposing a model of genes activated by phosphorylation at serine residues in the TAD domain (207).

Another study using knock-in mice to investigate the transactivation potential on common p53 target genes, showed that the TAD1-mutant p53 failed to induce p21, Noxa and Puma expression, but it was able to transactivate Bax and retained the tumour suppressing function (208). Overexpression of Δ40p53 regardless of p53α status (wt, mutant or null) has also been reported to suppress hepatocellular carcinoma cell growth (209). These studies showed that: (1) TAD1 is important for an appropriate response to DNA damaging agents, (2) Δ40p53, which lacks this domain, may have abnormal responses to DNA-damaging agents, or abnormal apoptotic responses, and (3) Δ40p53 may have independent function, rather than simply functioning as an antagonist of wtp53. Accordingly the ratio of Δ40p53/p53 was shown to be important in the regulatory function that Δ40p53 has towards wt p53. In 2013, Hafsi *et al.* found that if Δ40p53 was expressed at levels higher than p53 (≥3 fold), Δ40p53 could inhibit p53 function, whereas lower or equivalent levels of Δ40p53 compared to p53, had diverse effects that were based on the cell lines examined (159).

In vivo, it has been shown that a high expression level of Δ40p53 in early embryos and embryonic stem cells (ESCs), maintains a proliferative status, while in adult somatic cells, a high level of Δ40p53 reduces life span (210, 211). These facts further indicate that the role of Δ40p53 depends on the cellular context. *In vivo* experiments performed with zebrafish and mice showed that Δ40p53 overexpression alone does not affect phenotype in the absence of wtp53, but its increased dose impairs overall growth status (210, 212, 213). Interestingly, a homologue of Δ40p53 is present in *C. elegans* and *Drosophila*, and it is important for germline in response to stress such as starvation and DNA-stress (214-216); while in higher organisms such as mammals, p53 is present in both germline and somatic cells (including adult stem cells), maintaining the balance of apoptosis and tissue-regeneration, reviewed by Abhinav et.al (217). These studies indicate that from an evolutionary point of view,
Δ40p53 may be primitive to p53α (210), and plays a critical role in embryo development and survival.

The function of Δ40p53 in cancer is diverse. In mucinous ovarian cancer, Δ40p53 expression is high in tumour tissue when compared to the normal tissue, but its expression in tumour tissue is positively related to recurrence-free survival (218). In melanoma cell lines, Δ40p53 is detectable and inhibits cisplatin-induced expression of p21 and PUMA (192). Data from our lab has shown that Δ40p53 is upregulated in breast cancers and is positively correlated with triple negative breast cancer (17).

1.5.4 p53 isoforms and breast cancer

As mentioned previously, p53 mutations are rare in breast cancer and p53 isoforms play a role in regulating p53. There are very few studies that have been performed in breast cancer patients. Of the studies that have been done, Bourdon *et al* examined the expression of p53 isoforms in 30 breast cancer samples compared to 8 pooled normal tissues (219), as well as another study looking at p53β and p53γ in 127 primary breast cancer tissues (198). They showed that the isoforms were differentially

expressed in breast cancer and that p53γ was associated with better prognosis, suggesting p53 isoforms may regulate p53 function in breast cancer. Both studies used nested PCR, but were not quantitative and they didn't examine Δ40p53. A study from Gadea *et al* proposed that Δ133p53β was an independent factor leading to recurrence and mortality in breast cancer regardless of *TP53* mutation status (220).

Another study has examined Δp53 in 88 primary breast cancer tumours and found that it was correlated to wt p53 mRNA levels, and that patients with mutant p53 and non-mutated Δp53 (mutational hybrids) had worse prognosis than patients with both isoforms mutated (221). However, it has not been confirmed that Δp53 is a real splice variant as it does not conform to normal splicing rules and no corroborating studies have been published.

Previous studies from our laboratory looked at p53β, p53γ, Δ40p53 as well as Δ133p53 using semiquantitave real-time PCR, and showed that high p53β expression was protective especially in patients carrying mutant p53 (17). These studies also established a link between Δ40p53 and breast cancers.

1.5.4.1 Δ40p53 and breast cancer

Studies from our laboratory are the only ones to date that have examined the relationship of Δ40p53 expression level with breast cancer clinical features and outcome. At the mRNA level we have shown that Δ40p53 is the most highly expressed p53 isoform in breast cancer, being significantly up-regulated in tumour tissues and cell lines compared to normal breast cells, and instructively associated with the aggressive subtype TNBC (17). A high Δ40p53:p53 ratio (> 0.7) is significantly associated with worse disease-free survival (HR 2.713) (18). These findings were validated by Mehta and colleagues in the TCGA cohort using RNA-seq data, where aside from p53α, Δ40p53 was the most highly expressed p53 isoform in breast cancer; and in every other cancer examined, further exemplifying its significance (222). These studies suggest that Δ40p53 may be involved in cellular functions that promote the aggressiveness of breast cancer, but functional studies demonstrating this are lacking and the role of Δ40p53 in this context has not been examined.

1.6 Study rationale

Breast cancer is the most commonly diagnosed cancer and accounts for the second-leading cause of cancer-related death among women worldwide (1). The tumour suppressor gene TP53 is the most frequently mutated gene in cancer, but its mutation in breast cancer is relatively rare (< 25%) and predominantly in TNBC (accounts for 10 - 20% of all breast cancer cases) (9, 10). As mentioned previously, p53 dysregulated genes better predict outcome and therapeutic responses in breast cancers than TP53 mutation (11, 12), therefore it has become clear that wt p53 is functionally

inactivated in the majority of breast cancers, indicating other mechanisms are involved in regulating p53 and subsequently affect the biological responses through the p53 pathway.

The *TP53* gene encodes for 12 protein variants (isoforms) due to alternative internal promoter usage, alternative splicing and alternative initiation of translation (13-16). The 12 isoforms are N-/Cterminally truncated and have been reported to have p53 regulatory abilities, however, their functional role in breast cancer remains largely unknown. Previous studies from our laboratory have established a link for the p53 isoforms and breast cancer, where we showed that Δ40p53 is the most abundant isoform in breast cancer specimens and breast cancer cell lines, and is significantly higher in cancers than in normal adjacent tissues (17). Studies from our laboratory have also reported a worse disease-free survival related to a higher Δ40p53/p53 ratio (18). These findings imply a role for Δ40p53 in breast cancer progression and treatment resistance. However, the mechanisms underlying this have not been adequately studied and functional analyses are lacking. Emerging evidence suggests p53 can regulate methylation, but knowledge in cancer is limited and a role of p53 isoforms in methylation has yet to be investigated.

We hypothesize that high levels of Δ40p53 (as observed in breast cancer) will have a negative impact on p53 functional activities resulting in increased proliferation, migration and invasion, contributing to p53-mediated DNA methylation, as well as inhibition of apoptosis in response to DNA damaging therapies; and that this is responsible for the association of worse outcomes in breast cancer patients with high Δ40p53/p53 ratios.

1.7 Aims

The major aims addressed in this thesis are:

1. To investigate the functional role of Δ40p53 in breast cancer including the regulation of gene expression, proliferation, cell migration, invasion and EMT;
2. To characterise the epigenetic changes associated with altered Δ40p53 expression;
3. To investigate the role of Δ40p53 in the response to DNA-damaging agents used in the treatment of breast cancer.

Chapter 2 Methodology

Chapter 2 Materials and methods

2.1 Materials

2.1.1 Chemicals from commercial sources

All chemicals and reagents were of molecular biology grade or analytical grade and were stored at room temperature unless otherwise stated. The chemicals and reagents were purchased from SigmaAldrich (Castle Hill, NSW Australia), Life Technologies (North Ryde, NSW, Australia), Thermofisher Scientific (North Ryde, NSW, Australia), Millennium Science (Mulgrave, VIC, Australia), Bio-Rad (Gladesville, NSW, Australia) and Bovogen Biologicals (Melbourne, Australia) and are listed in Table 2.1 in categories based on experimental procedures. Note that chemicals used in multiple assays were only listed in the first category.

Table 2.1 Chemicals used in throughout this thesis.

Name	Abbreviation	Source
Transfection		
DharmaFECT transfection Reagent 1 (4 °C)		Millennium Science
Opti-MEM (4 °C)		Life Technologies
Cell Culture		
Phenol red-free Dulbecco's modified eagle medium (4 °C)	DMEM	Life Technologies
Human Insulin (4 °C)		Sigma-Aldrich
Foetal Bovine Serum (-20 °C)	FBS	Bovogen Biologicals
Trypsin (-20 °C)		Life Technologies
TripLE		Life Technologies
L-glutamine (-20 °C)		Life Technologies
RNA extraction		

TRIzol (4 °C)		Thermal Fisher Scientific
Ethyl alcohol, Pure		Sigma-Aldrich
2-proponal		Sigma-Aldrich
Western Blotting		
NP-40		Sigma-Aldrich
Sodium dodecyl sulphate	SDS	Sigma-Aldrich
trisaminomethane	Tris	Sigma-Aldrich
Glycine		Sigma-Aldrich
Casein blocking buffer (4 °C)		Millennium Science
cOmplete™, Mini Protease Inhibitor Cocktail (4 °C)		Sigma-Aldrich
Bromophenol blue		Sigma-Aldrich
β-mercaptoethanol		Sigma-Aldrich
Ponseau S		Sigma-Aldrich
Glycerol		Sigma-Aldrich
30% Acrylamide (4 °C)		Sigma-Aldrich
Ammonium persulphate (4 °C)	APS	Sigma-Aldrich
Tetramethylethylenediamine (4 °C)	TEMED	Sigma-Aldrich
Precision Plus Protein™ Kaleidoscope™ Prestained Protein Standards (-20 °C)		Bio-Rad
Tween-20 Detergent		Sigma-Aldrich
Zymograph		
$ZnCl_2$		Sigma-Aldrich
$CaCl_2$		Sigma-Aldrich
Triton X-100		Sigma-Aldrich
Coomassie blue G250		Sigma-Aldrich
Fluorescent staining		
Formaldehyde		Sigma-Aldrich
TRITC-phalloidin (-20 °C)		Sigma-Aldrich
Phosphate-buffered saline	PBS	Life Technologies
4′,6-diamidino-2-phenylindole (-20 °C)	DAPI	
Cell Cycle analysis		
FxCycle™ PI/RNase Staining Solution		Thermo Fisher Scientific
RNA-seq		
SuperScript II Reverse Transcriptase (-20 °C)		Thermo Fisher Scientific
AMPure XP Beads (4 °C)		Thermo Fisher Scientific
Cell transduction		
Hexadimethrine bromide (4 °C)		Sigma-Aldrich

2.1.2 Kits from commercial sources

The High Capacity Reverse Transcription kit with RNase Inhibitor used to reverse transcribe RNA to cDNA was purchased from Life Technologies, North Ryde NSW, Australia. The Trans-Blot® Turbo™ RTA

Mini Nitrocellulose Transfer Kit was used to transfer protein to the nitrocellulose membrane using the Bio-Rad Turbo Transfer System and was purchased from Bio-Rad Laboratories, Gladesville, NSW, Australia. The IncuCyte® Annexin V Red Reagent apoptosis assay was purchased from Sartorius Singapore (Singapore Science Park II, Singapore). The RealTime-Glo™ Annexin V Apoptosis Assay and CellTiter-Glo® 2.0 Cell Viability Assay were purchased from Promega (Alexandria, VIC, Australia). The EZ-96 DNA Methylation™ Kit used for bisulfite conversion of DNA samples was purchased from Zymo Research (Irvine, California, United States). Infinium® MethylationEPIC BeadChips and reagents used for methylation analysis were purchased from Illumina (Scoresby, VIC, Australia). NextSeq® 500/550 High Output Kit v2 (including the High Output Reagent Cartridge, High Output Flow Cell Cartridge, Buffer Cartridge and the High Output 400M Flowcell), the TruSeq RNA Single Indexes Set A/B, and TruSeq Stranded mRNA Library Prep Kit were used for RNA-seq and were purchased from Illumina (Scoresby, VIC, Australia). Universal Taqman Master Mix and Taqman gene expression assays were used for semi-quantitative real-time PCR and were purchased from Life Technologies (North Ryde, NSW, Australia). HumanGene 1.0 Arrays were purchased from Affymetrix (Santa Clara, California, United States).

2.1.3 Antibodies and reagents for immunofluorescence and western blotting

The primary antibody used to detect E-cadherin was mouse anti-human monoclonal antibody HECD1 (ab1416, Abcam, Cambridge, United Kingdom) with a working concentration of 1/100 dilution. Primary antibodies used to detect GAPDH were mouse/rabbit anti-human monoclonal antibodies CB1001 and ab128915, and these were purchased from Abcam (Cambridge, United Kingdom) and Merck Millipore (Darmstadt, Germany) respectively. Both antibodies were used at a working concentration of 1 µg/ml. Primary antibodies used to detect the p53α and Δ40p53 (rabbit anti-human) isoforms were generated by Dr Jean-Christophe Bourdon (University of Dundee, UK). The KJCM1 antibody detects several epitopes from amino acid 1 - 81 and as well as from amino acid 360 -393 of p53α, and the the KJCA40 detects the epitope MDDLMLSPDDIEQWFTE with post-translational modifications (PTMs) are specific of Δ40p53 isoforms (including α, β and γ forms). The working concentrations of these antibodies were 1 µg/ml (KJCM1) and 2.5 µg/ml (KJCA40) respectively.

Goat anti-Mouse IgG Secondary Antibody conjugated with Alexa Fluor® 594 was purchased from Life Technologies (North Ryde, NSW, Australia) and was used for immunofluorescent staining. Odyssey secondary antibodies used in western blot analysis were purchased from Li-COR Corporate (Lincoln, Nebraska, United States) and included: IRDye 800CW Goat anti-Rabbit IgG, IRDye 800CW Goat antiMouse IgG and IRDye 680LT Donkey anti-Mouse IgG, which were used at a working concentration of 1:50000 dilution.

2.1.4 Cell lines

The human breast cancer cell lines MCF-7 and ZR75-1, expressing wt p53 (223, 224), were kind gifts from Professor Christine Clarke (Westmead Millennium Institute, University of Sydney, Australia) and Dr Judith Weidenhofer (University of Newcastle, Australia), respectively. MCF-7 cells stably overexpressing Δ40p53 via lentiviral LeGO vector as well as the empty-vector control were kindly generated by Dr Hamish Campbell and Professor Antony Braithwaite (University of Otago, New Zealand). To generate the lentiviral construct, the empty vector LEGO-iG2-puro+ was linearized by digestion with restriction endonucleases BamH1 and Sbf1. Δ40p53 cDNA was amplified by PCR using primers which incorporated 14bps of sequence homologous to the LEGO-iG2-puro+vector. The insert was then incorporated into the LEGO-iG2-puro+ vector by recombination (In-Fusion, Clontech, CA, USA). Δ40p53 lentivirus was then produced in 293T cells and used to transduce MCF7 cells. The derived MCF-7 cells were then maintained by puromycin selection (1 mg/ml).

2.1.5 Breast cancer patient samples

All patient samples used in this document were provided by the Australian Breast Cancer Tissue Bank (Darcy Rd, Westmead, NSW, Australia). This included total RNA extracted from 38 ER+ and 16 ER- fresh frozen invasive ductal carcinomas (IDCs). This study complies with the Helsinki Declaration with ethical approval from the Hunter New England Human Research Ethics Committee (Approval number: 09/05/20/5.02). All patients have consented to their tissue and clinical information being used in this study (17, 225).

2.1.6 siRNA

Custom-designed and commercially available siRNAs were used to modify p53 isoform expression in breast cancer cell lines (Table 2.2). Three siRNAs targeting intron 2 were used to knockdown Δ40p53 only, but #3 had toxicity and results for this siRNA are not shown in this document. A custom-p53 siRNA sequence spanning exon 2/3 of mature p53 mRNA, was used to knockdown p53α but not Δ40p53, and is therefore referred to as p53α siRNA in this document. P53 pool siRNA including 4 siRNAs, was used to knockdown all p53 transcripts, and non-targeting siRNA was used as a control.

Table 2.2 siRNA information

ID	Sequence (5' to 3')	Catalogue No.	Company
Δ40p53 #1	AGACCTGTGGGAAGCGAAA	Custom	Dharmacon
Δ40p53 #2	GCGAAAATTCCATGGGACT	Custom	Dharmacon
Custom-p53 (p53α)	GAAACTACTTCCTGAAAAC	Custom	Dharmacon
On Target Plus SMARTpool TP53 (7157)	1:GCAGTCAGATCCTAGCGTC 2:GTGCAGCTGTGGGTTGATT 3:GAAATTTGCGTGTGGAGTA 4:GGAGAATATTTCACCCTTC	L-003329-00-0020	Dharmacon
Non-targeting siRNA (control, NT)	On Target Plus non-targeting siRNA #1	D-001810-01-20	Dharmacon

2.1.7 shRNA

shRNAs were designed according to the siRNA sequences above (Table 2.3), from which Δ40p53 siRNA #1/2 as well as p53α siRNA sequences were packaged into lentiviral plasmids (GFP-positive and puromycin-resistant) by Sigma-Aldrich. A non-targeting control was commercially available from Sigma-Aldrich and it was used as a negative control.

Table 2.3 shRNA information

ID	Sequence (5' to 3')	Catalogue No.	Company
shΔ40p53 #1	AGACCTGTGGGAAGCGAAA	Custom	Sigma-Aldrich
shΔ40p53 #2	GCGAAAATTCCATGGGACT	Custom	Sigma-Aldrich
Custom-p53 (shp53α)	GAAACTACTTCCTGAAAAC	Custom	Sigma-Aldrich
Non-target control (shNT)			Sigma-Aldrich

2.1.8 Drugs

Cisplatin (CDDP) and doxorubicin/Adriamycin (DOX) were purchased from Sigma-Aldrich (Castle Hill, NSW, Australia) and were under safety clearance for Research Project Reference No R21/2016.

2.2 Methods

All experimental procedures were performed at room temperature if not specified.

2.2.1 Cell culture of breast cancer cell lines

All cell culture was carried out in a biosafety cabinet if not stated otherwise. The biosafety cabinet UV was turned on for 20 min to sterilise the surface. Prior to beginning experiments, all surfaces were wiped and sprayed with 70% ethanol before placing them into the biosafety cabinet.

2.2.1.1 Recovery of breast cancer cell lines

Adherent breast cancer cell lines were retrieved from liquid nitrogen and thawed at 37°C for 1 minute before being gently resuspended into 5 ml pre-warmed normal cell culture media, namely 1x phenol red-free Dulbecco's Modified Eagle Medium (DMEM) supplemented with 200mM L-glutamine, 2µg/ml insulin and 10% foetal bovine serum (FBS) (see Materials, Table 2.1). Cells were centrifuged at 200 g for 5 minutes and supernatant containing the freezing solvent DMSO (dimethyl sulfoxide) was discarded. Cell pellets were gently resuspended again and transfered to a tissue culture flask and placed in a cell culture incubator equipped with humidity, 5% CO_2/20% O_2 and constant temperature control at 37 °C to allow recovery.

2.2.1.2 Cell culture passage

Cells were routinely maintained in a cell culture incubator equipped with humidity, 5% CO_2/20% O_2 and constant temperature control at 37 ^oC. Once cells reached 80 ~ 90% confluence in a tissue culture flask with 75 cm^2 growth area (T75 tissue culture flask), cells were passaged as follows: (1) culture media was poured off from the tissue culture flask and residue media was removed using a 5 ml serological pipet; (2) 2 ml pre-warmed 0.05% trypsin-EDTA was added to wash the cells; (3) another 2 ml pre-warmed trypsin-EDTA was added, and the flask was placed back into the cell culture incubator for 5 minutes; (4) the flask was gently tapped and inspected for cell detachment; (5) 10 ml pre-warmed culture media was added to quench the trypsin and the cell suspension was transferred into a 15 ml Falcon tube and centrifuged for 5 minutes at 200 g; (6) once the cells had been spun down, supernatant was removed and the cell pellet was resuspended with fresh pre-warmed culture media and transferred into a new T75 flask at a ratio of 1:5 - 1:8 with media change every 2-3 days.

2.2.1.3 Cell freezing down procedure

Cells that had reached ~80% confluence were trypsinized as above (Section 2.2.1.2). Once the cells had been spun down and the supernatant removed, freezing media (10% DMSO in FBS) was used to resuspend the cell pellets. One millilitre cell suspension aliquots were transferred into cryogenic storage vials. The cryovials were placed into an isopropanol chamber and stored at -80 ^oC overnight. The cryovials were kept in a liquid nitrogen tank for long-term storage.

2.2.1.4 Culturing cells in multiwall plates or chamber slides

In experiments where a certain number of cells was required, cells which had grown to ~80% confluence and were still in the exponential phase of growth, were trypsinized and resuspended with pre-warmed culture media. A small aliquot (10 -20 µl) of homogenous cell suspension was mixed with an equal amount of trypan-blue and 10 µl of the mixture was loaded onto a Countess® Cell Counting Chamber Slide and read by the Countess II FL Automated Cell Counter (ThermoFisher Scientific, Australia). The live cell count was recorded for downstream steps. An appropriate amount of cell suspension containing the desired number of cells was transferred to fresh media to achieve the required seeding density. Cells were plated into a cell culture flask/multi-well plate and then placed into a cell culture incubator for the required time period according to the different assays.

2.2.2 RNAi techniques to knockdown p53 isoforms

Two RNA interference (RNAi) techniques were used to specifically knockdown p53 isoforms. RNAi mainly works post-transcriptionally, where the final processed short-interference RNA (siRNA) is generated to target mRNA without a genomic change. Common RNAi methods include siRNA transfection and shRNA (short-hairpin RNA) transduction, with the former being a transient process

and the latter being stable. Transduction is carried out by lentiviral infection, which is more applicable to most cell types, as transfection may be cell line dependent (226).

2.2.2.1 siRNA transfection

siRNAs in Table 2.2 were used to transfect breast cancer cell lines. An optimized seeding density for each cell line was established according to the different assays. For example, for a proliferation assay, a seeding density of 5000-10000 cells/well in a 96-well plate was generally appropriate. For downstream gene expression analysis, 2-3 $x10^5$ cells/well in a 6-well plate were seeded. Cells were cultured under standard cell culture conditions to ~80% confluence before being seeded at the optimized cell density for 24 hours before transfection. siRNAs were diluted with 1x siRNA buffer and serum-reduced media (Opti-MEM) and mixed with Opti-MEM diluted DharmaFECT transfection reagent-1. This mixed solution was then diluted in pre-warmed media to achieve a final concentration of 25 nM siRNA. The original cell culture media was replaced by Opti-MEM and cells were allowed to incubate for at least 24 hours before being harvested for downstream analysis.

2.2.2.2 shRNA transduction

Multiplicity of Infection (MOI) optimization was performed on a panel of cell lines to determine the amount of lentiviral particles for transduction, based on GFP positivity (the lentiviral construct contains a GFP sequence that allows screening of successfully transduced cells). Cells were plated into 6-well plates and the optimized MOI of corresponding shRNAs was used to infect cells. A final concentration of 8 µg/ml Hexadimethrine bromide was added to enhance transduction. Cells were then placed under standard cell culture incubation conditions for 48 hours before changing to fresh complete cell culture media. Cells were allowed to grow for 24-48 hours before 1 µg/ml puromycin was added to the cell culture media to eliminate non-transduced cells. Cells were routinely cultured with puromycin-supplemented media (puro-media). Cells were continually cultured in puro-media and monitored in the IncuCyte live cell imager (Essen, United States), using phase contrast and GFP channels, in order to visualize the GFP positivity. Once GFP signal was present in >90% of the cells, each subline was seeded into a 6-well plate and harvested for mRNA and protein analysis to confirm altered expression.

2.2.3 Analysis of mRNA and protein expression in mammalian cells

2.2.3.1 Semi-quantitative real-time RT-PCR

2.2.3.1.1 Total RNA extraction

All procedures were carried out in a fume hood. Cells were seeded in 6-well plates for transfection/drug treatments for the appropriate amount of time. Media was removed and 400 µl TRIzol reagent was added to each well and mixed by pipeting up and down several times to

homogenize. After 5 minutes incubation at RT, the cell lysate was transferred to a 1.5 mL microcentrifuge tube and mixed with 80 µl chloroform. After 2-3 minutes incubation, samples were centrifuged at 12000 g for 15 minutes at 4°C. The top aqueous phase containing RNA was transferred to a fresh tube and mixed with 200 µl isopropanol. The mixture was incubated at RT for 10 minutes and centrifuged at 12000 g for 10 minutes at 4 °C. The supernatant was discarded and 400 µl 75% ethanol was added to the RNA pellet, vortexed gently and centrifuged at 7500 g for 5 minutes at 4°C. The supernatant was carefully discarded and allowed to air dry for 5-10 minutes in the fume hood. The RNA was rehydrated in 40 µl RNase-free water and incubated at 55 °C for 10 minutes.

2.2.3.1.2 Quantitation of RNA

The RNA yield was determined by the Qubit™ RNA BR (broad range) Assay Kit (ThermoFisher Scientific, Australia). The Qubit RNA BR reagent was diluted 1:200 in Qubit RNA BR buffer to make the working solution, mixed thoroughly and the assay tubes were prepared as follows:

Table 2.4 Qubit RNA BR Assay composition

Volume	standards (µl)	Samples (µl)
Working solution	190	199
Standard 1 and 2	10	
Samples		1
Total	200	200

Standards and samples were vortexed briefly and incubated at RT for 2 minutes before being read on a Qubit 2.0 Fluorometer (ThermoFisher, Australia).

2.2.3.1.3 Reverse Transcription

Five hundred nanograms of total RNA was reverse transcribed to ds cDNA using the High Capacity Reverse Transcription kit with the RNase inhibitor (Life Technologies) according to Table 2.5. Two controls were included to account for any contaminations in the mix, one without MultiScribe Reverse transcriptase and one without RNA.

Table 2.5 Reverse transcription recipe

Components
1 x RT buffer
1 x RT random primers
4 mM dNTP mix
100 Units RNase Inhibitor
250 Units MultiScribe Reverse transcriptase
500 ng RNA
Nuclease-free water to 20 µl

The mixture then underwent the following steps in a thermal cycler (Table 3 2.6):

Table 2.6 Reverse transcription conditions

	Step 1	Step 2	Step 3	Step 4
Temp (°C)	25	37	85	4
Time (min)	10	120	5	-

After reverse transcription, cDNA was diluted to 10 ng/µl with nuclease-free water and was stored at -20 °C.

2.2.3.1.4 Semi-quantitative real-time PCR

TaqMan Gene Expression Assays (Life Technologies) were used for real-time PCR and the principle is illustrated in Figure 2.1A. Each assay has a pair of validated primers and a probe (several nucleotides). The probe was dual-tagged with a fluorochrome (the reporter) on the 5' end, and a quencher molecule consisting of a minor groove binder (MGB) and a non-fluoresescent quencher (NFQ) on the 3' end. Prior to PCR, the reporter transfers the energy to the quencher, namely by fluorescence resonance energy transfer (FRET), and only emits fluorescence once they are separated. No fluorescence is therefore detected prior to the PCR, and once a PCR reaction initiates, primers and the probe anneal to the template while DNA polymerase extends from the primers to the probe, cleaving the reporter from the quencher by the 5' exonuclease activity. As PCR cycles increase, an increasing amount of fluorescence is generated.

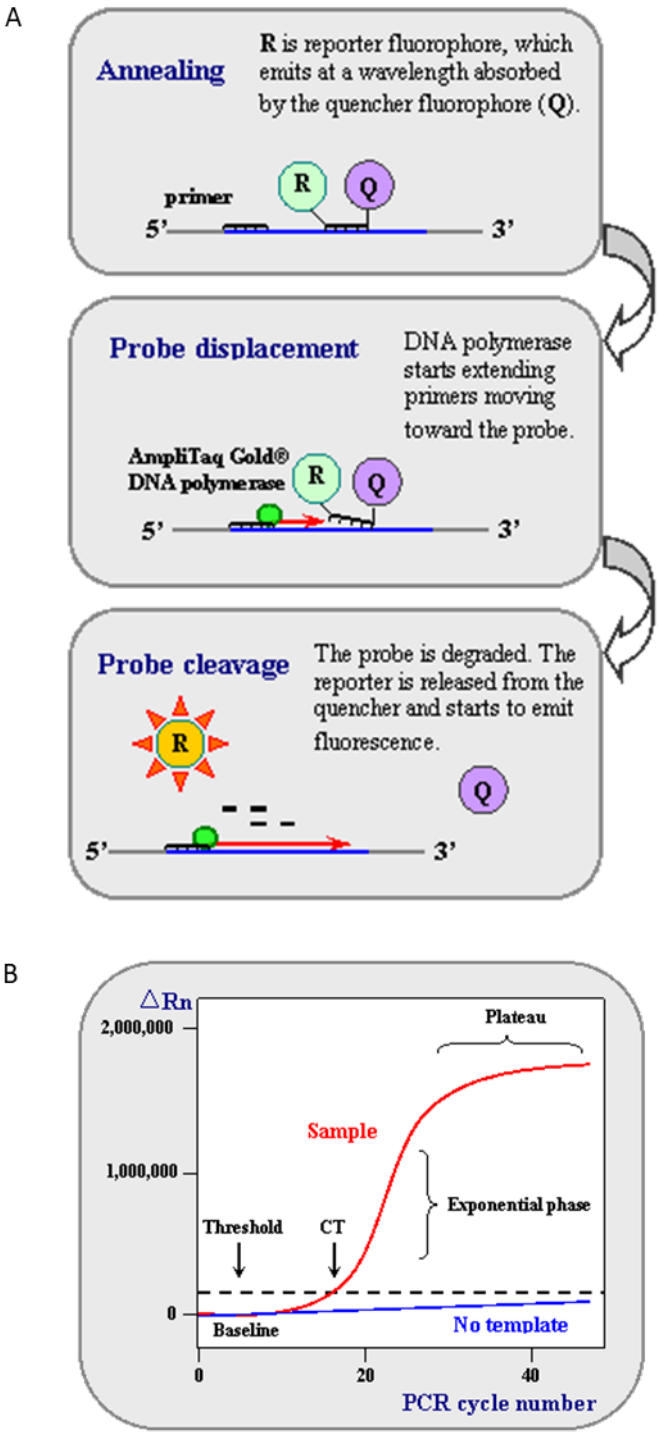

Figure 2.1 The principle of TaqMan gene expression assay and real-time quantitative PCR plot (227).

Briefly, 1 ng cDNA was mixed with 1x Taqman Universal PCR mix (LifeTechnologies), 900 nM Probe/Primer assay mix and brought to a final volume of 10 µl with nuclease-free water. The mixture underwent the following cycles (Table 2.7) in an Applied Biosystem 7500 Real-Time PCR machine (ThermoFisher Scientific, Australia):

Table 2.7 TaqMan Gene Expression Assay PCR condition

50°C for 2 minutes	1 cycle
95°C for 20 seconds	1 cycle
95°C for 3 seconds	40 cycles
60°C for 34 seconds	

Amplification of target genes was quantitated by the fluorescence detectors within the Applied Biosystems 7500 PCR-machine (Life Technologies) as the number of PCR cycles progressed (Figure 2.1B). A threshold was automatically generated by the Applied Biosystems software as 10-times the standard deviation of the average signal between 3-15 cycles, which could be adjusted manually afterwards. A real signal was greater than this threshold and the cycle number when a real signal appeared is the Ct value. Ct values were always read during the = exponentially amplification phase (Figure 2.1). Ct values are therefore more reliable than endpoint measurement of the PCR product.

2.2.3.1.5 Housekeeping genes and normalization

GAPDH and β-microglobulin (B2M) were the two housekeeping genes selected for normalization (228) because of minimal variation in breast cancer samples. Relative expression was calculated using the $2^{-\Delta\Delta Ct}$ method (229).

2.2.3.2 Western blot

2.2.3.2.1 Cell harvesting for protein extraction

Cells were harvested from a 6-well plate as follows: (1a) media was removed if cells were simply seeded or (1b) it was collected and spun at 200g for 5 min at 4°C if the cells were treated with drugs (to collect dead/dying cells). Once the cells were pelleted, the supernatant was discarded. (2) The cell monolayers were washed in twice with 1 ml cold PBS. (3) Fresh 500 µl cold PBS was added and a cellscraper was used to scrape the cells off, following their transfer to a fresh tube (from 1a) or combined with the previously saved cell pellet (1b). (4) The tubes were then centrifuged at 4500 g for 5 minutes at 4°C and the supernatant was discarded. Cell pellets were stored at -80 °C.

2.2.3.2.2 Protein extraction

Sixty microlitres of 1% NP-40 lysis buffer (50 mM Tris-HCl, 150 mM NaCl, 1% NP-40, pH 8.0, 1x Mini cOmplete Protease Inhibitor cocktail tablet per 10 ml) was added to the cell pellets and mixed by pipetting up and down several times or vortexing. Cell lysates were kept on ice for 10 minutes before sonication using the BioRupter sonicator (Diagenode, Belgium) using the following conditions: 30 seconds On, 30 seconds Off, for 3-5 cycles. Cell lysates were then centrifuged at 14000 g for 15 minutes at 4 °C to remove insoluble cell components. The clarified supernatant containing whole protein extract of cells was then transferred to a fresh new tube.

2.2.3.2.3 Determination of protein concentration

The protein concentration was determined using Bio-Rad dye reagent, which is a modified version of the Coomassie G250-based Bradford assay (230). A standard curve was prepared in duplicate using bovine serum albumin (BSA, 1.43 mg/ml) for the range of 0-20 µg per ml supplemented with 1x BioRad dye reagent and 2 µl of 1% NP-40 lysis buffer. Two microliters of protein sample was mixed with 798 µl MilliQ water and 200 µl 1x Bio-Rad dye reagent. Standard mixes and sample mixes were incubated at RT for 5 minutes before reading the absorbance at 595 nm on an Implen NanoPhotometer (München, Germany).

2.2.3.2.4 Sodium dodecyl sulphate polyacrylamide gel electrophoresis (SDS-PAGE)

Protein extracts were separated by electrophoresis on discontinuous acrylamide gels containing SDS, using a modification of the method described by Laemmli (231).

A 1 mm thickness gel was prepared using a 15 cm protein gel apparatus (Bio-Rad Laboratories, Regents Park, NSW, Australia). A resolving gel was prepared using 0.4 M Tris (pH 8.8), 0.1% (w/v) SDS and 6% or 8 or 10% (v/v) acrylamide (for molecular weight >100 kDa or between 50-100 kDa), 0.04% ammonium persulphate (APS) and 0.04% N,N,N',N'-tetramethylethylenediamine (TEMED). A stacking gel was layered on top of the resolving gel and consisted of 0.13 M Tris (pH 6.8), 0.1% (w/v) SDS, 3% (v/v) acrylamide, 0.04% APS and 0.04% TEMED.

10-50 µg of cell lysate was mixed with 1/3 cell lysate volume of 4x sample loading buffer containing bromophenol blue (40% glycerol, 8% SDS, 0.25 M Tris-HCl, pH6.8, 1% Bromophemol blue 0.01 g, 10% beta-mercaptoethanol before use). The samples were heated at 95 °C for 3minutes to denature the proteins, centrifuged and loaded onto the gel. Additionally, 5 µL of Precision Plus Protein™ prestained protein standards (Bio-Rad, Australia) was also loaded onto the gel to allow size determination of the proteins of interest. The protein standards include a mixture of 10 multi-coloured proteins with the different molecular weights (10-250 KDa) and can be detected by fluorescence when excited at appropriate wavelengths. The gel was placed in the reservoir buffer (25 mM Tris, 192 mM glycine, 0.1% SDS) and the samples were electrophoresed at constant volt (80-100 V). Electrophoresis was terminated when the dye front reached the end of the gel. Protein migration was compared to the Precision Plus Protein standards mentioned above.

2.2.3.2.5 Semi-dry Transfer

Proteins within the gel were transferred to a nitrocellulose membrane using the Bio-Rad Trans-Blot Turbo kit and System. Two ion reservoir stacks and a nitrocellulose membrane were merged into 1x Turbo transfer buffer for 5 min and assembled in the following order from bottom to top in a TranBlot Turbo tray: 1 pre-wet stack, 1 pre-wet nitrocellulose membrane, the gel and 1 pre-wet stack. A blot

roller was used to roll over the assembly to displace air bubbles. The Trans-Blot Turbo tray cover was placed into the tray by pressing firmly and turning to lock the tray. The tray was placed back into the Trans-Blot Turbo unit and the transfer condition was set up: 1.3 A, 25 V for 7 minutes. After the transfer, the gel and stacks were removed, and the rainbow markers were visible on the membrane. The membrane was washed twice with 1x PBST (1x PBS supplemented with 0.1% Tween-20) and stained with Ponceau S to visualize the separated proteins before rinsing off the stain with MilliQ water.

2.2.3.2.6 Blocking and blotting

The membrane was blocked by Casein Blocking Buffer (Millennium Science) at RT for 1 hour. The primary antibodies were diluted in blocking buffer (1 µg/ml and 2.5 µg/ml for KJCM1 and KJCA40 respectively) and added to the membrane allowing them to bind with rocking at 4 °C, overnight. The diluted primary antibody was collected to reuse and a 15-minute-wash was performed three times with PBST. Diluted secondary antibodies (1-5 µg/ml) in blocking buffer were added to the membrane and placed on a rocker for at least 1 hour at RT. GAPDH was used as loading control at a concentration of 1 µg/ml diluted in blocking buffer and allowed to bind at RT for 1 hour followed by 1 hour incubation with secondary antibody with 15-minute PBST washes as directed above.

2.2.3.2.7 Quantitation

The wet membrane was placed on an Odyssey CLx fluorescent imager (LI-COR Biosciences, United States) and the 700 and 800 CW channels were selected within the Image Studio Software program. The protein standards and fluorophore-conjugated secondary antibodies can be excited to emit fluorescent signals. Images were taken to record the membrane including the information of the protein standards as well as the proteins of interest detected by corresponding antibodies. The molecular weight can be identified by referring to the protein standards. The integrated software of the Odyssey imager was used to quantify the quantity of the proteins. By applying a rectangle selection over the detected protein bands, the intensity values of proteins of interest were recorded and then normalised to the intensity values of the loading control of the same lane. The relative change was then calculated between samples.

2.2.3.3 Gelatine zymograph to measure the activity of matrix metalloproteinases (MMPs)

Gelatine zymography was used to detect gelatinase enzymes, matrix metalloproteinases (MMPs) specifically in this thesis. Active gelatinases digest gelatine embedded in a polyacrylamide gel. After Coomassie staining, areas of degradation are visible as clear bands against a darkly stained background.

2.2.3.3.1 Collection of conditioned media

Cells were cultured in tissue culture flasks with 75 cm^2 growth area until around 80% confluent, then washed twice with 5 ml DMEM to remove FBS and then cultured for 24 hours in DMEM. Cells secreted MMPs into the media over this time period, namely the conditioned media. The conditioned media was collected and centrifuged at 200 g for 5 minutes at 4 °C to remove the unattached cells. The supernatant was transferred to a 10kDa cut-off centrifugal concentrator (Amicon, Merck Millipore) at 3000 g for 25 minutes at 4 °C.

2.2.3.3.2 Sodium dodecyl sulphate polyacrylamide gel electrophoresis (SDS-PAGE)

Protein concentration of the concentrated conditioned media was measured as described in Section 2.2.3.2 (2 µl of DMEM instead of 2 µl lysis buffer). 50 µg protein was mixed with 1/3 conditioned media volume of 4x native sample loading buffer (250 mM Tris-HCl, pH 6.8; 40% glycerol; 8% SDS; and 0.01% bromophenol blue) and SDS-PAGE with a7.5% acrylamide gel supplemented with 0.1% gelatine was performed with constant 90 V (Table 2.8 and 2.9).

Table 2.8 Migration gel

	1 mini gel
1.5M Tris pH 8.8	1.5 ml
30% Acrylamide	1.5 ml
MilliQ water	1.5 ml
Gelatine (4mg/ml)	1.5 ml
10% SDS	60 µl
10% APS	60 µl
TEMED	7.5 µl

Table 2.9 Stacking gel

	1 mini gel
0.5M Tris pH 6.8	1.25 ml
30% Acrylamide	670 µl
MilliQ water	3.075 ml
10% SDS	50 µl
10% APS	50 µl
TEMED	10 µl

2.2.3.3.3 Gel washing and developing

The gel was washed twice with the gel washing buffer (2% Triton X-100, 50 mM Tris-HCl pH 7.5, 5 mM $CaCl_2$ and 1 µM $ZnCl_2$, 30 minutes per wash) at RT. The gel was then incubated with incubation buffer (1% Triton X-100, 50 mM Tris-HCl, 5 mM $CaCl_2$ and 1 µM $ZnCl_2$) at 37 °C for 5 minutes, before being replaced by fresh and sufficient incubation buffer to incubate at 37 °C overnight with gentle agitation (at least 16 hours).

2.2.3.3.4 Gel staining and destaining

The gel was stained with staining buffer (5% Coomassie Blue R-250, 5% methanol, 10% acetic acid in MilliQ water) at RT for 1 hour until the gel was dark blue. The gel was destained with destaining buffer (10% methanol, 5% acetic acid in MilliQ water) until clear bands were visualized against the dark blue background.

2.2.3.3.5 Quantitation of the activity of MMPs

The gel was scanned with an Odyssey CLx fluorescent imager (LI-COR Corporates) using the 700 CW channel and quantified by ImageJ software (Figure 2.2). Briefly, the image was converted into an 8-bit image in black (background, highest on a grey scale) and white (clear bands where MMPs were activated, lowest on a grey scale). Each lane was selected by the rectangle selection tool and assigned numbers by selecting Analysis, Gels, select First/Next Lane. Plot Lanes was selected from the dropdown menu and a graph was shown including the intensity information of each of the bands along the length of lanes within each lane. The grey scale values decrease when a clear band appears and increases when the clear band ends in each lane. The MMP activity can be read by measuring the area of the inverted peak.

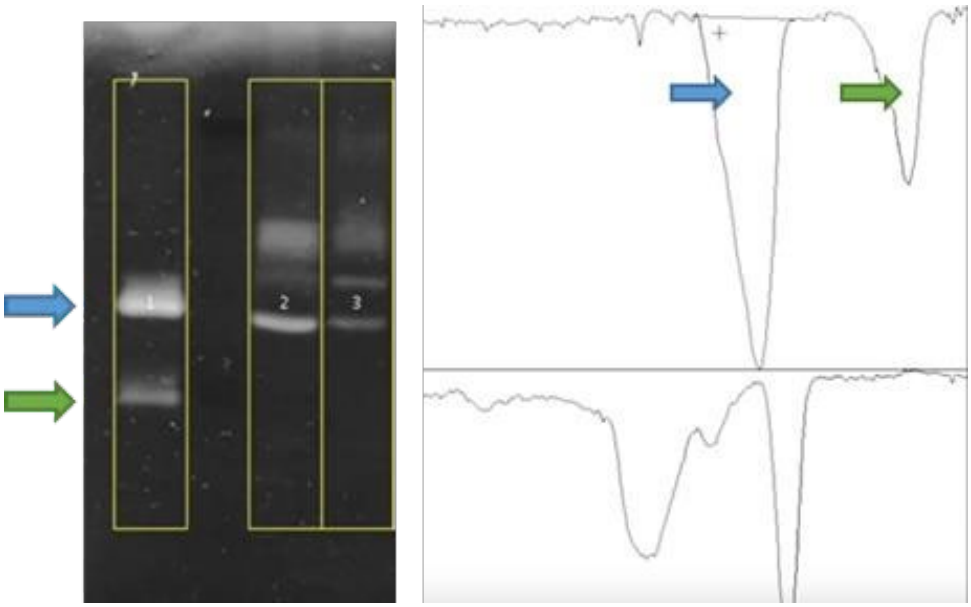

Figure 2.2 Measurement of MMP activity using Image J. The stained and destained gelatine-embedded gel was scanned and converted to 8-bit image in black and white. Black indicates the background and white indicates the clean bands, where active MMP have digested the gelatine. Lanes were selected and plotted on the left (digits indicate lanes selected). MMP activity can be read by the area of the inverted peak. Blue and green arrows indicate the clear bands on the gel and the related measurements (area of inverted peaks) (Image dapted from (232)).

2.2.4 Immunofluorescent staining

Immunofluorescent (IF) staining was performed to (1) visualize the distribution of a target protein via a fluorescent microscope and (2) to quantify the staining intensity of a target protein by applying the

correct masks. Both direct and indirect immunofluorescent staining methods were used in this document on fixed cells. Direct immunofluorescent staining used a single fluorophore-conjugated dye, while indirect immunofluorescent staining used a primary antibody, followed by detection with a secondary fluorophore-conjugated antibody.

2.2.4.1 Cell fixation and permeabilization

Media was carefully removed from cells growing in tissue culture plates or chamber slides without irritating the cells. Formaldehyde (3.7%) diluted in PBS was pre-warmed to 37 °C before being added to the well and incubation at RT for 15-20 minutes in a fume hood (100 µl/well of a 96-well plate and 200 µl/well of a 8-well chamber slide). Fixation solution was removed and cells were washed once with sufficient PBS (200 µl/well of a 96-well plate and 400 µl/well of a 8-well chamber slide).

Triton X-100 (0.1% v/v in PBS) was added to cells (100 µl/well of a 96-well plate and 200 µl/well of a 8-well chamber slide) and incubated at RT for 5 minutes and washed 1x with sufficient PBS.

2.2.4.2 Indirect immunofluorescent staining

2.2.4.2.1 Blocking

3% FBS diluted in PBS was added to cells (100 µl/well of a 96-well plate and 200 µl/well of a 8-well chamber slide) after removal of PBS and incubation at RT for 30 minutes to block non-specific targets. Cells were thoroughly washed by using sufficient PBS and removing PBS completely.

2.2.4.2.2 Primary antibody staining

HECD-1 primary antibody (Abcam, Australia, mouse anti-E-cadherin) was diluted to 10 µg/ml in 3% (w/v) FBS solution before being added to the cells and incubated at RT for at least 1 hour (50 µl/well of a 96-well plate and 100 µl/well of a 8-well chamber slide). Cells were washed three times with 100 µl PBS.

2.2.4.2.3 Secondary antibody staining

Alexa Fluor 594 goat anti-mouse IgG secondary antibody (Thermofisher Scientific) was diluted to 5 µg/ml in 3% (w/v) FBS solution before being added to the cells and incubated at RT, protected from light, for at least 30 minutes (50 µl/well of a 96-well plate and 100 µl/well of a 8-well chamber slide). Cells were thoroughly washed three times with 100 µl PBS. Cells were further stained with DAPI as required (Section 2.2.5.3) and cells then imaged according to Section 2.2.5.4.

2.2.4.3 Direct staining with DAPI

DAPI was used to visualize the nucleus. Fifty microliters/well in a 96-well plate and 100 µl/well in an 8-well chamber slide of 300 nM DAPI staining solution diluted in PBS was added to the cells and incubated at RT, protected from light, for 10 minutes and washed three times with sufficient PBS.

2.2.4.4 Immunofluorescence microscopy and digital imaging

Immunofluorescently stained cells were visualized and analysed using a Cytation 3 (BioTek, Australia) equipped with filters to resolve TXR (545-580nm), FITC (450-480nm) and DAPI (270-380nm) fluorochromes. Images were taken using the DAPI and TXR channels and the Gen5 software then used to process the images and analyse staining intensity by the following steps: (1) primary masks were applied to outline the nuclei (Figure 1, purple); (2) secondary masks were relative to the primary masks, extending to include each entire cell (Figure 2.3, red); and (3) the average staining intensity of each single cell/well was recorded.

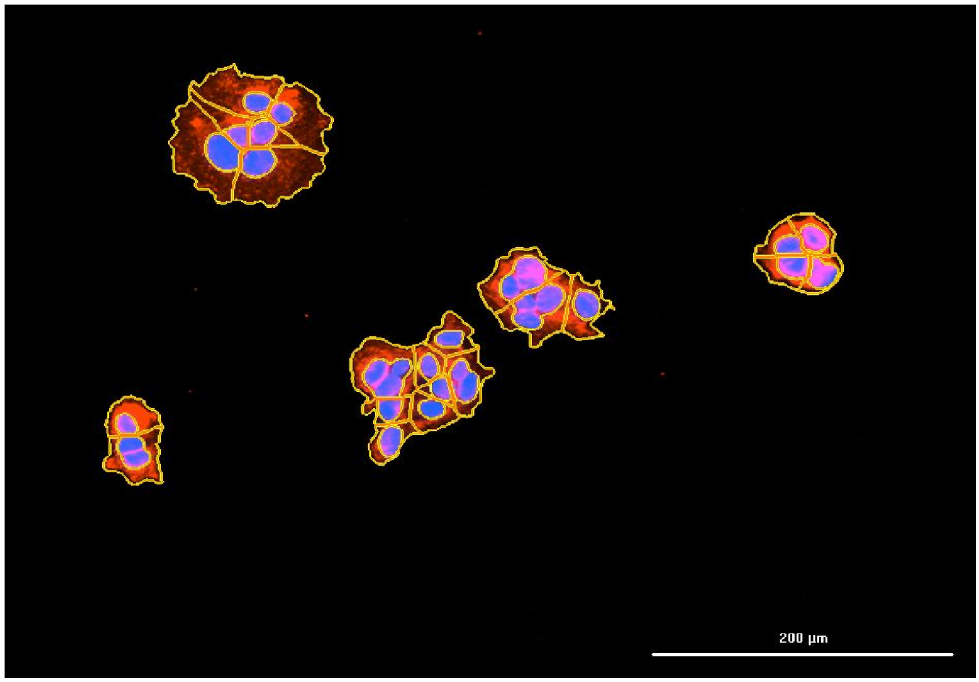

Figure 2.3 Quantification of E-cadherin staining intensity using Cytation 3. Cells stained for E-cadherin using HECD1 antibody (red) and nuclei using DAPI (purple) were imaged and analysed using the Cytation 3. Primary masks were applied to detect nuclei and secondary masks were applied based on the primary masks, therefore E-cadherin staining intensity of each single cell can be calculated.

2.2.5 Proliferation assay

2.2.5.1 Confluence-based proliferation assay

Cells were seeded at a low density (5,000 to 10,000 per well) into 96-well plates in triplicate and placed into an IncuCyte (Essen live-cell imager installed into a standard cell culture incubator). Time-lapse HD images were taken by the IncuCyte and were analysed using the IncuCyte Zoom software by applying

the correct cell masks to calculate the cell confluence with time. Cells were transfected with siRNAs as described previously and returned to the IncuCyte to monitor proliferation.

2.2.5.2 Metabolism-based proliferation assay

An alternative method to 2.2.5.1 was used to measure proliferation of cells not growing as monolayers and/or not having similar morphologies. The CellTiter-Glo® 2.0 assay measures the amount of ATP present in metabolically active cells, which reflects the amount of live cells. The principle is based on the light generation from catalysing the luciferin by luciferase included in CellTiter-Glo reagent and ATP, Mg^{2+} and O_2 present in cells (Figure 2.4). Briefly, cells were plated into 96-well white clear bottom plates in triplicate. Plates were equilibrated at RT for 30 minutes before 100 µl CellTiter Glo 2.0 reagent was added to the plates, scheduled for 24 hours, 48 hours, 72 hours and 96 hours. Plates were placed on an orbital shaker for 2 min to induce cell lysis and read using the Cytation3 (BioTek, United States) luminescent filter.

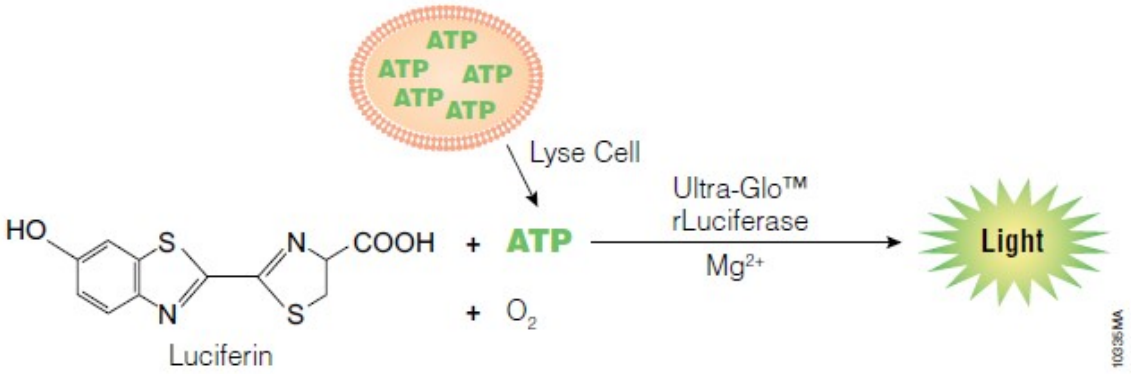

Figure 2.4 Principle of CellTiter-Glo® 2.0 assay. Metabolic active cells have O_2, Mg^{2+} and ATPs, which are important components to catalyse luciferin. The amount of light generated is positively associated with the number of cells. (Image source: Assay manual)

2.2.6 Migration/invasion assay

2.2.6.1 Migration/invasion assay based on wound healing method

This method was published as part of this PhD thesis (233). Briefly, a coated (100 µl/ml matrigel) 96well plate (invasion assay) or a non-coated 96-well plate (migration assay) was seeded with cells in triplicate until confluent and scratched using the 96-well WoundMaker™ (Essen) to generate scratch wounds throughout the plate. Dislodged cell sheets were washed with pre-warmed culture media and fresh media was added (migration assay). Additionally for the invasion assay, matrigel was diluted to 125 µg/ml (234) with cold fresh media, and 50 µl was added to plates before gelation in the standard cell culture incubator for 30 min, followed by topping up with another 50 µl of fresh warm media.

Wounded cells in the plates were placed into the IncuCyte (Essen, United States) and monitored until the wounds had closed (Figure 2.5).

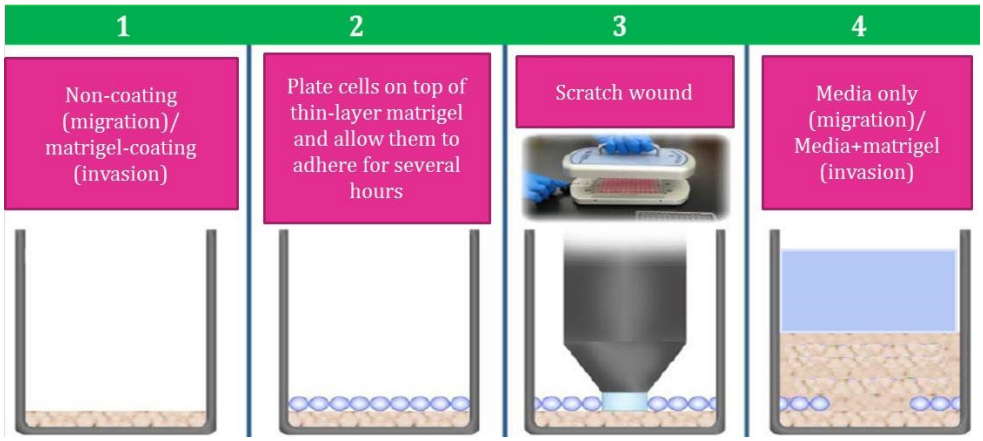

Figure 2.5 Experimental procedures of migration/invasion assay using the WoundMaker.

Collected images were analysed by the integrated wound scratch module of IncuCyte Zoom software. The initial scratch wound was established as a reference to the migration front. Relative wound density was used to quantify the speed of wound closure. It is a background-subtracted algorithm indicated by the following equation.

% Relative wound density = 100 * (w(t) – w(0)) / (c(t) – w(0)); t= at time t, w = density of the wound region, c = density of the cell region (Figure 2.6).

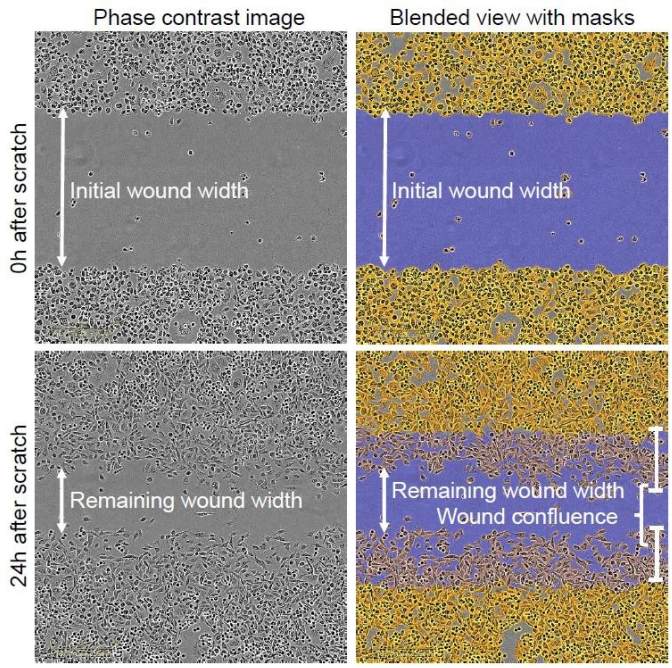

Figure 2.6 Illustration of migration/invasion assays using the WoundMaker and IncuCyte with phase contrast images and blended mode with masks. Blue, scratch wound; yellow, cells surrounding the scratch wound; pink, cells moved into the scratch wound at 24 hours after scratch.

2.2.6.2 Transwell migration/invasion assay

Wound scratch assays require a homogenous cell monolayer, therefore, transwell migration/invasion assay were used in cases where cells could not form a confluent monolayer.

For these assays, 1 x 10^5 cells were resuspended with DMEM supplemented with 0.1% FBS and seeded into transwell inserts (8 µm, polycarbonate membrane, 24-well format). Transwell inserts were uncoated for migration assays and coated with 0.125 µg/ml matrigel overnight for invasion assays. Complete media with 10% FBS media was added to the lower chamber and the transwell inserts were then seated on top to allow migration for 24 hours. Transwells were then fixed with 3.7% formaldehyde for 15 minutes. Non-migrated cells were wiped off from the inserts and crystal violet was used to stain the inserts. Five random views of each insert was chosen to count migrated cells using a 10x objective under a light microscope. An average count of 5 random spots was regarded as the read from one transwell insert. All experiments were repeated three times with duplicates of each subline/condition.

2.2.7 DNA-damaging agents treatment

The DNA-damaging agents, cisplatin (1 mM) and doxorubicin (1 µM), were used to treat cells with altered isoform levels and functional analyses were performed. The working concentrations of the DNA-damaging drugs used in this study were previously determined in our laboratory for the cell lines under study, according to their IC50 value. Sterile Distilled water was used as a vehicle control. Drug treatment times were assay-dependent and details are described in the following sections.

2.2.7.1 Real-time Annexin V apoptosis

Phosphatidylserine binds intracellularly to the plasma membrane of healthy, membrane-intact cells, and apoptotic cells lose the membrane integrity, exposing phosphatidylserine externally and allowing binding of Annexin V dye.

Apoptosis assays were performed on MCF-7 cells using the IncuCyte® Annexin V Red reagent and IncuCyte Red fluorescent channel to measure apoptosis over time. Cells were seeded in triplicate for 24 hours in a 96-well plate. 100 µl of 1 mM cisplatin and 1 µM doxorubicin mixed with diluted Annexin V reagent (1:200) respectively was added to cells and monitored by the IncuCyte using both phase and red fluorescent channels. The annexin V positive counts were normalized to the confluence of the corresponding subline at corresponding time points. Apoptosis assays performed on ZR75-1 cells used Promega RealTime-Glo™ Annexin V Apoptosis Assay. Cells were seeded in triplicate for 24 hours in a 96-well plate. 100 µl of 1 mM cisplatin and 1 µM doxorubicin mixed with diluted Detection Reagent including 1x final concentration of Annexin V-SmBiT, Annexin V-LgBiT and $CaCl_2$. The Cytation 3 was used to read the luminescent values every 24 hours starting from 0 hour. The luminescent value of

each subline at the specified time point was normalised to the untreated cells of the same subline at the same time point.

2.2.7.2 Cell cycle analysis

Propidium iodide (PI) binds to DNA by intercalating between bases, reflecting the content of DNA. DNA content allows cell cycle analysis: 2N DNA in G_0/G_1 phase, 4N DNA in G_2/M phase and S phase in between. Cells were seeded in triplicate in 6-well plates for 24 hours before fresh media supplemented with 1 mM CDDP or 1 µM DOX was added, followed by incubation for 24 hours. Cells were trypsinized and fixed with cold 70% ethanol for 1 hour at 4°C. Fixed cells were washed twice with cold PBS and stained with FxCycle™ PI/RNase Staining Solution for 15 minutes at RT, protected from the light. Data was acquired on FACSCanto™ flow cytometer (BD Biosciences, Australia) including an excitation source of three lasers: blue (488-nm, air-cooled, 20-mW solid state), red (633-nm, 17-mW HeNe), and violet (405-nm, 30-mW solid state). Laser excitation optics illuminate cells and collection optics direct light scatter and fluorescence signals through spectral filters to the detectors. 5000 events were collected for each sample.

Data was analysed using Kaluza™ (Beckman Coulter, United States). The fcs files were imported into Kaluza software. Data was firstly plotted by forward scatter and side scatter and a gate was drawn to remove doublets. Cell counts were plotted against PI staining intensity and gates were drawn to delineate G1, S and G2 cell populations.

2.2.8 HumanGene 1.0 Arrays

2.2.8.1 Breast cancer samples

Breast cancer samples were acquired from the Australian Breast Cancer Tissue Bank. Participation is entirely voluntary and written consent has already been given for the tissue specimens were used from the Australian Breast Cancer Tissue Bank for research purposes. All patients have an adequate understanding of the purpose, risks and potential benefits of the research. The consent to participate is of an unspecified and extended nature. A patient can withdraw at any time without having to give a reason.

Δ40p53 expression levels were measured in 38 ER+ and 16 ER- breast cancer tissues for which gene expression data has been previously published by our group (17, 225), using semi-quantitative realtime PCR. Both groups were separated further into two groups based on the median: high Δ40p53 and low Δ40p53 to identify genes that were differentially regulated by endogenously expressed Δ40p53.

To identify genes that were differentially regulated by endogenously expressed Δ40p53, expression microarray analyses were performed using breast cancer tissues. High Δ40p53 and low Δ40p53 groups were designated on the basis of median Δ40p53 expression as determined previously from a study of 38 ER+ and 16 ER- breast cancer tissues published by our group (17, 225). The HumanGene 1.0 arrays (Affymetrix) have a transcript coverage of 11,000 lncRNAs, 24,000 genes, and 30,000 coding transcripts.

2.2.8.2 RNA extraction and transcripts hybridization

100 ng total RNA of all FFPE samples was amplified (Ovation FFPE WTA kit) and biotinylated (Encore Biotin module) according to the manufacturers' instructions (Nugen, San Carlos, California, United States). The samples were hybridised to Affymetrix HuGene 1.0 and incubated for 17 hours before being washed and stained. The arrays were scanned on an Affymetrix GeneChip Scanner 3000 7G (Affymetrix, United States) and the data was imported to Genomic Suite 6.6 (Partek) and a robust multi-array analysis (RMA) was performed, which included log2 transformation, background correction, quantile normalisation and summarisation of the probe features resulting in a set of expression signal intensities.

2.2.8.3 Data Analysis

Unsupervised hierarchical clustering was performed on genes that were found to be significantly different in the comparison of all IDC vs all NAT samples ($p < 0.5$; fold change > 1.5 or < -1.5). Correction for multiple testing was performed using Benjamini – Hochberg procedure. Gene set enrichment analysis (GSEA) was performed to identify enriched pathways using the Gene List Analysis tool of Panther Classification System.

2.2.9 Illumina EPIC methylation arrays

2.2.9.1 DNA extraction

The Gentra Puregene Tissue Kit (Qiagen, Netherlands) was used to isolate DNA from cell pellets (1 x 10^6 cells/subline) with altered p53 isoform expression following the manufacturers' instructions. DNA was quantitated using the Qubit dsDNA BR Assay Kit according to the manufacturer's instructions (Life Technologies, Australia). Qubit dsDNA BR reagent was diluted 1:200 in Qubit dsDNA BR buffer to make the working solution, mixed thoroughly and the assay tubes prepared as follows:

Table 2.10 Qubit dsDNA BR Assay composition

Volume	standards (µl)	Samples (µl)
Working solution	190	199
Standard 1 and 2	10	
Samples		1
Total	200	200

Standards and samples were vortexed briefly and incubated at RT for 2 minutes before being read on a Qubit 2.0 Fluorometer (ThermoFisher, Australia).

2.2.9.2 Bisulfite conversion

Five hundred nanograms of DNA was diluted to 50 µl and underwent bisulfite conversion using the Zymo EZ DNA Methylation kit following the manufacturer's instructions. DNA was denatured with Dilution Buffer and incubated at 37 °C for 15 minutes before adding the CT Conversion Reagent. The mixture was put in a thermocycler with the following conditions: 40 cycles of incubation firstly at 95 °C for 30 seconds and then 50 °C for 60 minutes, hold at 4 °C. M-binding buffer and the converted DNA was added to Zymo-Spin™ I-96 Binding plate before being spun down at ≥ 3000 g for 5 minutes. The column was washed with M-Washing Buffer and then M-Desulphonation Buffer was added and incubated at RT for 20 minutes. The column was washed twice with M-Washing Buffer and 15 µl MElution Buffer was added. The bisulphite-converted DNA was stored at -80 °C until use.

2.2.9.3 EPIC 850k methylation array

2.2.9.3.1 Denaturation, amplification and precipitation of bisulfite-converted DNA

Bisulfite-converted DNA was denatured with 0.1 N NaOH at RT for 10 minutes before adding RPM to neutralize. Multi-Sample Amplification Master Mix was added to the mixture and incubated at 37 °C for 20-24 hours in an Illumina Hybridization Oven to allow amplification. The amplified products were enzymatically fragmented by Fragmentation solution and incubated on a 37 °C heat block for 1 hour. Precipitation solution and 2-propanol were added, followed by incubation at 4 °C for 30 minutes to precipitate the DNA samples before centrifugation at 3000 g at 4 °C for 20 minutes. The supernatant was removed and the pellet was allowed to dry at RT for 1 hour.

2.2.9.3.2 Rehydration and hybridization to BeadChips

The DNA precipitates were resuspended and incubated at 48 °C for 1 hour, before incubating at 95 °C for 20 minutes to denature. The BeadChips were prepared by assembling the Hyb Chambers with the BeadChip Hyb Chamber gaskets, and adding Humidifying buffer to the hybridisation chamber then closing the Hybridisation Chamber lid to prevent evaporation.

Twenty-six microliters of each DNA sample was loaded onto the BeadChip and placed into the prepared Hybridisation Chamber. The lid was locked and the chamber was placed in an Illumina Hybridization Oven at 48 °C for 16-24 hours.

2.2.9.3.3 Washing, staining and imaging the BeadChips

The BeadChips were washed twice using Preparation buffer 1 and then the flow-through chambers were assembled and placed into the Chamber Rack at 44 °C. The extension reagents (Resuspension, hybridization and wash solution; XStain BeadChip solution 1; XStain BeadChip solution 2; Two-Color Extensio nMaster Mix; 95% formamide/1 mM EDTA and XStain BeadChip solution 3), staining reagents (Superior Two-Color Master Mix, Anti-StainTwo-Color Master Mix) and washing reagents were dispensed following the manufacturer's instructions. The BeadChips were then coated with XC4 and dried in a vacuum desiccator for 50-55 minutes at 675 mm Hg. The BeadChips were imaged using an Illumina iScan system (Illumina, Scoresby, VIC, Australia).

2.2.9.4 Data Analysis

The bisulfite conversion efficiency was checked using Genome Studio (Illumina, Australia). The internal controls present on the beadchips use infinium I probe design and allele-specific single base extension to monitor the conversion efficiency of the bisulfite-treated DNA. All samples were within the range recommended by Illumina.

Data was analysed using the Chip Analysis Methylation Pipeline (ChAMP) developed by Yuan Tian etc. in RStudio (version 1.2.5001) (235). Script is indicated in bold and italic characters. ***Library (ChAMP)*** is used to open ChAMP vignette. The idat files exported from iScan as well a sample sheet (csv format) were loaded into RStudio to read the data (***myload <- champ.load (Arraytype = "EPIC"***). Script (***myLoadpdSlide <- as.factor(myLoadpdSlide***) was used to convert slide numbers to factors for downstream steps. Quality control (***champ.QC (Arraytype = "EPIC"***) was performed to assess whether it is suitable for downstream analysis, and this includes (1) multi-dimensional scaling plot, which displays the similarity of testing samples, (2) β-value distribution and (3) a dendrogram of all samples. Normalisation was performed by the script (***myNorm <- champ.norm(arraytype="EPIC"***)***.***

Significantly differentially methylated probes were identified when $p < 0.05$ using Benjamini-Hochberg adjustment method and the script was as follows:

```
champ.DMP (beta = myNorm,          pheno
= myLoad$pd$Sample_Group,
        adjPVal = 0.05,
adjust.method = "BH",
arraytype = "EPIC").
```

Differentially methylated regions (DMRs) were identified using the Probe lasso method (236), defining that a minimum distance between two DMRs is 1000 bp, minimum DMR size is 50 bp, minimum DMPs in one DMR is 7 and adjusted *p*-value is 0.05. The imported DMRs were annotated with annotated genes. The script is listed as follows.

```
champ.DMR(beta=myNorm,
        pheno=myLoad$pd$Sample_Group,
compare.group="type the names of sample group here"
arraytype="450K",
        method = "Probelasso",
        minProbes=5,
adjPvalDmr=0.05,
        cores=3,
        meanLassoRadius=375,
minDmrSep=1000,
minDmrSize=50,          arraytype
= "EPIC").
```

DMP and DMR results were exported and comparison between isoform-altered sublines to control cells were performed.

Gene enrichment analysis was performed with ChAMP with the following script:

```
champ.GSEA(beta=myNorm,
        DMR=myDMR,
        CpGlist=NULL,
        Genelist=NULL,
        pheno=myLoad$pd$Sample_Group,
method="fisher",
arraytype="450K",          Rplot=TRUE,
adjPval=0.05).
```

The GSEA uses the Exact Test method, which used information downloaded from MSigDB (The Molecular Signatures Database) to perform the Fisher exact test that calculates the enrichment status for each pathway (237).

2.2.10 RNA-seq

RNA-seq was used to identify differentially expressed genes (DEGs) among sublines or conditions, providing information on both genes and gene expression levels. Illumina sequencing chemistry utilises sequencing by synthesis, where during each cycle, a fluorophore-incorporated nucleotide was added and the fluorescent dye was cleaved by polymerase to emit the signal representing the identity of the nucleotide. RNA-seq was performed using NextSeq 500 (Illumina, Scoresby, VIC, Australia). A simplified overview is provided in Figure 2.7.

2.2.10.1 Total RNA extraction, quantitation and quantification

Breast cancer derived sublines were plated into 6-well plates for 24 hours before the culture media was removed. Cells were lysed using TRIzol Reagent and total RNA was extracted as described in 2.2.3.1. Alternative steps were applied when the cells were treated with DNA-damaging agents. Cells

were seeded in 6-well plates and allowed to grow overnight to reach a confluence at about 40-50% confluence. Culture media was replaced by 2 ml fresh culture media supplemented with DOX and cells were treated for 24 hours. Media containing DOX and floating cells potentially damaged by DOX were collected into a 2 ml microcentrifuge and spun at 200 g for 5 minutes at 4 °C before supernatant was removed. Attached cells in the plates were lysed with TRIzol Reagent and transferred into the 2 ml microcentrifuge tubes containing the previously spun-down media, in order to collect all cells from the treatments.

RNA was initially quantitated using the Qubit™ RNA BR Assay kit as described in section 2.2.3.1 before performing quality assessment using the Agilent 4200 Tapestation System and the Aligent High Sensitivity (HS) RNA ScreenTape assay (Agilent, Australia). Briefly, 2 µl RNA sample or HS RNA Ladder was mixed with 1 µl HS RNA Sample Buffer (final concentration 1x), vortexed at 2000 rpm at RT for 1 minute using IKA vortexer (IKA, Germany) and spun down. Samples and ladder were incubated at 72 °C for 3 minutes and placed on ice for 2 minutes. The HS RNA tape and samples were placed into the the Agilent 4200 Tapestation System and the start icon was selected. An RNA integrity number (RIN) was given for each sample. Samples with a RIN ≥7 were used for RNA-seq.

2.2.10.2 Library preparation

The library preparation for 24 samples was performed using the Illumina TruSeq® Stranded mRNA LT Sample Prep Kit. All procedures were performed as per the manufacturer's guide.

2.2.10.2.1 Purify and fragment RNA

600 ng total RNA of each sample was diluted to 50 µl with nuclease-free water. mRNA with a polyA tail was purified twice using poly-T oligo attached magnetic beads (RNA Purification Beads). mRNA was mixed with Fragment, Prime, Finish mix after the second wash. Random hexamers in the Fragment, Prime, Finish Mix were used to reverse transcribe the mRNA to ensure even priming across the transcripts in the next step.

2.2.10.2.2 1st strand cDNA

The fragmented RNA was reverse transcribed into first strand cDNA using random hexamers and SuperScript II Reverse Transcriptase (Thermofisher Scientific, Australia). During this step, the First Strand Synthesis Act D mix prevents DNA-dependent synthesis, allowing RNA-dependent synthesis.

2.2.10.2.3 2nd Strand cDNA synthesis

The complementary strand of the first strand cDNA was synthesized for adaptor ligation, but instead of dTTP, dUTP was incorporated into the synthesis, which cannot be amplified by DNA polymerase, ensuring strand specificity. The end products of this step are blunt-ended cDNA.

2.2.10.2.4 Adenylate 3’ Ends and ligate adapters

A single A-nucleotide was added prior to adapter ligation to the 3’ end of the above blunt-ended cDNA, which was complementary to the T-nucleotide at the 3’ end of the adapters and prevented the ds cDNAs from binding to one another. Twenty-four adapter indices were used for each round of library prep. The adapters were composed of two parts: a sequence complementary to the oligos on the flow cell surface and a sequence complementary to the sequencing primer region that initiates the sequencing.

2.2.10.2.5 Amplification of ds cDNA by PCR and library validation

PCR Primer Cocktail contained adapter specific primers in order to enrich the cDNA products with adapters on both ends of the fragment. cDNA libraries were quantified using Agilent D1000 ScreenTape assay and a ~260 bp cDNA size was expected. cDNA libraries were quantitated using a Qubit BR dsDNA Assay Kit according to Section 2.2.9.1.

2.2.10.2.6 Pool and denature libraries

Twenty-four libraries were diluted to 10 nM and pooled into a microcentrifuge tube. Pooled libraries were further diluted into 4 nM and mixed with equal amounts of 0.2 M NaOH to denature. Denatured libraries were finally diluted to 1.8 pM.

2.2.10.3 Creating a sequencing run using NextSeq

All information was registered in Illumina BaseSpace including sample ID, indices ID and flow cell type (HT, single end, 75 cycle). The NextSeq® 500/550 High Output Kit v2 (75 cycle, up to 400 million reads) was used for the purpose of identifying differentially expressed genes (DEGs). All 24 libraries were pooled together and run on one flow cell included in the kit, therefore, about 15 million reads were obtained for each sample.

1.3 ml of prepared 1.8 pM pooled libraries were loaded onto the Reagent Cartridge. The flow cell, Reagent Cartridge and the buffer Cartridge were loaded onto the NextSeq. The planned run was initiated by logging into BaseSpace on the NextSeq.

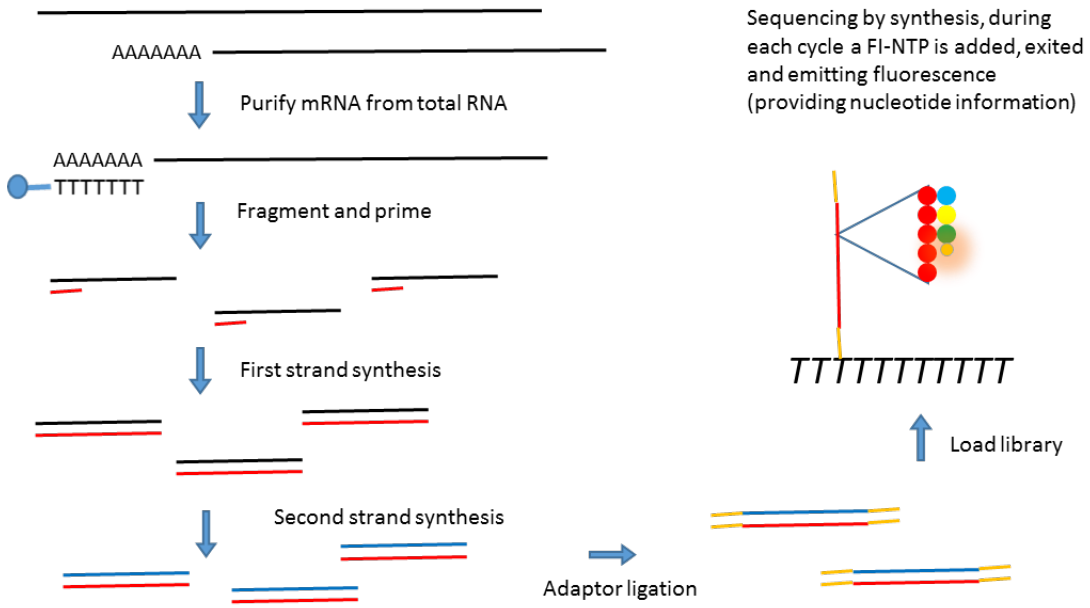

Figure 2.7 Overview of stranded mRNA sequencing. mRNA was purified from total mRNA by oligoT beads and then enzymatically fragmented and primed with random hexamer. First strand cDNA is initially synthesized and followed by second strand synthesis. Sequencing by synthesis is the Illumina sequencing principle. Each cycle, a fluorophore-conjugated NTP is added and excited to reveal the information of each base.

2.2.10.4 Data analysis

FASTQ files were generated by BaseSpace supported by Illumina with indices being trimmed off. The quality control of the raw data was examined using FastQC (Babraham Bioinformatics, United Kingdom). Sequencing data was then mapped to GRCh37 assembly using STAR. Mapped BAM files were imported into SeqMonk (Babraham Bioinformatics, United Kingdom) for quantification. RNA-seq QC of the mapped data was further performed in SeqMonk and libraries with good quality should have a high percentage of the reads falling into genes, a high percentage of the reads of the genes falling into exons, no ribosome RNA reads and no mitochondrial reads. Data was quantified using the integrated RNA-seq pipeline to firstly quantify the raw counts for DESeq2 statistical analysis. DESeq2 is a binomial statistical test, and normalizes for sample size and composition. DESeq2 performs an internal normalisation where the geometric mean was calculated for each gene of all samples and a dispersion value is estimated for each gene by a model fit procedure. Outliers are automatically removed by DESeq2. By performing the RNA-seq pipeline with the selection of log transformation, data was quantified further into $\log_2$RPM (reads per million base pairs) for visualisation and intensity filter. Intensity statistical analysis is a continuous test on the normalised data. DEGs were identified between sublines and the corresponding control sublines at the basal level, and between untreated and DOX-treated conditions of each subline in drug treatment experiments.

Chapter 3

Investigation of the role of Δ40p53 in breast cancer progression

Chapter 3 Investigation of the role of Δ40p53 in breast cancer progression

3.1 Introduction

Somatic *TP53* mutations have been found in over 80% of all human cancer cases, but the mutation rate is not ubiquitous in breast cancer (<25%) (9, 10), indicating other mechanisms are involved in ablating the canonical p53 function. The studies described in this thesis are focused on Δ40p53, an isoform that is truncated from the N-terminus of the full-length p53 and therefore lacks TAD1 (13-16). Previous studies from our laboratory showed that Δ40p53 mRNA expression level was higher in breast tumour samples compared to the matched normal adjacent tissue and that a high Δ40p53/p53 ratio (> 0.7) was significantly associated with worse disease-free survival (HR 2.713, p = 0.1243) (17, 18). These studies suggest that Δ40p53 may be involved in cellular functions that promote the aggressiveness of breast cancer, but functional studies demonstrating this are lacking.

The function of Δ40p53 is poorly understood. As mentioned in Section 1.5.1, Δ40p53 can form a hetero-tetramer with p53 that can stably bind to the consensus DNA sequence within target genes

(14, 16, 159, 160). The TAD1 (lacking in Δ40p53) at the N-terminus is crucial for target gene transactivation, therefore a hetero-tetramer that incorporates Δ40p53 may compromise the canonical p53 function. In this respect, Δ40p53 has been shown to exert a negative impact on p53 functional activities when highly expressed (14, 16). On the other hand, Δ40p53 lacks the HDM2-binding domain and cannot undergo HDM2-mediated degradation, which may protect p53α from degradation. At least regarding apoptosis it has been reported that Δ40p53 has p53α-independent functions (206), however, its functional impact on tumour progression and metastasis-related processes are still unknown.

Tumorigenesis in the breast occurs in the epithelia lining the ducts or lobules (20). Under normal conditions, this structure separates the stroma and the lumen, and exhibits well-arranged morphology owing to cell polarity and cell-cell connections (53). The cell adhesion molecule E-cadherin links cells of the same type through the extracellular domains and binds in the cytoplasm to cytoskeleton, stabilizing the epithelial structure (113). Loss of E-cadherin is a key indicator of the breakdown of the epithelial phenotype and represents one of the complex molecular changes that permit the initial steps of the metastatic cascade through the EMT.

As described in Section 1.2.4 and 1.3.1.4, EMT describes the transition from epithelial phenotype to mesenchymal phenotype, when E-cadherin expression is lost and mesenchymal markers are expressed (51). p53 is involved in metastasis-related processes including EMT and cell migration/invasion, in particular, p53 maintains E-cadherin expression by opposing its negative regulators and this interaction can be direct or indirect (112, 117). Once EMT is achieved, loosened cell-cell connection facilitates cell mobility. Cancer cells then contact with other cell types and the extracellular matrix (ECM) and invade through these barriers by secreting catalytic molecules such as MMPs (57, 58).

Given that previous studies from our laboratory indicate a negative association between Δ40p53/p53 ratio and disease-free survival in breast cancer, it was hypothesised that Δ40p53 may have a functional role in processes that modulate breast cancer progression, such as EMT and cell migration/invasion.

3.2 Aims

The overall aim of the work described in this Chapter is to determine whether Δ40p53 has a role in metastasis-related processes including EMT and cell migration/invasion. Specifically, the aims are:

(1) To characterise genes associated with high endogenous expression of Δ40p53 in breast cancer specimens;

(2) To investigate the function of Δ40p53 in EMT and cell migration/invasion using the cell line models established in Aim 1;

(3) To determine if inhibition of Δ40p53 expression results in molecular changes associated with EMT.

3.3 Approach

Δ40p53 expression levels were measured in 38 ER+ and 16 ER- breast cancer tissues for which gene expression data has been previously published by our group (17, 225), using semi-quantitative realtime PCR and separated into two groups based on the median: high Δ40p53 and low Δ40p53 to identify genes that were differentially regulated by endogenously expressed Δ40p53. Gene set enrichment analysis (GSEA) was performed to identify enriched pathways using Enrichr (developed by the Ma'ayan Lab) using Ontologies libraries (238, 239). Enrichr calculated for adjusted *p*-value, odds ratio and combined scores (which multiplies the log of the p-value computed with the Fisher exact test) and the significantly enriched GO terms and the top 10 GO terms ranked by adjusted *p*-value is listed in this Chapter.

RNAi techniques were utilized to knock down Δ40p53 expression in MCF-7 and ZR75-1 breast cancer cell lines, which have wt p53 and are ER positive (223, 224). This included siRNA transfection and shRNA transduction (refer to Chapter 2 Section 2.2.2 for detailed methodology). Initially, two siRNAs targeting □40p53, one specifically targeting p53α but not □40p53, and one targeting all isoforms were investigated for their knockdown efficiency, before moving to shRNA transduction experiments. The use of different siRNAs was to generate isoform-specific knockdown, thus modifying the Δ40p53/p53α ratio in these cells. Following confirmation that the siRNAs were able to specifically knockdown □40p53 and/or p53α, shRNA experiments were conducted to establish the long-term effects of the knockdown model. These experiments were performed according to Section 2.2.2.2.

After transfection/transduction, selected knockdown cell lines as well as previously established Δ40p53-overexpression MCF-7 cells (stable Δ40p53-overexpression by LeGO vector) (as described in (240)) were subjected to functional analysis, including cell proliferation and cell migration/invasion. Cell migration assessed 2D cell mobility, while cell invasion was used to assess 3D cell mobility. Cell invasion requires not only force to progress, but also the ability to degrade ECM. In these experiments, an ECM barrier was created using Matrigel. Different cell mobility assays were performed based on

the nature of the cells. Wound healing-based migration/invasion assays can only be performed on cells that can form a confluent monolayer, and are ideal to study cell morphology; while transwell migration/invasion assay can be performed with most cell types, but are not suitable to study cell morphology in these assays.

To study the molecular mechanisms of Δ40p53 in regulating EMT, the expression levels of E-cadherin, its negative regulators, as well as a panel of metastasis-related genes were investigated. In addition, RNA-seq was used to identify genes whose expression was associated with altered endogenous Δ40p53 expression level in the stably transduced cell lines.

3.4 Results

3.4.1 Differentially expressed genes in breast cancers with high or low Δ40p53 expression

To determine genes that are affected endogenously in breast cancers with high levels of Δ40p53 expression, 38 ER+ and 16 ER- primary IDCs (Grade 1 and 2) were subjected to HumanGene 1.0 Array (Affymetrix) analysis. Figure 3.1A showed that the relative expression of Δ40p53 was significantly higher in the high Δ40p53 breast cancers compared to the low Δ40p53 breast cancers. Fifty-nine annotated genes (out of 72 transcripts, Table 3.1) were identified as being differentially expressed (> 1.5 fold, $p < 0.05$, FDR 5%) when ER+ breast cancers expressing high levels of Δ40p53 (red branches) were compared to those expressing low Δ40p53 (blue branches), and these genes clearly separated these breast cancers into two distinct groups by hierarchical clustering, indicating distinct gene expression patterns between the two groups (Figure 3.1B). However, the same genes did not show any distinct clusters in ER- breast cancer samples (Figure 3.1C). Additionally, no genes were identified as being differentially expressed (>1.5 fold, $p < 0.05$, FDR 5%) when ER- breast cancers with high levels of Δ40p53 expression were compared to those with low levels of Δ40p53 expression (data not shown).

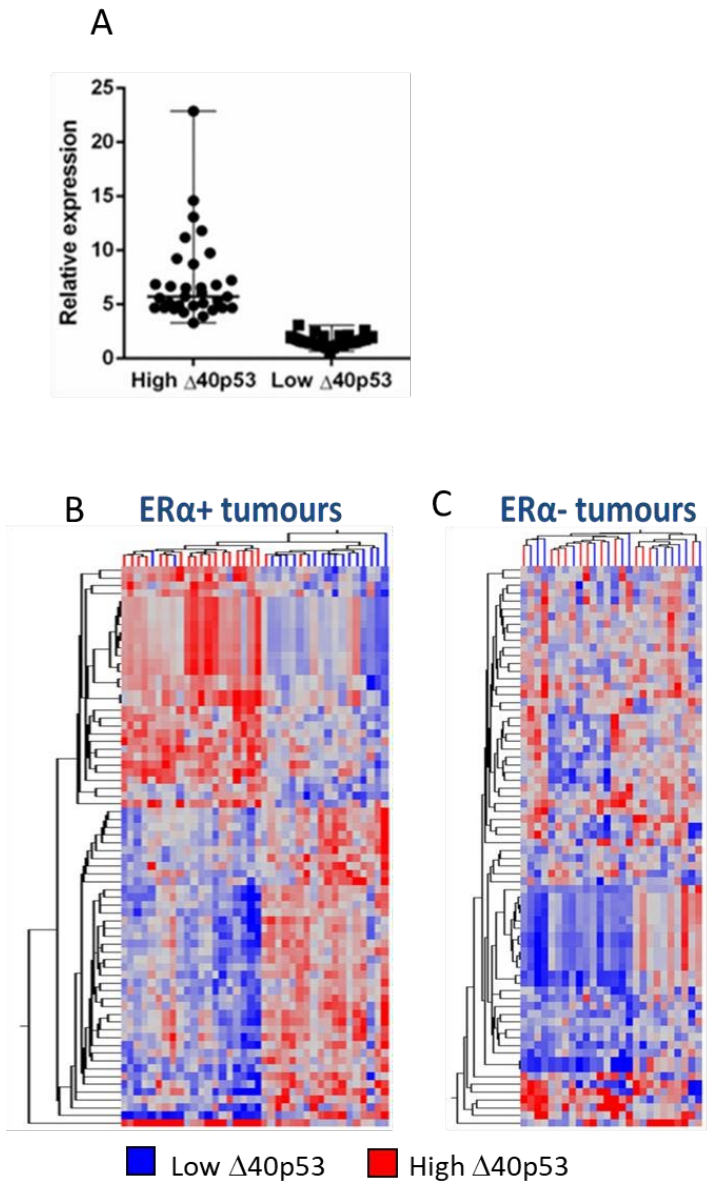

Figure 3.1 High Δ40p53 expression is associated with altered gene expression in 38 ERα+ and 16 ER- breast tumours. A, The expression of 28,869 genes was analysed by gene expression profiling in 38 ER+ and 16 ER- breast tumours expressing high or low Δ40p53 (as determined by qPCR). B, Hierarchical clustering was performed on 72 transcripts found to be differentially expressed in high (red branches) vs low (blue branches) expressing ERα+ tumours. C, the 72 differentially expressed transcripts were hierarchically clustered in ER- breast cancers in high (red) vs low (blue). Similarity in the expression between genes (branches on left) and between samples (branches on top) was measured using Euclidean correlation. Distances between clustered branches represent the average distances. Up-regulated expression is represented by red, down-regulated expression is represented by blue, and equal expression is represented by grey.

Table 3.1 59 annotated differentially expressed genes in ER+ breast cancers.

Gene	Gene description	Regulation by high Δ40p53	FC (abs)	*p*-value
C14orf174	chromosome 14 open reading frame 174	up	1.632	0.006
C5orf30	chromosome 5 open reading frame 30	up	1.580	0.045
CCDC125	coiled-coil domain containing 125	up	1.636	0.014
CYFIP2	cytoplasmic FMR1 interacting protein 2	up	1.673	0.043

DNAJC12	DnaJ (Hsp40) homolog, subfamily C, member 12	up	2.340	0.029
EFHC1	EF-hand domain (C-terminal) containing 1	up	1.528	0.015
FAM174A	family with sequence similarity 174, member A	up	1.515	0.021
GUSBP1	glucuronidase, beta pseudogene 1	up	1.609	0.009
GUSBP3	glucuronidase, beta pseudogene 3	up	1.773	0.008
HSD17B7	hydroxysteroid (17-beta) dehydrogenase 7	up	1.720	0.011
HSD17B7P2	hydroxysteroid (17-beta) dehydrogenase 7 pseudogene 2	up	1.719	0.045
KIF3A	kinesin family member 3A	up	1.511	0.010
KLHDC1	kelch domain containing 1	up	1.518	0.030
MCCC2	methylcrotonoyl-CoA carboxylase 2 (beta)	up	1.618	0.036
MIPOL1	mirror-image polydactyly 1	up	1.632	0.021
NUCB2	nucleobindin 2	up	1.541	0.021
NUDT12	nudix (nucleoside diphosphate linked moiety X)-type motif 12	up	1.592	0.027
SNORA48	small nucleolar RNA, H/ACA box 48	up	1.533	0.012
SSBP2	single-stranded DNA binding protein 2	up	1.578	0.027
ACTN1	actinin, alpha 1	down	1.515	0.016
ARL4C	ADP-ribosylation factor-like 4C	down	1.654	0.005
C1R	complement component 1, r subcomponent	down	1.778	0.022
CCR1	chemokine (C-C motif) receptor 1	down	1.586	0.041
CD4	cluster of differentiation 4	down	1.513	0.034
CERCAM	cerebral endothelial cell adhesion molecule	down	1.525	0.018
CHI3L1	chitinase 3-like 1 (cartilage glycoprotein-39)	down	2.532	0.013
CHST11	carbohydrate (chondroitin 4) sulfotransferase 11	down	1.517	0.019
CNN2	calponin 2	down	1.708	0.013
CTSD	cathepsin D	down	1.760	0.039
CYB5R3	cytochrome b5 reductase 3	down	1.533	0.004
DPP4	dipeptidyl-peptidase 4	down	2.048	0.039
FBLN1	fibulin 1	down	1.648	0.043
FLNA	filamin A, alpha	down	1.688	0.004
FPR1	formyl peptide receptor 1	down	1.513	0.006
GREM1	gremlin 1, cysteine knot superfamily, homolog (Xenopus laevis)	down	1.847	0.027
HAS2	hyaluronan synthase 2	down	1.763	0.030
ITGB2	integrin, beta 2 (complement component 3 receptor 3 and 4 subunit)	down	1.564	0.037
KCNJ15	potassium inwardly-rectifying channel, subfamily J, member 15	down	1.547	0.032
LAPTM5	lysosomal protein transmembrane 5	down	1.612	0.013
LGALS1	lectin, galactoside-binding, soluble, 1	down	1.630	0.013
LILRB4	leukocyte immunoglobulin-like receptor, subfamily B (with TM and ITIM domains), member 4	down	1.572	0.016
LRP1	low density lipoprotein receptor-related protein 1	down	1.790	0.014
MFGE8	milk fat globule-EGF factor 8 protein	down	1.732	0.007
MMP9	matrix metallopeptidase 9 (gelatinase B, 92kDa gelatinase, 92kDa type IV collagenase)	down	1.680	0.038
MYL9	myosin, light chain 9, regulatory	down	1.539	0.032
PCOLCE	procollagen C-endopeptidase enhancer	down	1.778	0.030
PFKFB3	6-phosphofructo-2-kinase/fructose-2,6-biphosphatase 3	down	1.597	0.032
PLAUR	plasminogen activator, urokinase receptor	down	1.554	0.015
PLTP	phospholipid transfer protein	down	1.616	0.027

SERPING1	serpin peptidase inhibitor, clade G (C1 inhibitor), member 1	down	1.504	0.045
SIRPB1	signal-regulatory protein beta 1	down	1.537	0.047
SLC43A3	solute carrier family 43, member 3	down	1.579	0.010
SRPX	sushi-repeat-containing protein, X-linked	down	1.817	0.027
STARD3	StAR-related lipid transfer (START) domain containing 3	down	1.645	0.030
TAGLN	transgelin	down	1.697	0.032
TGM2	transglutaminase 2 (C polypeptide, protein-glutamine-gammaglutamyltransferase)	down	1.630	0.008
TIMP1	TIMP metallopeptidase inhibitor 1	down	1.572	0.013
TMEM45A	transmembrane protein 45A	down	1.867	0.047
TNFRSF21	tumor necrosis factor receptor superfamily, member 21	down	1.744	0.004

Gene set enrichment analysis (GSEA) was performed by Enrichr using GO Biological Process 2018 on the 59 annotated DEGs. The top 10 GO terms ranked by adjusted *p*-value are listed in Table 3.2. The most enriched GO terms are neutrophil mediated immunity (GO:0002446), neutrophil activation involved in immune response (GO:0002283), negative regulation of cellular component movement (GO:0051271), neutrophil degranulation (GO:0043312) and cellular response to cytokine stimulus (GO:0071345); other top enriched GO terms include positive regulation of viral entry into host cell (GO:0046598), regulation of cysteine-type endopeptidase activity involved in apoptotic signaling pathway (GO:2001267), cytokine-mediated signaling pathway (GO:0019221), extracellular matrix organization (GO:0030198) and positive regulation of cholesterol efflux (GO:0010875). These GO terms are mostly associated with immune responses mediated by cytokines, which is not surprising given the fact that the breast cancer specimens includes all cell types including the tumour cells, stroma cells, epithelia as well as the lymphatic cells. These genes also overlap with cellular component movement and extracellular matrix organisation, in line with our hypothesised association between Δ40p53 and cell mobility. In addition, genes involved in these two GO terms were all down-regulated, such as *ACTN1* (actinin 1), *FBLN1* (fibulin 1) and *ITGB2* (integrin 2), indicating endogenously higher level of Δ40p53 is associated with down-regulated cell mobility.

Table 3.2 Gene set enrichment analysis of 69 annotated DEGs in ER+ breast cancers.

GO biological Process Term	P-value	Adjusted P-value	Odds Ratio	Combined Score	Genes
neutrophil mediated immunity (GO:0002446)	1.21E-05	0.01	6.25	70.78	CNN2;CYB5R3;ITGB2;PLAUR;FPR1;CHI3L1;CTSD;MMP9;SIRPB1
neutrophil activation involved in immune response (GO:0002283)	1.13E-05	0.01	6.30	71.78	CNN2;CYB5R3;ITGB2;PLAUR;FPR1;CHI3L1;CTSD;MMP9;SIRPB1
negative regulation of cellular component movement (GO:0051271)	1.08E-05	0.02	67.80	775.20	ACTN1;CCDC125;FBLN1
neutrophil degranulation (GO:0043312)	1.06E-05	0.03	6.36	72.80	CNN2;CYB5R3;ITGB2;PLAUR;FPR1;CHI3L1;CTSD;MMP9;SIRPB1
cellular response to cytokine stimulus (GO:0071345)	7.16E-06	0.04	6.68	79.09	CCR1;CD4;ITGB2;FPR1;CHI3L1;HAS2;TIMP1;MMP9;TNFRSF21
positive regulation of viral entry into host cell (GO:0046598)	2.37E-04	0.20	84.75	707.47	CD4;LGALS1
regulation of cysteine-type endopeptidase activity involved in apoptotic signaling pathway (GO:2001267)	3.04E-04	0.22	75.33	610.08	PLAUR;MMP9
cytokine-mediated signaling pathway (GO:0019221)	5.20E-04	0.24	4.28	32.35	CNN2;CCR1;CD4;ITGB2;FPR1;TIMP1;MMP9;TNFRSF21
extracellular matrix organization (GO:0030198)	5.82E-04	0.25	7.37	54.90	GREM1;ITGB2;HAS2;TIMP1;MMP9
positive regulation of cholesterol efflux (GO:0010875)	6.54E-04	0.26	52.15	382.43	LRP1;PLTP

3.4.2 Molecular inhibition of Δ40p53 expression

3.4.2.1 Endogenous **Δ**40p53 mRNA level can be specifically down-regulated by RNAi

Following the findings above, which showed that high Δ40p53 was associated with cell motility, I designed knockdown breast cancer cell line models to examine the effects of altered ratio of Δ40p53/p53α on cell motility. This was done by RNAi techniques.

Two breast cancer cell lines, which both have wt p53, were tested for knockdown of p53 isoforms using siRNA transfection. In all cell lines, custom-designed siRNA to knockdown p53α (targeted to exon 2/3, the region not included in Δ40p53) was specific (it only altered p53α and not Δ40p53) and effective (67% for ZR75-1 cells and more than 80% for MCF-7) (Figure 3.2A and C). The Δ40p53 siRNAs inhibited the mRNA expression by 34-44% in MCF-7 and 64-66% in ZR75-1 cells (Figure 3.2B and D). The p53α mRNA expression level was unchanged in ZR75-1 when they were transfected with either of the Δ40p53 siRNAs, but was increased in MCF-7 cells by approximately 2-fold (Figure 3.2A and C). The p53 pool siRNA (four pooled siRNAs targeting all p53 isoforms) reduced the expression of p53α to the same extent as p53α specific siRNA and also depleted Δ40p53 levels to the same extent as the Δ40p53 targeting siRNAs (Figure 3.2A and C). Hence, these experiments show that the expression of Δ40p53 or p53Δ can be specifically altered using isoform-specific siRNAs.

Alternative experiments using shRNAs demonstrated that shp53α was able to inhibit the expression of the full-length p53α but not Δ40p53 in both MCF-7 and ZR75-1 cells by approximately 80% and 75% at the mRNA level (Fig 3.2E and G). Transduction with either shΔ40p53 #1 or #2 did not change the expression level of p53α, but shΔ40p53 #1 knocked down Δ40p53 specifically by about 65% in MCF-7 cells and about 55% in ZR75-1 cells, without altering the mRNA level of p53α (Figure 3.2F and H). For this reason shΔ40p53 #2 was not used for further experimentation throughout this thesis and therefore shΔ40p53 #1 is herein referred to as shΔ40p53. Interestingly in the MCF-7 shp53α subline, the Δ40p53 mRNA level was increased by about 1.4 fold compared to the non-targeting control (Figure 3.2F).

The KJCM1 and KJCA40 antibodies directed against p53α and Δ40p53, respectively, were then used to examine protein expression changes in the Δ40p53 overexpressing MCF-7 cells and shRNAmanipulated MCF-7 and ZR75-1 sublines. Compared with control cells there was increased levels of immunoreactivity detected using KJCM1 and KJCA40 in MCF-7-Δ40p53 cells (Fig. 3.2I, left), consistent with the stabilising effects of Δ40p53 on p53α (240). In contrast, there were selectively reduced levels of Δ40p53 (KJCA40) and p53α (KJCM1) in both MCF-7 and ZR75-1 sublines following transduction of isoform-specific shRNAs (Fig. 3.2I, right and 3.2J). Hence, these experiments show that the shRNAs can

specifically alter the expression of Δ40p53 or p53 mRNA and protein and propose these cell lines are appropriate models for investigating the isoform-specific effect of Δ40p53 and p53α in breast cancer.

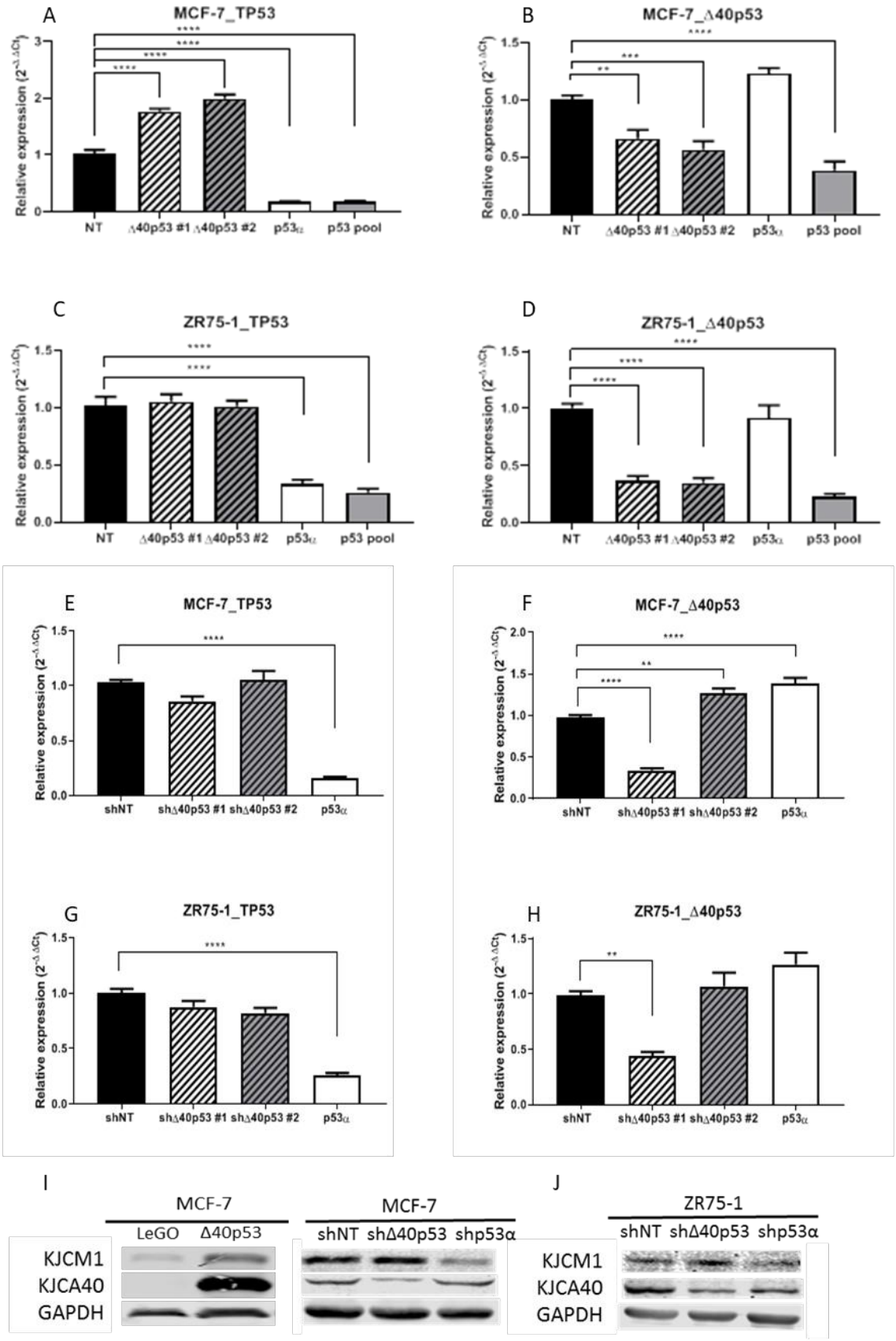

Figure 3.2 Targeted knockdown of Δ40p53 and FLp53 in MCF-7 and ZR75-1 cells using siRNA and shRNA. mRNA expression levels of p53α (A and C) and Δ40p53 (B and D) was measured using semi-quantitative real-time PCR following transfection of MCF-7 (A and B) and ZR75-1 (C and D) cells with 25 nM Δ40p53-siRNA (#1, #2), p53 pool siRNA and custom p53 siRNA

(p53□). All real-time PCR results were normalised to the housekeeping gene, β-microglobulin, and transfection conditions were compared to the non-targeting siRNA control (NT) which was set to 1. mRNA expression levels of p53α (E and G) and Δ40p53 (F and H) were measured using semi-quantitative real-time PCR of transduced MCF-7 (E and F) and ZR75-1 (G and H) cells Δ40p53-shRNA (#1, #2) and custom p53 siRNA (p53□). All real-time PCR results were normalised to the housekeeping gene, β-microglobulin, and transduction conditions were compared to the non-targeting shRNA control (NT) which was set to 1. Relative expression was calculated using 2-ΔΔCt method as described (229). Experiments were repeated three times in triplicate. Results are the mean of three independent experiments and error bars represent the standard error of the mean (SEM). Significant differences are indicated with brackets and stars by one-way ANOVA. * $p < 0.05$, ** $p < 0.01$, **** $p < 0.0001$. The p53α and Δ40p53 protein levels were detected by western blot using KJCM1 (specific for p53α) and KJCA40 (specific for Δ40p53) antibodies respectively in the MCF-7 sublines (I) including the pre-established Δ40p53-overexpression cells (MCF-7-Δ40p53 and its control MCF-7-LeGO) and the shRNA-transduced sublines, as well as the transduced ZR75-1 sublines (J).

3.4.3 Cell morphology was altered in the Δ40p53-shRNA transduced ZR75-1 subline.

Following the successful knockdown of Δ40p53 or p53α by shRNA transduction in MCF-7 and ZR75-1 cell lines, we next determined if the long-term knockdown resulted in overt morphological changes. These results were compared to MCF-7 cells which had been transduced with a Δ40p53overexpression vector (MCF-7-Δ40p53) or empty control vector (MCF-7-LeGO) previously published by our group, with increased p53α and Δ40p53 protein levels in the former (Figure 3.2I) (240).

All MCF-7 sublines displayed identical morphology to the parental MCF-7 cell line despite altered Δ40p53/p53α, and were able to form a confluent monolayer when cultured in tissue culture flasks or plates (Figure 3.3A, B, C, E and G). In contrast, ZR75-1 sublines (Figure 3,3D, F and H), showed distinct morphological differences between the conditions. ZR75-1-shNT cells (Figure 3.3D) had identical morphology to the parental ZR75-1 cells (not shown), but ZR75-1-shΔ40p53 (Figure 3.3F) cells aggregated into islands of cells and lost the ability to form a monolayer. In contrast, ZR75-1-shp53α cells (Figure 3.3H) had a similar morphology to ZR75-1-shNT cells.

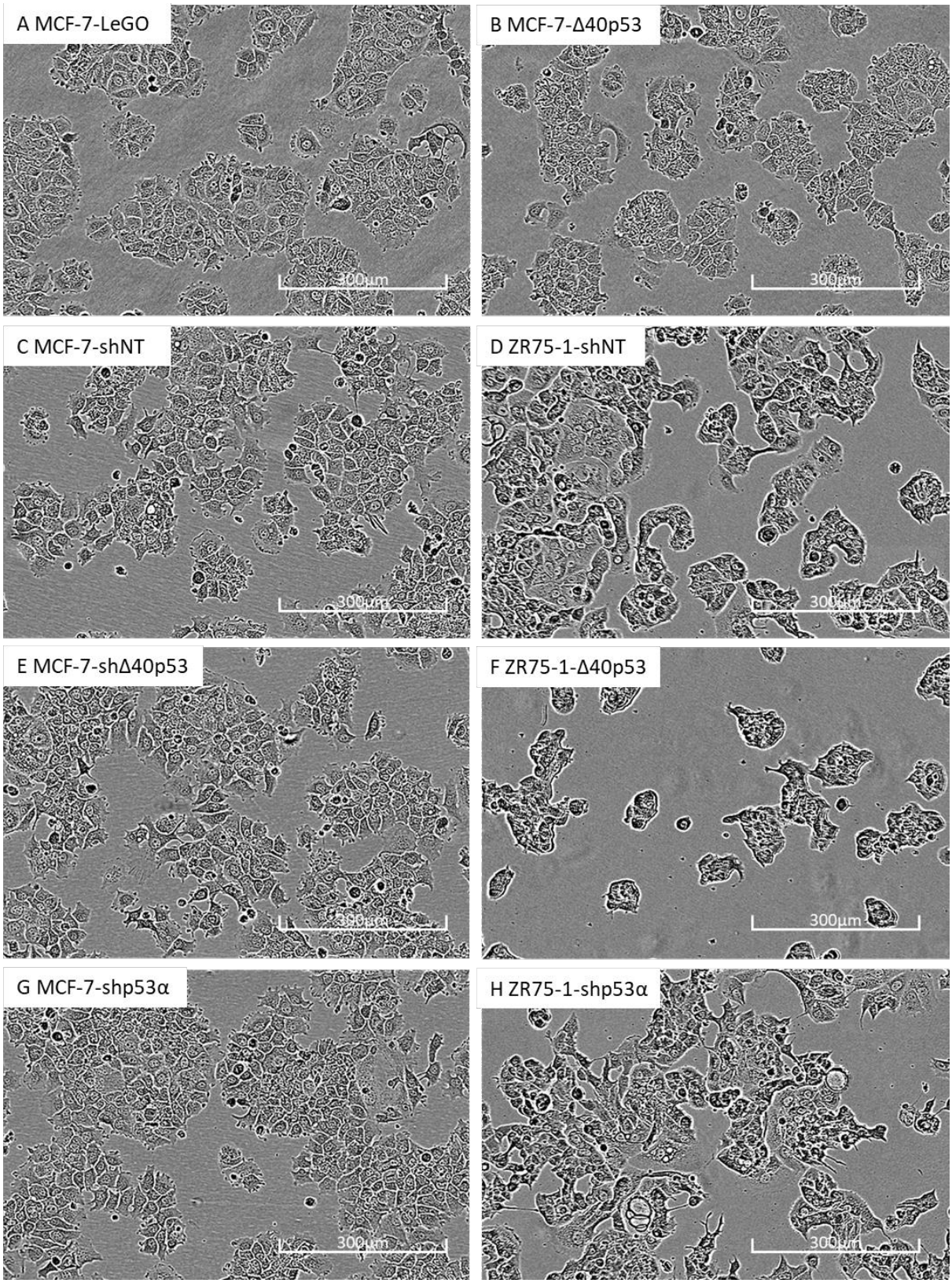

Figure 3.3 Morphology of MCF-7 and ZR75-1 breast cancer cell lines stably transduced to alter the expression levels of Δ40p53 or p53. The top panel shows the high definition image of Δ40p53-overexpression MCF-7 cells (MCF-7-Δ40p53) (B) and its empty vector control (MCF-7-LeGO) (A). C, E and G show stable knockdown of Δ40p53 and p53α in MCF-7 cells as well as the non-targeting control. E, F and H show stable knockdown of Δ40p53 and p53α in ZR75-1 cells as well as the nontargeting control. Images were taken by IncuCyte equipped with 10x objective.

3.4.4 Cell proliferation was differentially altered in MCF-7 and ZR75-1 sublines

3.4.4.1 Cell proliferation was negatively associated with the level of **Δ**40p53 in MCF-7 sublines

Cell proliferation was evaluated by measuring confluence on the IncuCyte live cell imager (233). Images were automatically analysed using confluence masks within the Incucyte software analysis suite (Section 2.2.5.1).

In MCF-7 cells, Δ40p53-overexpression led to reduced cell proliferation compared to the control (Figure 3.4A), while Δ40p53 knockdown led to increased cell proliferation (Figure 3.4B). Similarly, knockdown of p53α in MCF-7 cells led to the most significant increase in cell proliferation, consistent with its role as a tumour suppressor. In comparison, Figure 3.4C showed a similar growth rate between ZR75-1-shNT and ZR75-1-shp53α sublines, but the ZR75-1-shΔ40p53 subline had significantly slower growth rate when compared by the confluence-based assay. However, confluence-based proliferation assays rely on two assumptions: the ability of forming a confluent monolayer and identical morphology. The unique morphologies amongst the ZR75-1 sublines, especially the shΔ40p53 cells which grew in islands of cells (if allowed to grow for an extended length of time) that were not distinguishable under a light microscope may therefore have affected the reading in the confluencebased proliferation assays.

Alternatively to compare cell proliferation between the ZR75-1 sublines, the CellTiter Glo® 2.0 endpoint Assay was used to measure cell proliferation based on cellular metabolism (Section 2.2.5.2) over four time points (24 hours, 48 hours, 72 hours and 96 hours). These individual plates were scanned by the IncuCyte prior to adding CellTiter Glo® 2.0 reagent in order to record the confluence at the corresponding time points (Figure 3.4C). All measurements were normalised to the value at 24 hours within each subline. As shown in Figure 3.4D, the CellTiter Glo® 2.0 luminescence assay indicated that there was no difference in proliferation when metabolism of each subline was measured, indicating no impact of either Δ40p53 or p53α knockdown on ZR75-1 cell proliferation.

The above results showed cell line-dependent results, where Δ40p53 inhibition led to increased cell proliferation in MCF-7 cells but not ZR75-1 cells, even though both cell lines contain wt p53 and are ER positive. Hence, it is likely that the function of Δ40p53 is cell-line dependent.

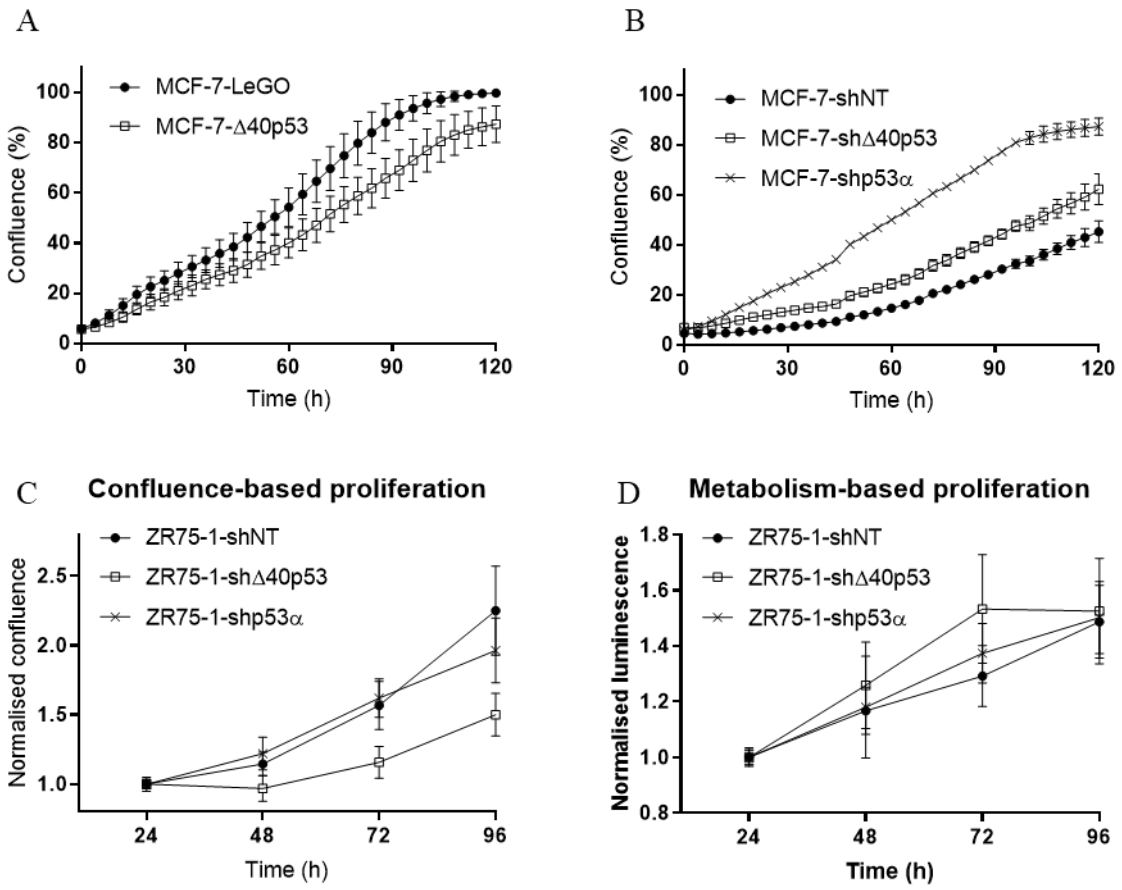

Figure 3.4 Δ40p53 was negatively associated with cell proliferation of MCF-7 sublines, but not of ZR75-1 sublines. Cell proliferation was measured by confluence using the IncuCyte in Δ40p53-overexpression MCF-7 sublines (A) and Δ40p53/p53α knockdown MCF-7 sublines (B). Cell proliferation of ZR75-1 sublines was measured by confluence using the IncuCyte (C) and by metabolism using CellTiter Glo® (D), normalising to the value of 24 hours within each subline. Experiments were repeated three time in triplicate with the error bar representing mean ± SD.

3.4.5 Cell mobility was altered by altered level of **Δ**40p53 or p53**α**

Two types of methods were used to evaluate cell mobility: the scratch wound assay and the Transwell assay, both of which can be modified for analysis of migration (no ECM coating) or invasion (ECM coating). In my previously published JoVE protocol (233), 5 mg/ml ECM gel (Matrigel) was used as the ECM barrier for MDA-MB-231 cells, but ZR75-1 cells were unable to invade through this barrier. Based on the less-invasive nature of the two wt p53 cell lines MCF-7 and ZR75-1, a more diluted Matrigel concentration (125 μg/ml) was applied (234). The scratch wound assay evaluates the speed of cells occupying the cell free area (the wound), and the Transwell assay accounts for the number of cells that have passed through the pores of the membrane.

Initially scratch wound migration/invasion assays were performed on Δ40p53-overxpression MCF-7 cells according to the protocol outlined in Section 2.2.6.1. MCF-7 cells overexpressing Δ40p53 migrated slower compared to the empty vector control MCF-7-LeGO cells, and the wound remained significantly larger than the MCF-7-LeGO cells (compare Figure 3.5B with 3.5C). Both sublines exhibited enlarged cells at the migratory front from the bilateral cell sheets and protruding edges stretching toward the cell-free area, but the extent was less in MCF-7-Δ40p53 cells when compared to MCF-7LeGO cells.

To assess the invasive ability of these sublines, cell invasion assays were performed according to Section 2.2.6.1. MCF-7-Δ40p53 cells had significantly impaired invasion capacity compared to MCF-7LeGO cells (Figure 3.5D) and thus a wider wound (Figure 3.5E and F). Both sublines showed a smaller and tighter migratory front cells in the invasion assay compared to that of the migration assay with no protruding spikes, which are common in invasive cell lines such as MDA-MB-231 (233).

We then sought to assess cell migration/invasion in the shRNA-transduced MCF-7 sublines. However, as previously established in Figure 3.4B, MCF-7 shRNA knockdown Δ40p53 and p53α cells displayed increased proliferation rates over controls and hence, achieving similar confluency that is required for wound-healing assays is difficult and the altered proliferation would be expected to skew the results. Transwell assays were therefore employed according to Section 2.2.6.2 to measure migration and invasion, since these assays readily utilise the same seeding densities and do not require preincubation to establish confluence. As shown in Figure 3.5, the number of cells that migrated (Figure 3.5G) or invaded (Figure 3.5H) through the membrane of the Transwell inserts was not significantly different when MCF-7-shΔ40p53 cells were compared to MCF-7-shNT cells. In contrast, MCF-7-shp53α cells had acquired significantly increased cell mobility, indicating p53α as the major modulator of migration and invasion in MCF-7 cells (Figure 3.5G and H).

We next assessed the effect of Δ40p53 knockdown on migration and invasion in the ZR75-1 cells. Overall, ZR75-1 cells had 10 fold less mobility than MCF-7 cells in migration and invasion assays (compare Figure 3.5G and I, Figure 3.5H and J, respectively). Notably however, consistent with the findings observed in MCF-7 cells, ZR75-1-shp53α cells had significantly increased cell migration and invasion compared to ZR75-1-shNT cells; whilst ZR75-1-shΔ40p53 cells had the least cell mobility, albeit, not significantly changed relative to the shNT control cells (Figure 3.5I and J).

Thus, knockdown of p53α resulted in significant increased cell migration and invasion in both MCF-7 and ZR75-1 cells, demonstrating a dominant role. In contrast, Δ40p53-overexpression led to reduced cell mobility while Δ40p53 knockdown had no significant effect on MCF-7 and ZR75-1 cell lines.

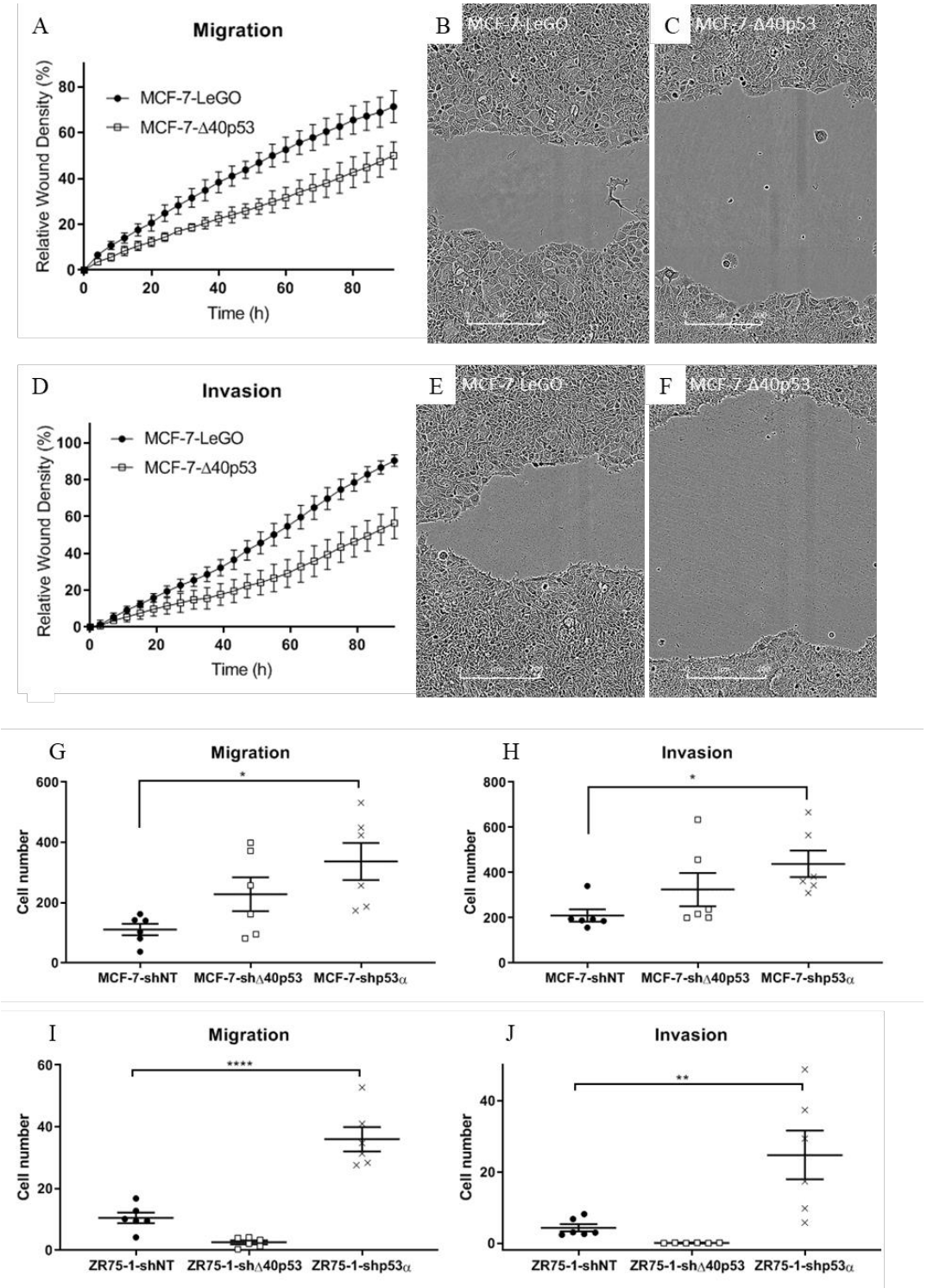

Figure 3.5 Altered Δ40p53 or p53α led to altered cell migration and invasion in MCF-7 and ZR75-1 cells. The metric Relative Wound Density was used to quantitate cell migration (A) and invasion (B). B and C, at 72 hours after wounds had been made in the migration assay, the remaining wound width of MCF-7-Δ40p53 cells was larger than that of MCF-7-LeGO cells and the migratory front of MCF-7-Δ40p53 cells appeared less active than that of MCF-7-LeGO cells. E and F, at 72 hours after wounds had been made in the invasion assay, MCF-7-Δ40p53 cells showed impaired invasion (E) compared to MCF-7-LeGO cells (F). Experiments were repeated three times in triplicate. Representative results and images are shown. In MCF-7 cells, transwell migration (G) and invasion (H) showed no significant increase in cell mobility when Δ40p53 was knocked down but increased cell mobility when p53α was knocked down. In ZR75-1 cells, transwell migration (I) and invasion (J) showed no significant increase in cell mobility when Δ40p53 was knocked down but increased cell mobility when p53α was knocked down. Results are the mean of three independent experiments, and error bars represent the standard error of the mean (SEM).
Experiments were repeated three times in triplicate. Significant differences are indicated with brackets and stars by one-way

ANOVA. * $p < 0.05$, ** $p < 0.01$, **** $p < 0.0001$.

3.4.6 Altered isoform levels were not significantly associated with MMP activity

As anticipated from prior studies (105), knock down of p53α resulted in enhanced invasiveness of sublines derived from MCF-7 and ZR75-1 cells, whereas knockdown of Δ40p53 had limited effects. A further aspect of cell invasion *in vivo* involves remodelling the microenvironment. For cancer cells to be able to penetrate into the surrounding tissue, i.e. lymphatic and/or blood systems, they must degrade the extracellular matrix, commonly by secreting MMPs. Gelatine zymograph was used to visualize and quantitate MMPs secreted by cancer cells (see Section 2.2.3.3 for further details on the method). The gel was incubated with incubation buffer which enables the gelatinase reaction and then stained with G250 Coomassie blue. Active MMPs can digest the gelatine, leaving clear bands which can be used to identity specific MMPs on the basis of electrophoretic mobility and their activities on the basis of the size of the cleared areas. As shown in Figure 3.6A, all sublines showed pro-MMP9, active MMP9, pro-MMP2 and active MMP2 activities, of which active-MMP2 was the most abundant. In both MCF-7 and ZR75-1 sublines, no statistically significant changes occurred in the MMP secretome after Δ40p53 or p53α knockdown.

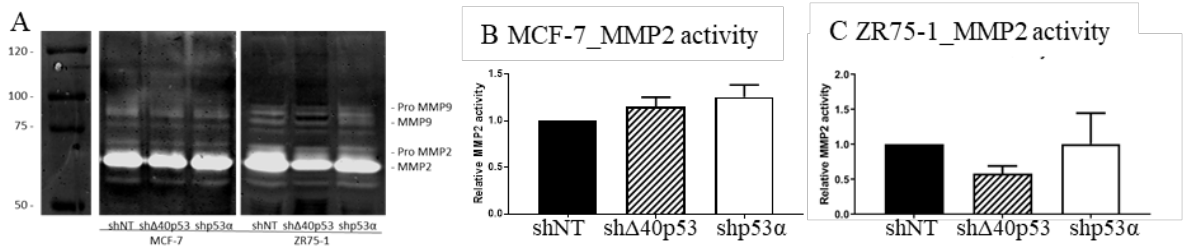

Figure 3.6 **The activities of MMPs were measured using gelatine zymography.** A, MMP profiles of MCF-7 (left) and ZR75-1 (right) sublines are shown by gelatine zymograph, where the area of the clear bands indicates the activity of corresponding MMPs. The activity of active-MMP2 was quantified using Image J of MCF-7 sublines (C) and ZR75-1 sublines (D). Results are the mean of three independent experiments and the error bars are the standard error of the mean (SEM). No significant difference was detected by one-way ANOVA.

3.4.7 E-cadherin expression was altered by **Δ**40p53 or p53**α**

As loss of E-cadherin (encoded by the *CDH1* gene) is the hallmark of EMT and p53 has a role in regulating E-cadherin (Section 1.3.1.4), we first investigated if altering expression of the Δ40p53 isoform had an effect on E-cadherin mRNA and protein expression. Western blotting was initially used to detect E-cadherin protein expression, but multiple non-specific bands were detected (data not shown). This might have resulted from dissociation of E-cadherin extracellular and intracellular domains during harvesting using trypsin and lysis. Alternatively, indirect immunofluorescent staining (Section 2.2.4) was used to detect quantitated E-cadherin levels based on the average staining intensity of each cell (Figure 3.7G-N).

Using this approach, Δ40p53-overexpression in MCF-7 cells was associated with significantly elevated E-cadherin expression at the mRNA and protein levels (Figure 3.7A and D), but Δ40p53 knockdown did not result in altered E-cadherin mRNA and protein levels (Figure 3.7B and E). Knockdown of p53α in MCF-7 cells was associated with a small but significant reduction (~20%) of E-cadherin mRNA expression (Figure 3.7B) and a small reduction in protein expression (albeit not significant) (Figure 3.7E). Knockdown of Δ40p53 in ZR75-1 cells resulted in a significant increase (1.5 fold) in E-cadherin expression at the mRNA and protein levels, but intriguingly, knockdown of p53α also resulted in 1.5fold increased E-cadherin protein expression (Figure 3.7C and F). Hence, the effect of altered Δ40p53 and p53 expression on E-cadherin was not consistent, suggesting cell-line dependent effects.

Next, we examined the effect of altered expression of the Δ40p53 isoform on the mRNA levels of Ecadherin negative regulators Snail, Slug, Zeb1 and the EMT marker vimentin, encoded by *SNAI1, SNAI2, ZEB1* and *VIM* respectively. These markers had overall lower expression in MCF-7-Δ40p53 cells than in MCF-7-LeGO cells with the exception of *ZEB1* (Figure 3.8A, D, G and J), indicating a weaker suppression on E-cadherin, thus enhancing E-cadherin up-regulation in MCF-7-Δ40p53 cells consistent with the results of Figure 3.7A and D. These markers were not differentially expressed when knocking down Δ40p53 or p53α in MCF-7 cells, with the exception of elevated expression of the mesenchymal marker *VIM* in MCF-7-shp53α transduced cells (Figure 3.8B, E, H and K).

SNAI2 and *VIM* gene expression levels were significantly down-regulated in ZR75-1-shΔ40p53 transduced cells, indicating a less mesenchymal phenotype, and supporting the fact that these cells were less migratory and expressed higher levels of E-cadherin (Figure 3.8F and L). In contrast to our hypothesis, *SNAI2* and *VIM* gene expression levels in ZR75-1-shp53α cells were significantly downregulated as well, even though the reduction was not as obvious as that of ZR75-1-shΔ40p53 (Figure
3.8C, F, I and L).

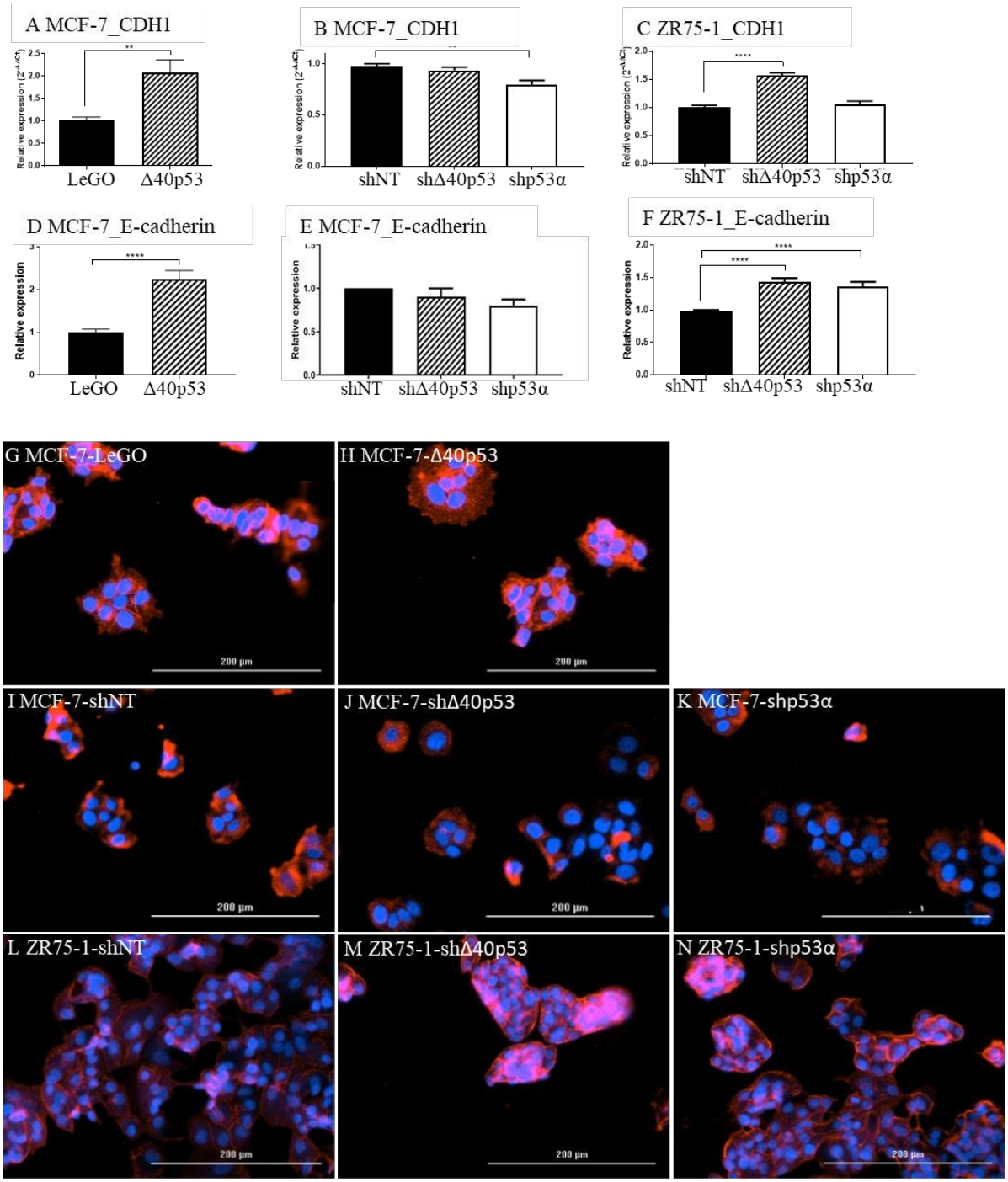

Figure 3.7 Altered E-cadherin expression in MCF-7 and ZR75-1 sublines. A-C, E-cadherin (encoded by CDH1 gene) mRNA level was quantified using semi-quantitative real-time PCR and normalized to the house-keeping gene β2-microglobulin in MCF-7 and ZR75-1 sublines. D-F, E-cadherin protein level was quantified using immunofluorescent staining. Experiments were repeated three times in triplicate and results are the mean of three independent experiments and error bars represent the standard error of the mean (SEM). Significant differences are indicated with brackets and stars by student t-test (2 groups) or one-way ANOVA (three groups). * $p < 0.05$, ** $p < 0.01$, **** $p < 0.0001$. G-N, representative images of immunofluorescent staining of E-cadherin (red) and nuclei (DAPI, purple). Images were captured using Cytation 3 equipped with a 10x objective and with the same settings including excitation, exposure time and camera gain.

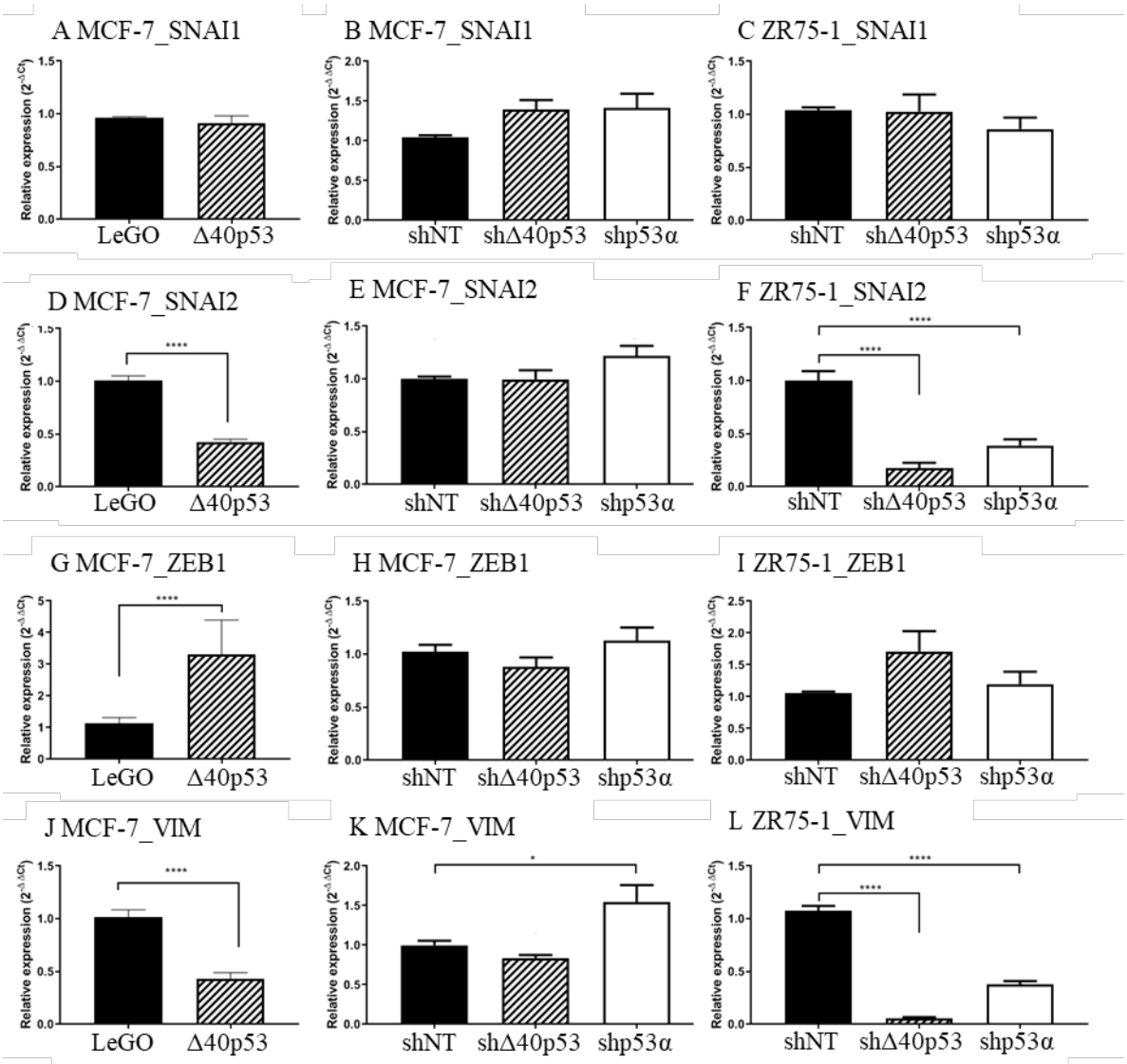

Figure 3.8 mRNA level of the negative regulators of E-cadherin and a mesenchymal marker in MCF-7 and ZR75-1 sublines. mRNA expression levels of *SNAI1* (A - C), *SNAI2* (B - D), *ZEB1* (G – I) and *VIM* (J – L) were measured using semi-quantitative real-time PCR in MCF-7 cells overexpressing Δ40p53 (A, D, G and J) or transduction of shRNA to Δ40p53/p53 in MCF-7 cells (B, E, H and K) and in ZR75-1 cells (C, F, I and L). Results were normalised to the housekeeping gene, β2-microglobulin, and compared to the corresponsive control (empty vector LeGO or shNT cells). Relative expression was calculated using 2-ΔΔCt method as described (229). Experiments were repeated three times in triplicate. Results are the mean of three independent experiments and error bars represent the standard error of the mean (SEM). Significant differences are indicated with brackets and stars by t-test or one-way ANOVA. * $p < 0.05$, ** $p < 0.01$, **** $p < 0.0001$.

3.4.8 Characterization of molecular profiles of MCF-7 and ZR75-1 sublines

To investigate the inconsistencies observed between MCF-7 and ZR75-1 sublines when Δ40p53 was knocked down in functional assays, we used RNA-seq to determine the molecular profiles of these sublines and identify reasons for these differences. Analysis of mRNA expression profiles showed that MCF-7 and ZR75-1 derived sublines were distinct in hierarchical cluster analysis and that theoverexpression and knockdown sublines of MCF-7 also formed separate clusters (Fig 3.9A). We next determined which genes were differentially expressed at the basal level when Δ40p53 and p53 expression were modulated. Figure 3.9B-E show the heatmaps of the hierarchical clustering of

differentially expressed genes (DEGs) when comparing the isoform-overexpression/knockdown sublines to their control sublines. One hundred DEGs were identified when comparing MCF-7-Δ40p53 to MCF-7-LeGO cells (Figure 3.9B). The MCF-7 knockdown experimental groups had less DEGs than the Δ40p53 overexpressing cell line (21 for Δ40p53-shRNA and 36 for p53α-shRNA) when they were compared to the MCF-7-shNT cells (Figure 3.9C and D). The ZR75-1 knockdown experimental groups had a much higher number of DEGs than the MCF-7 cell lines (201 for Δ40p53-shRNA and 104 for p53α-shRNA) when compared to ZR75-1-shNT cells (Figure 3.9D and E), indicating that isoform changes induced more diverse changes in ZR75-1. This was also reflected in Figure 3.9A, as the length of the branches illustrates the similarity between the groups and ZR75-1-shΔ40p53 are clearly separated from both shp53α and shNT cells. Additionally, this also suggests that endogenous Δ40p53 regulates a similar number of transcripts as p53α in MCF-7 cells, but almost double the number of transcripts when compared to p53α in ZR75-1 cells.

We next attempted to identify common DEGs within the different comparison groups and DEGs that were unique to each of the sublines (Figure 3.9G-J), which are shown in Table 3.3 with gene symbols and $\log_2$FC, where FC is the fold change of normalized gene expression. A $\log_2$FC = 0.58 reflects a fold change of 1.5 and a $\log_2$FC = 1 reflects a fold change of 2.

Initially, we asked whether the same targets were regulated by p53 and Δ40p53. There was very little overlap in the number of targets that were regulated endogenously by both p53 and Δ40p53 in either of the cell lines (three in MCF-7 and 25 in ZR75-1) (Figure 3.9G and H, Table 3.3), indicating that knocking down of Δ40p53 or p53α at the basal level had regulated a different set of genes. The three common DEGs were all down-regulated by Δ40p53 or p53α knockdown in MCF-7 cells and they are *OR10J1* (Olfactory receptor 10J1), *ABCC11* (ATP-binding cassette transporter sub-family C member 11) and *MARCKS* (Myristoylated Alanine Rich Protein Kinase C Substrate) ($\log_2$FC between -1.5 ~ -4), all encoding for membrane proteins and among which the first two genes are odour-associated and the last one is associated with cytoskeleton. Twenty-five DEGs were identified in ZR75-1, and there was no overlap with the three DEGs identified in MCF-7 cells. Nine out of these 25 DEGs were downregulated by Δ40p53 or p53α knockdown and five out of these 25 DEGs (light blue shading, Table 3.3) were up-regulated by knockdown of either isoform. These genes may require both isoforms to maintain or suppress their gene expression, therefore knockdown of either led to down-regulation or up-regulation compared to shNT cells. Several of these genes including *TFF1* (trefoil factor 1), *SCGB1A* (secretoglobin family 1A member 1) and *ACACB* (Acetyl-CoA Carboxylase Beta) are involved in regulation of metabolism. One DEG, namely *CEL* was up-regulated in ZR75-1-shΔ40p53 and downregulated in ZR75-1-shp53α (shaded in dark grey in Table 3.3). The other 10 DEGs were downregulated by knockdown of Δ40p53 and up-regulated by knockdown of p53α (shaded grey in

Table 3.3). Surprisingly, a number of tumour suppressor genes were down-regulated by Δ40p53-knockdown and up-regulated by p53α-knockdown, and these including *DLC1* (DLC1 Rho GTPase Activating Protein), *SCUBE2* (Signal Peptide, CUB Domain and EGF Like Domain Containing 2), *SLFN11* (schlafen family member 11) and *HSPB8* (heat shock protein 8). Two movement-restraining genes were downregulated by Δ40p53 and up-regulated by p53α and these including *GJA1* (Gap Junction Protein Alpha 1) and *TUBB3* (Tubulin Beta 3). GSEA generally applies to gene sets containing 25-500 genes to rule out invalid normalization in the analysis (241). Therefore, gene sets that fall out of the range will not be as accurate. The 25 DEGs did not have significantly enriched GO Biological Process terms based on the adjusted *p*-value.

We next went on to determine what genes were regulated independently by Δ40p53 or p53. In MCF7 cells, 18 genes were regulated independently by Δ40p53 endogenously and four of these (*COL3A1, PEG10, SERPINA3, SLITRK6*) were also regulated when Δ40p53 was overexpressed (Figure 3.9G). *COL3A1* (collagen, type III, alpha 1) was up-regulated when Δ40p53 was either overexpressed or knocked down; and *PEG10* (paternally expressed 10) and *SERPINA3* (serpin peptidase inhibitor, clade A, member 3) were down-regulated when Δ40p53 was either overexpressed or knocked down. *SLITRK6* (SLIT and NTRK-like family, member 6) was up-regulated ($log_2FC = 3.78$) in cell lines overexpressing Δ40p53 and down-regulated ($log_2FC = -3.67$) when Δ40p53 was knocked down compared to the corresponding control cells. Thirty-three genes were regulated independently by p53α endogenously and four of these *(TMEM64, TRGC1, TP53, PLS3*) were also regulated when Δ40p53 was overexpressed (Figure 3.9G). *TMEM64* (transmembrane protein 64) was down-regulated when Δ40p53 was overexpressed or p53α was knocked down. *TRGC1* (T cell receptor gamma constant 1) was down-regulated by overexpressing Δ40p53 and down-regulated by knocking down p53α. Both *TP53* and *PLS3* (plastin 3) were up-regulated by overexpressing Δ40p53 and down-regulated by knocking down p53α. Only one common DEG (*MARCKS*) was identified when Δ40p53 or p53α level was altered in MCF-7 cells (Figure 3.9G). MARCKS was up-regulated in MCF-7-Δ40p53 sublines ($log_2FC = 2.31$), however it was down-regulated in both MCF-7-shΔ40p53 and MCF-7-shp53α ($log_2FC = -1.67$ and -2.05 respectively).

From Figure 3.9G, 14, 29 and 91 DEGs were regulated independently by Δ40p53-knockdown, p53αknockdown and Δ40p53-overexpression respectively in MCF-7 cells. Knocking down of either isoform did not introduce a great difference to the basal gene expression of MCF-7 cells, which is in line with the fact that EMT was not greatly affected at the basal level in MCF-7 cells. Even though only a limited number of genes were affected independently through knockdown of either isoform at the basal level, the number of DEGs following p53α-knockdown was double the number of DEGs following Δ40p53knockdown, indicating that endogenously, Δ40p53 has little impact on MCF-7 cells, which explains the little change on EMT by Δ40p53-knockdown. Of importance, there were a number of

genes that were regulated whose function was consistent with the known roles of p53; there were growth factors down-regulated in MCF-7-shΔ40p53 cells, *BMP2* (bone morphogenetic protein 2. Log_2FC = -3), *GRB14* (growth factor receptor-bound protein 14, Log_2FC = -1.58) and *PTGER4* (prostaglandin E Receptor 4, log_2FC = -2.88) for example, and interestingly some proliferation-stimulating genes like *BMP7* (bone morphogenetic protein 7) and *MUCL1* (mucin-like 1) were up-regulated (Log_2FC 1.12 and 1.63 respectively) in MCF-7-shp53α cells. This partially explains the significantly accelerated proliferation of MCF-7-shp53α compared to the shNT cells, but cannot explain the slightly accelerated proliferation of MCF-7-shΔ40p53 cells, indicating other factors are involved. The number of DEGs (14) regulated by Δ40p53 was only ~15% of the number of DEGs (91) regulated by Δ40p53-overexpression, which was expected, given that-overexpression is ubiquitous in every cell, but the knockdown was incomplete as demonstrated by the gene expression and western blot results (Figure 3.2). Therefore, a higher number of genes were affected by Δ40p53-overexpression. Fifty-four out of 91 genes were upregulated (59%) and 37 out of 91 genes were down-regulated (41%), indicating Δ40p53overexpression has almost equally induced and inhibited the same amount of genes. There were 176 and 79 DEGs regulated independently by Δ40p53-knockdown and p53α-knockdown in ZR75-1 cells, indicating Δ40p53-knockdown affected a larger number of genes than p53α-knockdown in ZR75-1 cells, this explains the distinct morphological changes. Thirty-seven out of 176 genes were upregulated (21%) and 139 out of 176 genes were down-regulated (79%) by Δ40p53-knockdown; 47 out of 79 genes were up-regulated (59%) and 32 out of 79 genes were down-regulated (41%) by p53αknockdown. From the unique gene lists of ZR75-1-shΔ40p53 and ZR75-1-shp53α, we identified quite a few tumour suppressor/potential tumour suppressor candidates as well as oncogene-like/potential oncogene-like candidates, however there was no absolute link between isoform-knockdown and tumour suppression. For example, *RERG* (RAS Like Estrogen Regulated Growth Inhibitor) was downregulated and *CXCL17* (Chemokine ligand 17, oncogenic) was up-regulated by Δ40p53-knockdown in ZR75-1 cells; meanwhile *ANXA1* (annexin A1) and *BCAS1* (breast carcinoma amplified sequence 1), both tumour-associated were down-regulated by Δ40p53-kockdown. Similarly, proliferation inhibiting *BTG2* (BTG family member 2) by p53α-knockdown and cancer-associated *FGFR2* (fibroblast growth factor receptor 2) was up-regulated by p53α-knockdown; meanwhile tumour-associated genes such as *EGFR* (epidermal growth factor receptor) and *MUCL1* (mucin-like 1) were down-regulated. Overall, this shows the impact of altering endogenous Δ40p53 or p53α was cell-line dependent.

3.4.9 Pathway profiling of MCF-7 and ZR75-1 sublines

Enrichr GO Biological Process was used for GSEA (238, 239). The top 10 most significant GO Terms ranked by adjusted *p*-value are listed in Table 3.4. The DEGs unique to MCF-7-Δ40p53 were mostly

involved in the response to viral infection, as well as biological processes such as the response to interferon, regulation of viral genome replication and life cycle. The 14 and 29 unique genes regulated in MCF-7-shΔ40p53 and MCF-7-shp53α showed no significant enriched GO biological processes, and the top GO term gene sets were limited with less than four DEGs in each category. The MCF-7shΔ40p53 unique DEG *BMP2* appears most frequently in the top 10 GO Biological Process terms including muscle tissue morphogenesis, neurogenesis and steroid biosynthesis. Along with another two DEGs *PTGER4* (prostaglandin E Receptor 4) and *GNAI1* (Guanine nucleotide-binding protein G(i), alpha-1 subunit), unique to MCF-7-shΔ40p53, were all down-regulated (Log_2FC -1.41, -1.81 and -3.44 respectively) and were associated with pathways in cancer (Enrichr, KEGG 2019 Human), suggesting a beneficial effect of Δ40p53-knockdown. The 29 DEGs unique to MCF-7-shp53α cells appear to be associated with multiple metabolic processes and developmental processes, among which *CDKN1A* (cyclin-dependent kinase inhibitor 1) and *FAS* (Fas (tumor Necrosis Factor Receptor Superfamily, Member 6) are categorized into GO term cellular response to amino acid starvation (GO:0034198), and they are also involved in p53 pathways. Both were down regulated (log_2FC -1.09 for *CDKN1A* and -1.65 for *FAS*), indicating p53-dependent cell cycle arrest and apoptosis were suppressed.

The 176 and 79 DEGs unique to ZR75-1-shΔ40p53 and ZR75-1-shp53α respectively, were enriched in different GO biological process categories. Even though the largest number of DEGs were found to be affected independently by Δ40p53-knockdown in ZR75-1 cells, only one GO Term (regulation of calcium ion-dependent exocytosis) had an adjusted *p*-value < 0.05. Other GO Terms had no more than three genes. This suggests that Δ40p53-knockdown in ZR75-1 cells had an impact on multiple biological processes. The GO Term with the highest combined score was regulation of extent of cell growth, which may extrapolate to some extent of the more aggregated morphology of ZR75-1shΔ40p53 cells. Unique DEGs to ZR75-1-shp53α cells were mostly involved in glucuronidation of multiple substances due to the elevated multiple *UGT1A* (uridine diphosphate glucuronosyltransferase 1A) isoforms ($log_2FC > 4.7$). The GO term gland morphogenesis had an adjusted *p*-value of 0.1 and includes *TGFB2* (Transforming Growth Factor Beta 2) and *FGFR2* (fibroblast growth factor receptor 2), both of which were up-regulated in ZR75-1-shp53α (log_2FC 1.52 and 1.06 respectively) and down-regulated in ZR75-1-shΔ40p53 cells (log_2FC -5.03 and -2.51 respectively); indicating that knockdown of Δ40p53 rather than p53α in ZR75-1 cells affects gland morphogenesis. The GO term negative regulation of lymphocyte migration has an adjusted *p*-value of 0.09, including the genes *PADI2* (Protein-arginine deiminase type-2) and *APOD* (Apolipoprotein D), both of which were down-regulated (log_2FC -0.95 and -1.68 respectively).

Lastly, we tried to identify similarity between MCF-7 and ZR75-1 cells with Δ40p53 or p53α knockdown. There were very few genes in common. One gene, *UBE2QL1* (ubiquitin-Conjugating Enzyme E2Q-Like

Protein 1), was down-regulated in both MCF-7-shΔ40p53 and ZR75-1-shΔ40p53 (log_2FC -5.85 and 1.62 respectively) when compared to shNT cells. Two genes *MUCL1* and *TP53* were found in common when comparing p53α-knockdown to shNT cells in MCF-7 and ZR75-1 cells, *TP53* was down-regulated in both MCF-7 and ZR75-1 cells (log_2FC -1.48 and -1.43 respectively), but *MUCL1* was up-regulated in MCF-7-shp53α (log_2FC -1.63) and down-regulated in ZR75-1-shp53α (log_2FC -1.28). This showed that endogenous Δ40p53 or p53α knockdown mostly altered a distinct set of genes and knock down of Δ40p53 or p53α, induced distinct transcript profiles in the derived cell lines.

The above RNA-seq results showed that Δ40p53-overexpression, Δ40p53-knockdown or p53αknockdown in MCF-7 and ZR75-1 cells regulated very few genes in common, indicating that genes regulated by each isoform were relatively independent. In addition, very few genes were found in common when comparing MCF-7 to ZR75-1 by knocking down Δ40p53 or p53α, confirming further that the altered level of each isoform had an independent impact on gene expression in MCF-7 or ZR75-1 cells. Notably, the number of differentially expressed genes induced by isoform-knockdown in MCF-7 cells was much less than those of ZR75-1 cells, suggesting that endogenously, isoform level did not affect MCF-7 to an as great extent as ZR75-1 cells. The unique differentially expressed genes were enriched in different GO Biological Process terms, where Δ40p53-overexpression in MCF-7 was associated with the response to viral infection, Δ40p53-knockdown in ZR75-1 cells was associated with cell growth and ion homeostasis and p53α-knockdown in ZR75-1 was associated with glucuronidation. Overall, we did not see a similar impact by knocking down endogenous Δ40p53 or p53α in MCF-7 and ZR75-1 cells.

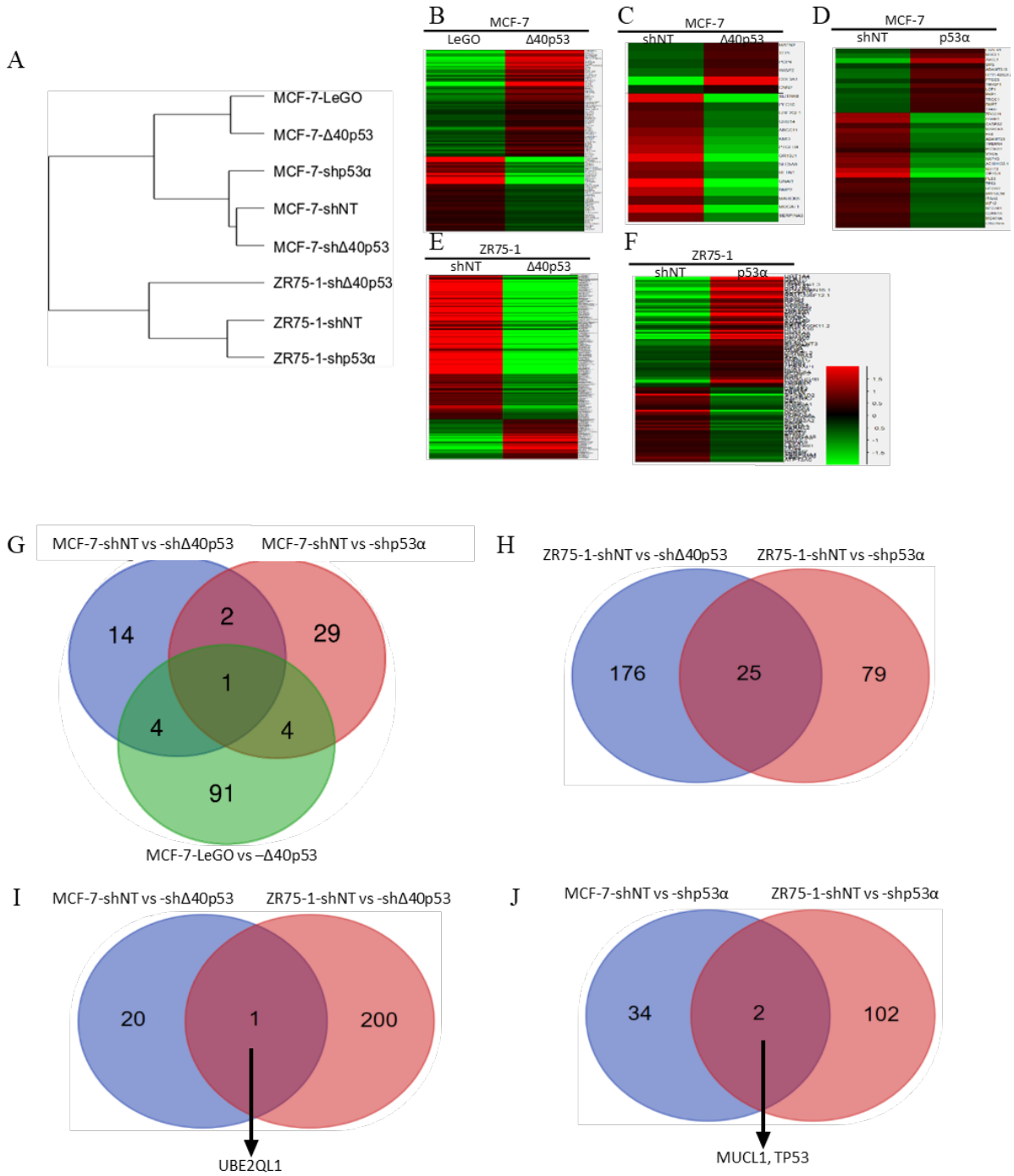

Figure 3.9 Differentially expressed genes (DEG) detected by RNA-seq of MCF-7 and ZR75-1 sublines. A, Sample similarity based on total mRNA expression profiles of all sublines. B – F, Differentially expressed genes (DEGs) are hierarchically clustered and illustrated in heatmaps of individual comparisons: MCF-7-Δ40p53 to MCF-7-LeGO (B), MCF-7-shΔ40p53 to MCF-7-shNT (C), MCF-7-shp53α to MCF-7-shNT (D), ZR75-1-shΔ40p53 to ZR75-1-shNT (E) and ZR75-1-shp53α to ZR75-1-shNT (F). H – K, Venn diagrams show common and unique DEGs between comparisons between sublines and subline-specific DEGs.

Table 3.3 Common and unique DEGs in MCF -7 and ZR 75-1 sublines at basal level with expression log_2FC indicated.

				log_2FC to control cell lines (LeGO/shNT)		
Names	**total**	**Gene**	**description**	**Δ40p53-overexpression**	**shΔ40p53**	**shp53α**
Common DEGs between sublines and their corresponding control sublines						
All isoformaltered MCF-7 sublines to controls	1	MARCKS	myristoylated alanine-rich protein kinase C substrate [Source:HGNC Symbol;Acc:6759]	2.31	-1.68	-2.05
MCF-7-Δ40p53 vs MCF-7-LeGO and MCF-7-shΔ40p53 vs MCF-7-shNT	4	COL3A1	collagen, type III, alpha 1 [Source:HGNC Symbol;Acc:2201]	2.22	3.86	\
		PEG10	paternally expressed 10 [Source:HGNC Symbol;Acc:14005]	-4.92	-1.30	\
		SERPINA3	serpin peptidase inhibitor, clade A (alpha-1 antiproteinase, antitrypsin), member 3 [Source:HGNC Symbol;Acc:16]	-1.22	-1.87	\
		SLITRK6	SLIT and NTRK-like family, member 6 [Source:HGNC Symbol;Acc:23503]	3.78	-3.67	\
MCF-7-shΔ40p53 vs MCF-7-shNT and MCF-7-shp53α vs MCF-7-shNT	2	ABCC11	ATP-binding cassette, sub-family C (CFTR/MRP), member 11 [Source:HGNC Symbol;Acc:14639]	\	-2.10	-2.44
		OR10J1	olfactory receptor, family 10, subfamily J, member 1 [Source:HGNC Symbol;Acc:8175]	\	-3.79	-3.63
MCF-7-Δ40p53 vs MCF-7-LeGO and MCF-7-shp53α vs MCF-7-shNT	4	PLS3	plastin 3 [Source:HGNC Symbol;Acc:9091]	2.00	\	-1.13
		TMEM64	transmembrane protein 64 [Source:HGNC Symbol;Acc:25441]	-1.06	\	-1.44
		TP53	tumor protein p53 [Source:HGNC Symbol;Acc:11998]	2.26	\	-1.48
		TRGC1	T cell receptor gamma constant 1 [Source:HGNC Symbol;Acc:12275]	-2.24	\	1.17
ZR75-1-shΔ40p53 vs ZR75-1-shp53α and ZR75-1-shp53α vs ZR75-1-shΔ40p53	25	ACACB	acetyl-CoA carboxylase beta [Source:HGNC Symbol;Acc:85]	\	-1.81	-1.82
		C1orf64	chromosome 1 open reading frame 64 [Source:HGNC Symbol;Acc:28339]	\	-2.23	-1.53
		CEACAM6	carcinoembryonic antigen-related cell adhesion molecule 6 (non-specific cross reacting antigen) [Source:HGNC Symbol;Acc:1818]	\	-1.81	-1.79
		SCGB1D2	secretoglobin, family 1D, member 2 [Source:HGNC Symbol;Acc:18396]	\	-9.85	-1.49
		SCGB2A2	secretoglobin, family 2A, member 2 [Source:HGNC Symbol;Acc:7050]	\	-9.98	-1.66

		SERPINA1	serpin peptidase inhibitor, clade A (alpha-1 antiproteinase, antitrypsin), member 1 [Source:HGNC Symbol;Acc:8941]	\	-1.78	-1.22
		SLC34A2	solute carrier family 34 (sodium phosphate), member 2 [Source:HGNC Symbol;Acc:11020]	\	-5.09	-1.61
		SYT13	synaptotagmin XIII [Source:HGNC Symbol;Acc:14962]	\	-6.84	-4.27
		TFF3	trefoil factor 3 (intestinal) [Source:HGNC Symbol;Acc:11757]	\	-4.39	-0.99

		GABRQ	gamma-aminobutyric acid (GABA) receptor, theta [Source:HGNC Symbol;Acc:14454]	\	3.15	1.87
		NR2F1	nuclear receptor subfamily 2, group F, member 1 [Source:HGNC Symbol;Acc:7975]	\	3.21	1.69
		PCDH10	protocadherin 10 [Source:HGNC Symbol;Acc:13404]	\	3.70	3.43
		UGT1A4	UDP glucuronosyltransferase 1 family, polypeptide A4 [Source:HGNC Symbol;Acc:12536]	\	4.55	4.70
		UGT1A6	UDP glucuronosyltransferase 1 family, polypeptide A6 [Source:HGNC Symbol;Acc:12538]	\	4.67	4.85
		DLC1	deleted in liver cancer 1 [Source:HGNC Symbol;Acc:2897]	\	-3.27	1.03
		EGR3	early growth response 3 [Source:HGNC Symbol;Acc:3240]	\	-6.29	1.52
		GJA1	gap junction protein, alpha 1, 43kDa [Source:HGNC Symbol;Acc:4274]	\	-8.56	0.86
		HSPB8	heat shock 22kDa protein 8 [Source:HGNC Symbol;Acc:30171]	\	-3.02	0.86
		KRT80	keratin 80 [Source:HGNC Symbol;Acc:27056]	\	-1.66	0.90
		LONRF2	LON peptidase N-terminal domain and ring finger 2 [Source:HGNC Symbol;Acc:24788]	\	-2.90	1.06
		SCUBE2	signal peptide, CUB domain, EGF-like 2 [Source:HGNC Symbol;Acc:30425]	\	-7.32	1.09
		SLFN11	schlafen family member 11 [Source:HGNC Symbol;Acc:26633]	\	-7.05	1.53
		TMSB4X	thymosin beta 4, X-linked [Source:HGNC Symbol;Acc:11881]	\	-5.48	0.75
		TUBB3	tubulin, beta 3 class III [Source:HGNC Symbol;Acc:20772]	\	-4.18	0.91
		CEL	carboxyl ester lipase (bile salt-stimulated lipase) [Source:HGNC Symbol;Acc:1848]	\	1.49	-1.43

Unique DEGs						
Unique to MCF-7-Δ40p53	91	A2M*	alpha-2-macroglobulin [Source:HGNC Symbol;Acc:7]	2.97	\	\
		ACSL1*	acyl-CoA synthetase long-chain family member 1 [Source:HGNC Symbol;Acc:3569]	1.00	\	\
		ATP10D*	ATPase, class V, type 10D [Source:HGNC Symbol;Acc:13549]	1.77	\	\
		BST2*	bone marrow stromal cell antigen 2 [Source:HGNC Symbol;Acc:1119]	1.37	\	\
		CLSTN3*	calsyntenin 3 [Source:HGNC Symbol;Acc:18371]	1.23	\	\
		CRIP2*	cysteine-rich protein 2 [Source:HGNC Symbol;Acc:2361]	1.07	\	\
		CRISP3*	cysteine-rich secretory protein 3 [Source:HGNC Symbol;Acc:16904]	2.02	\	\
		DDX60*	DEAD (Asp-Glu-Ala-Asp) box polypeptide 60 [Source:HGNC Symbol;Acc:25942]	2.24	\	\
		EHF*	ets homologous factor [Source:HGNC Symbol;Acc:3246]	1.85	\	\
		EPHA3*	EPH receptor A3 [Source:HGNC Symbol;Acc:3387]	1.87	\	\
		EVPL*	envoplakin [Source:HGNC Symbol;Acc:3503]	0.71	\	\
		FRMPD1*	FERM and PDZ domain containing 1 [Source:HGNC Symbol;Acc:29159]	6.38	\	\
		HERC6*	hect domain and RLD 6 [Source:HGNC Symbol;Acc:26072]	1.33	\	\
		IFI27*	interferon, alpha-inducible protein 27 [Source:HGNC Symbol;Acc:5397]	3.43	\	\
		IFI44*	interferon-induced protein 44 [Source:HGNC Symbol;Acc:16938]	4.98	\	\
		IFI44L*	interferon-induced protein 44-like [Source:HGNC Symbol;Acc:17817]	3.82	\	\
		IFI6*	interferon, alpha-inducible protein 6 [Source:HGNC Symbol;Acc:4054]	1.81	\	\
		IFIH1*	interferon induced with helicase C domain 1 [Source:HGNC Symbol;Acc:18873]	1.20	\	\
		IFITM1*	interferon induced transmembrane protein 1 (9-27) [Source:HGNC Symbol;Acc:5412]	1.17	\	\
		IFITM3*	interferon induced transmembrane protein 3 [Source:HGNC Symbol;Acc:5414]	0.70	\	\
		IL1R1*	interleukin 1 receptor, type I [Source:HGNC Symbol;Acc:5993]	0.81	\	\

		IRF9*	interferon regulatory factor 9 [Source:HGNC Symbol;Acc:6131]	1.13	\	\
		ISG15*	ISG15 ubiquitin-like modifier [Source:HGNC Symbol;Acc:4053]	1.81	\	\
		KCNK2*	potassium channel, subfamily K, member 2 [Source:HGNC Symbol;Acc:6277]	1.30	\	\
		KIF20A*	kinesin family member 20A [Source:HGNC Symbol;Acc:9787]	0.65	\	\
		KRT17*	keratin 17 [Source:HGNC Symbol;Acc:6427]	2.33	\	\
		LGALS3BP*	lectin, galactoside-binding, soluble, 3 binding protein [Source:HGNC Symbol;Acc:6564]	0.78	\	\
		NAA15*	N(alpha)-acetyltransferase 15, NatA auxiliary subunit [Source:HGNC Symbol;Acc:30782]	0.65	\	\
		NDUFC1*	NADH dehydrogenase (ubiquinone) 1, subcomplex unknown, 1, 6kDa [Source:HGNC Symbol;Acc:7705]	0.77	\	\
		NFIA*	nuclear factor I/A [Source:HGNC Symbol;Acc:7784]	0.80	\	\
		NGFRAP1*	nerve growth factor receptor (TNFRSF16) associated protein 1 [Source:HGNC Symbol;Acc:13388]	0.66	\	\
		OAS1*	2'-5'-oligoadenylate synthetase 1, 40/46kDa [Source:HGNC Symbol;Acc:8086]	1.32	\	\
		OASL*	2'-5'-oligoadenylate synthetase-like [Source:HGNC Symbol;Acc:8090]	1.68	\	\
		PARP10*	poly (ADP-ribose) polymerase family, member 10 [Source:HGNC Symbol;Acc:25895]	1.62	\	\

		PARP12*	poly (ADP-ribose) polymerase family, member 12 [Source:HGNC Symbol;Acc:21919]	1.06	\	\
		PARP14*	poly (ADP-ribose) polymerase family, member 14 [Source:HGNC Symbol;Acc:29232]	1.17	\	\
		PARP9*	poly (ADP-ribose) polymerase family, member 9 [Source:HGNC Symbol;Acc:24118]	0.82	\	\
		PHF17*	PHD finger protein 17 [Source:HGNC Symbol;Acc:30027]	1.15	\	\
		PLK1*	polo-like kinase 1 [Source:HGNC Symbol;Acc:9077]	0.77	\	\
		RCN1*	reticulocalbin 1, EF-hand calcium binding domain [Source:HGNC Symbol;Acc:9934]	1.77	\	\

		RP11-234O6.2*	No description	3.59	\	\
		RP11-865I6.2*	No description	2.67	\	\
		RP4-697K14.7*	Peroxisomal proliferator-activated receptor A-interacting complex 285 kDa protein [Source:UniProtKB/Swiss-Prot;Acc:Q9BYK8]	0.93	\	\
		SAMD9*	sterile alpha motif domain containing 9 [Source:HGNC Symbol;Acc:1348]	2.77	\	\
		SAMHD1*	SAM domain and HD domain 1 [Source:HGNC Symbol;Acc:15925]	1.00	\	\
		SCLT1*	sodium channel and clathrin linker 1 [Source:HGNC Symbol;Acc:26406]	1.22	\	\
		SCNN1A*	sodium channel, nonvoltage-gated 1 alpha [Source:HGNC Symbol;Acc:10599]	1.28	\	\
		SCOC*	short coiled-coil protein [Source:HGNC Symbol;Acc:20335]	0.80	\	\
		SETD7*	SET domain containing (lysine methyltransferase) 7 [Source:HGNC Symbol;Acc:30412]	0.59	\	\
		SOX2*	SRY (sex determining region Y)-box 2 [Source:HGNC Symbol;Acc:11195]	2.90	\	\
		STAT6*	signal transducer and activator of transcription 6, interleukin-4 induced [Source:HGNC Symbol;Acc:11368]	0.89	\	\
		SULF1*	sulfatase 1 [Source:HGNC Symbol;Acc:20391]	3.91	\	\
		TCIRG1*	T-cell, immune regulator 1, ATPase, H+ transporting, lysosomal V0 subunit A3 [Source:HGNC Symbol;Acc:11647]	2.53	\	\
		UBE2L6*	ubiquitin-conjugating enzyme E2L 6 [Source:HGNC Symbol;Acc:12490]	1.60	\	\
		ABCG2**	ATP-binding cassette, sub-family G (WHITE), member 2 [Source:HGNC Symbol;Acc:74]	-0.98	\	\
		AC110619.2**	Uncharacterized protein [Source:UniProtKB/TrEMBL;Acc:B5MC12]	-1.59	\	\
		ANXA3**	annexin A3 [Source:HGNC Symbol;Acc:541]	-0.93	\	\
		APOD**	apolipoprotein D [Source:HGNC Symbol;Acc:612]	-1.03	\	\
		ARHGDIB**	Rho GDP dissociation inhibitor (GDI) beta [Source:HGNC Symbol;Acc:679]	-2.22	\	\

		C10orf112**	chromosome 10 open reading frame 112 [Source:HGNC Symbol;Acc:24331]	-0.79	\	\
		C19orf63**	chromosome 19 open reading frame 63 [Source:HGNC Symbol;Acc:27609]	-6.17	\	\

C1orf21**	chromosome 1 open reading frame 21 [Source:HGNC Symbol;Acc:15494]	-0.77	\	\
C6orf97**	chromosome 6 open reading frame 97 [Source:HGNC Symbol;Acc:21177]	-0.91	\	\
CEACAM6**	carcinoembryonic antigen-related cell adhesion molecule 6 (non-specific cross reacting antigen) [Source:HGNC Symbol;Acc:1818]	-1.17	\	\
DHRS2**	dehydrogenase/reductase (SDR family) member 2 [Source:HGNC Symbol;Acc:18349]	-0.74	\	\
DNAJA4**	DnaJ (Hsp40) homolog, subfamily A, member 4 [Source:HGNC Symbol;Acc:14885]	-5.21	\	\
EVL**	Enah/Vasp-like [Source:HGNC Symbol;Acc:20234]	-0.79	\	\
FAM124B**	family with sequence similarity 124B [Source:HGNC Symbol;Acc:26224]	-4.58	\	\
GPRIN3**	GPRIN family member 3 [Source:HGNC Symbol;Acc:27733]	-4.99	\	\
GSTM3**	glutathione S-transferase mu 3 (brain) [Source:HGNC Symbol;Acc:4635]	-0.79	\	\
GUSB**	glucuronidase, beta [Source:HGNC Symbol;Acc:4696]	-0.65	\	\
INHBB**	inhibin, beta B [Source:HGNC Symbol;Acc:6067]	-0.71	\	\
KLHL5**	kelch-like 5 (Drosophila) [Source:HGNC Symbol;Acc:6356]	-0.67	\	\
LIN7A**	lin-7 homolog A (C. elegans) [Source:HGNC Symbol;Acc:17787]	-0.93	\	\
MMP16**	matrix metallopeptidase 16 (membrane-inserted) [Source:HGNC Symbol;Acc:7162]	-0.90	\	\
NPAS3**	neuronal PAS domain protein 3 [Source:HGNC Symbol;Acc:19311]	-1.38	\	\
NT5E**	5'-nucleotidase, ecto (CD73) [Source:HGNC Symbol;Acc:8021]	-1.30	\	\
PLXNA4**	plexin A4 [Source:HGNC Symbol;Acc:9102]	-1.73	\	\
POF1B**	premature ovarian failure, 1B [Source:HGNC Symbol;Acc:13711]	-1.15	\	\
POLR3G**	polymerase (RNA) III (DNA directed) polypeptide G (32kD) [Source:HGNC Symbol;Acc:30075]	-2.36	\	\
RCAN1**	regulator of calcineurin 1 [Source:HGNC Symbol;Acc:3040]	-0.89	\	\
RP11-206M11.7**	No description	-1.12	\	\
RP11-662G23.1**	No description	-1.87	\	\

		SERPINA5**	serpin peptidase inhibitor, clade A (alpha-1 antiproteinase, antitrypsin), member 5 [Source:HGNC Symbol;Acc:8723]	-1.00	\	\
		SGCE**	sarcoglycan, epsilon [Source:HGNC Symbol;Acc:10808]	-4.59	\	\
		SGCG**	sarcoglycan, gamma (35kDa dystrophin-associated glycoprotein) [Source:HGNC Symbol;Acc:10809]	-0.72	\	\
		SLC25A30**	solute carrier family 25, member 30 [Source:HGNC Symbol;Acc:27371]	-0.67	\	\
		SPATA6**	spermatogenesis associated 6 [Source:HGNC Symbol;Acc:18309]	-3.83	\	\
		TFF1**	trefoil factor 1 [Source:HGNC Symbol;Acc:11755]	-0.67	\	\
		TNIK**	TRAF2 and NCK interacting kinase [Source:HGNC Symbol;Acc:30765]	-1.02	\	\
		TRIM22**	tripartite motif containing 22 [Source:HGNC Symbol;Acc:16379]	-5.05	\	\
Unique to MCF-7-shΔ40p53	14	CNN2*	calponin 2 [Source:HGNC Symbol;Acc:2156]	\	0.65	\
		MATN2*	matrilin 2 [Source:HGNC Symbol;Acc:6908]	\	1.17	\
		PCP4*	Purkinje cell protein 4 [Source:HGNC Symbol;Acc:8742]	\	1.08	\
		TFPI*	tissue factor pathway inhibitor (lipoprotein-associated coagulation inhibitor) [Source:HGNC Symbol;Acc:11760]	\	1.35	\
		WISP2*	WNT1 inducible signaling pathway protein 2 [Source:HGNC Symbol;Acc:12770]	\	1.46	\
		BMP2**	bone morphogenetic protein 2 [Source:HGNC Symbol;Acc:1069]	\	-3.00	\
		GNAI1**	guanine nucleotide binding protein (G protein), alpha inhibiting activity polypeptide 1 [Source:HGNC Symbol;Acc:4384]	\	-4.21	\
		GRB14**	growth factor receptor-bound protein 14 [Source:HGNC Symbol;Acc:4565]	\	-1.58	\
		KMO**	kynurenine 3-monooxygenase (kynurenine 3-hydroxylase) [Source:HGNC Symbol;Acc:6381]	\	-2.58	\
		MOGAT1**	monoacylglycerol O-acyltransferase 1 [Source:HGNC Symbol;Acc:18210]	\	-3.63	\
		PTGER4**	prostaglandin E receptor 4 (subtype EP4) [Source:HGNC Symbol;Acc:9596]	\	-2.88	\
		RFTN1**	raftlin, lipid raft linker 1 [Source:HGNC Symbol;Acc:30278]	\	-1.92	\
		SLC5A8**	solute carrier family 5 (iodide transporter), member 8 [Source:HGNC Symbol;Acc:19119]	\	-2.12	\

		UBE2QL1**	ubiquitin-conjugating enzyme E2Q family-like 1 [Source:HGNC Symbol;Acc:37269]	\	-1.62	\
Unique to MCF-7-shp53α	29	ADAMTS19*	ADAM metallopeptidase with thrombospondin type 1 motif, 19 [Source:HGNC Symbol;Acc:17111]	\	\	1.46
		ASCL1*	achaete-scute complex homolog 1 (Drosophila) [Source:HGNC Symbol;Acc:738]	\	\	2.86
		BMP7*	bone morphogenetic protein 7 [Source:HGNC Symbol;Acc:1074]	\	\	1.12
		LCP1*	lymphocyte cytosolic protein 1 (L-plastin) [Source:HGNC Symbol;Acc:6528]	\	\	1.03
		LGALS1*	lectin, galactoside-binding, soluble, 1 [Source:HGNC Symbol;Acc:6561]	\	\	1.11
		MUCL1*	mucin-like 1 [Source:HGNC Symbol;Acc:30588]	\	\	1.63
		PKP1*	plakophilin 1 (ectodermal dysplasia/skin fragility syndrome) [Source:HGNC Symbol;Acc:9023]	\	\	1.35
		PTGES*	prostaglandin E synthase [Source:HGNC Symbol;Acc:9599]	\	\	0.90
		RP11-428L9.2*	No description	\	\	1.55
		SMS*	spermine synthase [Source:HGNC Symbol;Acc:11123]	\	\	0.85
		TM4SF1*	transmembrane 4 L six family member 1 [Source:HGNC Symbol;Acc:11853]	\	\	1.55
		TSKU*	tsukushi small leucine rich proteoglycan homolog (Xenopus laevis) [Source:HGNC Symbol;Acc:28850]	\	\	1.09
		AC104135.4**	No description	\	\	-1.87
		ADAMTS9**	ADAM metallopeptidase with thrombospondin type 1 motif, 9 [Source:HGNC Symbol;Acc:13202]	\	\	-1.65
		C1QTNF6**	C1q and tumor necrosis factor related protein 6 [Source:HGNC Symbol;Acc:14343]	\	\	-0.99
		CADPS2**	Ca++-dependent secretion activator 2 [Source:HGNC Symbol;Acc:16018]	\	\	-1.34
		CDKN1A**	cyclin-dependent kinase inhibitor 1A (p21, Cip1) [Source:HGNC Symbol;Acc:1784]	\	\	-1.09
		FAS**	Fas (TNF receptor superfamily, member 6) [Source:HGNC Symbol;Acc:11920]	\	\	-1.65

		HECW2**	HECT, C2 and WW domain containing E3 ubiquitin protein ligase 2 [Source:HGNC Symbol;Acc:29853]	\	\	-1.34
		ITGA5**	integrin, alpha 5 (fibronectin receptor, alpha polypeptide) [Source:HGNC Symbol;Acc:6141]	\	\	-1.18
		KIF12**	kinesin family member 12 [Source:HGNC Symbol;Acc:21495]	\	\	-1.33
		KRT13**	keratin 13 [Source:HGNC Symbol;Acc:6415]	\	\	-2.88
		MGAT4A**	mannosyl (alpha-1,3-)-glycoprotein beta-1,4-N-acetylglucosaminyltransferase, isozyme A [Source:HGNC Symbol;Acc:7047]	\	\	-1.20
		NECAB1**	N-terminal EF-hand calcium binding protein 1 [Source:HGNC Symbol;Acc:20983]	\	\	-1.41
		NXPH3**	neurexophilin 3 [Source:HGNC Symbol;Acc:8077]	\	\	-2.08
		PARM1**	prostate androgen-regulated mucin-like protein 1 [Source:HGNC Symbol;Acc:24536]	\	\	-2.57
		PCDHA1**	protocadherin alpha 1 [Source:HGNC Symbol;Acc:8663]	\	\	-0.92
		SMPDL3B**	sphingomyelin phosphodiesterase, acid-like 3B [Source:HGNC Symbol;Acc:21416]	\	\	-1.04
		VWDE**	von Willebrand factor D and EGF domains [Source:HGNC Symbol;Acc:21897]	\	\	-1.80

Unique to ZR75-1-shΔ40p53	176	ADARB2*	adenosine deaminase, RNA-specific, B2 [Source:HGNC Symbol;Acc:227]	\	6.57	\
		APOL4*	apolipoprotein L, 4 [Source:HGNC Symbol;Acc:14867]	\	2.59	\
		AQP3*	aquaporin 3 (Gill blood group) [Source:HGNC Symbol;Acc:636]	\	1.41	\
		BAMBI*	BMP and activin membrane-bound inhibitor homolog (Xenopus laevis) [Source:HGNC Symbol;Acc:30251]	\	1.56	\
		CA2*	carbonic anhydrase II [Source:HGNC Symbol;Acc:1373]	\	1.36	\
		CECR1*	cat eye syndrome chromosome region, candidate 1 [Source:HGNC Symbol;Acc:1839]	\	1.88	\
		CERS4*	ceramide synthase 4 [Source:HGNC Symbol;Acc:23747]	\	1.26	\
		CLCA2*	chloride channel accessory 2 [Source:HGNC Symbol;Acc:2016]	\	1.33	\
		CRABP1*	cellular retinoic acid binding protein 1 [Source:HGNC Symbol;Acc:2338]	\	1.88	\

		CXCL17*	chemokine (C-X-C motif) ligand 17 [Source:HGNC Symbol;Acc:19232]	\	2.35	\
		CXCR7*	chemokine (C-X-C motif) receptor 7 [Source:HGNC Symbol;Acc:23692]	\	2.10	\
		DENND1B*	DENN/MADD domain containing 1B [Source:HGNC Symbol;Acc:28404]	\	1.17	\
		DPYS*	dihydropyrimidinase [Source:HGNC Symbol;Acc:3013]	\	5.12	\
		ELF5*	E74-like factor 5 (ets domain transcription factor) [Source:HGNC Symbol;Acc:3320]	\	2.77	\
		ELK3*	ELK3, ETS-domain protein (SRF accessory protein 2) [Source:HGNC Symbol;Acc:3325]	\	3.88	\
		FAM113B*	family with sequence similarity 113, member B [Source:HGNC Symbol;Acc:28255]	\	1.27	\
		FAM129A*	family with sequence similarity 129, member A [Source:HGNC Symbol;Acc:16784]	\	1.38	\
		FGG*	fibrinogen gamma chain [Source:HGNC Symbol;Acc:3694]	\	2.63	\
		GATM*	glycine amidinotransferase (L-arginine:glycine amidinotransferase) [Source:HGNC Symbol;Acc:4175]	\	1.17	\
		HMGCS2*	3-hydroxy-3-methylglutaryl-CoA synthase 2 (mitochondrial) [Source:HGNC Symbol;Acc:5008]	\	1.14	\
		KCNMA1*	potassium large conductance calcium-activated channel, subfamily M, alpha member 1 [Source:HGNC Symbol;Acc:6284]	\	1.28	\
		LHX9*	LIM homeobox 9 [Source:HGNC Symbol;Acc:14222]	\	4.48	\
		LMO3*	LIM domain only 3 (rhombotin-like 2) [Source:HGNC Symbol;Acc:6643]	\	2.27	\
		LRRK2*	leucine-rich repeat kinase 2 [Source:HGNC Symbol;Acc:18618]	\	1.07	\
		LUZP2*	leucine zipper protein 2 [Source:HGNC Symbol;Acc:23206]	\	4.11	\

		MBNL2*	muscleblind-like 2 (Drosophila) [Source:HGNC Symbol;Acc:16746]	\	1.40	\
		NFIX*	nuclear factor I/X (CCAAT-binding transcription factor) [Source:HGNC Symbol;Acc:7788]	\	1.25	\
		PKHD1L1*	polycystic kidney and hepatic disease 1 (autosomal recessive)-like 1 [Source:HGNC Symbol;Acc:20313]	\	1.40	\

PTPRQ*	protein tyrosine phosphatase, receptor type, Q [Source:HGNC Symbol;Acc:9679]	\	4.21	\
RIMS2*	regulating synaptic membrane exocytosis 2 [Source:HGNC Symbol;Acc:17283]	\	1.47	\
RP11-279F6.1*	No description	\	1.71	\
RP11-369C8.1*	No description	\	2.08	\
S100P*	S100 calcium binding protein P [Source:HGNC Symbol;Acc:10504]	\	1.33	\
S1PR3*	sphingosine-1-phosphate receptor 3 [Source:HGNC Symbol;Acc:3167]	\	1.07	\
SH3RF1*	SH3 domain containing ring finger 1 [Source:HGNC Symbol;Acc:17650]	\	1.06	\
SLC12A1*	solute carrier family 12 (sodium/potassium/chloride transporters), member 1 [Source:HGNC Symbol;Acc:10910]	\	3.12	\
TMEM134*	transmembrane protein 134 [Source:HGNC Symbol;Acc:26142]	\	0.96	\
ABAT**	4-aminobutyrate aminotransferase [Source:HGNC Symbol;Acc:23]	\	-2.47	\
ABCC3**	ATP-binding cassette, sub-family C (CFTR/MRP), member 3 [Source:HGNC Symbol;Acc:54]	\	-4.51	\
AC005544.1**	No description	\	-6.82	\
AC008537.3**	CYP2B proteinCytochrome P450 2B7 short isoformUncharacterized protein [Source:UniProtKB/TrEMBL;Acc:Q14097]	\	-4.93	\
AGPS**	alkylglycerone phosphate synthase [Source:HGNC Symbol;Acc:327]	\	-4.64	\
AGR2**	anterior gradient homolog 2 (Xenopus laevis) [Source:HGNC Symbol;Acc:328]	\	-1.91	\
AGR3**	anterior gradient homolog 3 (Xenopus laevis) [Source:HGNC Symbol;Acc:24167]	\	-1.69	\
AHR**	aryl hydrocarbon receptor [Source:HGNC Symbol;Acc:348]	\	-1.53	\
AMOTL1**	angiomotin like 1 [Source:HGNC Symbol;Acc:17811]	\	-1.31	\
AMOTL2**	angiomotin like 2 [Source:HGNC Symbol;Acc:17812]	\	-1.57	\
ANXA1**	annexin A1 [Source:HGNC Symbol;Acc:533]	\	-6.92	\
ARPC1B**	actin related protein 2/3 complex, subunit 1B, 41kDa [Source:HGNC Symbol;Acc:704]	\	-1.02	\

		ASPH**	aspartate beta-hydroxylase [Source:HGNC Symbol;Acc:757]	\	-1.11	\

		ATP6V0A4**	ATPase, H+ transporting, lysosomal V0 subunit a4 [Source:HGNC Symbol;Acc:866]	\	-1.74	\
		BCAS1**	breast carcinoma amplified sequence 1 [Source:HGNC Symbol;Acc:974]	\	-1.52	\
		BMPR1B**	bone morphogenetic protein receptor, type IB [Source:HGNC Symbol;Acc:1077]	\	-2.10	\
		C10orf81**	chromosome 10 open reading frame 81 [Source:HGNC Symbol;Acc:26285]	\	-1.18	\
		C19orf33**	chromosome 19 open reading frame 33 [Source:HGNC Symbol;Acc:16668]	\	-6.56	\
		C20orf3**	chromosome 20 open reading frame 3 [Source:HGNC Symbol;Acc:13238]	\	-0.96	\
		C2orf43**	chromosome 2 open reading frame 43 [Source:HGNC Symbol;Acc:26145]	\	-5.76	\
		C4orf19**	chromosome 4 open reading frame 19 [Source:HGNC Symbol;Acc:25618]	\	-4.01	\
		C8orf73**	chromosome 8 open reading frame 73 [Source:HGNC Symbol;Acc:27814]	\	-1.78	\
		CACNA1H**	calcium channel, voltage-dependent, T type, alpha 1H subunit [Source:HGNC Symbol;Acc:1395]	\	-7.64	\
		CACNG4**	calcium channel, voltage-dependent, gamma subunit 4 [Source:HGNC Symbol;Acc:1408]	\	-7.49	\
		CAPN8**	calpain 8 [Source:HGNC Symbol;Acc:1485]	\	-2.82	\
		CCL28**	chemokine (C-C motif) ligand 28 [Source:HGNC Symbol;Acc:17700]	\	-3.66	\
		CELSR2**	cadherin, EGF LAG seven-pass G-type receptor 2 (flamingo homolog, Drosophila) [Source:HGNC Symbol;Acc:3231]	\	-1.47	\
		CLDN3**	claudin 3 [Source:HGNC Symbol;Acc:2045]	\	-6.84	\
		CLEC3A**	C-type lectin domain family 3, member A [Source:HGNC Symbol;Acc:2052]	\	-4.85	\
		COL12A1**	collagen, type XII, alpha 1 [Source:HGNC Symbol;Acc:2188]	\	-3.45	\
		COL6A1**	collagen, type VI, alpha 1 [Source:HGNC Symbol;Acc:2211]	\	-4.60	\
		CREB3L1**	cAMP responsive element binding protein 3-like 1 [Source:HGNC Symbol;Acc:18856]	\	-2.96	\
		CRIM1**	cysteine rich transmembrane BMP regulator 1 (chordin-like) [Source:HGNC Symbol;Acc:2359]	\	-3.20	\

		CRMP1**	collapsin response mediator protein 1 [Source:HGNC Symbol;Acc:2365]	\	-6.02	\
		CTSD**	cathepsin D [Source:HGNC Symbol;Acc:2529]	\	-4.17	\
		CYFIP2**	cytoplasmic FMR1 interacting protein 2 [Source:HGNC Symbol;Acc:13760]	\	-1.37	\
		DNAJC15**	DnaJ (Hsp40) homolog, subfamily C, member 15 [Source:HGNC Symbol;Acc:20325]	\	-6.31	\
		DOK7**	docking protein 7 [Source:HGNC Symbol;Acc:26594]	\	-6.44	\
		DSTN**	destrin (actin depolymerizing factor) [Source:HGNC Symbol;Acc:15750]	\	-1.00	\

		EGLN2**	egl nine homolog 2 (C. elegans) [Source:HGNC Symbol;Acc:14660]	\	-1.26	\
		EHD2**	EH-domain containing 2 [Source:HGNC Symbol;Acc:3243]	\	-1.76	\
		ENDOD1**	endonuclease domain containing 1 [Source:HGNC Symbol;Acc:29129]	\	-1.44	\
		ESR1**	estrogen receptor 1 [Source:HGNC Symbol;Acc:3467]	\	-1.58	\
		ETNK2**	ethanolamine kinase 2 [Source:HGNC Symbol;Acc:25575]	\	-1.26	\
		FADS1**	fatty acid desaturase 1 [Source:HGNC Symbol;Acc:3574]	\	-1.85	\
		FADS2**	fatty acid desaturase 2 [Source:HGNC Symbol;Acc:3575]	\	-1.13	\
		FBLN2**	fibulin 2 [Source:HGNC Symbol;Acc:3601]	\	-3.41	\
		FOXI1**	forkhead box I1 [Source:HGNC Symbol;Acc:3815]	\	-5.72	\
		FREM2**	FRAS1 related extracellular matrix protein 2 [Source:HGNC Symbol;Acc:25396]	\	-6.09	\
		FXYD3**	FXYD domain containing ion transport regulator 3 [Source:HGNC Symbol;Acc:4027]	\	-1.04	\
		FXYD5**	FXYD domain containing ion transport regulator 5 [Source:HGNC Symbol;Acc:4029]	\	-6.32	\
		GFRA1**	GDNF family receptor alpha 1 [Source:HGNC Symbol;Acc:4243]	\	-5.74	\
		GOLM1**	golgi membrane protein 1 [Source:HGNC Symbol;Acc:15451]	\	-6.08	\
		GPX1**	glutathione peroxidase 1 [Source:HGNC Symbol;Acc:4553]	\	-6.26	\
		GREB1**	growth regulation by estrogen in breast cancer 1 [Source:HGNC Symbol;Acc:24885]	\	-5.01	\

		GRIK3**	glutamate receptor, ionotropic, kainate 3 [Source:HGNC Symbol;Acc:4581]	\	-8.69	\
		HEXA**	hexosaminidase A (alpha polypeptide) [Source:HGNC Symbol;Acc:4878]	\	-1.10	\
		HPGD**	hydroxyprostaglandin dehydrogenase 15-(NAD) [Source:HGNC Symbol;Acc:5154]	\	-6.04	\
		HSD17B4**	hydroxysteroid (17-beta) dehydrogenase 4 [Source:HGNC Symbol;Acc:5213]	\	-1.34	\
		IFITM10**	interferon induced transmembrane protein 10 [Source:HGNC Symbol;Acc:40022]	\	-5.47	\
		IGFBP4**	insulin-like growth factor binding protein 4 [Source:HGNC Symbol;Acc:5473]	\	-3.41	\
		IL6ST**	interleukin 6 signal transducer (gp130, oncostatin M receptor) [Source:HGNC Symbol;Acc:6021]	\	-1.75	\
		INPP4B**	inositol polyphosphate-4-phosphatase, type II, 105kDa [Source:HGNC Symbol;Acc:6075]	\	-2.68	\
		KCND2**	potassium voltage-gated channel, Shal-related subfamily, member 2 [Source:HGNC Symbol;Acc:6238]	\	-5.90	\

		KCNE4**	potassium voltage-gated channel, Isk-related family, member 4 [Source:HGNC Symbol;Acc:6244]	\	-4.18	\
		KCNH1**	potassium voltage-gated channel, subfamily H (eag-related), member 1 [Source:HGNC Symbol;Acc:6250]	\	-6.85	\
		KCNK2**	potassium channel, subfamily K, member 2 [Source:HGNC Symbol;Acc:6277]	\	-4.68	\
		KCNK5**	potassium channel, subfamily K, member 5 [Source:HGNC Symbol;Acc:6280]	\	-4.63	\
		KIF16B**	kinesin family member 16B [Source:HGNC Symbol;Acc:15869]	\	-1.10	\
		KRT15**	keratin 15 [Source:HGNC Symbol;Acc:6421]	\	-2.11	\
		KRT8**	keratin 8 [Source:HGNC Symbol;Acc:6446]	\	-1.81	\
		LAMB3**	laminin, beta 3 [Source:HGNC Symbol;Acc:6490]	\	-2.33	\
		LDHB**	lactate dehydrogenase B [Source:HGNC Symbol;Acc:6541]	\	-6.30	\
		LGALS1**	lectin, galactoside-binding, soluble, 1 [Source:HGNC Symbol;Acc:6561]	\	-6.63	\
		LGALS3BP**	lectin, galactoside-binding, soluble, 3 binding protein [Source:HGNC Symbol;Acc:6564]	\	-2.38	\

		LRG1**	leucine-rich alpha-2-glycoprotein 1 [Source:HGNC Symbol;Acc:29480]	\	-3.60	\
		MAOB**	monoamine oxidase B [Source:HGNC Symbol;Acc:6834]	\	-8.72	\
		MDK**	midkine (neurite growth-promoting factor 2) [Source:HGNC Symbol;Acc:6972]	\	-4.29	\
		MID1**	midline 1 (Opitz/BBB syndrome) [Source:HGNC Symbol;Acc:7095]	\	-1.90	\
		MPPED2**	metallophosphoesterase domain containing 2 [Source:HGNC Symbol;Acc:1180]	\	-6.30	\
		MUC5B**	mucin 5B, oligomeric mucus/gel-forming [Source:HGNC Symbol;Acc:7516]	\	-5.94	\
		MYEOV**	myeloma overexpressed (in a subset of t(11;14) positive multiple myelomas) [Source:HGNC Symbol;Acc:7563]	\	-6.62	\
		NBL1**	neuroblastoma, suppression of tumorigenicity 1 [Source:HGNC Symbol;Acc:7650]	\	-2.11	\
		NBPF1**	neuroblastoma breakpoint family, member 1 [Source:HGNC Symbol;Acc:26088]	\	-1.30	\
		NCRNA00052**	No description	\	-6.51	\
		NECAB1**	N-terminal EF-hand calcium binding protein 1 [Source:HGNC Symbol;Acc:20983]	\	-7.13	\
		NKAIN1**	Na+/K+ transporting ATPase interacting 1 [Source:HGNC Symbol;Acc:25743]	\	-3.04	\
		NNT**	nicotinamide nucleotide transhydrogenase [Source:HGNC Symbol;Acc:7863]	\	-1.76	\
		NPNT**	nephronectin [Source:HGNC Symbol;Acc:27405]	\	-3.10	\

		NPY1R**	neuropeptide Y receptor Y1 [Source:HGNC Symbol;Acc:7956]	\	-3.24	\
		NRCAM**	neuronal cell adhesion molecule [Source:HGNC Symbol;Acc:7994]	\	-3.76	\
		NRP1**	neuropilin 1 [Source:HGNC Symbol;Acc:8004]	\	-4.86	\
		NUDT12**	nudix (nucleoside diphosphate linked moiety X)-type motif 12 [Source:HGNC Symbol;Acc:18826]	\	-7.90	\
		OLFM1**	olfactomedin 1 [Source:HGNC Symbol;Acc:17187]	\	-2.25	\
		OLFML3**	olfactomedin-like 3 [Source:HGNC Symbol;Acc:24956]	\	-6.73	\

		PAPSS2**	3'-phosphoadenosine 5'-phosphosulfate synthase 2 [Source:HGNC Symbol;Acc:8604]	\	-1.03	\
		PARD6B**	par-6 partitioning defective 6 homolog beta (C. elegans) [Source:HGNC Symbol;Acc:16245]	\	-1.42	\
		PCDH19**	protocadherin 19 [Source:HGNC Symbol;Acc:14270]	\	-5.91	\
		PDZK1**	PDZ domain containing 1 [Source:HGNC Symbol;Acc:8821]	\	-7.60	\
		PGM5**	phosphoglucomutase 5 [Source:HGNC Symbol;Acc:8908]	\	-6.86	\
		PGR**	progesterone receptor [Source:HGNC Symbol;Acc:8910]	\	-3.16	\
		PITX1**	paired-like homeodomain 1 [Source:HGNC Symbol;Acc:9004]	\	-1.70	\
		PLCD3**	phospholipase C, delta 3 [Source:HGNC Symbol;Acc:9061]	\	-1.77	\
		PLCE1**	phospholipase C, epsilon 1 [Source:HGNC Symbol;Acc:17175]	\	-6.29	\
		PMP22**	peripheral myelin protein 22 [Source:HGNC Symbol;Acc:9118]	\	-2.14	\
		PREX1**	No description	\	-3.45	\
		PXDN**	peroxidasin homolog (Drosophila) [Source:HGNC Symbol;Acc:14966]	\	-1.25	\
		QSOX1**	quiescin Q6 sulfhydryl oxidase 1 [Source:HGNC Symbol;Acc:9756]	\	-4.00	\
		RAB31**	RAB31, member RAS oncogene family [Source:HGNC Symbol;Acc:9771]	\	-1.61	\
		RCAN1**	regulator of calcineurin 1 [Source:HGNC Symbol;Acc:3040]	\	-1.63	\
		RERG**	RAS-like, estrogen-regulated, growth inhibitor [Source:HGNC Symbol;Acc:15980]	\	-1.47	\
		RP11-295K3.1**	No description	\	-4.25	\
		RP11-662G23.1**	No description	\	-6.20	\
		RP4-754E20__A.5**	No description	\	-6.19	\
		SAT1**	spermidine/spermine N1-acetyltransferase 1 [Source:HGNC Symbol;Acc:10540]	\	-1.68	\
		SCIN**	scinderin [Source:HGNC Symbol;Acc:21695]	\	-5.97	\

		SDR42E1**	short chain dehydrogenase/reductase family 42E, member 1 [Source:HGNC Symbol;Acc:29834]	\	-7.53	\
		SLC12A4**	solute carrier family 12 (potassium/chloride transporters), member 4 [Source:HGNC Symbol;Acc:10913]	\	-1.75	\
		SLC2A1**	solute carrier family 2 (facilitated glucose transporter), member 1 [Source:HGNC Symbol;Acc:11005]	\	-1.22	\
		SLC2A14**	solute carrier family 2 (facilitated glucose transporter), member 14 [Source:HGNC Symbol;Acc:18301]	\	-7.17	\
		SLC7A2**	solute carrier family 7 (cationic amino acid transporter, y+ system), member 2 [Source:HGNC Symbol;Acc:11060]	\	-2.17	\
		SLFN5**	schlafen family member 5 [Source:HGNC Symbol;Acc:28286]	\	-6.82	\
		SPTSSB**	serine palmitoyltransferase, small subunit B [Source:HGNC Symbol;Acc:24045]	\	-5.35	\
		STMN3**	stathmin-like 3 [Source:HGNC Symbol;Acc:15926]	\	-1.56	\
		STS**	steroid sulfatase (microsomal), isozyme S [Source:HGNC Symbol;Acc:11425]	\	-1.75	\
		SUSD3**	sushi domain containing 3 [Source:HGNC Symbol;Acc:28391]	\	-6.27	\
		SYT8**	synaptotagmin VIII [Source:HGNC Symbol;Acc:19264]	\	-9.44	\
		SYTL2**	synaptotagmin-like 2 [Source:HGNC Symbol;Acc:15585]	\	-2.53	\
		SYTL5**	synaptotagmin-like 5 [Source:HGNC Symbol;Acc:15589]	\	-6.33	\
		TFF1**	trefoil factor 1 [Source:HGNC Symbol;Acc:11755]	\	-6.20	\
		TMEM2**	transmembrane protein 2 [Source:HGNC Symbol;Acc:11869]	\	-1.66	\
		TMTC1**	transmembrane and tetratricopeptide repeat containing 1 [Source:HGNC Symbol;Acc:24099]	\	-2.18	\
		TNNI2**	troponin I type 2 (skeletal, fast) [Source:HGNC Symbol;Acc:11946]	\	-7.12	\
		TSKU**	tsukushi small leucine rich proteoglycan homolog (Xenopus laevis) [Source:HGNC Symbol;Acc:28850]	\	-4.05	\
		TSPAN1**	tetraspanin 1 [Source:HGNC Symbol;Acc:20657]	\	-1.63	\
		UBE2QL1**	ubiquitin-conjugating enzyme E2Q family-like 1 [Source:HGNC Symbol;Acc:37269]	\	-5.85	\
		UNC13D**	unc-13 homolog D (C. elegans) [Source:HGNC Symbol;Acc:23147]	\	-5.12	\

		UST**	uronyl-2-sulfotransferase [Source:HGNC Symbol;Acc:17223]	\	-2.40	\
		VTCN1**	V-set domain containing T cell activation inhibitor 1 [Source:HGNC Symbol;Acc:28873]	\	-1.06	\
Unique to	79	A4GALT*	alpha 1,4-galactosyltransferase [Source:HGNC Symbol;Acc:18149]	\	\	1.30

ZR75-1-shp53α		ATP8A2*	ATPase, aminophospholipid transporter, class I, type 8A, member 2 [Source:HGNC Symbol;Acc:13533]	\	\	2.28
		B4GALNT3*	beta-1,4-N-acetyl-galactosaminyl transferase 3 [Source:HGNC Symbol;Acc:24137]	\	\	1.58
		BCAT1*	branched chain amino-acid transaminase 1, cytosolic [Source:HGNC Symbol;Acc:976]	\	\	2.02
		C12orf53*	chromosome 12 open reading frame 53 [Source:HGNC Symbol;Acc:25338]	\	\	2.68
		C12orf59*	chromosome 12 open reading frame 59 [Source:HGNC Symbol;Acc:26438]	\	\	3.22
		CBLN2*	cerebellin 2 precursor [Source:HGNC Symbol;Acc:1544]	\	\	1.92
		CBS*	cystathionine-beta-synthase [Source:HGNC Symbol;Acc:1550]	\	\	1.92
		CD9*	CD9 molecule [Source:HGNC Symbol;Acc:1709]	\	\	0.69
		CDK2AP1*	cyclin-dependent kinase 2 associated protein 1 [Source:HGNC Symbol;Acc:14002]	\	\	0.68
		DLX3**	distal-less homeobox 3 [Source:HGNC Symbol;Acc:2916]	\	\	1.75
		DPYSL5*	dihydropyrimidinase-like 5 [Source:HGNC Symbol;Acc:20637]	\	\	1.26
		FGFR2*	fibroblast growth factor receptor 2 [Source:HGNC Symbol;Acc:3689]	\	\	1.06
		FRAS1*	Fraser syndrome 1 [Source:HGNC Symbol;Acc:19185]	\	\	2.16
		GCGR*	glucagon receptor [Source:HGNC Symbol;Acc:4192]	\	\	2.83
		GPRC5A*	G protein-coupled receptor, family C, group 5, member A [Source:HGNC Symbol;Acc:9836]	\	\	1.12
		GSTP1*	glutathione S-transferase pi 1 [Source:HGNC Symbol;Acc:4638]	\	\	3.31
		IL20*	interleukin 20 [Source:HGNC Symbol;Acc:6002]	\	\	1.96
		ITPRIPL2*	inositol 1,4,5-trisphosphate receptor interacting protein-like 2 [Source:HGNC Symbol;Acc:27257]	\	\	0.97

		KIF1A*	kinesin family member 1A [Source:HGNC Symbol;Acc:888]	\	\	1.13
		KIF5C*	kinesin family member 5C [Source:HGNC Symbol;Acc:6325]	\	\	1.74
		MESP1*	mesoderm posterior 1 homolog (mouse) [Source:HGNC Symbol;Acc:29658]	\	\	2.00
		MPP2*	membrane protein, palmitoylated 2 (MAGUK p55 subfamily member 2) [Source:HGNC Symbol;Acc:7220]	\	\	1.10
		OLR1*	oxidized low density lipoprotein (lectin-like) receptor 1 [Source:HGNC Symbol;Acc:8133]	\	\	1.95
		PLEKHG4B*	pleckstrin homology domain containing, family G (with RhoGef domain) member 4B [Source:HGNC Symbol;Acc:29399]	\	\	3.64
		RIMS4*	regulating synaptic membrane exocytosis 4 [Source:HGNC Symbol;Acc:16183]	\	\	1.43

		ROBO2*	roundabout, axon guidance receptor, homolog 2 (Drosophila) [Source:HGNC Symbol;Acc:10250]	\	\	2.83
		RP11-398F12.1*	No description	\	\	7.34
		RP11-438N16.1*	No description	\	\	2.22
		RP11-566K11.2*	Melanocyte-stimulating hormone receptor [Source:UniProtKB/SwissProt;Acc:Q01726]	\	\	0.84
		RP11-9G1.3*	No description	\	\	2.51
		SLC16A3*	solute carrier family 16, member 3 (monocarboxylic acid transporter 4) [Source:HGNC Symbol;Acc:10924]	\	\	0.90
		SLC6A15*	solute carrier family 6 (neutral amino acid transporter), member 15 [Source:HGNC Symbol;Acc:13621]	\	\	2.57
		SLC6A6*	solute carrier family 6 (neurotransmitter transporter, taurine), member 6 [Source:HGNC Symbol;Acc:11052]	\	\	1.01
		SYNPO*	synaptopodin [Source:HGNC Symbol;Acc:30672]	\	\	1.35
		TGFB2*	transforming growth factor, beta 2 [Source:HGNC Symbol;Acc:11768]	\	\	1.52
		THBS1*	thrombospondin 1 [Source:HGNC Symbol;Acc:11785]	\	\	1.01
		TIMP2*	TIMP metallopeptidase inhibitor 2 [Source:HGNC Symbol;Acc:11821]	\	\	0.83
		TMEM98*	transmembrane protein 98 [Source:HGNC Symbol;Acc:24529]	\	\	1.90

		UGT1A1*	UDP glucuronosyltransferase 1 family, polypeptide A1 [Source:HGNC Symbol;Acc:12530]	\	\	4.86
		UGT1A10*	UDP glucuronosyltransferase 1 family, polypeptide A10 [Source:HGNC Symbol;Acc:12531]	\	\	4.77
		UGT1A3*	UDP glucuronosyltransferase 1 family, polypeptide A3 [Source:HGNC Symbol;Acc:12535]	\	\	4.71
		UGT1A5*	UDP glucuronosyltransferase 1 family, polypeptide A5 [Source:HGNC Symbol;Acc:12537]	\	\	4.71
		UGT1A7*	UDP glucuronosyltransferase 1 family, polypeptide A7 [Source:HGNC Symbol;Acc:12539]	\	\	4.76
		UGT1A8*	UDP glucuronosyltransferase 1 family, polypeptide A8 [Source:HGNC Symbol;Acc:12540]	\	\	4.71
		UGT1A9*	UDP glucuronosyltransferase 1 family, polypeptide A9 [Source:HGNC Symbol;Acc:12541]	\	\	4.71
		ZNF300*	zinc finger protein 300 [Source:HGNC Symbol;Acc:13091]	\	\	4.01
		AKR7A3**	aldo-keto reductase family 7, member A3 (aflatoxin aldehyde reductase) [Source:HGNC Symbol;Acc:390]	\	\	-1.11
		APOD**	apolipoprotein D [Source:HGNC Symbol;Acc:612]	\	\	-1.68

		ATP13A5**	ATPase type 13A5 [Source:HGNC Symbol;Acc:31789]	\	\	-1.24
		BTG2**	BTG family, member 2 [Source:HGNC Symbol;Acc:1131]	\	\	-1.03
		C2orf72**	chromosome 2 open reading frame 72 [Source:HGNC Symbol;Acc:27418]	\	\	-0.91
		CD44*	calmodulin-like 3 [Source:HGNC Symbol;Acc:1452]	\	\	-5.55
		CALML3**	CD44 molecule (Indian blood group) [Source:HGNC Symbol;Acc:1681]	\	\	-0.81
		CORO2A**	coronin, actin binding protein, 2A [Source:HGNC Symbol;Acc:2255]	\	\	-0.83
		CRISP3**	cysteine-rich secretory protein 3 [Source:HGNC Symbol;Acc:16904]	\	\	-1.26
		EGFR**	epidermal growth factor receptor [Source:HGNC Symbol;Acc:3236]	\	\	-1.17
		FAM198B**	family with sequence similarity 198, member B [Source:HGNC Symbol;Acc:25312]	\	\	-0.81
		FMOD**	fibromodulin [Source:HGNC Symbol;Acc:3774]	\	\	-0.75

		GGT1**	gamma-glutamyltransferase 1 [Source:HGNC Symbol;Acc:4250]	\	\	-0.84
		MUCL1**	mucin-like 1 [Source:HGNC Symbol;Acc:30588]	\	\	-1.28
		PADI2**	peptidyl arginine deiminase, type II [Source:HGNC Symbol;Acc:18341]	\	\	-0.95
		PIK3R1**	phosphoinositide-3-kinase, regulatory subunit 1 (alpha) [Source:HGNC Symbol;Acc:8979]	\	\	-0.75
		PRLR**	prolactin receptor [Source:HGNC Symbol;Acc:9446]	\	\	-1.26
		RBM20**	RNA binding motif protein 20 [Source:HGNC Symbol;Acc:27424]	\	\	-0.76
		SEPP1**	selenoprotein P, plasma, 1 [Source:HGNC Symbol;Acc:10751]	\	\	-0.87
		SERHL2**	serine hydrolase-like 2 [Source:HGNC Symbol;Acc:29446]	\	\	-1.82
		SH3BGRL**	SH3 domain binding glutamic acid-rich protein like [Source:HGNC Symbol;Acc:10823]	\	\	-1.06
		SLC1A4**	solute carrier family 1 (glutamate/neutral amino acid transporter), member 4 [Source:HGNC Symbol;Acc:10942]	\	\	-0.73
		SLC25A18**	solute carrier family 25 (mitochondrial carrier), member 18 [Source:HGNC Symbol;Acc:10988]	\	\	-0.83
		SLC40A1**	solute carrier family 40 (iron-regulated transporter), member 1 [Source:HGNC Symbol;Acc:10909]	\	\	-0.88
		SPINK8**	serine peptidase inhibitor, Kazal type 8 (putative) [Source:HGNC Symbol;Acc:33160]	\	\	-0.92
		TDO2**	tryptophan 2,3-dioxygenase [Source:HGNC Symbol;Acc:11708]	\	\	-0.89
		THRSP**	thyroid hormone responsive [Source:HGNC Symbol;Acc:11800]	\	\	-1.13
		TMEM86A**	transmembrane protein 86A [Source:HGNC Symbol;Acc:26890]	\	\	-0.75
		TP53**	tumor protein p53 [Source:HGNC Symbol;Acc:11998]	\	\	-1.45
		TRPV6**	transient receptor potential cation channel, subfamily V, member 6 [Source:HGNC Symbol;Acc:14006]	\	\	-0.93
		WDR44**	WD repeat domain 44 [Source:HGNC Symbol;Acc:30512]	\	\	-0.74
		ZMAT3**	zinc finger, matrin-type 3 [Source:HGNC Symbol;Acc:29983]	\	\	-0.85

Common genes from multiple lists are listed alphabetically and unique genes are grouped into up-(*) and down-regulated (**) genes and then listed alphabetically. The 25 common DEGs between ZR75-1-shΔ40p53 vs ZR75-1-shNT and ZR75-1-shp53α vs ZR75-1-shNT are further color-coded into 4 subgroups: DEGs with no shading were down-regulated by knockdown of either Δ40p53 or p53α; DEGs with blue shading were up-regulated by Δ40p53 and p53α-knockdown; DEGs with grey shading were down-regulated by Δ40p53-knockdown and up-regulated by

p53αknockdown; one DEG with dark grey shading was up-regulated by Δ40p53-knockdown and down-regulated by p53α-knockdown. Values irrelevant to each condition (common of more than one comparisons or unique gene lists) are indicated with "\".

Table 3.4 Top 10 enriched GO Biological Process Terms of the unique DEGs in each subline

GO Biological Process 2018 Term	P-value	Adjusted P-value	Odds Ratio	Combined Score	Genes
MCF-7-Δ40p53					
type I interferon signaling pathway (GO:0060337)	3.91E-13	9.99E-10	33.30	951.34	IFITM3;BST2;IFITM1;OAS1;IFI27;IFI6;ISG15;SAMHD1;IRF9;OASL
cellular response to type I interferon (GO:0071357)	3.91E-13	2.00E-09	33.30	951.34	IFITM3;BST2;IFITM1;OAS1;IFI27;IFI6;ISG15;SAMHD1;IRF9;OASL
negative regulation of viral genome replication (GO:0045071)	3.14E-09	5.34E-06	30.17	590.61	IFITM3;BST2;PARP10;IFITM1;OAS1;ISG15;OASL
negative regulation of viral life cycle (GO:1903901)	1.28E-08	1.63E-05	24.81	450.94	IFITM3;BST2;PARP10;IFITM1;OAS1;ISG15;OASL
regulation of viral genome replication (GO:0045069)	1.61E-08	1.64E-05	24.04	431.41	IFITM3;BST2;PARP10;IFITM1;OAS1;ISG15;OASL
cytokine-mediated signaling pathway (GO:0019221)	1.01E-06	8.58E-04	4.85	67.01	IFITM3;IFITM1;IL1R1;IFI6;ISG15;SAMHD1;OASL;SOX2;BST2;OAS1;IFI27;STAT6;TRIM22;IRF9
regulation of type I interferon production (GO:0032479)	4.55E-05	0.033	12.78	127.76	IFIH1;POLR3G;UBE2L6;STAT6;ISG15
response to interferon-alpha (GO:0035455)	5.92E-05	0.04	38.78	377.58	IFITM3;BST2;IFITM1
response to interferon-beta (GO:0035456)	8.38E-05	0.04	34.70	325.77	IFITM3;BST2;IFITM1
protein ADP-ribosylation (GO:0006471)	8.38E-05	0.047	34.70	325.77	PARP10;PARP14;PARP9
MCF-7-shΔ40p53					
cellular response to ketone (GO:1901655)	1.83E-04	0.93	98.52	848.02	PTGER4;GNAI1
muscle tissue morphogenesis (GO:0060415)	0.013	0.98	75.19	325.25	BMP2
ureteric bud morphogenesis (GO:0060675)	0.014	0.99	71.43	305.35	BMP2
tryptophan metabolic process (GO:0006568)	0.007	0.99	142.86	709.25	KMO
acylglycerol biosynthetic process (GO:0046463)	0.013	0.99	75.19	325.25	MOGAT1
ERK1 and ERK2 cascade (GO:0070371)	0.015	0.99	68.03	287.51	PTGER4
negative regulation of steroid biosynthetic process (GO:0010894)	0.011	1	89.29	401.49	BMP2

cellular response to mechanical stimulus (GO:0071260)	0.001	1	58.31	440.34	PTGER4;CNN2
positive regulation of neurogenesis (GO:0050769)	0.001	1	40.82	279.21	PCP4;BMP2
regulation of neuron differentiation (GO:0045664)	0.002	1	33.61	217.00	PCP4;BMP2
MCF-7-shp53α					
negative regulation of phosphate metabolic process (GO:0045936)	3.80E-04	0.97	68.97	543.22	CDKN1A;BMP7

regulation of sprouting angiogenesis (GO:1903670)	3.42E-04	1	72.60	579.39	ITGA5;ADAMTS9
negative regulation of neurogenesis (GO:0050768)	0.001	1	40.57	276.13	ASCL1;BMP7
cardiac muscle tissue development (GO:0048738)	0.001	1	37.28	247.44	ADAMTS9;BMP7
regulation of dendrite development (GO:0050773)	0.001	1	36.30	239.00	HECW2;BMP7
cellular response to amino acid starvation (GO:0034198)	0.002	1	34.48	223.53	CDKN1A;FAS
glycoprotein metabolic process (GO:0009100)	0.002	1	28.15	171.14	MGAT4A;ADAMTS9
positive regulation of protein phosphorylation (GO:0001934)	0.003	1	6.68	39.20	CDKN1A;FAS;ITGA5;BMP7
negative regulation of neuron differentiation (GO:0045665)	0.004	1	21.22	117.22	ASCL1;BMP7
extracellular matrix organization (GO:0030198)	0.004	1	9.00	48.81	ITGA5;LCP1;ADAMTS9
ZR75-1-shΔ40p53					
regulation of calcium ion-dependent exocytosis (GO:0017158)	7.76E-06	0.04	12.63	148.57	RIMS2;LRRK2;SYTL5;SYT8;CACNA1H;SYTL2
positive regulation of cell-substrate adhesion (GO:0010811)	1.02E-04	0.26	10.72	98.56	NRP1;FGG;AGR2;NPNT;CCL28
alpha-linolenic acid metabolic process (GO:0036109)	1.80E-04	0.31	26.22	226.18	FADS2;HSD17B4;FADS1
regulated exocytosis (GO:0045055)	3.56E-04	0.36	5.34	42.39	RIMS2;LGALS3BP;RAB31;SCIN;FGG;ENDOD1;QSOX1
regulation of regulated secretory pathway (GO:1903305)	3.39E-04	0.43	11.96	95.58	SYTL5;SYT8;UNC13D;SYTL2
nervous system development (GO:0007399)	7.40E-04	0.54	2.99	21.56	OLFM1;RCAN1;MDK;MPPED2;CRIM1;PMP22;STMN3;CRMP1;NRCAM;GFRA1;PCDH19;NBL1
hydrogen peroxide metabolic process (GO:0042743)	6.84E-04	0.58	17.05	124.22	GPX1;MAOB;PXDN

regulation of exocytosis (GO:0017157)	0.001	0.64	8.74	59.32	RIMS2;ANXA1;FGG;UNC13D
monovalent inorganic cation homeostasis (GO:0055067)	0.002	0.66	12.63	80.69	SLC12A4;SLC12A1;ATP6V0A4
myoblast fusion (GO:0007520)	0.002	0.67	32.47	209.62	CACNA1H;KCNH1
ZR75-1-shp53α					
flavonoid glucuronidation (GO:0052696)	4.08E-16	2.08E-12	196.91	6977.17	UGT1A10;UGT1A1;UGT1A5;UGT1A3;UGT1A9;UGT1A8;UGT1A7
xenobiotic glucuronidation (GO:0052697)	3.72E-15	9.49E-12	161.10	5352.66	UGT1A10;UGT1A1;UGT1A5;UGT1A3;UGT1A9;UGT1A8;UGT1A7
cellular glucuronidation (GO:0052695)	2.15E-13	3.66E-10	104.24	3040.50	UGT1A10;UGT1A1;UGT1A5;UGT1A3;UGT1A9;UGT1A8;UGT1A7
glucuronate metabolic process (GO:0019585)	1.65E-09	2.10E-06	90.42	1828.65	UGT1A10;UGT1A1;UGT1A3;UGT1A9;UGT1A7
retinoic acid metabolic process (GO:0042573)	2.46E-09	2.51E-06	84.39	1672.78	UGT1A1;UGT1A3;UGT1A9;UGT1A8;UGT1A7
monocarboxylic acid metabolic process (GO:0032787)	2.47E-07	2.10E-04	16.26	247.37	UGT1A1;UGT1A3;GGT1;UGT1A9;SLC16A3;UGT1A8;UGT1A7
retinoid metabolic process (GO:0001523)	1.25E-05	0.01	16.66	187.97	UGT1A1;UGT1A3;UGT1A9;UGT1A8;UGT1A7
negative regulation of lipid metabolic process (GO:0045833)	5.49E-05	0.03	39.97	392.13	UGT1A1;APOD;UGT1A8
carboxylic acid transport (GO:0046942)	5.28E-05	0.03	19.47	191.78	SLC6A6;SLC6A15;SLC1A4;SLC16A3
regulation of biosynthetic process (GO:0009889)	2.29E-04	0.08	84.39	707.43	GSTP1;THRSP

3.5 Discussion

The *TP53* gene is regarded as the guardian of genome because the translated full-length p53 protein is involved in a large network of biological processes including regulation of proliferation/apoptosis, DNA repair, tumour inhibition and metabolism, thus maintaining the balance of proliferation and apoptosis. The *TP53* gene is the most frequently mutated gene in human cancers albeit not in breast cancer. The majority of breast cancer cases have wt p53, which has lost the tumour inhibition ability, but the exact mechanisms are unknown in most cases.

In our previous studies, we have shown that a high Δ40p53/p53 ratio is associated with worse diseasefree survival in breast cancer patients, suggesting the canonical function of wt p53 is compromised due to the increased endogenous Δ40p53 level (18). This led to our hypothesis that Δ40p53 plays a role in breast cancer progression. We performed gene expression array analysis on previously published breast cancer specimens, which were separated into two groups based on the median of the mRNA expression of Δ40p53 in all cases. We observed a distinct separation of differentially expressed genes clustered by higher or lower Δ40p53 level in ER+ cases, but not in ER- cases. A relationship between Δ40p53 and ER+ breast cancers is therefore evident and amongst those cases with high Δ40p53 expression, the differentially expressed genes were mostly associated with immune responses. As analyses were conducted on clinical tissues the inclusion of multiple cell types including normal/malignant cells, stroma cells and immune cells was expected. Nevertheless, the stronger association of immune response pathway genes with high Δ40p53 levels indicates that Δ40p53 could participate in modulating p53-mediated immune-responses, at least in ER+ tumours. Indeed, another p53 isoform, Δ133p53, was associated with immunity, interfering with p53-mediated anti-viral response and inducing inflammation and autoimmunity in mouse models (242, 243). In contrast, the down-regulated genes in the presence of high Δ40p53 expression were mostly cytoskeletal components such as *ACTN1* and *FBLN1*, agreeing with our hypothesis of Δ40p53's regulation of cell motility.

To better elucidate the function of Δ40p53 in breast cancers, we utilised gene overexpression as well as RNAi techniques to establish breast cancer cell line models. The choice of MCF-7 and ZR75-1 lies in the fact that both are ER+ and both have wt p53. Initially, two siRNAs were used to test whether the customized sequences could specifically inhibit the transcription of the Δ40p53 isoforms, before the utilisation of shRNAs to generate stable knockdowns. We observed an improved knockdown efficiency in MCF-7 cells by using shRNA at the RNA level and also observed specific down-regulation at the protein level using isoform specific antibodies in both cell lines.

Together with the previously established Δ40p53-overexpression MCF-7 cell model, we were able to perform a series of functional analysis experiments and by specific overexpression/knockdown of Δ40p53 as well as knockdown of p53α, we aimed to dissect the functions independently affected by different levels of Δ40p53 or p53α. The ZR75-1-derived sublines showed distinct morphological changes when Δ40p53 was knocked down, showing a more aggregated phenotype, but the MCF-7derived sublines showed identical morphology regardless of isoform status. This suggested a greater impact of Δ40p53 on ZR75-1 cells.

The canonical function of p53 is to monitor the integrity of DNA by inducing DNA-repair, cell cycle arrest and apoptosis, while halting proliferation; whereas loss of p53 or mutation of p53 induces cell proliferation (9, 103). Consistently, proliferation was accelerated when either isoform was knocked down in MCF-7 cells, but p53α-knockdown led to a greater augmentation of cell proliferation; Δ40p53ovexpression MCF-7 cells exhibited slightly less proliferative potential compared to the empty-vector control MCF-7 cells. This proposes a similar role for Δ40p53 and p53α in proliferation suppression in MCF-7 cells. In ZR75-1 cells, no differences in proliferation were seen by knockdown of either isoform despite the morphological changes imparted to the cells. Others have reported a proliferation suppression effect by Δ40p53 either by overexpression of vector transfection into p53-null cells, similar to the canonical function of p53 (206). Our results have shown that in ZR75-1 cells, there was no evident difference regarding isoform knockdown status. However, in MCF-7 cells, Δ40p53 suppressed cell proliferation when overexpressed; and knockdown of either isoform contributed to increased cell proliferation, suggesting at least, in both MCF-7 cell lines, Δ40p53 and p53α seemed to exert a similar level of control over cell proliferation at the basal level.

In contrast to a benign tumour, cancers are invasive locally or distally, namely carcinoma in situ or metastatic cancers. Metastasis is the primary reason for cancer-related deaths, describing the ability of cancer cells in extravasating, relocating and initiating secondary growth elsewhere.

Next we went on to investigate whether p53 isoforms have a role in EMT. EMT is regarded as the first step of metastasis, when the molecular feature has changed in epithelial cells, leading to a mesenchymal phenotype. The epithelial cells lose the apical-basal polarity and the cell-cell connection, becoming mobile. There has been raised awareness of p53 in EMT suppression mainly through maintaining E-cadherin expression, in prevention of ECM degradation by suppression of MMP secretion and in restraining cell mobility by, for example, inhibition of membrane protrusions. The breast cancer cell lines, MCF-7 and ZR75-1, maintain epithelial morphology, expressing epithelial markers including E-cadherin and exhibiting tight cell-cell connections. The epithelia-like breast cancer cell migration and invasion is generally through a migratory cell front, which passively drags the

following cells, therefore, scratch wound assays are ideal to record morphological changes. We initially used scratch wound migration/invasion assays on the MCF-7-Δ40p53 and the empty-vector control MCF-7-LeGO cells. Figure 3.5B and C showed a relatively high migratory front of both sublines with enlarged cell size and protruding spikes toward the cell-free area, but the MCF-7-LeGO cell front appeared to be more active. In the scratch wound invasion assay, a diluted matrigel layer was adequate to halt cells occupying the cell-free area and the moving front was less active in both MCF7 and MCF-7-LeGO cells. MCF-7 cells overexpressing Δ40p53 were overall less migratory and invasive compared to the MCF-7-LeGO cells, implying a role of Δ40p53 in inhibiting cell mobility. This is in good agreement with the characterisation of the EMT-related markers, where Δ40p53-overexpression led to increased E-cadherin at the mRNA and protein levels, decreased mRNA level of the mesenchymal marker vimentin and of the E-cadherin negative regulator Slug, showing Δ40p53 suppresses EMT. It has been reported that Slug mRNA is stabilized by HDM2 in the absence of p53, but not in the presence of p53 by HDM2-mediated degradation. As shown in Figure 3.2I that both p53 and Δ40p53 protein levels were enhanced in MCF-7-Δ40p53 cells, therefore the down-regulated Slug mRNA level may be due to the elevated p53 protein level, which might also explain the decreased cell proliferation and cell mobility. Strikingly, Zeb1 mRNA level was significantly up-regulated, which is also a negative Ecadherin regulator and has been reported to be indirectly suppressed by p53 through miR-200c. Apart from being a negative regulator of E-cadherin, Zeb1 is also a critical factor regulating cell stemness. Chaffer *et al* reported Zeb1 to be the switch from non-cancer stem cells (non-CSC) to CSC if the promotor region is accessible and also reported *ZEB1* promoter regions of MCF-7 and ZR75-1 cell lines are methylated and therefore, hard to transit to a mesenchymal phenotype (244). The up-regulated Zeb1 mRNA level following Δ40p53-overexpression could have a potential role in altering the methylation status of *ZEB1* gene, and thereby enhancing the stem cell potential of MCF-7-Δ40p53 cells.

In fact, a role for Δ40p53 in embryonic stem cells has been established previously, but the level of Δ40p53 was dominant during embryo development and then decreased when p53 level was increased.

Due to the effects on cell proliferation rate in the shRNA-transduced MCF-7 cells and morphological changes in shRNA-transduced ZR75-1 cells, scratch wound assays were considered inaccurate. Transwell assays performed on transduced MCF-7 and ZR75-1 sublines showed significantly increased cell migration/invasion in both cell lines transduced with p53α-shRNA, indicating that full-length p53 is a critical safeguard preventing cell mobility. Δ40p53-shRNA, on the other hand impaired ZR75-1 but not MCF-7 cell mobility. The investigation of EMT-related molecular markers showed very diverse results. In MCF-7-shp53α cells, E-cadherin was down-regulated significantly at the mRNA level, but not at protein level and only vimentin was up-regulated at the mRNA level, indicating a more

mesenchymal phenotype. In MCF-7-shΔ40p53 cells, we did not see any significant changes in any of these markers. These results showed p53α-knockdown but not Δ40p53-knockdown has an impact on EMT in MCF-7 cells. As mentioned earlier, ZR75-1-shp53α cells had a more aggregated morphology and it is therefore not surprising to see a decreased cell mobility accompanied by up-regulated Ecadherin and down-regulated Slug and vimentin. ZR75-1-shp53α cells, though having increased cell mobility, had the same up-regulation of E-cadherin, Slug and vimentin as in ZR75-1-shΔ40p53 cells. It has been reported that re-expression of E-cadherin has been associated with metastatic cancer cell relocation *in vivo* (245), but this cannot explain the *in vitro* results.

It was speculated that the inconsistencies in function after altering levels of Δ40p53 and p53α may be due to intrinsic differences between the cell lines. RNA-seq analyses showed that knockdown of either p53 isoform introduced greater changes in gene expression profiles of ZR75-1 compared to MCF-7 cells and in ZR75-1 cells, the number of differentially expressed genes induced by Δ40p53-shRNA was almost twice of that induced by p53α-shRNA. This likely explains the identifiable morphological changes evident in ZR75-1-shΔ40p53 cells. Addtionally, Δ40p53-overexpression led to greater changes than either knockdown of Δ40p53 or p53α. It is unclear if this difference results from biological or technical reasons, the latter may be possible if the efficacy of shRNA knockdown was not homogenous amongst the cell population. It is highly possible that this difference is caused by the type of gene expression modification method: cDNA of Δ40p53 was cloned into the LeGO-vector and therefore all MCF-7-Δ40p53 are Δ40p53-positive; while shRNAs to knockdown endogenous Δ40p53/p53α level may not be homogenous between different cells, thus the impact was relatively less.

Notably, there was not much overlap when comparing each of the sublines to their corresponding control sublines (LeGO or shNT cells) and then cross-comparing the above comparisons. The lengths of the branches of the dendrogram also reflect this (Figure 3.9A). It also illustrates that at the basal level, knockdown of either isoform led to minor changes to the mRNA expression profiles in MCF-7 cells, with MCF-7-shΔ40p53 more similar to MCF-7-shNT; on the contrary, ZR75-1-shΔ40p53 cells were much less similar to ZR75-1-shNT cells than ZR75-1-shp53α cells, showing the importance of cell context when it comes to Δ40p53 function. The highest overlap (25 genes) occurred when comparing shΔ40p53 and shp53α to shNT in ZR75-1 cells. Among these, *PCDH10* (procadherin 10) was almost equally up-regulated in ZR75-1-shΔ40p53 and ZR75-1-shp53α cells (log_2FC 3.43 and 3.7 respectively), and this may help explain the increased E-cadherin expression in these cells. Ten of the 25 genes were differentially regulated by Δ40p53- or p53α-shRNA, and several tumour-suppression-associated genes were included such as *GJA1* (gap junction protein alpha 1), *SCUBE2* (signal peptide-CUB-EGF domaincontaining protein 2) and *SLFN11* (schlafen family member 11) (246-248). These genes were

downregulated by Δ40p53-knockdown and up-regulated by p53α-knockdown, suggesting a role of Δ40p53 in maintaining these tumour suppressing genes in ZR75-1 cells. The abs (log_2FC) values of these genes was much greater when knocking down Δ40p53 compared to those when knocking down p53α (Figure 3.3, grey shading). Together with the fact that these genes were expressed in shNT cells, it is possible that Δ40p53 outweighs p53α in maintaining the expression of these genes. When knocking down p53α, Δ40p53 led to a higher transactivation of these genes, and when knocking down Δ40p53, this function was greatly inhibited.

We performed GSEA analysis on subline-unique genes. Δ40p53-overexpression is associated with elevated PARP family members (PARP10/12 etc.), suggesting a similar role as p53 has in stress and DNA-repair. Δ40p53-overexpression is also associated with elevated immune response to virus and this is in good agreement with the gene expression analysis of breast cancer specimens, where we showed the most enriched GO biological process was “neutrophil mediated immunity” when comparing samples between a higher and a lower Δ40p53/p53 ratio. As mentioned above, growth related genes were also down-regulated in MCF-7-shΔ40p53 and several other growth-related genes were up-regulated in MCF-7-shp53α cells, which explains increased proliferation of MCF-7-shp53α cells, but cannot explain a slightly increased proliferation of MCF-7-shΔ40p53 cells. We have also noticed that some p53 target genes including *CDKN1A* and *FAS* were down-regulated in MCF-7-shp53α cells, indicating these cells not only gained potential to grow, but also potentially gained resistance to cell-cycle arrest and apoptosis.

In ZR75-1 cells, Δ40p53-knockdown had the largest number of differentially regulated genes, but they were categorised into various gene ontology terms, the most enriched GO terms were associated with exocytosis, which requires membrane-trafficking. In addition, several genes are involved in estrogensignaling pathways such as *ESR1, PGR and TFF1* (Trefoil Factor 1) (249) and they were all downregulated, indicating that Δ40p53 is important for the regulation by estrogen and that Δ40p53knockdown in ZR75-1 cells potentially decreased the sensitivity to estrogen. The knockdown of p53α is mostly associated with glucuronidation of exogenous substances and the related genes were all upregulated ($_{log2}$FC > 4.7). An increased glucuronidation is commonly associated with drug efficacy (250), indicating p53α-knockdown potentially increases the metabolism of drugs, thus potentially leading to loss of drug potency following drug treatment in these cells. However, we also pointed out that in ZR75-1 cells, it is difficult to evaluate the tumour suppression-associated function of either isoform, as knockdown of either isoform showed simultaneous tumour suppressing and tumour promoting features. These results implied that other factors were involved in directing p53 function in ZR75-1 cells.

In summary, examining the role of Δ40p53 in two ER+ breast cancer cell lines revealed differential effects on EMT-associated processes including cell motility in MCF-7 cells but not in ZR75-1 cells. In contrast, p53α, acted to restrain cell motility in both cell lines suggesting it plays a more dominant regulatory role in this context. Δ40p53, when overexpressed, has an impact on suppressing tumorigenic genes, similar to p53; and when it was knocked down, down-regulated cell-proliferation markers were seen in MCF-7 cells and genes associated with a lower response to estrogen was seen in ZR75-1 cell, indicating that proliferation was interrupted on some level.

Chapter 4
Investigation of the impact of Δ40p53 on DNA methylation

Chapter 4 Δ40p53 and DNA methylation

4.1 Introduction

In Chapter 3 we investigated the functional and molecular consequences of altering the endogenous Δ40p53/p53α ratio in breast cancer cells. As mentioned in Chapter 1 (Section 1.3.1.5), epigenetic factors can regulate the function of p53, and conversely, p53 can control methylation regulators such as DNMT1 (130), but nothing is known about the role of p53 isoforms in regulating methylation.

Epigenetic modifications are of great importance when it comes to regulation of gene expression. For example, histone modifications such as acetylation affect the accessibility of transcriptional machinery to DNA, thus influencing altered gene expression (124, 251). Another very common epigenetic modification is DNA methylation, typically a methyl group is added to a cytosine residue, which similarly impacts gene expression and notably without changing the original DNA sequence (252). Extensive DNA methylation often occurs in CpG islands, where a high content of CG repeats are observed (252). About 75% of CpG islands are methylated in somatic cells, while less methylation is seen in stem cells including embryonic and hematopoietic stem cells as well as during neurological development (253-256). In cancer, hypomethylation is associated with global genomic instability and activation of oncogene expression, while hypermethylation is regularly associated with inhibition of oncogene inhibitors/tumour suppressor genes (252, 257).

Given the knowledge that p53 influences the epigenome and that p53 isoforms impact p53 function, it is plausible that p53 isoforms could also contribute to epigenetic regulation.

4.2 Aims

The specific role of Δ40p53 in DNA methylation has not been previously examined. The primary aim of this Chapter was to investigate the impact of Δ40p53 expression on global DNA methylation profiles using the validated sublines of MCF-7 and ZR75-1 cells developed in the previous Chapter. Comparisons will be made between controls and sublines bearing stable alterations in Δ40p53 and p53α expression to identify differentially methylated genes.

4.3 Approach

The established breast cancer cell line models (MCF-7 cells with stable Δ40p53-overexpression, Δ40p53-knockdown and p53α knockdown; and ZR75-1 cells with stable Δ40p53-knockdown and p53α knockdown) were harvested from three independent experiments and DNA was extracted using the Gentra Puregene DNA Extraction Kit (Section 2.2.9.1). DNA samples (500 ng) were subjected to bisulfite conversion (Section 2.2.9.2). The samples were then hybridised to Illumina EPIC 850k Beadchips (Section 2.2.9.3) and a methylation signature for each subline obtained after analysis using the Chip Analysis Methylation Pipeline (ChAMP) developed by Yuan Tian etc (235). Differentially methylated probes (DMP) were identified between each of the isoform-altered sublines compared to the control sublines and significance was granted if $p < 0.05$ (Benjamini-Hochberg as the p-value adjustment method for limma analysis) (235, 258, 259). These analyses were performed on single probes (DMPs) and on differentially methylated regions (DMR, minimum 1000 bp distance between two DMRs, minimum 50 bp of the DMR size and minimum 5 DMPs within one DMR) (260) (Section 2.2.9.4).

4.4 Results

4.4.1 Differentially methylated probes

The methylation landscape of all sublines was obtained and samples were clustered in the dendrogram, where the length of the branches illustrates the similarity between each sample. Figure 4.1A showed good that triplicates of each sample were closely clustered as expected, as well as cell line-dependent clustering, where the MCF-7 and ZR75-1 derived sublines were more tightly clustered, rather than clustering by knockdown condition. The methylation signatures of transduced MCF-7 sublines showed a higher similarity between MCF-7-shNT and MCF-7-shΔ40p53 rather than between MCF-7-shNT and MCF-7-shp53α cells; while ZR75-1-shΔ40p53 cells were less similar to shNT cells than to ZR75-1-shp53α cells.

Differentially methylated probe analysis was performed on each subline compared to their corresponding control subline and the results are summarized in Table 4.1. When compared to MCF7-LeGO cells, there were 131860 DMPs in MCF-7-Δ40p53 cells; when compared to MCF-7-shNT cells, there were 156745 and 177772 DMPs in MCF-7-shΔ40p53 and MCF-7-shp53α cells respectively; and when compared to ZR75-1-shNT cells, there were 134158 and 123675 DMPs in ZR75-1-shΔ40p53 and ZR75-1-shp53α cells respectively. In MCF-7 cells, the lowest number of DMPs was found in the Δ40p53-overexpression cell line, followed by the Δ40p53-knockdown cell line, whilst p53αknockdown had the highest number of DMPs (> 1.3 fold of DMPs in MCF-7-Δ40p53). In ZR75-1 cells, the numbers of DMPs when knocking down Δ40p53 and p53α were similar (134158 and 123675 respectively). These results showed that the influence of isoform knockdown are cell-line dependent, where p53α-knockdown altered the methylation profile to a greater extent in MCF-7 cells and Δ40p53knockdown altered the methylation profile to a greater extent in ZR75-1 cells.

Assessment of the genomic location of the DMPs showed that these were mostly located within the gene body (32-45%) and the intergenic regions (IGR) (32-52%). This was followed by the occurrences in the TSS1500 (1500 bp upstream of the transcription starting site, 10-17%), followed by the 5'UTR region (7-11%) and TSS200 (200 bp upstream of the transcription starting site) (~5%) (Table 4.1). DMPs occurred rarely at the 3'UTR and were less common in the first exon, suggesting the majority of DMPs in the gene body are actually further downstream of the transcription start sites. Overall, the methylation affected similar UCSC Gene groups in all contrasted conditions. We next looked whether the DMPs occurred within annotated CpG islands using the annotation "Relation to USCS CpG Islands". Table 4.1 showed that most CpG-island-associated DMPs are located within the gene body. In ZR75-1 sublines, over 11% of all DMPs were located within CpG islands and in MCF-7 sublines about 9% of DMPs were located within CpG islands when compared to the control sublines. In MCF-7 cells, 8.4% of DMPs were located in CpG islands in MCF-7-shp53α, which was slightly lower than those in MCF-7shΔ40p53 cells when compared to the shNT cells, and in MCF-7-Δ40p53 cells when compared to LeGO cells (9.08% and 9.05% respectively); suggesting that knockdown of p53α has a smaller impact on the methylation of CpG sites methylation within the CpG islands.

Of all CpG sites, the proportion of hypomethylated and hypermethylated probes were different when comparing the isoform-altered sublines to their corresponding control sublines (Table 4.2). In MCF-7 cells, 50.66% probes were hypomethylated and 49.34% probes were hypermethylated when Δ40p53 was overexpressed and when Δ40p53 was knocked down in MCF-7 cells, 38.95% probes were hypomethylated and 61.05% probes were hypermethylated. When p53α was knocked down, fewer (24.17%) probes were hypomethylated and a higher number (75.83%) of probes were hypermethylated when compared to Δ40p53 knockdown. These results indicate that knockdown of

either isoform in MCF-7 cells has a different impact on single probe methylation compared to Δ40p53overexpression, which resulted in an almost equal number of hypomethylated and hypermethylated probes. In ZR75-1 cells, the number of hypomethylated and hypermethylated probes found to be differentially regulated when comparing the p53α-knockdown cells to shNT cells were almost equal, but when Δ40p53 was knocked down, more hypermethylated probes (67.12%) and less hypomethylated probes (32.88%) were found, showing a different influence of isoforms in the alteration of single probe methylation profiles in ZR75-1 cells.

4.4.2 Differentially methylated regions

Changes in the methylation status of an individual CpG island is not likely to reflect changes in neighbouring gene expression. It was therefore important to consider methylation changes across entire regulatory regions. Therefore, we performed differentially methylated region (DMR) analysis using the Probe lasso method (260), specifying a minimum 1000 bp distance between two DMRs, a minimum 50 bp DMR size and a minimum of 5 DMPs within one DMR.

The aforementioned analysis identified 103, 173, and 259 DMRs when overexpressing Δ40p53, knocking down Δ40p53 and knocking down p53α in MCF-7 sublines compared to the corresponding controls respectively. Moreover, 189 and 179 DMRs were detected when knocking down Δ40p53 and p53α in ZR75-1 cells compared to the shNT controls respectively (Table 4.2). Knockdown of p53α in MCF-7 cells led to the largest number of DMRs in MCF-7 although not in ZR75-1 cells (Table 4.2), emphasizing the greater impact of p53α on methylation landscapes in MCF-7 cells. Interestingly, there was no correlation between the number of DMPs and the number of DMRs in either cell line (Table 4.2). For example, the number of DMP were similar in Δ40p53-overexpressing MCF-7 cells and both knockdown sublines of ZR75-1 cells, however, corresponding numbers of DMRs in Δ40p53overexpressing MCF-7 cells were almost half of the number of DMRs of isoform-altered ZR75-1 cells. This suggests methylation changes at single probe locations when overexpressing Δ40p53 were quite sporadic. Table 4.2 also lists the hypermethylated and hypomethylated regions within each subline in comparison to the corresponding control sublines. Sixty hypomethylated regions (58.25%) and 43 (41.75%) hypermethylated regions were found when overexpressing Δ40p53 in MCF-7 cells. Knockdown of either Δ40p53 or p53α in MCF-7 cells resulted in a fold increase between two-three in hypermethylated regions compared to hypomethylated regions. In ZR75-1 cells, the number of the hypermethylated regions was similar to that of the hypomethylated regions (~50%).

To identify the specific genes likely affected by DNA methylation changes, the Homo sapiens (human) genome assembly GRCh37 (hg19) was used to annotate the DMRs and define differentially methylated genes (DMGs). Venn diagrams of DMGs comparing isoform-altered sublines with their corresponding

controls are shown in Figures 4.1B-E. There were 87, 147 and 219 DMGs when overexpressing Δ40p53, knocking down Δ40p53 and knocking down p53α respectively in MCF-7 cells (Figure 4.1B). When comparing MCF-7-shΔ40p53 and MCF-7-shp53α to the shNT cells there were 90 DMGs in common, accounting for approximately half of all DMGs, indicating that knockdown of either p53 isoform affected a high proportion of the same genes. Thirty-six out of 87 DMGs when overexpressing Δ40p53 were found in common with DMGs when knocking down Δ40p53 (Figure 4.1B) and 45 out of 87 DMGs were found in common with DMGs when knocking down p53α. There were 29 DMGs found to be differentially methylated in all MCF-7 isoform-altered cells. There were 155 and 146 DMGs when knocking down Δ40p53 and p53α in ZR75-1 cells, and 73 DMGs were in common, which is about 50% of the DMGs between p53α-knockdown and Δ40p53-knockdown when compared to shNT. Knockdown of either isoform in both MCF-7 and ZR75-1 cells showed an about 50% overlap of DMGs (Figure 4.1C).

To further investigate the impact of altered DMG expression on biological processes, functional classifications were derived using Panther from the overrepresented gene lists. Analyses were performed with the 90 and 73 common DMGs between Δ40p53 and p53α-knockdown in MCF-7 (Figure 4.2A) and ZR75-1 (Figure 4.2B) respectively. The category "Cellular process" contained the highest number of DMGs (25 and 18 out of 44 DMGs in MCF-7 and ZR75-1 respectively). Subcategory classification of Cellular process highlighted processes including cell communication, cell cycle, cell death, cellular component, cellular developmental process, cellular metabolic process, cellular response to stimulus, execution phase of apoptosis, protein folding and signal transduction (Figures 4.2C and 4.2D for MCF-7 and ZR75-1, respectively). The overrepresentation of genes falling into each of the subcategories were very similar, indicating that in MCF-7 and ZR75-1 cells, knocking down either isoform affected similar cellular processes.

To delve further into the genes most commonly affected when the Δ40p53 isoform were altered, further pairwise comparisons were made between all Δ40p53 isoform-modified cells, both MCF-7 and ZR75-1 cells, and their respective controls as shown in the Venn diagram (Figure 4.1D). Further comparisons were made between DMGs observed between MCF-7 Δ40p53 and controls versus changes in both MCF-7 and ZR75-1 p53α knockdown cell lines (Figure 4.1E). By this analysis, limited genes were found in common; whilst 44 DMGs were found in when knocking down Δ40p53 between MCF-7 and ZR75-1 cells, the same number of DMGs were found when knocking down p53α between these two cell lines. Panther gene list analysis was used to illustrate the classification of biological process of the common DMGs between MCF-7 and ZR75-1 when Δ40p53 was knocked down (Figure 4.3A) and when p53α was knocked down (Figure 4.3B). As before, most genes in each test were classified into the category "Cellular process") (11 for Δ40p53-knockdown and 14 for

p53αknockdown). Subcategories of cellular process were shown in Figure 4.3C and D for Δ40p53- and p53αknockdown. Two DMGs were categorised as "cellular response to stimulus" and "signal transduction" when knocking down Δ40p53 (Figure 4.3C). They are *UBD* (ubiquitin D) and *RAB1B* (Ras-related protein Rab-1B, RAS oncogene family), with the former being hypermethylated (Δβ = 0.031) compared to shNT cells, and the latter being hypomethylated (Δβ = -.0.103) in MCF-7 but hypermethylated in ZR75-1 compared (Δβ = 0.073) to shNT cells, where Δβ indicates the regional average difference compared to shNT cells (Δβ = 0.1 or -0.1 indicate 10% hypermethylation or 10% hypomethylation). When knocking down p53α, five common DMGs between MCF-7 and ZR75-1 cells were categorised as "cellular response to stimulus" and "signal transduction" (Figure 4.3D). They are *CCRL2* (C-C chemokine receptor), *TSHR* (Thyrotropin receptor), *UBD*, *GPR133* (Adhesion G-protein coupled receptor D1) and *PLA2G6* (Neurodegeneration With Brain Iron Accumulation 2), with the first three being hypermethylated when p53α was knocked down (Δβ ranging from 0.02 to 0.2), and the last one being hypomethylated (Δβ = -0.07 for MCF-7 and Δβ = -0.03 for ZR75-1). Note that Δβ values are the average difference of the indicated DMR region with at least 5 DMPs, which are significant between selected contrasts based on the *p*-value, therefore a small Δβ value was expected.

4.4.3 GSEA pathway analysis of differentially methylated regions

To better understand the biological significance of the DMR-associated genes. GSEA was performed using the ChAMP pipeline, which downloaded the information from MSigDB (The Molecular Signatures Database) and Fishers exact test was performed to calculate enrichment status of the pathways, and significantly enriched pathways (adjusted *p* value < 0.05) were returned.

By this analysis, there were 14, 36 and 103 enriched pathways when Δ40p53 was overexpressed, Δ40p53 was knocked down and p53α was knocked down in MCF-7 cells; and 49 and 44 when Δ40p53 was knocked down and when p53α was knocked down in ZR75-1 cells. The full table can be found in Appendix 3 and 4 including genes and the *p*-values, and concise tables are shown in Table 4.4 for MCF7 and Table 4.5 for ZR75-1. Pathways were interpreted by consulting the GSEA database from the Broad Institute (261, 262) and listed in column "Description". Pathways in all contrasts were arranged by similarity with color-coding and selected pathways were followed by included gene symbols shaded grey. There were three GSEA categories found in all contrasts of MCF-7 cells (Table 4.3 yellow) and 17 and 34 common categories between Δ40p53-knockdown and p53α-knockdown in MCF-7 and ZR75-1 respectively (Table 4.3 and 4.4 ,green). Only one GSEA category "chr6p21" was found in all 5 contrasts and was indicated in bold/italic red characters (Table 4.3 and 4.4), which is a cytoband region on chromosome 6. The associated genes within each of the contrasts were also listed in Table 4.3 and 4.4, and shared a high level of similarity among contrasts (*LTA, TNF, TNXB* and TRIM family, to name a few). This indicates that isoform-alteration has a global impact on this region.

When comparing p53α-knockdwon to shNT cells, three more GSEA categories were found in common when comparing between MCF-7 and ZR75-1 cells, these being "BENPORATH_ES_WITH_H3K27ME3", "CAGGTG_V$E12_Q6" and "TGGAAA_V$NFAT_Q4_01". BENPORATH_ES_WITH_H3K27ME3 includes genes with the trimethylated H3K27 mark in the promoters of embryo stem cell transcriptional regulators, and the last two include genes associated with E-box binding motif CAGGTG and TGGAAA, and are related to transcription factor and T-cell maturation, demonstrating a connection between p53α-knockdown and these biological activities. There were no other overlapping enriched pathways when isoforms were knocked down between MCF-7 and ZR75-1 cells. The common pathways when Δ40p53 or p53α was knocked down included transcription factor binding, immune and inflammation response, Cytoxan sensitivity, etc. in MCF-7 cells; while in ZR75-1 cells the enriched pathways were associated with micro-RNA, developmental process, stem cell features and membrane-associated components. These results showed that the pathways that both isoforms were involved in were quite different. The common pathways between contrast MCF-7-Δ40p53 vs. MCF-7-LeGO and contrast MCF-7-shp53α and MCF-7 shNT included genes associated with hepatocellular carcinoma, Type 1 diabetes and genes with low CpG density promoters but bearing a trimethylation mark (Figure 4.3, blue). The common pathways between contrast MCF-7-Δ40p53 vs. MCF-7-LeGO and contrast MCF-7shΔ40p53 and MCF-7 shNT included genes associated with micro-RNA (Figure 4.3, purple).

Distinctive pathways were indicated in Table 4.3 and 4.4 with no shading. The unique pathways when overexpressing Δ40p53 were cell fate commitment, module_543 (annexin, MHCII and lectins) and transcription factor binding (Figure 4.3). Unique pathways when knocking down Δ40p53 in MCF-7 were involved in several cancers (liver, melanoma and prostate) and binding including NFκB binding. A large number of unique pathways enriched when p53α was knocked down included multiple cancerrelated subcategories, organ development (breast, heart, muscle, etc.), DNA-binding, stress responses, immune responses and apoptosis. In ZR75-1 cells, unique enriched pathways when knocking down Δ40p53 included metabolism, immune responses, transcription factor binding, and mostly membrane components, and unique pathways enriched when knocking down p53α in ZR75-1 cells included transcription factor binding, myc-associated proliferation and several breast cancer-associated categories (Table .4.4).

These GSEA results showed that isoform alterations in p53 isoforms affected similar but also distinct biological activities.

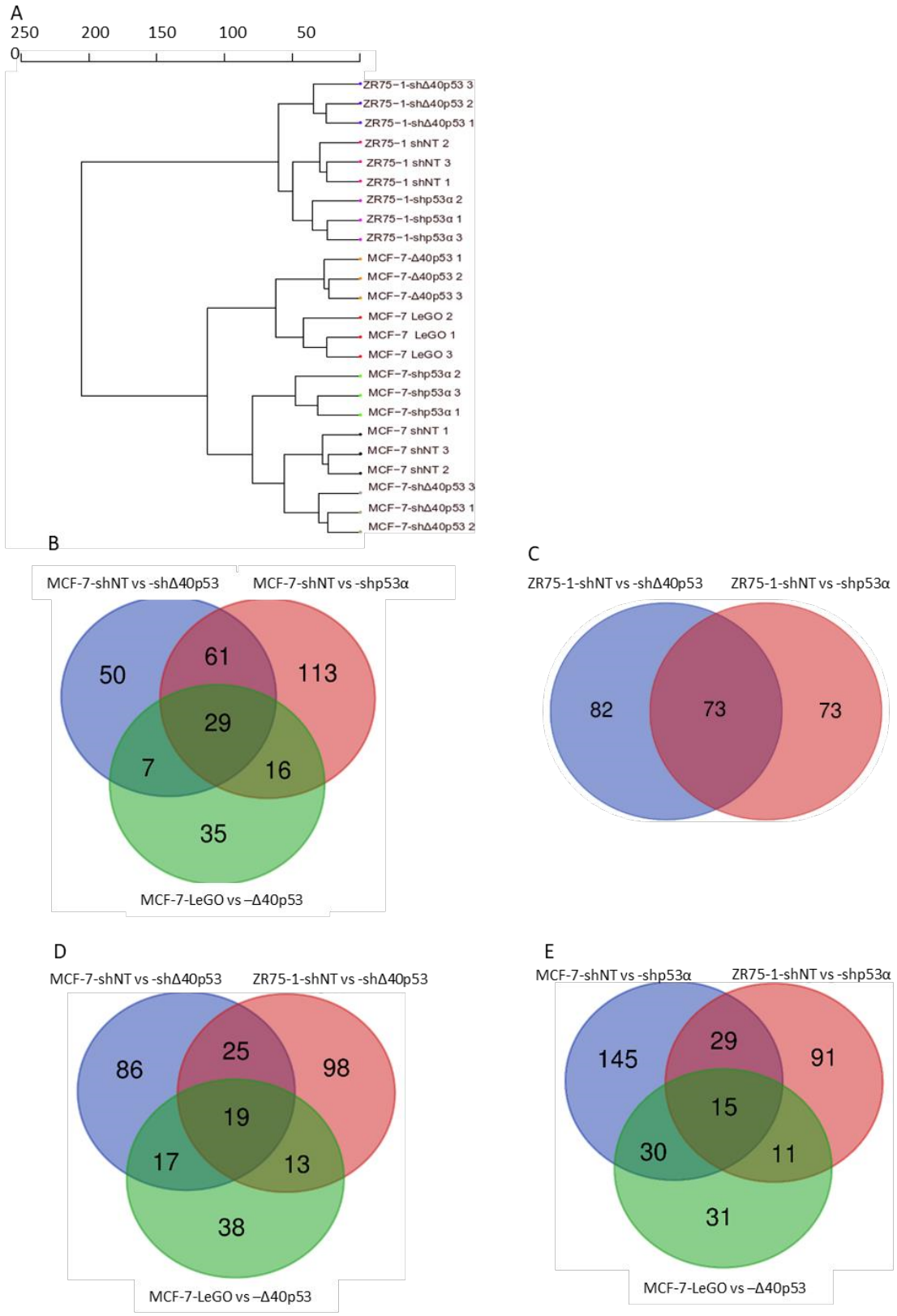

Figure 4.1 Overview of sample clusters and commonality between genes associated with differentially methylated regions. A, Dendrogram of clusters of all samples (in triplicates). B-E, commonality between isoform altered DMRassociated genes when compared to the corresponding controls in MCF-7/ZR75-1 cells or between MCF-7 and ZR75-1 cells.

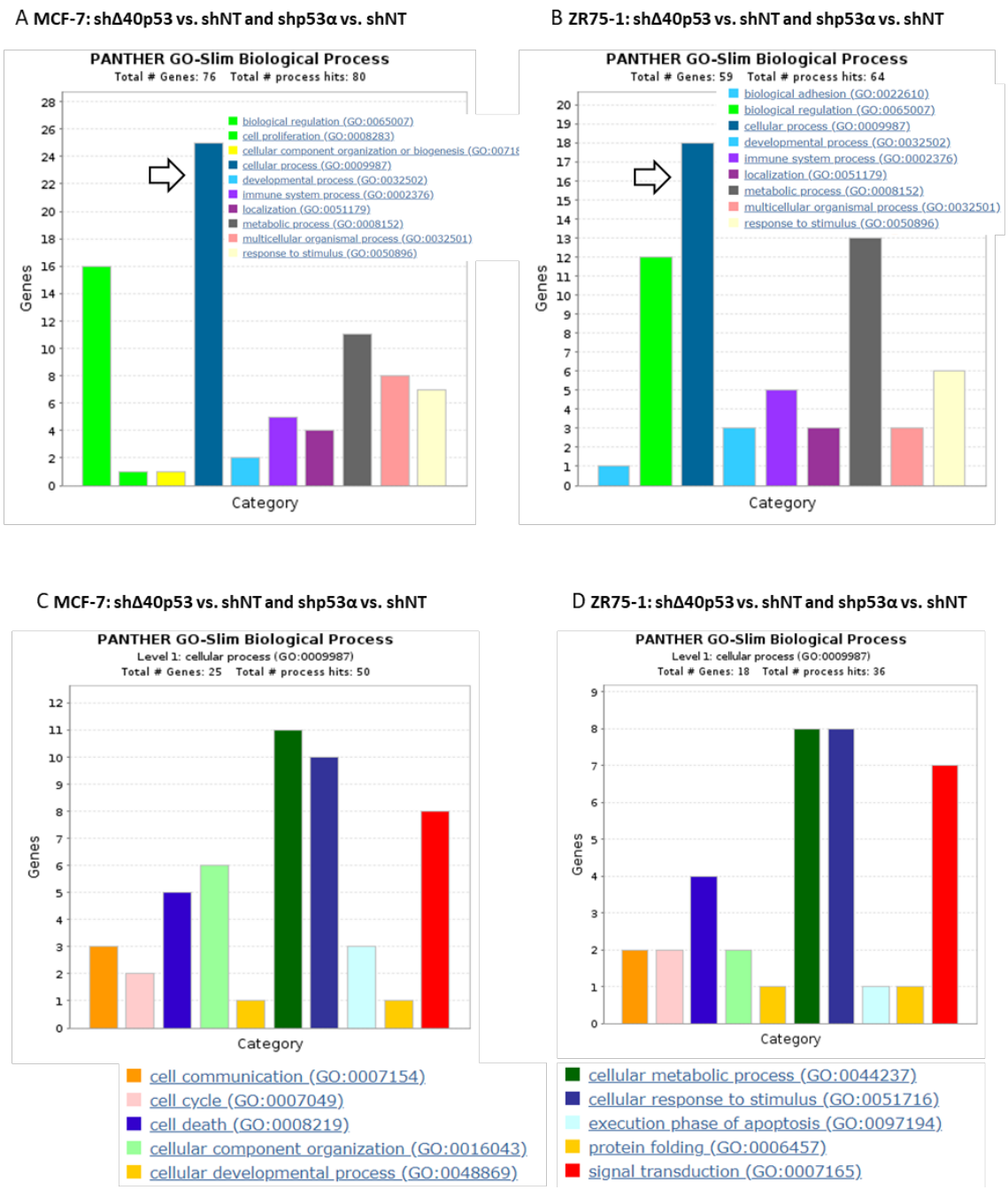

Figure 4.2 Functional classification of common genes associated with identified DMRs between Δ40p53-knockdown and p53α knockdown within MCF-7 and ZR75-1 cells. A and B, common genes classified by Panther GO-Slim biological process with categories indicated by colour, and the number of genes of such categories can be read from the Y-axis. C and D, category cellular processes with the highest number of genes (indicated with arrows) were further classified into subcategories

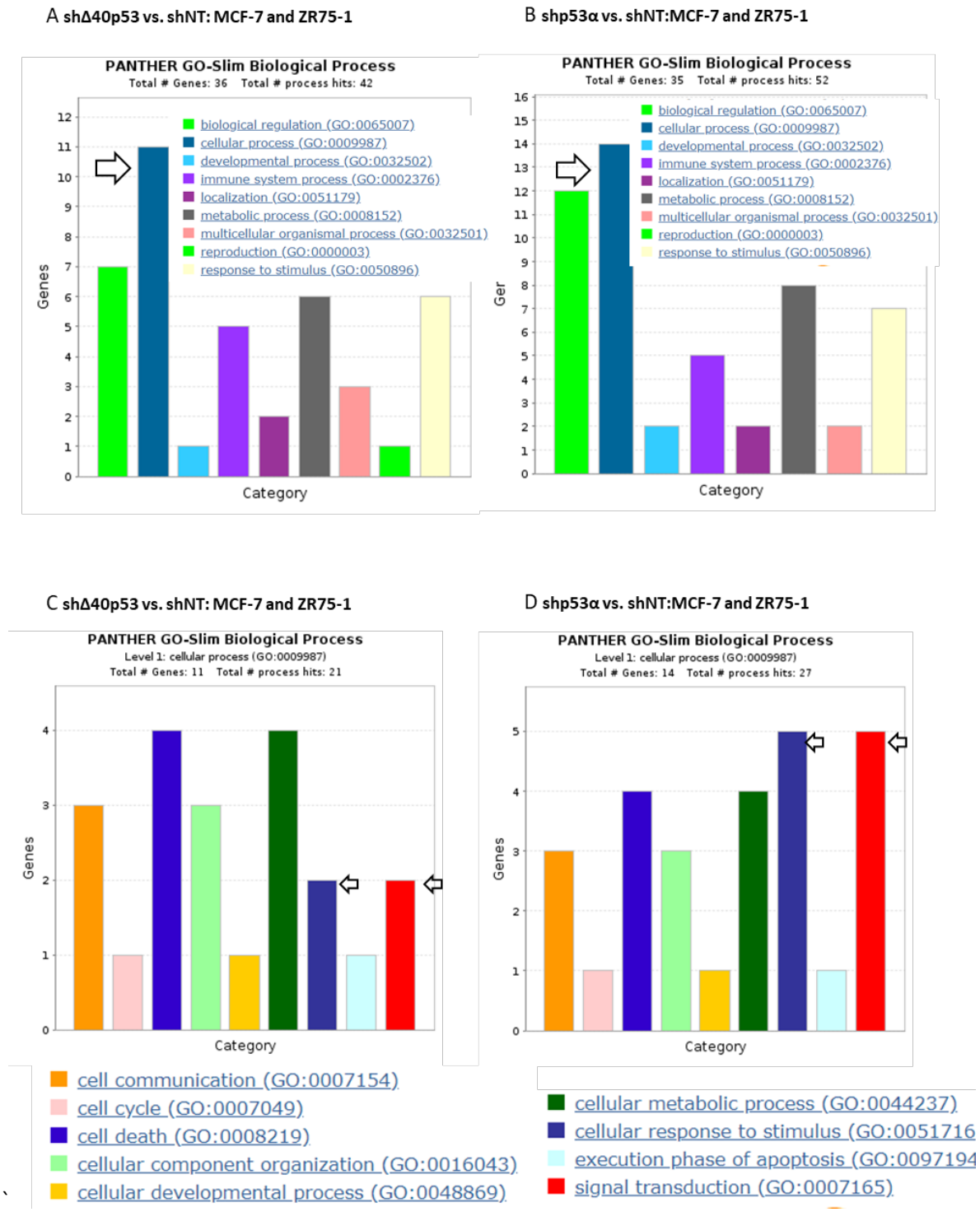

Figure 4.3 Functional classification of common genes associated with identified DMRs between MCF-7 and ZR75-1 when knocking down Δ40p53 or p53α. A and B, common genes classified by Panther GO-Slim biological process with categories indicated by colour, and the number of genes of such categories can be read from the Y-axis. C and D, category cellular processes with the highest number of genes (indicated with arrows) were further classified into subcategories. Two subcategories (cellular response to stimulus and signal transduction) showed different proportions between Δ40p53 or p53α-knockdown.

Table

4.1 Differentially expressed probes (DMPs) by altered isoforms in MCF-7 and ZR75-1 cells.

UCSC Gene Group	Relation to UCSC CpG Island	MCF-7									ZR75-1					
		Δ40p53 vs LeGO			shΔ40p53 vs shNT			shp53α vs shNT			shΔ40p53 vs shNT			shp53α vs shNT		
		Count		%	Count		%	Count		%	Count		%	Count		%
Body	Body-island	3608	46086	34.95	3960	53012	40.20	3991	58209	44.14	4442	47337	35.90	4317	43429	32.94
	Body-opensea	32439			37981			42542			32636			29274		
	Body-shelf	3283			3648			3828			3514			3286		
	Body-shore	6756			7423			7848			6745			6552		
TSS1500 (1500 bp upstream of TSS)	TSS1500-island	1879	16675	12.65	2168	19370	14.69	2393	22526	17.08	2230	16530	12.54	2143	15663	11.88
	TSS1500-opensea	5501			6422			7536			5414			4911		
	TSS1500-shelf	465			523			536			473			464		
	TSS1500-shore	8830			10257			12061			8413			8145		
TSS200 (200 bp upstream of TSS)	TSS200-island	1474	5349	4.06	1943	6672	5.06	2108	7386	5.60	2203	6421	4.87	2061	5948	4.51
	TSS200-opensea	2313			2840			3284			2441			2228		
	TSS200-shelf	182			210			214			237			202		
	TSS200-shore	1380			1679			1780			1540			1457		
5'UTR	5'UTR-island	1179	9811	7.44	1507	11807	8.95	1591	13308	10.09	1533	10585	8.03	1383	9448	7.17
	5'UTR-opensea	5682			6941			7870			5959			5274		
	5'UTR-shelf	800			890			978			913			787		
	5'UTR-shore	2150			2469			2869			2180			2004		
1stExon	3'UTR-island	211	2942	2.23	202	3091	2.34	245	3387	2.57	261	2806	2.13	262	2571	1.95
	3'UTR-opensea	1864			2052			2241			1753			1537		
	3'UTR-shelf	265			265			275			250			225		
	3'UTR-shore	602			572			626			542			547		
ExonBnd	1stExon-island	914	2512	1.91	1202	3084	2.34	1275	3433	2.60	1281	2931	2.22	1039	2571	1.95
	1stExon-opensea	1048			1246			1464			1097			990		
	1stExon-shelf	75			86			105			79			80		
	1stExon-shore	475			550			589			474			462		
3'UTR	ExonBnd-island	12	753	0.57	13	735	0.56	17	845	0.64	12	673	0.51	12	594	0.45
	ExonBnd-opensea	642			643			741			568			492		
	ExonBnd-shelf	46			32			25			47			39		
	ExonBnd-shore	53			47			62			46			51		
IGR (intergenic regions)	IGR-island	2696	47732	36.20	3194	58974	44.72	3310	68678	52.08	3411	46875	35.55	3209	43451	32.95
	IGR-opensea	36588			46102			54730			35245			32313		
	IGR-shelf	3881			4347			4842			3662			3435		
	IGR-shore	4567			5331			5796			4557			4494		
Sum	islands	11973	-	9.08	14189	-	9.05	14930	-	8.40	15373	-	11.46	14426	-	11.66

Table

(relation to UCSC CpG island)	opensea	86080	-	65.28	104227	-	66.49	120408	-	67.73	85113	-	63.44	77019	-	62.28
	shelf	8998	-	6.82	10001	-	6.38	10803	-	6.08	9175	-	6.84	8518	-	6.89
	shore	24813	-	18.82	28328	-	18.07	31631	-	17.79	24497	-	18.26	23712	-	19.17
Total		131860			156745			177772			134158			123675		

4.2 Summaries of hypomethylated and hypermethylated probes and regions by altered isoforms in MCF-7 and ZR75-1 cells.

Comparison between Sublines		**MCF-7**						**ZR75-1**			
		Δ40p53 vs LeGO		**shΔ40p53 vs shNT**		**Shp53α vs shNT**		**shΔ40p53 vs shNT**		**Shp53α vs shNT**	
		count	%	count	%	count	%	count	%	count	%
DMP compared to control sublines	Hypomethylated	66792	50.66	61060	38.95	42969	24.17	44113	32.88	62414	50.47
	hypermethylated	65068	49.34	95685	61.05	134803	75.83	90045	67.12	61261	49.53
Total DMPs		131860		156745		177772		134158		123675	
DMR compared to control sublines	Hypomethylated	60	58.25	64	36.99	65	25.10	79	41.80	93	51.96
	hypermethylated	43	41.75	109	63.01	194	74.90	110	58.20	86	48.04
Total DMRs		103		173		259		189		179	

Table

4.3 GSEA pathways with descriptions when isoform levels were altered in MCF-7 cells.

MCF-7-Δ40p53 vs. MCF-7-LeGO	MCF-7-shΔ40p53 vs. MCF-7-shNT	MCF-7-shp53α vs. MCF-7 shNT	Short description if applicable
BRIDEAU_IMPRINTED_GENES	BRIDEAU_IMPRINTED_GENES	BRIDEAU_IMPRINTED_GENES	
chr6p21	***chr6p21***	***chr6p21***	
RXRB; HLA-DRA; PPT2; MAS1L; TRIM15; TRIM10; SLC44A4; NEU1; DPCR1; SYNGAP1; HLA-DMB; GPSM3; VARS; PRRT1; NOTCH4; COL11A2; PBX2; RNF39; TRIM40; PSMB9; LTA; TNF; TNXB	ZNF192P1; DDAH2; HLA-DRA; PPT2; DAXX; EGFL8; TRIM10; C2; HSD17B8; HLA-J; UBD; HCG4; GPSM3; VARS; FKBPL; CFB; GPX5; COL11A2; PBX2; TRIM38; ATF6B; LTA; BTNL2; TNF; TNXB	ZNF192P1; DDAH2; HLA-DRA; PPT2; LY6G5C; DAXX; MAS1L; ZBTB9; SKIV2L; TRIM15; TRIM10; C2; HSD17B8; PPP1R10; HLA-J; HLA-DMB; UBD; GPSM3; FKBPL; CFB; NOTCH4; GPX5; COL11A2; OR2H1; PLA2G7; PBX2; ATF6B; LTA; DDR1; TNF; TAP2; TNXB	
GGGAGGRR_V$MAZ_Q6	GGGAGGRR_V$MAZ_Q6	GGGAGGRR_V$MAZ_Q6	Genes with 3'UTR containing motif GGGAGGRR which matches annotation for MAZ: MYC-associated zinc finger protein (purine-binding transcription factor)
	AACTTT_UNKNOWN	AACTTT_UNKNOWN	
	CATTGTYY_V$SOX9_B1	CATTGTYY_V$SOX9_B1	Genes with 3'UTR containing motif CATTGTYY which matches annotation for SOX9: SRY (sex determining region Y)-box 9 (campomelic dysplasia, autosomal sex-reversal)
	CTTTGA_V$LEF1_Q2	CTTTGA_V$LEF1_Q2	Genes with 3'UTR containing motif CTTTGA which matches annotation for LEF1: lymphoid enhancer-binding factor 1
	MODULE_84	MODULE_84	Immune (humoral) and inflammatory response.
	POTTI_CYTOXAN_SENSITIVITY	POTTI_CYTOXAN_SENSITIVITY	
	TAATTA_V$CHX10_01	TAATTA_V$CHX10_01	Genes with 3'UTR containing motif TAATTA which matches annotation for VSX1: visual system homeobox 1 homolog, CHX10-like (zebrafish)
	TGATTTRY_V$GFI1_01	TGATTTRY_V$GFI1_01	Genes having at least one occurence of the highly conserved motif M94 TGATTTRY sites. The motif matches transcription factor binding site V$GFI1_01 (v7.4 TRANSFAC).
	V$AFP1_Q6	V$AFP1_Q6	Genes with 3'UTR containing motif ATTAAYTRCAC which matches annotation for ZHX2: transcription factor ZHX2
	V$CEBPDELTA_Q6	V$CEBPDELTA_Q6	Genes with 3'UTR containing motif MATTKCNTMAYY which matches annotation for CEBPD: CCAAT/enhancer binding protein (C/EBP), delta
	V$COMP1_01	V$COMP1_01	Genes with 3'UTR containing motif NVTNWTGATTGACNACAAVARRBN which matches annotation for MYOG: myogenin (myogenic factor 4)

Table

	V$NFKAPPAB_01	V$NFKAPPAB_01	Genes having at least one occurence of the transcription factor binding site V$NFKAPPAB_01 (v7.4 TRANSFAC) in the regions spanning up to 4 kb around their transcription starting sites.
	V$NKX61_01	V$NKX61_01	
	V$PAX4_02	V$PAX4_02	Genes with 3'UTR containing motif NAAWAATTANS which matches annotation for PAX4: paired box gene 4
	YCATTAA_UNKNOWN	YCATTAA_UNKNOWN	
CERVERA_SDHB_TARGETS_1_DN		CERVERA_SDHB_TARGETS_1_DN	Genes turned off in Hep3B cells (hepatocellular carcinoma, HCC)

KEGG_TYPE_I_DIABETES_MELLITUS		KEGG_TYPE_I_DIABETES_MELLITUS	
MIKKELSEN_MCV6_LCP_WITH_H3K4ME3		MIKKELSEN_MCV6_LCP_WITH_H3K4ME3	Genes with low-CpG-density promoters (LCP) bearing the tri-methylation mark at H3K4 (H3K4me3) in MCV6 cells (embryonic fibroblasts trapped in a differentiated state).
ATATGCA.MIR-448	ATATGCA.MIR-448		
chr5q31	chr5q31		
GGGACCA.MIR-133A.MIR-133B	GGGACCA.MIR-133A.MIR-133B		
TCCAGAG.MIR-518C	TCCAGAG.MIR-518C		
CELL_FATE_COMMITMENT			
chr6q23			
MODULE_543			Annexin, MHCII, and lectins.
V$AR_03			Genes having at least one occurence of the transcription factor binding site V$AR_03 (v7.4 TRANSFAC) in the regions spanning up to 4 kb around their transcription starting sites.
	ACEVEDO_LIVER_CANCER_WITH_H3K27ME3_DN		
	CAGTATT.MIR-200B.MIR-200C.MIR429		
	CHIARADONNA_NEOPLASTIC_TRANSFORMATION_KRAS_DN		
	FIGUEROA_AML_METHYLATION_CLUSTER_3_UP		
	KEGG_MELANOGENESIS		
	MIKKELSEN_MCV6_ICP_WITH_H3K27ME3		Genes with intermediate-CpG-density promoters (ICP) bearing the trimethylation mark at H3K27 (H3K27me3) in MCV6 cells (embryonic fibroblasts trapped in a differentiated state).
	SCHAEFFER_PROSTATE_DEVELOPMENT_AND_CANCER_BOX1_DN		
	TGTTTGY_V$HNF3_Q6		Genes with 3'UTR containing motif TGTTTGY which matches annotation for FOXA1: forkhead box A1
	TRANSC_FACT		

	V$AP1_Q2_01		Genes with 3'UTR containing motif TGACTCANNSKN which matches annotation for JUN: v-jun sarcoma virus 17 oncogene homolog (avian)
	V$GFI1_01		Genes with 3'UTR containing motif NNNNNNNAAATCACWGYNNNNNNN which matches annotation for GFI1: growth factor independent 1
	V$HFH8_01		Genes having at least one occurence of the transcription factor binding site V$HFH8_01 (v7.4 TRANSFAC) in the regions spanning up to 4 kb around their transcription starting sites.
	V$NFKB_Q6_01		Genes having at least one occurence of the transcription factor binding site V$NFKB_Q6_01 (v7.4 TRANSFAC) in the regions spanning up to 4 kb around their transcription starting sites.

	WGTTNNNNNAAA_UNKNOWN		
	YAATNRNNNYNATT_UNKNOWN		
		ACEVEDO_METHYLATED_IN_LIVER_CANCER_DN	
		ANATOMICAL_STRUCTURE_DEVELOPMENT	
		APOPTOSIS_GO	
		ARGGGTTAA_UNKNOWN	
		ATGCAGT.MIR-217	
		AZARE_NEOPLASTIC_TRANSFORMATION_BY_STAT3_DN	
		BENPORATH_EED_TARGETS	Set 'Eed targets': genes identified by ChIP on chip as targets of the Polycomb protein EED [GeneID=8726] in human embryonic stem cells.
		BENPORATH_ES_WITH_H3K27ME3	Set 'H3K27 bound': genes posessing the trimethylated H3K27 (H3K27me3) mark in their promoters in Set 'Core 9': 'embryonic stem cell' transcription regulators that are preferentially and coordinately overexpressed in the highgrade, ER-negative breast cancer tumors.
		NEUROD1; MAPT; SFRP1; ZIC4; ESR1; FLRT2; SLC6A3; MSC; RPS6KA2; SLC24A4; EYA4; CD8A; FOXF2; EGFLAM; CRMP1; ALX4; PITX2; PTPRN2; NGF; TWIST1; IGFBP3; FLI1; CHST8; SLITRK3; CSMD2; CHN2; ZEB2; DLX5; CACNB4	

		BENPORATH_SUZ12_TARGETS	Set 'Suz12 targets': genes identified by ChIP on chip as targets of the Polycomb protein SUZ12 [GeneID=23512] in human embryonic stem cells.
		BOQUEST_STEM_CELL_UP	
		CAGGTG_V$E12_Q6	Genes with 3'UTR containing motif CAGGTG which matches annotation for TCF3: Transcription factor 3 (E2A immunoglobulin enhancer binding factors E12/E47)
		TRIM15; CRMP1; ALX4; DDR1; DDAH2; PPT2; MAPT; GNAS; TMEM105; ZEB2; AFF3; ZIC4; MTNR1A; ESR1; SNCA; BMP7; NOS1; ITPR2; NEUROD1; SLITRK3; PAK6; SDPR; LTA; FGF1; STRA6; PLA2G6; MSC; EYA4; CHST8; NGF; MGAT5B; LY6G5C; ELAVL4; SLC7A8; PDE4B; GCNT3; SFRP1; COL11A2; PHYHIP; LDB3; GHDC	
		CELL_DEVELOPMENT	
		CHEN_METABOLIC_SYNDROM_NETWORK	
		DAVICIONI_RHABDOMYOSARCOMA_PAX_FOXO1_FUSION_DN	
		EGFR1	
		FULCHER_INFLAMMATORY_RESPONSE_LECTIN_VS_LPS_DN	
		GATAAGR_V$GATA_C	Genes with 3'UTR containing motif GATAAGR. Motif does not match any known transcription factor
		GAURNIER_PSMD4_TARGETS	
		GNF2_DNM1 HELLER_SILENCED_BY_METHYLATION_UP	Neighborhood of DNM1 dynamin 1 in the GNF2 expression compendium
		KAAB_HEART_ATRIUM_VS_VENTRICLE_UP	
		KAYO_CALORIE_RESTRICTION_MUSCLE_DN	
		LIM_MAMMARY_LUMINAL_MATURE_DN	
		MALIK_REPRESSED_BY_ESTROGEN	Genes consistently and robustly repressed by estradiol [PubChem=5757] in MCF7 cells (breast cancer); this reperession was prevented by fulvestrant [PubChem=3478439].
		MCLACHLAN_DENTAL_CARIES_DN	

		MCLACHLAN_DENTAL_CARIES_UP	
		MEISSNER_NPC_HCP_WITH_H3K4ME2_AND_H3K27ME3	Genes with high-CpG-density promoters (HCP) bearing histone H3 dimethylation mark at K4 (H3K4me2) and trimethylation mark at K27 (H3K27me3) in neural precursor cells (NPC).
		MIKKELSEN_ES_ICP_WITH_H3K27ME3	
		MODULE_1	Ovary genes.
		MODULE_100	Genes in the cancer module 100.
		MODULE_11	Genes in the cancer module 11
		MODULE_117	Signaling
		MODULE_118	cell line expressed genes.
		MODULE_12	Spinal cord (neuro-development) genes
		MODULE_137	CNS genes
		MODULE_2	DRG (dorsal root ganglia) genes
		MODULE_220	Developmental processes
		MODULE_23	Liver genes - metabolism and xenobiotics
		MODULE_41	Genes in the cancer module 41.
		MODULE_44	Thymus genes
		MODULE_45	Whole blood genes
		MODULE_55	Genes in the cancer module 55
		MODULE_6	Trachea genes
		MODULE_66	Genes in the cancer module 66
		MODULE_88	Heart, liver, kidney and pancreas metabolic and xenobiotic response genes
		MOREAUX_MULTIPLE_MYELOMA_BY_TACI_UP	
		MULTICELLULAR_ORGANISMAL_DEVELOPMENT	
		PLASMA_MEMBRANE	
		PROGRAMMED_CELL_DEATH	

		QI_HYPOXIA_TARGETS_OF_HIF1A_AND_FOXA2	
		REACTOME_INITIAL_TRIGGERING_OF_COMPLEMENT	
		REGULATION_OF_APOPTOSIS	
		REGULATION_OF_DEVELOPMENTAL_PROCESS	
		REGULATION_OF_PROGRAMMED_CELL_DEATH	
		RPS14_DN.V1_UP	Genes up-regulated in CD34+ hematopoietic progenitor cells after knockdown of RPS14 [GeneID=6208] by RNAi.
		RTTTNNNYTGGM_UNKNOWN	
		RYTTCCTG_V$ETS2_B	Genes with 3'UTR containing motif RYTTCCTG which matches annotation for ETS2: v-ets erythroblastosis virus E26 oncogene homolog 2 (avian)
		SCHAEFFER_PROSTATE_DEVELOPMENT_12HR_DN	
		SCHUETZ_BREAST_CANCER_DUCTAL_INVASIVE_UP	
		SHEPARD_BMYB_MORPHOLINO_DN	
		SMID_BREAST_CANCER_LUMINAL_B_DN	
		SMID_BREAST_CANCER_NORMAL_LIKE_UP	
		SNF5_DN.V1_DN	Genes down-regulated in MEF cells (embryonic fibroblasts) with knockout of SNF5 [GeneID=6598] gene.
		ST_ADRENERGIC	
		ST_G_ALPHA_I_PATHWAY	G alpha i Pathway
		ST_MYOCYTE_AD_PATHWAY	
		TARTE_PLASMA_CELL_VS_PLASMABLAST_UP	
		TGGAAA_V$NFAT_Q4_01	Genes with 3'UTR containing motif TGGAAA which matches annotation for NFAT: nuclear factor of activated T-cells.

		□ FOXF2; LRRC2; UBD; TNF; FLI1; PPT2; GNAS; CREM; ZEB2; AFF3; ZIC4; ESR1; ADCY2; TWIST1; NOS1; RBFOX1; SLITRK3; CALD1; TNXB; DBN1; RIN2; CYFIP2; NGF; IGFBP3; EGFLAM; PPP1R10; ELAVL4; SLC7A8; PDE4B; TNFAIP8; CREB5; ADORA1; PITX2; TREX1; CCDC80; LDB3	
		TTGTTT_V$FOXO4_01	Genes with 3'UTR containing motif TTGTTT which matches annotation for MLLT7: myeloid/lymphoid or mixed-lineage leukemia (trithorax homolog, Drosophila); translocated to, 7
		V$ALPHACP1_01	Genes having at least one occurence of the transcription factor binding site V$ALPHACP1_01 (v7.4 TRANSFAC) in the regions spanning up to 4 kb around their transcription starting sites.
		V$CEBP_01	Genes with 3'UTR containing motif NNTKTGGWNANNN which matches annotation for CEBPA: CCAAT/enhancer binding protein (C/EBP), alpha
		V$CP2_01	Genes with 3'UTR containing motif GCHCDAMCCAG which matches annotation for TFCP2: transcription factor CP2
		V$FOXD3_01	Genes with 3'UTR containing motif NAWTGTTTRTTT which matches annotation for FOXD3: forkhead box D3
		V$GATA1_03	Genes with 3'UTR containing motif ANGNDGATAANNGN which matches annotation for GATA1: GATA binding protein 1 (globin transcription factor 1)
		V$GATA1_04	Genes with 3'UTR containing motif ANGNDGATAANNGN which matches annotation for GATA1: GATA binding protein 1 (globin transcription factor 1)
		V$GATA1_05	Genes with 3'UTR containing motif ANGNDGATAANNGN which matches annotation for GATA1: GATA binding protein 1 (globin transcription factor 1)
		V$GATA3_01	Genes with 3'UTR containing motif NNGATARNG which matches annotation for GATA3: GATA binding protein 3
		V$IRF7_01	Genes with 3'UTR containing motif TNSGAAWNCGAAANTNNN which matches annotation for IRF7: interferon regulatory factor 7
		V$LHX3_01	Genes with 3'UTR containing motif AATTAATTAA which matches annotation for LHX3: LIM homeobox 3
		V$MEIS1AHOXA9_01	Genes having at least one occurence of the transcription factor binding site V$MEIS1AHOXA9_01 (v7.4 TRANSFAC) in the regions spanning up to 4 kb around their transcription starting sites.
		V$NKX62_Q2	Genes with 3'UTR containing motif NWADTAAWTANN which matches annotation for NKX6-2: NK6 transcription factor related, locus 2 (Drosophila)
		WOO_LIVER_CANCER_RECURRENCE_UP	

		YOSHIMURA_MAPK8_TARGETS_UP	

Common pathways are indicated by colours: yellow, present in all MCF-7 sublines with alteration of isoforms; green, present in MCF-7 cells with Δ40p53/p53α-knockdown; blue, present in MCF-7 with Δ40p53-overexpression and p53α-knockdown; purple, present in MCF-7 with Δ40p53-overexpression and p53α-knockdown. Pathways enriched in ZR75-1 cells are indicated with red bold italic characters with associated genes of each contrast listed in cells below with grey shading. Full table can be find in Appendix 3.

Table 4.4 GSEA enriched pathways with descriptions when isoform levels were altered in ZR75-1 cells.

ZR75-1-shΔ40p53 vs. ZR75-1-shNT	ZR75-1-shp53α vs. ZR75-1 shNT	Short description if applicable
AAGCACA,MIR-218	AAGCACA,MIR-218	
ACCAATC,MIR-509	**ACCAATC,MIR-509**	
AGCACTT,MIR-93,MIR-302A,MIR-302B,MIR-302C,MIR-302D,MIR372,MIR-373,MIR-520E,MIR-520A,MIR-526B,MIR-520B,MIR-520C,MIR-520D	AGCACTT,MIR-93,MIR-302A,MIR-302B,MIR-302C,MIR-302D,MIR372,MIR-373,MIR-520E,MIR-520A,MIR-526B,MIR-520B,MIR-520C,MIR-520D	
AGGGCAG,MIR-18A	AGGGCAG,MIR-18A	
ANATOMICAL_STRUCTURE_DEVELOPMENT	ANATOMICAL_STRUCTURE_DEVELOPMENT	
ATGTAGC,MIR-221,MIR-222	ATGTAGC,MIR-221,MIR-222	
ATTCTTT,MIR-186	ATTCTTT,MIR-186	
CACTTTG,MIR-520G,MIR-520H	CACTTTG,MIR-520G,MIR-520H	
CAGCACT,MIR-512-3P	CAGCACT,MIR-512-3P	
CAGCTTT,MIR-320	CAGCTTT,MIR-320	
chr5q31	chr5q31	
chr6p21	***chr6p21***	
DDAH2; RXRB; HLA-DRA; PPT2; EGFL8; TRIM15; TRIM10; DOM3Z; C2; SLC44A4; RGL2; HLA-J; HLA-E; NEU1; STK19; EHMT2; ZNF311; SYNGAP1; GABBR1; UBD; GPSM3; PRRT1; CFB; PSORS1C1; NOTCH4; CDSN; GPX5; ZBTB22; OR2H1; PLA2G7; RNF39; TAPBP; TRIM31; PSMB8; LTA; TNF; TNXB	DDAH2; HLA-DRA; PPT2; GTF2H4; EGFL8; TRIM10; TRIM26; SLC44A4; RGL2; HLA-J; NEU1; EHMT2; ZNF311; SYNGAP1; VARS2; UBD; PRRT1; PSORS1C2; PSORS1C1; COL11A2; OR2H1; LTA; TNF; TNXB	

GCACTTT,MIR-17-5P,MIR-20A,MIR-106A,MIR-106B,MIR-20B,MIR-519D	GCACTTT,MIR-17-5P,MIR-20A,MIR-106A,MIR-106B,MIR-20B,MIR-519D	
GGTGTGT,MIR-329	GGTGTGT,MIR-329	
GTATTAT,MIR-369-3P	GTATTAT,MIR-369-3P	
GTGCCTT,MIR-506	GTGCCTT,MIR-506	
GTTTGTT,MIR-495	GTTTGTT,MIR-495	
INTEGRAL_TO_PLASMA_MEMBRANE	INTEGRAL_TO_PLASMA_MEMBRANE	
INTRINSIC_TO_PLASMA_MEMBRANE	INTRINSIC_TO_PLASMA_MEMBRANE	
KEGG_TYPE_I_DIABETES_MELLITUS	KEGG_TYPE_I_DIABETES_MELLITUS	
MIKKELSEN_ES_HCP_WITH_H3K27ME3	MIKKELSEN_ES_HCP_WITH_H3K27ME3	Genes with high-CpG-density promoters (HCP) bearing histone H3 K27 trimethylation mark (H327me3) in embryonic stem cells (ES).
MIKKELSEN_IPS_WITH_HCP_H3K27ME3	MIKKELSEN_IPS_WITH_HCP_H3K27ME3	Genes with high-CpG-density promoters (HCP) bearing the tri-methylation mark at H3K27 (H3K27me3) in MCV8.1 (induced pluripotent cells, iPS).
MIKKELSEN_MEF_HCP_WITH_H3_UNMETHYLATED	MIKKELSEN_MEF_HCP_WITH_H3_UNMETHYLATED	Genes with high-CpG-density promoters (HCP) with unmethylated histone H3 in MEF cells (embryonic fibroblast).
MULTICELLULAR_ORGANISMAL_DEVELOPMENT	MULTICELLULAR_ORGANISMAL_DEVELOPMENT	
NERVOUS_SYSTEM_DEVELOPMENT	NERVOUS_SYSTEM_DEVELOPMENT	
SYSTEM_DEVELOPMENT	SYSTEM_DEVELOPMENT	
TAATAAT,MIR-126	TAATAAT,MIR-126	
TCTCTCC,MIR-185	TCTCTCC,MIR-185	
TGAATGT,MIR-181A,MIR-181B,MIR181C,MIR-181D	TGAATGT,MIR-181A,MIR-181B,MIR181C,MIR-181D	
TGCACTT,MIR-519C,MIR-519B,MIR519A	TGCACTT,MIR-519C,MIR-519B,MIR519A	
TGCTGCT,MIR-15A,MIR-16,MIR15B,MIR-195,MIR-424,MIR-497	TGCTGCT,MIR-15A,MIR-16,MIR15B,MIR-195,MIR-424,MIR-497	
TGCTTTG,MIR-330	TGCTTTG,MIR-330	
TGGTGCT,MIR-29A,MIR-29B,MIR-29C	TGGTGCT,MIR-29A,MIR-29B,MIR-29C	
TTTGCAC,MIR-19A,MIR-19B	TTTGCAC,MIR-19A,MIR-19B	

INTEGRAL_TO_MEMBRANE		
INTRINSIC_TO_MEMBRANE		
MEMBRANE		
MEMBRANE_PART		
MODULE_11		Genes in the cancer module 11
MODULE_118		cell line expressed genes
MODULE_55		Genes in the cancer module 55.
MODULE_84		mmune (humoral) and inflammatory response
MODULE_88		Heart, liver, kidney and pancreas metabolic and xenobiotic response genes.
PLASMA_MEMBRANE		
PLASMA_MEMBRANE_PART		
RTAAACA_V$FREAC2_01		Genes with 3'UTR containing motif RTAAACA which matches annotation for FOXF2: forkhead box F2
V$HFH4_01		Genes with 3'UTR containing motif AWKTGTTTGTTTA which matches annotation for FOXJ1: forkhead box J1
V$POU3F2_01		Genes with 3'UTR containing motif ATGMATWWATTCAT which matches annotation for POU3F2: POU domain, class 3, transcription factor 2
YCATTAA_UNKNOWN		
	ACOSTA_PROLIFERATION_INDEPENDENT_MYC_TARGETS_DN	
	BENPORATH_ES_WITH_H3K27ME3	Set 'H3K27 bound': genes posessing the trimethylated H3K27 (H3K27me3) mark in their promoters in Set 'Core 9': 'embryonic stem cell' transcription regulators that are preferentially and coordinately overexpressed in the high-grade, ERnegative breast cancer tumors.
	LRFN5; CSMD3; SIX1; KCNIP4; GNAO1; SFRP1; ESR1; HOXA3; CDH23; KCNIP2; PTPRN2; LOC84931; TWIST1; CHST8; PRRT1; DLX5; FAM5C; SEMA3B; GUCY1A3	
	CAGGTG_V$E12_Q6	Genes with 3'UTR containing motif CAGGTG which matches annotation for TCF3: Transcription factor 3 (E2A immunoglobulin enhancer binding factors E12/E47)

	▯ SDK1; IGF2; RGL2; PCDHA6; PCDHA1; SEMA3B; CBFA2T3; ARHGAP24; DDAH2; PPT2; GUCY1A3; SIPA1; ESR1; PRDM16; GNAO1; BDNF; PSORS1C2; HOXA3; LTA; ELF5; STRA6; PCDHA10; EXPH5; KCNIP2; KCNIP4; PLA2G6; PEX10; CAST; CHST8; TNNI2; SYT8; MACF1; SFRP1; SORBS2; COL11A2; LRFN5	
	CATTGTYY_V$SOX9_B1	
	LEE_METASTASIS_AND_ALTERNATIVE_SPLICING_DN	
	TGGAAA_V$NFAT_Q4_01	Genes with 3'UTR containing motif TGGAAA which matches annotation for NFAT: nuclear factor of activated T-cells
	▯ RGL2; UBD; PCDHA6; FOXP2; TNF; FAM5C; PPT2; CREM; SIPA1; ESR1; GNAO1; BDNF; TWIST1; LGALS1; HOXA3; CALD1; TNXB; ELF5; PCDHA11; PCDHA13; KCNIP2; CAST; C1RL; KCNJ1; EHMT2; TNFAIP8; LAMB3; TREX1	
	TURASHVILI_BREAST_DUCTAL_CARCINOMA_VS_DUCTAL_NORMAL_DN	
	TURASHVILI_BREAST_LOBULAR_CARCINOMA_VS_DUCTAL_NORMAL_DN	
	V$HNF6_Q6	
	V$OCT1_Q6	Genes having at least one occurence of the transcription factor binding site V$OCT1_Q6 (v7.4 TRANSFAC) in the regions spanning up to 4 kb around their transcription starting sites.

Common pathways between Δ40p53 and p53α-knockdown are indicated in green. Pathways enriched in MCF-7 cells are indicated with red bold italic characters with associated genes of each contrast listed in cells below with grey shading. Full table can be find in Appendix 4.

4.5 Discussion

This Chapter examined the methylation profiles of the isoform-altered breast cancer cell line models established in Chapter 3. Both MCF-7 and ZR75-1 cells are classified as luminal breast cancers and both exhibit wt p53. However, the impact of manipulating p53 produced different outcomes for each cell line with respect to EMT-associated gene expression as well as functional assays. This was also reflected in RNA-seq analyses where comparisons performed at the basal level and following p53 isoform manipulations indicated that Δ40p53 and p53α regulate different sets of genes, and that endogenous isoform knockdown did not have the same effect in MCF-7 and ZR75-1 cells. However, since p53 is a transcription factor that is largely associated with stress stimuli and DNA integrity, endogenously modified p53 isoform levels may not introduce a great differences when no internal or external stress is present. The TP53 gene is reported to control epigenetic factors and the mutation status is also reported to be associated with methylation landscape of multiple cancer types, including breast cancer. We hypothesized therefore that Δ40p53 would also be involved in modulating DNA methylation.

Using microarrays in the form of the Illumina EPIC 850k BeadChip, a technology which covers >90% of the known CpG features in the human genome at single base resolution, we identified a range of 120,000-180,000 DMPs when comparing p53 isoform manipulated cells with their respective controls. The lowest number of differences in DMPs occurred between MCF-7-Δ40p53 and MCF-7-LeGO cells while the highest numbers were found when either Δ40p53 or p53α were knocked down in MCF-7 cells. It is important to point out when overexpressing or knocking down Δ40p53 occurs in a background of endogenous p53α expression, and changes in p53α accompany manipulations of Δ40p53, suggesting p53α has the most impact on the scale of methylation change in MCF-7 cells. In ZR75-1 cells in contrast, almost the same number of DMPs were identified after Δ40p53-knockdown or p53α-knockdown.

Looking at the location of DMP sites in related to genes (UCSC Gene Group) showed most were located in the gene body and IGRs. Some work has shown that gene body methylation is associated with transcript splicing and the response to environmental changes (263, 264), thus affecting the scale of gene expression. In addition, it has been reported that the gene body methylation is coupled with transcriptional elongation and affect RNA polymerase II binding to the DNA (265), thus affecting the scale of gene expression. These suggest that isoform alteration potentially altered gene transcriptions via gene body methylation. This is surprising, as the transctivation activity carried on by p53 is mostly via the p53RE located in for example the promoter region; our data, in contrast, has shown a link between p53 isoforms and change of gene body methylation. The gene body methylation is regulated by the *de novo* DNA methyltransferase (DNMT3), responsible for establishing methylation profiles

after replication. An interaction of DNMT3a and p53 has been reported, that protein interaction between p53 and DNMT3a was observed in 293T cells, where p53 lost the ability to transactivate p21 (266); in return, p53 suppressed DNMT3a expression in mouse embryo stem cells and p53 deficiency led to clone heterogeneity due to change of DNA methylation (267). The p53 isoform can potentially be involved in modulate methylation regulators. This also proposed an addition mechanism of transcription regulation mediated by p53 via gene body methylation. Another hotspot for methylation change mediated by p53 isoforms is the intergenic region (IGR). Not much was known about IGR methylation; however, IGR may contain enhancer sequences, which has been reported by multiple studies (268-270). As found by Sammons and colleagues, p53 binds to enhancers, but enhancer licensing is cell context dependent (271), and this may require other p53 family members such as p63 (272). Dynamic methylation super enhancer has been reported in embryo stem cells (273), and Δ40p53 has been reported to maintain pluripotency in embryo stem cells (211), establishing a potential link between Δ40p53 and stemness over enhancer regulation. As such, p53 isoforms may have a role regulating enhancer methylation, affecting downstream gene transactivation activities.

When looking at the methylation changes in relation to CpG clusters, the DMPs were mostly located in the islands (except opensea). DMPs in CpG islands represented about 9% of all DMPs in MCF-7 and around 11% in ZR75-1 cells, showing cell line dependent differences (Table 4.1).

The shift from DMP analysis to DMR analysis is extensively adapted recently due to statistical and biological reasons. By combining DMPs, effect size is increased, leading to increased power and effectiveness. Furthermore, DMR is more representative in certain disease and often replicates better than DMP (274, 275). Based on these DMPs, DMRs were identified using the ChAMP pipeline applying the Probe lasso method. Similarly to DMPs, the highest DMRs were observed when p53α was knocked down, whereas only 103 DMRs were found when Δ40p53 was overexpressed in MCF-7 cells. The DMP/DMR ratio when Δ40p53 was overexpressed was almost twice of that when p53α was knocked down, indicating that DMPs when overexpressing Δ40p53 were more sporadic and less ingegrated than the DMPs resulting from p53α knockdown. In fact, the DMP/DMR ratios detected after isoform knockdown in MCF-7 and ZR75-1 cells were lower than those resulting from Δ40p53-overexpression.

In Chapter 3, we reported at the basal level that there was very little commonality in differentially expressed genes between Δ40p53-knockdown or p53α knockdown within either MCF-7 or ZR75-1 cells, as well as specific knockdown between MCF-7 and ZR75-1 cells. In contrast, the methylation landscapes altered by isoform-alteration shared higher similarity, especially in isoform-knockdown cases (Figure 5.1B and C). DMR-associated genes (DMGs) were investigated by panther gene list classification function. The commonly affected genes by knockdown of either isoform in MCF-7 and

ZR75-1 cells showed similar GO biological processes (Figure 5.2). In addition, isoform-knockdown led to a good number of common DMR-associated genes between MCF-7 and ZR75-1 cells (Figure 5.1D and E). By further looking into the GO biological process term "cellular process" we observed that the methylation profiles of more genes were affected by p53α-knockdown than Δ40p53-knockdown in the subcategories "cellular response to stimulus" and "signal transduction" indicating p53αknockdown is likely to have a greater impact on the methylation of genes involved in these functions (Figure 5.3). Genes in the above two subcategories are reported to have a prognostic importance in multiple cancers, for example, UBD expression is associated with colon cancer progression and a higher disease-recurrence rate (276), which was hypermethylated by isoform-knockdown compared to the shNT cells. CCL2 was reported to be highly expressed in breast cancers, and was associated with tumour recurrence when CD14-positive tumour-associated macrophages were increased (277). P53 suppresses CCL2 by binding to the promoter region (278), but there is no report on how p53-mediated methylation can affect CCL2. *TSHR* promoter was methylated in thyroid cancers but normal thyroid tissues and benign adenomas (279), but *TP53* mutation is not common in thyroid cancers, yet a defective p53 is detected (280), indicating the methylation of *TSHR* could be regulated by other mechanisms including p53 isoforms. These results and reports promoted us to investigate the role of p53 isoforms in DNA methylation, through which gene expression can be regulated.

GSEA analysis performed with ChAMP on the DMR-associated genes gave us some insight into interpreting these methylation changes altered by Δ40p53 or p53α knockdowns. We have found a cytoband region chr6p21, which was affected by either isoform change in both MCF-7 and ZR75-1 cells compared to the corresponding control cells, and the genes in each contrast showed a number of common genes such as *TNF, LTA, TNXB, COL11A2 and HLA-DRA.* In 2013, Vijai et al. reported that chr6p21.32 was one of the susceptible regions associated with lymphoid malignancies using Affymetrix genotyping 6.0 SNP array (281); in 2017, Lee et al. reported copy number variation in chr6p21.32 in metastatic thymic adenocarcinoma (282). The hypomethylation of chr6p21.3 was reported to be associated with attenuated recurrence of high grade serous epithelial ovarian cancer via modulated immune responses (283). Here we reported an impact of p53 isoform alteration in regulating this region that included several genes of great biological significance. The tumour necrosis factors can be double-sided in cancers. TNF and LTA are both cytokines and pro-inflammatory factors that are involved in inflammation-associated carcinogenesis (284, 285). It has been proposed that TNF proteins activate NF-κB (286, 287), which inhibits carcinogen-induced cytotoxicity, facilitating malignant transformation (288). High expression of TNFα and polymorphism of LTA are reported to

be associated with breast cancers (289, 290). Wt p53 aided TNF-induced apoptosis in prostate cancer cells (291), while mutant p53 can inhibit TNF-induced apoptosis and enhance activation of NF-κB (292). A number of studies have demonstrated a role for Δ133p53 (N-terminus deletion encompassing both TADs) in inflammation. The study by Braithwaite and colleagues using mouse models showed that Δ122p53 (counterpart of Δ133p53 in humans) was pro-inflammatory and led to increased expression of pro-inflammatory cytokines (242). These studies highlight the role of p53 in regulating inflammatory events in cancers. *TNXB* and *COL11A2* encode an essential component of extracellular matrix. The former has been shown to have an anti-adhesion role thus promoting cancer cell mobility (293, 294) and the latter has been found to be affected by DNA methylation in a pan-cancer analysis (295). These facts indicates that regional methylation at chr6p21 was profoundly affected by p53 isoforms, where both isoforms are critical in modelling this event.

Three other regions were affected by p53-knockdown in both MCF-7 and ZR75-1 cells. "BENPORATH_ES_WITH_H3K27ME3" includes genes that present the H3K27 trimethylation mark in the promoters and they are transcriptional regulators primarily in embryonic stem cells and highgrade ER-negative breast cancers according to MSigDB databases. Most of the genes are transcriptional factors. The other two categories "CAGGTG_V$E12_Q6" and
"TGGAAA_V$NFAT_Q4_01" include various transcription factors presenting the two motifs CAGGTA and TGGAAA in the promoters of immunoglobulin enhancer binding factors and nuclear factors of activated T-cells. These results further supported the theory of p53α in epigenetic changes. As mentioned in Section 1.3.1.5, drugs blocking epigenetic changes have the most success in treating p53-deficient cancers, but not in cancer with wt p53 (129), suggesting a role for p53 in maintaining the stability of the methylome. Inducible pluripotent stem (iPS) cells are a good example of reprogrammed epigenetic features, where the methylation profiles of iPS cells exhibit dynamic changes during reprogramming according to a study of 22 iPS cel lines derived from five different human cell types (296). The Yakahashi reprogramming factors including SOX2 were found to have a higher efficiency in producing mouse iPS in the absence of the functional wt p53 (297), stressing the potential of p53 in DNA methylation particularly in stem cell studies. The fact that p53 expression is hardly detectable in stem cells, and is re-expressed during differentiation and organ generation through multiple epigenetic changes (297), and that Δ40p53-haploinsuffiency caused loss of mouse embryo stem cell pluripotency indicate a link between p53 isoforms and DNA methylation. However, this study is mostly carried out in stem cells studies, and most studies examined post-translational inactivation of p53 such as ATM-mediated phosphorylation at serine residue and deacetylation at lysine residue (298, 299). The direct effect on methylation by p53 has not been looked at. Our results

supported a role for p53 in DNA methylation in stem cell studies and also showed an impact on immunogenic events.

Δ40p53-overexpression had the least impact on regional DNA methylation, whereas Δ40p53 and p53α knockdown in both MCF-7 and ZR75-1 cells showed a greater overlap of enriched pathways (18 and 34 respectively) (Table 4.3 and 4.4), showing p53α and Δ40p53 knockdown commonly affected DNA methylation in these biological pathways including development, immune and inflammation responses and binding of transcription factors. This is not surprising given the discussion above that p53 and Δ40p53 was involved in developmental processes and that p53 is involved in antiinflammation-induced carcinogenesis. However, these pathways were also cell line distinct. Particularly in ZR75-1 cells, membrane-associated genes exhibited methylation changes, including *PTPRN2* and *PCDH.* PTPRN2 is reported to promote cell migration by actin-remodelling in mice (300) and PCDH family members are involved in generating multiple cadherins, which are critical membrane proteins mediating cell-cell connection and cell-matrix connection (301). This is in good agreement with the morphological changes altered by Δ40p53-knockdown in Chapter 3, indicating these morphological changes were governed by DNA methylation.

The uniquely enriched pathways were investigated to dissect the functions by Δ40p53 or p53α knockdown in MCF-7 and ZR75-1 cells. Most of the enriched pathways were again associated with developmental processes and transcription factor binding, however in different sub-categories. Notably, isoform-knockdown in ZR75-1 cells affected a much greater number of micro-RNA via DNA methylation. p53 has been reported to activate miR-34a and miR-145 (302), suppressing reprogramming factors, and miR-34a can stabilize p53 by suppressing SIRT1 (122). However, regulation of micro-RNA by p53-mediated methylation has not been investigated. Δ40p53-knockdown in both MCF-7 and ZR75-1 cells exhibited genes associated with cancers and immune responses, but in different GSEA modules. P53α-knockdown in both MCF-7 and ZR75-1 cells were enriched in oncogene regulation and multiple cancer types, where p53α-knockdown in ZR75-1 cells preferentially affected breast cancer-associated genes and p53α-knockdown in MCF-7 cells affected genes in more cancer types including breast cancer and liver cancer. In addition, p53α-knockdown also affected DNA methylation of genes involved in apoptosis and programmed cell death. These genes include *DDAH2, DAXX, APOE, CASP8, SNCA* and *ADORA1,* among which the first three were hypomethylated, and the last three were hypermethylated. Of note, DDAH2 (dimethylarginine dimethylaminohydrolase 2) has been reported to promote invasiveness of lung adenocarcinoma (303), and CASP8 (caspase 8) is a wellestablished p53-dependent apoptosis regulator (103, 304). This correlation of increased malignancy and decreased apoptosis in MCF-7-shp53α has been described in Chapter 3 by RNA-seq, and here again, we showed that DNA methylation also contributes to this effect in MCF-7 cells.

To summarise, in this Chapter we showed that DNA methylation was affected by p53 isoforms in inflammation, development, and cancers. The affected genes were cell line dependent. This Chapter has identified a new role for the Δ40p53 isoform in the regulation of gene methylation in unstressed conditions.

Chapter 5
Investigation of the functional role of Δ40p53/p53α in response to DNA-damaging agents

Chapter 5 Investigation of the functional role of **Δ**40p53/p53**α** in response to DNA-damaging agents

5.1 Introduction

In Chapter 3, cell models with stable knockdown of Δ40p53 or p53α were established using MCF-7 and ZR75-1 cells. Knockdown of p53α in both cell lines increased cell migration/invasion and enriched for genes affecting the extracellular components, indicating a dominant role for full-length p53 in these processes. However, we found cell line dependent effects at the basal level when knocking down Δ40p53 in MCF-7 or ZR75-1 cells regarding EMT and cell migration/invasion. In Chapter 4, we investigated the methylation profiles of these breast cancer cell line models and found p53αknockdown affected the highest number of differentially methylated regions compared to the control cells in both MCF-7 and ZR75-1; Δ40p53-knockdown, on the other hand, had diverse effects on methylation alteration. Altered isoforms mostly affected genes involved in immune responses, signal transduction and multiple binding proteins. These experiments were performed with no external stimulation or treatment. An essential aspect of p53 in tumour suppression lies in the fact that p53 reacts to various stress stimuli to induce downstream responses accordingly, thereby maintaining genomic stability (89, 90). There have been reports of an independent role for Δ40p53 in inducing G2 arrest in response to ER stress, while p53α induced G1 arrest but was not required for G2 arrest (160). To date, there have been no studies which have analysed the effect of endogenous alterations in the Δ40p53/p53α ratio in response to DNA damage. It is possible that the shift between Δ40p53 and p53α will have an impact on the decision of cell fate in response to DNA damage.

In this Chapter, we investigated how alterations in the endogenous expression of Δ40p53 or p53α affect the response of breast cancer cells to two commonly used DNA-damaging therapies used to treat the disease, cisplatin (CDDP) and doxorubicin (DOX) and that have been reported to be involved in p53-dependent pathways. Cisplatin intercalates into the DNA and introduces breaks (305, 306), while doxorubicin attacks topoisomerase II during the DNA synthesis phase (307), both resulting in DNA damage. p53 is activated in response to the damage and may lead to DNA repair, cell cycle arrest or apoptosis, but the contribution of endogenous Δ40p53 in this context is not known.

5.2 Aim

We hypothesise that the ratio of Δ40p53/p53α will affect the response to DNA damage. Therefore, the main aim of this Chapter was to determine whether cells treated with DNA-damaging agents have an outcome that is associated with altered Δ40p53/p53α ratio. Specifically, by using our cell line models, the aims were:

144

(1) To investigate the function of Δ40p53 in regulating the cell cycle in response to CDDP/DOX;
(2) To investigate the function of Δ40p53 in apoptosis in response to CDDP/DOX;
(3) To investigate the function of Δ40p53 in p53-dependent gene regulation in response to the DNA-damaging agents CDDP/DOX.

5.3 Approach

In Chapter 3, we established cell line models using MCF-7 and ZR75-1 with stable knockdown of Δ40p53 or p53α. Together with the Δ40p53-overexpression MCF-7 cells, we tested whether EMTrelated functions and EMT-related gene expression were altered by p53 isoform expression at the basal level. In this Chapter, these sublines were treated with physiological relevant concentrations of the DNA damaging agents CDDP and DOX.

Cell cycle analysis was performed using propidium iodide (PI) staining on treated cells. PI intercalates into the DNA double strand with no sequence preference, proportionally reflecting the content of DNA. By running the stained cells on a flow cytometer, cell cycle information of untreated and treated cells was obtained. Given the fact that p53 and Δ40p53 were reported to have different roles on G1 and G2 phases respectively (160), the relative change of cell populations at G1 and G2 phases was studied by normalizing to the untreated cells at the corresponding phases of each subline and comparing the scale of changes when the p53 isoform levels were altered.

We next attempted to investigate the apoptotic differences introduced by altered isoform expression level in response to DNA-damaging agents. Since these cells were adherent and the process of PI staining including typsinization, fixation and multiple washes might introduce variability, we performed real-time Annexin V assays. Annexin V detects deformed early apoptotic cells by binding to exposed cytosolic phosphatidylserine (PS), and by conjugating with a fluorescent dye or a luminescent signal, apoptosis can be quantified in real-time, with minimal disturbance of the cells. As shown in Chapter 3, ZR75-1-derived cells had changed morphology, especially the ZR75-1-shΔ40p53 cells which grew in an aggregative manner, therefore confluence-based assays were not applicable. The IncuCyte Red Annexin V Reagent (apoptotic cells quantitated by red fluorescent cell count) was used for the MCF-7 sublines. MCF-7 sublines were grown to 30~40% confluence then treated with 1 mM CDDP or 1 μM DOX and monitored by the IncuCyte in both phase and red fluorescent channels. The Annexin V positive counts were normalized to the confluence of the corresponding subline at corresponding time points. The Promega RealTime-Glo Annexin V Assay (apoptotic cells quantitated by luminescent value) was used for ZR75-1 sublines. All ZR75-1 sublines were seeded at 20,000 cells per well for 24 h and treated with 1 mM CDDP or 1 μM DOX with the Annexin luminescent assay

reagents. Luminescent Annexin V signal was measured every 24 h from 0 h (commencement of treatment). The luminescent value of each subline at the measured time point was normalised to the untreated cells of the same subline at the same time point, therefore the slopes represent how rapid apoptosis occurred in response to the drugs.

To characterise the molecular mechanisms associated with altered p53 isoform ratio, including p53dependent gene expression of the pro-apoptotic markers Bax, Puma and Noxa as well as p21, western blotting and semi-quantitative real-time PCR were used.

To further characterize the molecular profiles of the cell sublines following treatment, RNA-seq was performed. RNA was extracted from cell pellets harvested from 24 hours after treatment followed by library preparation, converting to ds cDNA. The Illumina next generation sequencing method was used, followed by analysis of the data using an R-based program called Seqmonk (308). Normalized data is shown as log_2RPM, which represents the expression of a certain gene (Section 2.2.11). The DESeq2 vignette was used to filter out genes that were differentially expressed between any two groups using "likelihood ratio test" with a *p*-value cut-off set to 0.05. The results were further filtered using an intensity test to account for the statistical magnitude of effect test. The final list of genes was visualised using hierarchical clustering.

5.4 Results

5.4.1 The altered Δ40p53/p53α ratio is associated with altered G1 and G2 arrest in response to DNA-damaging agents

Initially, we performed cell cycle analysis at the basal level in the cell line models with altered levels of Δ40p53 or p53α. Figure 5.1 showed that at the basal level without treatment, transduction of p53 shRNA had no effect in MCF-7 or ZR-75-1 cells on any of the cell cycle phases when compared to the corresponding shNT control cell lines, and very little apoptosis was detected regardless of the isoform status and cell line (Appendix 1). However, the cell populations within G1 were slightly yet significantly reduced, when Δ40p53 was overexpressed in MCF-7 (Figure 5.1A, 73.40 % to 71.17 %), or knocked down in MCF-7 (Figure 5.1B, 74.70% to 66.63 %) or ZR75-1 cells (Figure 5.1C, 79.58 % to 74.25 %).

Following this, the cells were treated with physiologically relevant concentrations of CDDP and DOX (1 mM and 1 μM respectively) for 24 hours then collected for cell cycle analysis. Cell populations at G1, S and G2 after treatment were normalised to untreated cells within the same phase in order to identify the relative changes (Table 5.1).

Figure 5.2 and Table 5.1 (column G1) show that less cells were in G1 phase following treatment with both DNA-damaging agents in all sublines (except MCF-7-LeGO and MCF-7-shΔ40p53 treated with CDDP), when comparing treated groups to untreated control groups respectively, indicating a general trend of an induction in G1-S transition in response to DNA damage regardless of p53 isoform status. Overall, this reduction in G1 was much greater in response to DOX than CDDP. Knockdown of either isoform in MCF-7 cells led to a significant reduction in the G1 population. MCF-7 sublines illustrated a negative association between Δ40p53 and G1 arrest. Δ40p53 overexpression was associated with a more reduced G1 population when cells were treated with DOX but not CDDP (Figure 5.2A and B), while Δ40p53 knockdown was associated with less reduced G1 population when cells were treated with either drug (Figure 5.2C and D). These results were not seen in ZR75-1-shΔ40p53 cells in response to any drug treatments (Figure 5.2E and F). When knocking down p53α, a more reduced G1 population was seen in both MCF-7 and ZR75-1 cells treated with either drug when compared with the shNT cells, and surprisingly this pattern was similar to that of Δ40p53-overexpression in MCF-7 cells in response to DOX.

Table 5.1 Relative change of cell population at each cell cycle phase after CDDP/DOX treatment.

Treatment	**Sublines**	**G1**	**S**	**G2**
MCF-7-Δ40p53 vs MCF-7-LeGO				
CDDP	MCF-7-LeGO	0.968 ± 0.008	1.126 ± 0.079	0.926 ± 0.099
	MCF-7-Δ40p53	1.031 ± 0.006	0.995 ± 0.014*	0.847 ± 0.015
DOX	MCF-7-LeGO	0.653 ± 0.003	2.237 ± 0.026	1.672 ± 0.001
	MCF-7-Δ40p53	0.493 ± 0.018*	2.196 ± 0.022	2.324 ± 0.066*
MCF-7-shΔ40p53 and MCF-7-shp53α vs MCF-7-shNT				
CDDP	MCF-7-shNT	0.791 ± 0.012	1.569 ± 0.077	1.655 ± 0.004
	MCF-7-shΔ40p53	0.892 ± 0.014*	1.137 ± 0.112	1.298 ± 0.133
	MCF-7-shp53α	0.720 ± 0.007*	1.813 ± 0.096	2.279 ± 0.038*
DOX	MCF-7-shNT	0.511 ± 0.014	1.891 ± 0.022	2.909 ± 0.094
	MCF-7-shΔ40p53	0.642 ± 0.010*	1.101 ± 0.091*	1.993 ± 0.168*
	MCF-7-shp53α	0.366 ± 0.031*	2.531 ± 0.044*	4.165 ± 0.198*
ZR75-1-shΔ40p53 and ZR75-1-shp53α vs ZR75-1 shNT				
CDDP	ZR75-1-shNT	0.781 ± 0.013	2.432 ± 0.094	1.441 ± 0.142
	ZR75-1-shΔ40p53	0.786 ± 0.004	2.768 ± 0.125	1.027 ± 0.096*
	ZR75-1-shp53α	0.714 ± 0.011*	2.807 ± 0.133	1.711 ± 0.127
DOX	ZR75-1-shNT	0.805 ± 0.004	1.275 ± 0.118	2.262 ± 0.127
	ZR75-1-shΔ40p53	0.812 ± 0.018	1.202 ± 0.008	1.906 ± 0.099*
	ZR75-1-shp53α	0.679 ± 0.022*	1.789 ± 0.197	3.044 ± 0.044*

Cell populations at each phase after CDDP (no shading) or DOX (grey shading) treatment was normalised to cell populations prior to CDDP/DOX treatment of each sublines. Significance ($p < 0.05$, compared to the corresponding treated control sublines

at the same phase) of CDDP or DOX is indicated with *. All experiments were repeated three time in triplicate and results are the mean ± standard error of mean (SEM).

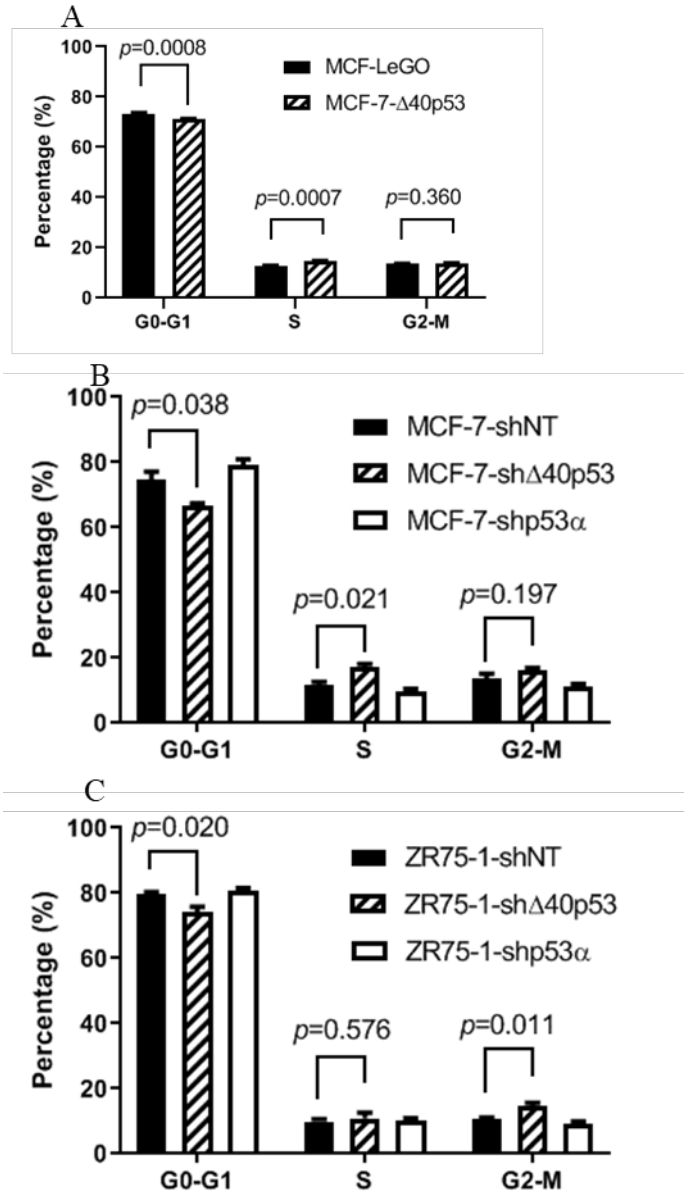

Figure 5.1 Cell cycle analysis of untreated MCF-7 and ZR75-1 sublines. Fixed cells were stained using FxCycle PI Reagent and data were acquired using a flow cytometer. Single living cells were gated out for cell cycle analysis. Gates were drawn for each phase and the percentages of cell populations of each phase were plotted as bar graph. Results were the mean of three independent experiments in triplicate and error bars indicate the standard error of the mean (SEM). Unpaired t-tests were used to identify significance and p-values are shown above the brackets.

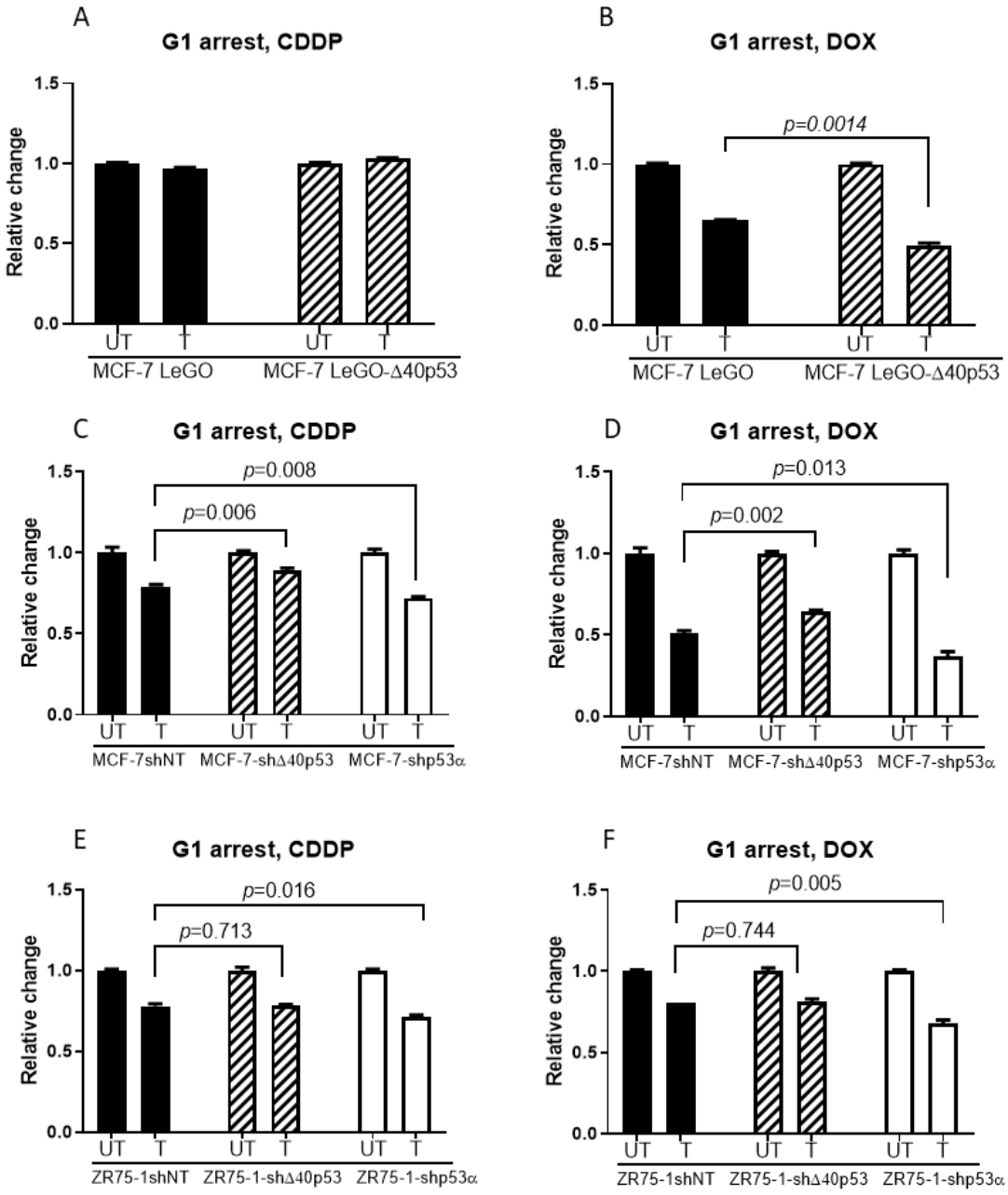

Figure 5.2 G1 arrest was not affected by the ratio of Δ40p53/p53α in MCF-7 and ZR75-1 sublines in response to CDDP and DOX. The cell population at G1 phase after treatment (UT) was normalised to that of before treatment (T). Results were the mean of three independent experiments in triplicate and error bars indicate the standard error of the mean (SEM). Unpaired t-tests were used to identify significance and p-values are shown above the brackets.

In response to either CDDP or DOX, all control cell lines underwent an increase in the proportion of cells in G2 phase of the cell cycle, with the exception of MCF-7-LeGO to CDDP (Fig 4.3, Table 5.1 column G2). Overexpression or knockdown of Δ40p53 had limited effect on G2 arrest in response to CDDP in MCF-7 cells when compared to untreated cells, while knockdown of p53 resulted in a 2.3 fold enhancement of CDDP-induced G2 arrest (Fig 4.3A and C). Similar results were observed in ZR75-1

cells, with the exception of Δ40p53, whose knockdown significantly inhibited CDDP-induced G2-arrest (Fig 4.3E). In response to DOX, overexpression of Δ40p53 significantly increased G2 arrest, while knockdown of Δ40p53 significantly inhibited G2 arrest in both MCF-7 and ZR75-1 (Fig 4.3B, D and F). In contrast, p53 knockdown significantly enhanced G2 arrest suggesting that the function of Δ40p53 and p53 in G2 arrest induced by DOX are distinct.

In response to both CDDP and DOX there was a significant increase in the proportion of cells in S-phase in the control lines (Fig 4.4, LeGO and shNT). Neither Δ40p53 nor p53 expression had a significant effect on the CDDP-induced enhancement of S-phase (Fig 4.4.A, C and E). However, there was a trend for Δ40p53 knockdown to inhibit S-phase progression, whilst p53 knockdown enhanced S-phase progression in DOX-treated cells (Fig 4.4B, D and F).

To sum up, CDDP and DOX led to a decreased cell population in G1 and an increased cell population in S and G2, but DOX had, in general, a greater effect. Δ40p53-overexpression attenuated the response to CDDP in all cell cycle phases in MCF-7 cells, while it inhibited G1 arrest and induced G2 arrest when compared to MCF-7-LeGO cells in response to DOX (Figure 5.2 and 5.3). In knockdown cell models, knockdown of p53α led to a more reduced G1 arrest and more induced G2 arrest in both MCF-7 and ZR75-1 cells under CDDP and DOX treatment when compared to treated shNT cells, which coincides with DOX-treated Δ40p53-overexpressing MCF-7 cells (Figure 5.2 and 5.3). Δ40p53-knockdown in ZR75-1 cells had limited impact on G1 and S phases, but led to less induced G2 arrest in response to both drugs. Δ40p53-knockdown affected all cell cycle phases, where the cell population was less reduced in G1 and less induced in S and G2 (Figure 5.3-5.5). Overall DOX led to a greater change in cell cycle phases in contrast to CDDP. A high Δ40p53/p53α ratio (Δ40p53-overexpression or p53αknockdown) was negatively associated with G1 arrest and positively associated with G2 arrest; while a low Δ40p53/p53α ratio (Δ40p53-knockdown) was positively associated with G1 arrest and negatively associated with G2 arrest in MCF-7 but not ZR75-1 cells. DOX-treatment had the most consistent correlation with the ratio of Δ40p53/p53α in MCF-7 cells in the overexpression and knockdown models.

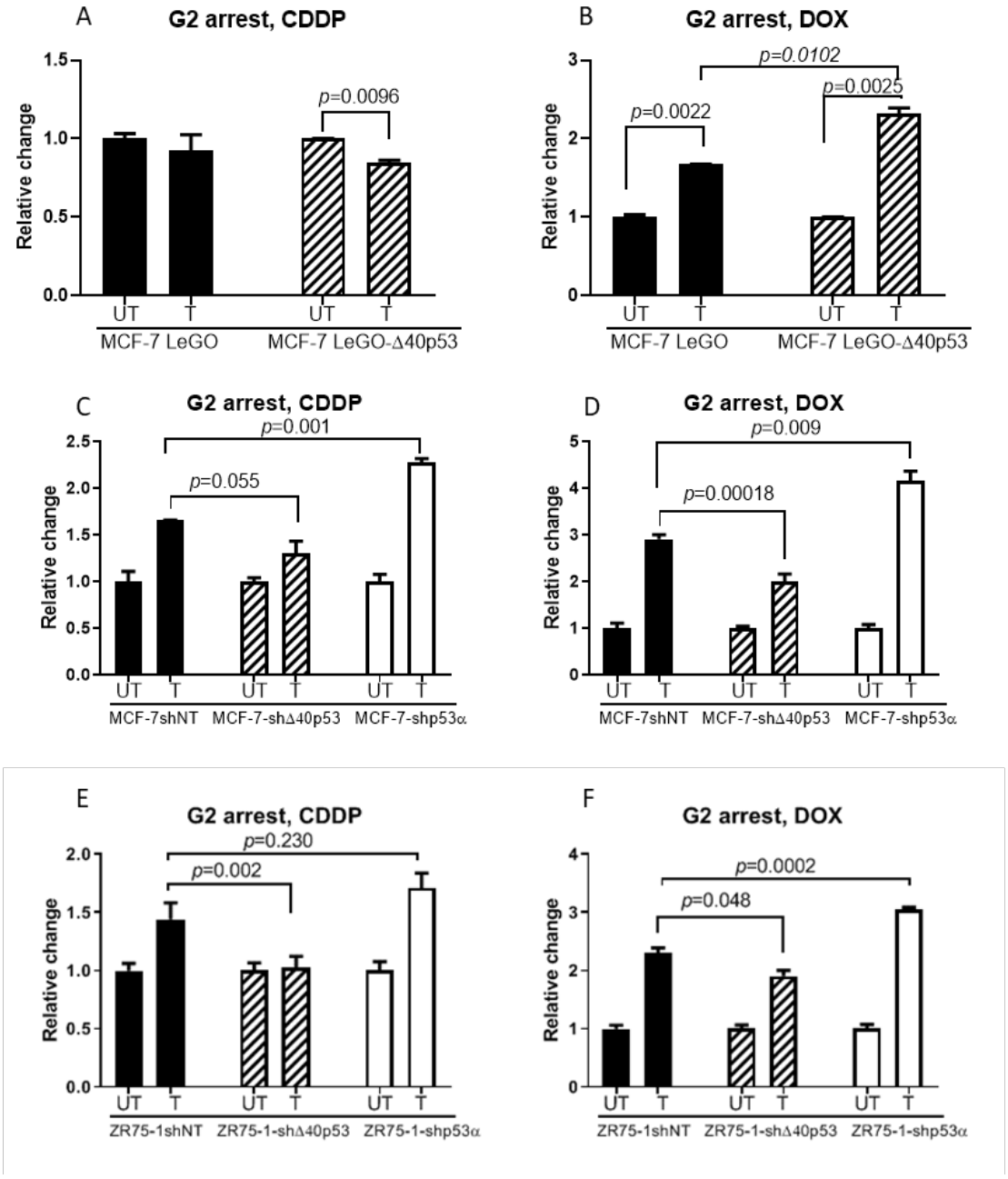

Figure 5.3 G2 arrest was affected by the ratio of Δ40p53/p53α in MCF-7 and ZR75-1 sublines in response to CDDP and DOX. The cell population at G2 phase before treatment (UT) was normalised to that of after treatment (T). Results were the mean of three independent experiments in triplicate and error bars indicate the standard error of the mean (SEM). Unpaired ttests were used to identify significance and p-values are shown with brackets.

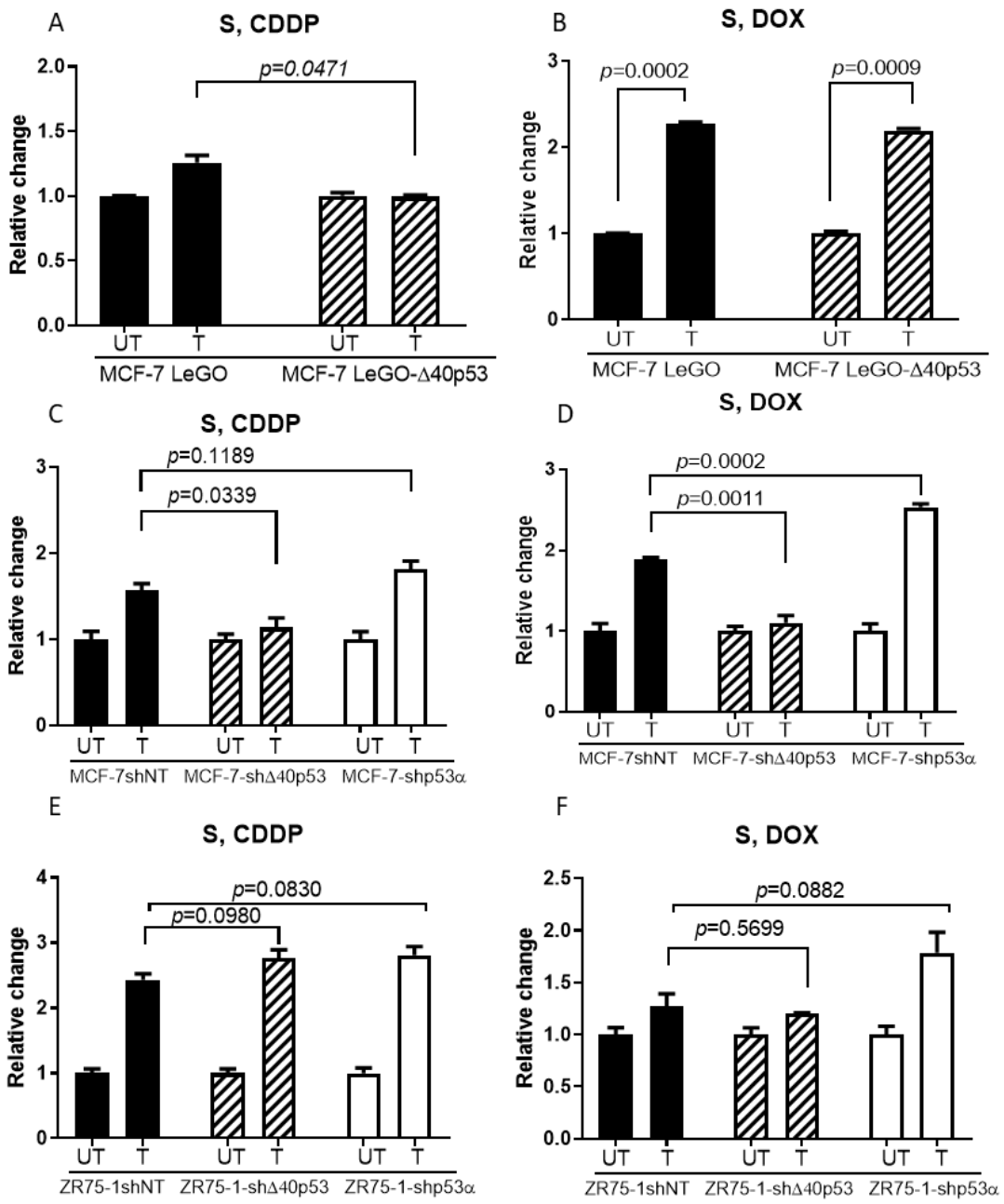

Figure 5.4 S phase was affected by the ratio of Δ40p53/p53α in MCF-7 and ZR75-1 sublines in response to CDDP and DOX. The cell population at S phase before treatment (UT) was normalised to that of after treatment (T). Results were the mean of three independent experiments in triplicate and error bars indicate the standard error of the mean (SEM). Unpaired t-tests were used to identify significance and p-values are shown with brackets.

5.4.2 Altered **Δ**40p53 and p53α expression levels are associated with apoptosis

DNA damage can lead to two outcomes: cell cycle arrest to allow DNA repair or apoptosis. We have seen in the above results that an altered Δ40p53/p53α ratio was related to cell cycle arrest at specific phases, but whether the cell repaired the damaged DNA and continued to survive or underwent apoptosis was unknown. Therefore, we investigated whether alteration in Δ40p53 or p53 expression affected apoptosis induced by these DNA-damaging agents.

All MCF-7 and ZR75-1 sublines showed increased apoptosis over time in response to both DNAdamaging drugs (Figure 5.5). In MCF-7 cells, Δ40p53 overexpression attenuated apoptosis, and Δ40p53 knockdown increased the rate of apoptosis in response to CDDP and DOX treatments. Knockdown of p53α had limited effect on the apoptosis rate when compared to shNT cells.

In ZR75-1 cells, knockdown of both Δ40p53 and p53α resulted in a significant reduction in the apoptosis rate induced by both agents when compared to NT cells, in contrast to what was observed in MCF-7 cells.

These results showed that in response to two DNA damaging agents, Δ40p53 inhibited apoptosis in MCF-7 cells but had the opposite effect in ZR75-1 cells. We therefore next focused on MCF-7 cells with stable Δ40p53-overexpression or Δ40p53/p53α-knockdown to unveil the molecular mechanisms of these contrasting results.

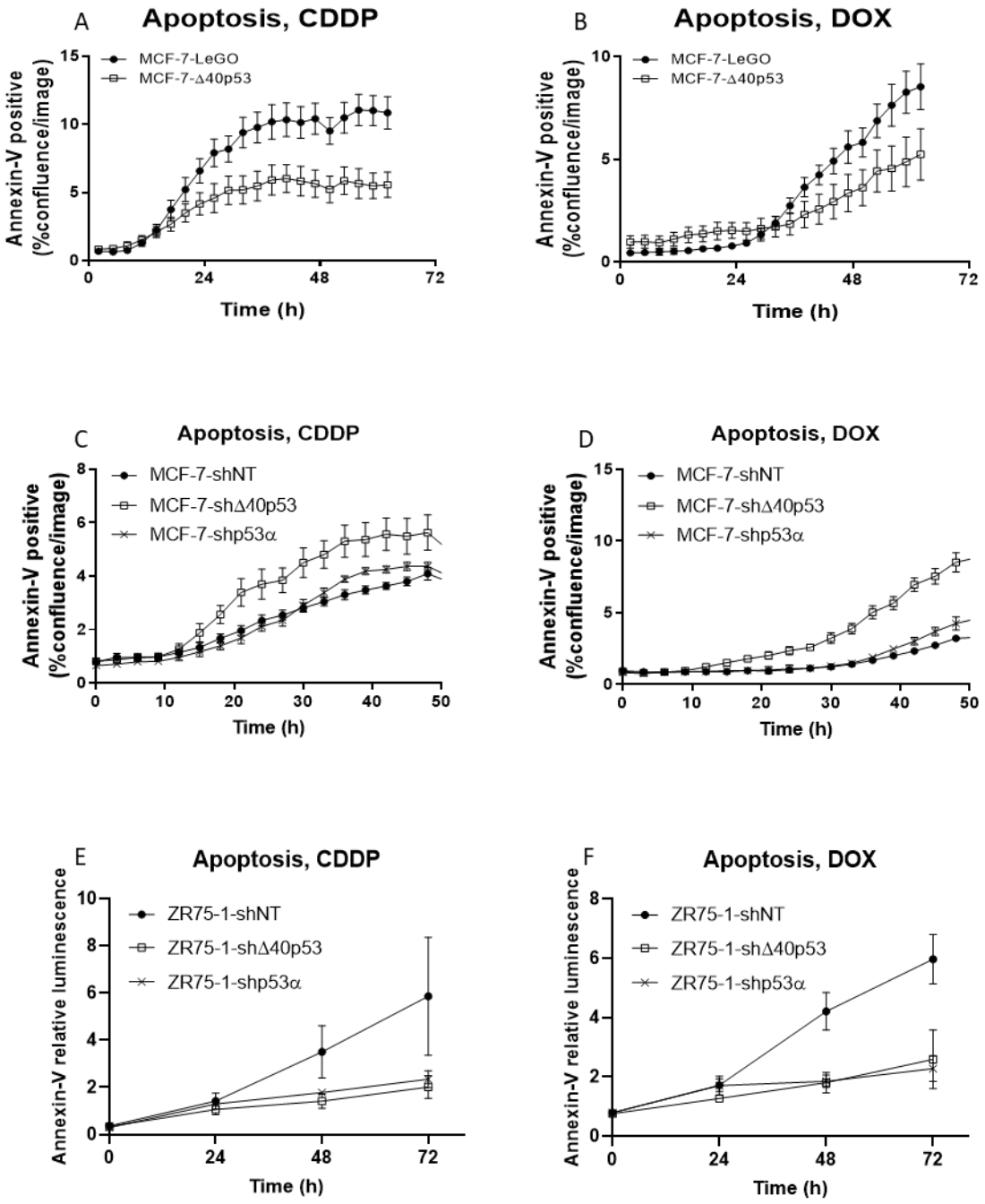

Figure 5.5 p53 isoform levels affect cell apoptosis in response to CDDP and DOX. A-D, Cell apoptosis of MCF-7 derived sublines in response to CDDP and DOX was measured using the IncuCyte Annexin V assay and positive annexin counts were normalised to the confluence at the same time points. E and F, Cell apoptosis of ZR75-1 derived sublines in response to CDDP and DOX was measured using the Promega luminescent Annexin V assay and luminescent values were normalised to the luminescent value at 0 hour for each subline. Results are from three independent experiments in triplicate and error bars are the standard deviation (SD) of the mean.

5.4.3 p53 and p53-dependent gene expression was elevated by DOX in MCF-7 cells

5.4.3.1 p53 protein level was up-regulated by DOX

The above results showed that when Δ40p53 was down-regulated in MCF-7 cells, significantly increased apoptosis was observed. To investigate the molecular mechanisms of this, the protein level of p53α was firstly examined by western blotting and the mRNA level by RT-qPCR in MCF-7 cells. Interestingly, there was a time-dependent increase in p53α levels in all MCF-7 sublines when treated with either drug, with the exception of MCF-7-Δ40p53 cells (Figure 5.6A). In MCF-7-Δ40p53 cells, elevated p53α was observed at the basal level and its expression at the protein level did not increase following DNA-damaging treatments. Only a slight increase (1.4 fold) was observed at the mRNA level in CDDP-treated cells but not following DOX. The lack of p53 induction may explain the reduced apoptosis rate observed in these cells when compared to LeGO controls (Figure 5.5A and B). Induction of p53 at the protein level following DNA damage in Δ40p53 knock down cells was significantly enhanced when compared to NT cells (Figure 5.6B) and this may explain the increased apoptosis induction in these cells. As expected, p53 was not induced by CDDP in p53 knockdown cells; and its induction was significantly delayed in DOX-treated cells (owing to incomplete p53 knockdown). A general trend of increased p53α as well as Δ40p53 expression was seen by 24 hours after drug treatment (Figure 5.6D – I), but no difference was observed between sublines and their corresponding control sublines indicating a post-transcriptional regulation on p53. Noting that the Δ40p53 primer targets intron 2, which is not present in MCF-7-Δ40p53 cells, therefore Δ40p53 mRNA level was not measured by RT-qPCR.

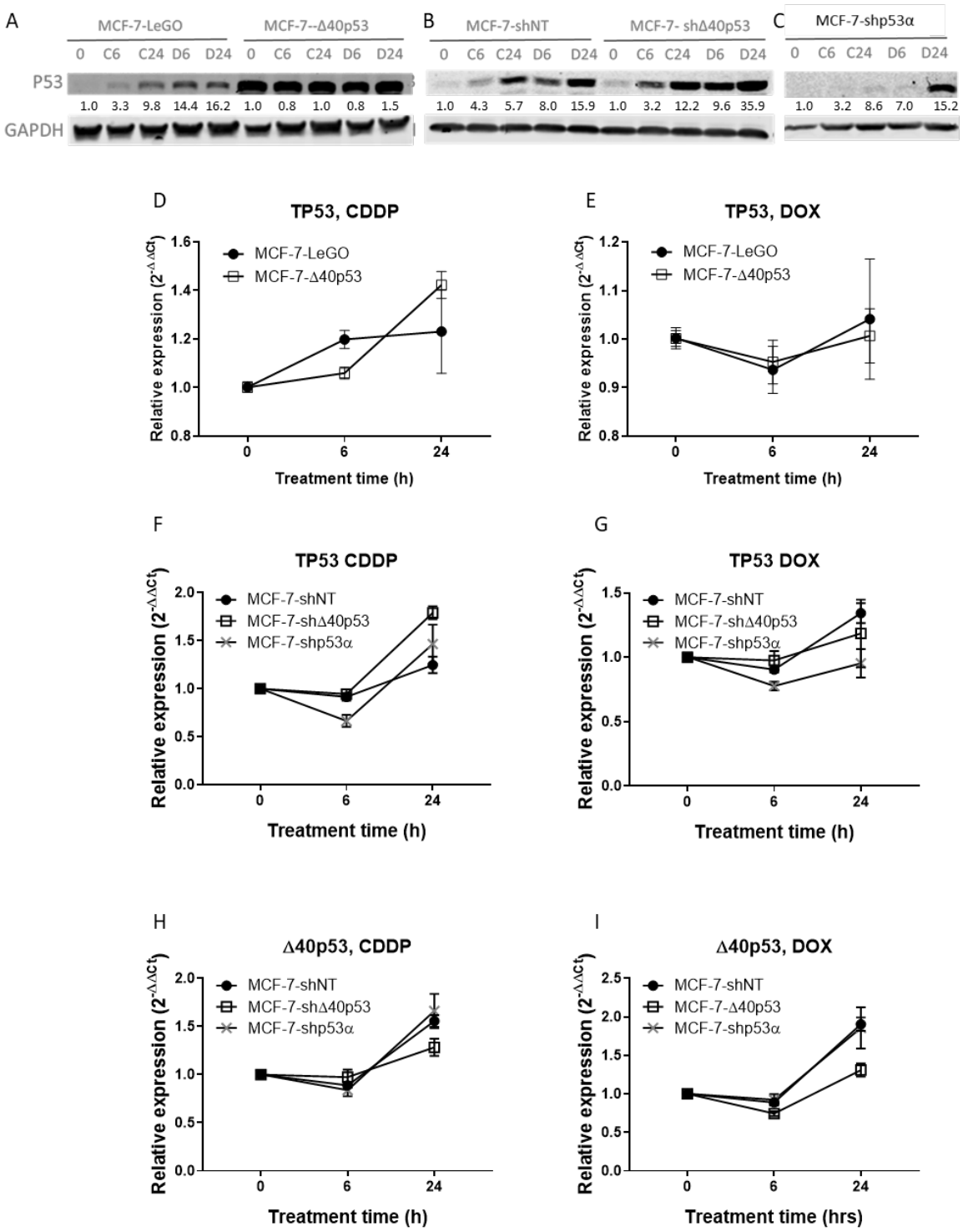

Figure 5.6 p53 protein level was significantly up-regulated in response to CDDP and DOX when Δ40p53 was knocked down in MCF-7 cells. A – C, Representative western blot analysis showed up-regulated p53 protein level after CDDP and DOX treatment (C and D as CDDP and DOX respectively and digits indicate time after treatment), when knocking down isoforms, but not overexpressing Δ40p53. The p53 protein levels of each treated time points are normalised to those of the untreated (at 0 h) within each of the sublines and quantification was shown of the representative western blot. p53 mRNA levels in response to CDDP (D and F) and DOX (E and G) and Δ40p53 mRNA level (H and I) were measured using semi-quantitative real-time PCR and quantified by 2-ΔΔCt method, normalising to untreated cells (0 h). Results are from three independent experiments in triplicate and error bars are the standard error of the mean (SEM). Significant results are shown with stars indicating the p-value. *, p<0.05; **, p< 0.01 and ****, p< 0001.

5.4.3.2 p53-dependent gene expression in response to DNA damaging agents in MCF-7 sublines The above results showed that in MCF-7 sublines, knocking down Δ40p53 decreased G2 arrest and increased cell death, and this was accompanied by increased p53 protein level, hence we next investigated p53-dependent cell cycle and apoptosis-related gene expression by RT-qPCR.

We looked at the relative mRNA expression changes of four commonly known p53-dependent target genes including p21 and three pro-apoptotic markers Bax, Puma and Noxa (Figure 5.7). Regardless of Δ40p53 and p53α levels, all genes showed a trend of up-regulation 24 hours after treatment with either DNA-damaging agent. The expression level of Bax, Noxa, Puma and p21 in MCF-7-Δ40p53 cells was equal to that of LeGO cells following CDDP treatment, but was significantly inhibited following DOX treatment, indicating that the transactivation of these genes by p53 was inhibited when Δ40p53 was overexpressed (Figure 5.7A, B, E, F, I, J, M and N). In contrast, the expression level of all three proapoptotic genes was significantly up-regulated when Δ40p53 was knocked down and significantly down-regulated (except Bax) when p53α was knocked down (Figure 5.7C, D, G, H, K and L), indicating that these p53-dependent pro-apoptotic genes were more highly activated as a result of Δ40p53 knockdown and less activated as a result of p53α knockdown. The gene expression of the cyclindependent inhibitor, p21, was not significantly changed among the MCF-7 sublines in response to DNA-damage (Figure 5.7M, N O and P). These results correlate with our results on p53α protein expression level and apoptosis in response to DNA-damaging agents, indicating Δ40p53 knockdown led to increased p53 induction when DNA was damaged, which led to increased apoptosis.

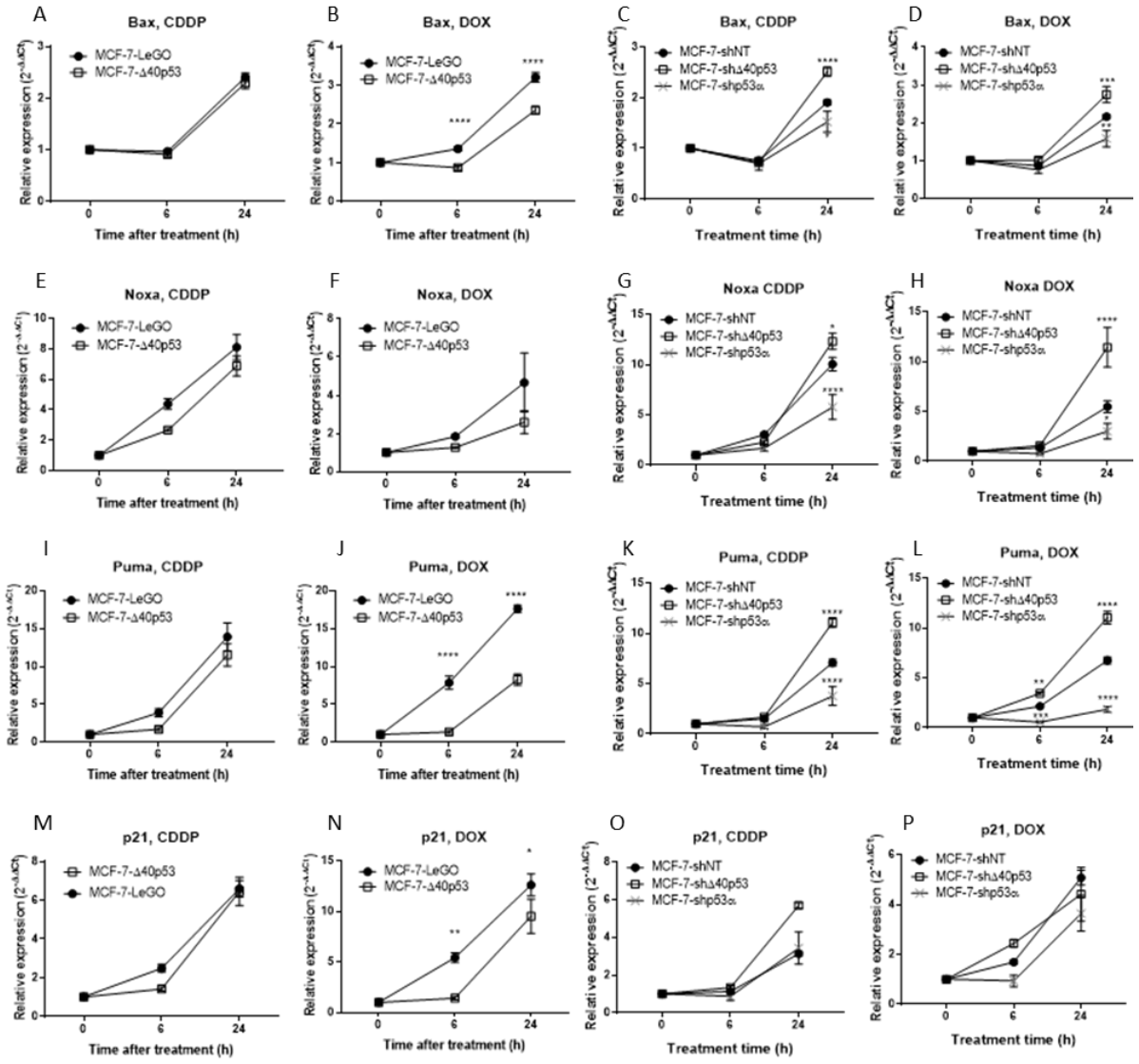

Figure 5.7 The mRNA expression level of p53-dependent genes was up-regulated in response to CDDP and DOX when Δ40p53 was knocked down in MCF-7 cells. mRNA levels of Bax (A-D), Noxa (E-H), Puma (I-L) and p21 (M-P) in response to CDDP and using semi-quantitative real-time PCR and quantified by 2-ΔΔCt method, normalising to untreated cells (0 h). Results are from three independent experiments in triplicate and error bars are the standard error of the mean (SEM). Significant results are shown with stars indicating the p-value. *, p<0.05; **, p< 0.01 and ****, p< 0001.

5.4.4 Characterisation of molecular profiles of DOX-treated sublines

The above results showed that an altered Δ40p53/p53α ratio is associated with altered G2 cell cycle arrest in both MCF-7 and ZR75-1 derived sublines. In MCF-7 sublines, a low level of Δ40p53 was associated with decreased G2 arrest as well as increased apoptosis and up-regulated p53-dependent pro-apoptotic gene expression, indicating enhanced p53 regulation of apoptosis in response to DNA damage. On the contrary, a high level of Δ40p53, either by knocking down p53α or overexpressing Δ40p53, led to an increased cell population at G2, when DNA synthesis is complete; and decreased expression of p53-dependent pro-apoptotic markers Bax and Puma at the mRNA level.

It is obvious from the above results that DOX has the most consistent impact on both MCF-7 and ZR751 cells and this was more noticeable at 24 hours after treatment compared to 6 hours after treatment. We therefore performed RNA-seq on these sublines treated with DOX and sought to identify genes whose expression in response to DOX was significantly different when Δ40p53 expression was inhibited or overexpressed, compared to the control sublines.

Hierarchical clustering of the mRNA expression profiles of all genes (Figure 5.8A) demonstrated that ZR75-1 and MCF-7 derived sublines formed clusters based on their treatment group: untreated (UT) and DOX-treated (T). Of all untreated MCF-7 sublines, the Δ40p53-overexpressing subline was closer to its corresponding control and Δ40p53/p53α isoform knockdown sublines were closer to their corresponding shNT subline, with less similarity between shΔ40p53 and shNT than shp53α to shNT. However, when treated with DOX, the expression profile of shp53α was more similar to shNT than shΔ40p53, indicating a relationship between DOX and an altered Δ40p53/p53 ratio. In contrast, the ZR75-1-shΔ40p53 subline was separated from the ZR75-1-shNT and ZR75-1-shp53α sublines before and after DOX treatment (Figure 5.8A).

MCF-7 sublines

We used DESeq2 and intensity statistical tests to identify differentially expressed genes after DOX treatment in each subline. Individually, there were 74, 51, 20, 77 and 22 DEGs after DOX treatment in the MCF-7-LeGO, MCF-7-Δ40p53, MCF-7-shNT, MCF-7-shΔ40p53 and MCF-7-shp53α sublines respectively, and Venn diagrams were drawn comparing these groups to the corresponding control groups (Figure 5.7B and C). A lower number of genes (31%, 51 genes vs 74 genes) were differentially regulated when Δ40p53 was overexpressed and compared to LeGO control cells in MCF-7 cells, whereas more genes (74%, 77 genes vs 20 genes) were differentially regulated when Δ40p53 was knocked down compared to NT cells; and almost equal numbers of genes were differentially regulated when p53α was knocked down in MCF-7 cells compared to shNT cells (22 genes vs 20 genes). Δ40p53knockdown led to the highest number (77) of differentially expressed genes in the knockdown group, followed by the number of DEGs (74) in MCF-7-LeGO cells, indicating a lower Δ40p53/p53α ratio is associated with more genes being regulated in response to DOX.

We then attempted to identify common DEGs between the sublines and unique genes within each subline in response to DOX. Twenty-five genes were found to be regulated in both MCF-7-LeGO and MCF-7-Δ40p53 cells after DOX treatment, whilst 26 genes (~50% of the MCF-7-Δ40p53 DEGs) were regulated independently by Δ40p53-overexpression. Nine genes were found to be commonly regulated among MCF-7-shNT, MCF-7-shΔ40p53 and MCF-7-shp53α sublines after treatment and four, nine and 57 genes were found to be regulated independently within each subline. Seven genes

were found to be commonly regulated after DOX treatment in all MCF-7 sublines, and they were regulated by DOX-treatment regardless of the isoform status, among which one gene, *BTG2* (BTG AntiProliferation Factor 2), was up-regulated in all sublines, indicating an anti-proliferative role for DOX on these cell lines.

The above comparisons were all performed within each subline, and we next proceeded to compare how these genes were modulated within all sublines. A total of 136 genes were found at least one of the MCF-7 sublines when comparing their gene expression profiles before DOX-treatment (UT) to those after DOX-treatment (T). These genes were hierarchically clustered by expression and are shown in Figure 5.8E. Up-regulated and down-regulated genes are shown in a colour scale ranging from green (lowest, down-regulated) to red (highest, up-regulated), showing DOX-related clusters of genes in the MCF-7 sublines. A distinct pattern of the down-regulated genes was seen in the MCF-7 sublines treated with DOX, where the expression profile of a cluster of down-regulated genes (Figure 5.8E, highlighted with white dashes) within MCF-7-Δ40p53 showed high resemblance to that of MCF-7-shNT cells, and the expression profiles of MCF-7-LeGO and MCF-7-shΔ40p53 cells were very similar for this gene cluster (Figure 5.8E). This indicated that this cluster of genes was strongly decreased in LeGO cells and that suppression of these genes was abrogated in Δ40p53-overexpression cells, whereas the opposite was observed in the Δ40p53-shRNA transduced subline. This links the Δ40p53/p53α ratio and the suppression of these genes together, showing that a high Δ40p53/p53α ratio was negatively associated with the inhibition of these genes. Therefore, we attempted to dissect these genes according to their mRNA expression profiles. The 136 DEGs are listed in Table 5.2 with the log_2FC values relative to untreated cells (minus values indicate down-regulation and vice versa). Significant DEGs in each group were indicated with bold characters, where some of these genes were unique to one group and some of them were common genes in multiple groups. Some of these log_2FC values may seem significant in sublines other than those indicated by bold, but they did not pass DESeq2 and the intensity filter within the certain group and are therefore, not significantly regulated. The values indicate a general trend of the 136 genes in all MCF-7 sublines after DOX-treatment compared to untreated cells: genes were almost uniformly up- or down-regulated. There were 73 down-regulated (blue shading) genes and 59 up-regulated (orange shading) genes following DOX-treatment in all MCF7 sublines, and only four DEGs did not follow this trend.

The white dashes highlight genes (59) within the hierarchical cluster analysis in Figure 5.9 that fall mostly into the down-regulated genes except one ATAD2 (ATPase family, AAA domain 2), which showed a very weak up-regulation in MCF-7-shp53α cells (log2FC = 0.11) (Table 5.2). Within each subline after DOX treatment there were 21, 19, four, 23 and five unique DEGs in LeGO,

Δ40p53overexpresion, shNT, shΔ40p53 and shp53α MCF-7 cells respectively, of which 4/21 in LeGO, 10/19 in Δ40p53-overexpression, 2/4 in shNT, 5/23 in shΔ40p53 and 4/5 in shp53α cells were independently up-regulated, and 17/21 in LeGO, 8/18 in Δ40p53-overexpression, 0/4 in MCF-7-shNT, 17/23 in shΔ40p53 and 0/5 in shp53α cells were independently down-regulated. Twenty-seven genes were down-regulated in both MCF-7-LeGO and MCF-7-shΔ40p53 cells. Altogether, these 61 DEGs showed stronger inhibition by DOX-treatment in MCF-LeGO and –Δ40p53 cells compared to the other three. GSEA analysis was performed by Enrichr GO Biological Process and Significant (< 0.05) GO terms and the top 10 GO terms ranked by adjusted *p*-values are listed in Table 5.3. The down-regulated genes were mostly enriched in all cell cycle phases and cell cycle phase transitions, indicating a greater susceptibility of LeGO and shΔ40p53 cells to DOX-induced cell cycle arrest. On inspection of the downregulated DEGs, they all exhibited a trend of the least suppression or highest expression in shp53α cells followed by shNT cells compared to shΔ40p53 cells, further implying that the ratio of Δ40p53/p53α affects MCF-7 cells in response to DNA-damage. The 59 up-regulated genes were enriched in the GO term "cellular response to amino acid starvation" with elevated gene expression of *CDKN1A, FAS* and *SESN1/2* (sestrin 1/2), which are all transactivation targets of p53.

ZR75-1 sublines

There were 93, 90 and 64 differentially expressed genes following DOX treatment in the ZR75-1-shNT, ZR75-1-shΔ40p53 and ZR75-1-shp53α cells respectively, and Venn diagrams were drawn comparing the knockdown groups to shNT group (Figure 5.8D). Almost equal numbers of genes were differentially regulated in response to DOX in the ZR75-1-shΔ40p53 and ZR75-1-shp53α, and ~30% less genes were differentially regulated in ZR75-1-shp53α cells. There were 25, 24 and 16 genes regulated independently within each of the sublines by DOX-treatment. Sixty-two genes were commonly regulated, when comparing ZR75-1-shΔ40p53 to ZR75-1-shNT cells, and 38 of them (61%) were also found in ZR75-1-shp53α after DOX-treatment. Forty-four genes were found to be co-regulated when comparing ZR75-1-shp53α to ZR75-1-shNT cells, and 38 of them (86%) were also found to be regulated in ZR75-1-shΔ40p53 cells after DOX-treatment. These 38 genes were not significantly enriched in any GO Biological Process terms, however, *TP53I3* (tumour protein p53 inducible protein 3), *GDF15* (growth differentiation factor 15), *TP53INP1* (tumour protein p53 inducible nuclear protein 1), *TNFRSF10C* (tumour necrosis factor superfamily, member 10C) were categorized into the term regulation of programmed cell death (GO:0043067) (p = 0.001, adjusted p = 1, odds ratio = 7.826 and combined score= 50.149), indicating DOX-treatment had triggered this p53-associated biological process in ZR75-1 cells. The 25 unique genes in ZR75-1-shNT cells in response to DOX were enriched in only one GO Biological Process term mitotic spindle organization (GO:0007052) (adjust p = 0.01, odds ratio = 42.67 and combined score = 556.34). The 24 unique genes in ZR75-1-shΔ40p53 in

response to DOX were not significantly enriched in any GO terms. The 16 unique genes regulated in ZR75-1-shp53α in response to DOX were not significantly enriched in any GO terms, but a few genes such as *CDKN1A* (cyclin-dependent kinase inhibitor 1A), *GADD45A* (growth arrest and DNA-damageinducible, alpha) and *DDB2* (damage-specific DNA binding protein 2) were known to be involved in the p53-associated response to DNA-damage.

A total of 137 differentially expressed genes were found to be differentially expressed in at least one subline after DOX-treatment and they were hierarchically clustered by expression and are shown in Figure 5.7F. Up-regulated and down-regulated genes are shown in a colour scale ranging from green (lowest, down-regulated) to red (highest, up-regulated). Consistent with what we observed in MCF-7 sublines, genes differentially regulated by DOX-treatment were clustered into up- and down-regulated groups, but were different from the pattern we observed in MCF-7 sublines, a Δ40p53/53α ratioassociated gene expression pattern was not observed. The gene expression profiles based on these 137 genes showed that untreated ZR75-1-shp53α cells were similar to ZR75-1-shNT cells, however after DOX-treatment, ZR75-1-shΔ40p53 cells were more similar to ZR75-1-shNT cells, indicating p53αknockdown rather than Δ40p53-knockdown had led to critical changes in response to DOX. The 137 genes are listed in Table 5.4 with the $\log_2$FC values to untreated cells (minus values indicate downregulation and vice versa). GSEA was performed using Enrichr on GO Biological Process and results are listed in Table 5.5.

The 137 genes are enriched in 10 GO Biological process terms: regulation of mitotic cell cycle phase transition (GO:1901990), signal transduction involved in mitotic G1 DNA damage checkpoint (GO:0072431), regulation of cell proliferation (GO:0042127), mitotic spindle organization (GO:0007052), positive regulation of cell cycle arrest (GO:0071158), positive regulation of protein phosphorylation (GO:0001934), DNA damage response, signal transduction by p53 class mediator (GO:0030330), DNA damage response, signal transduction by p53 class mediator resulting in cell cycle arrest (GO:0006977), regulation of apoptotic process (GO:0042981) and regulation of MAPK cascade (GO:0043408). These GO terms overlap nicely with those in MCF-7 cells, confirming a role for DOX in activating the p53 pathway and regulating the cell cycle and cell proliferation. There are 104 genes (76%, shaded in orange) and 33 genes (24%, shaded in blue) that were up- or down-regulated by DOXtreatment respectively, showing a well-separated regulation by DOX in ZR75-1 cells regardless of isoform status. The up-regulated genes were not significantly enriched in any GO terms, but the top GO-terms include signal transduction, cell proliferation, DNA-damage and apoptosis. The downregulated 33 genes are enriched in 35 GO terms including regulation of cell cycle phases and ubiquitinprotein ligase activity, very much like the enriched GO term of the DOX-down-regulated genes in MCF7 sublines. Twenty-four of the genes (72%, Table 5.4, pink) were less down-regulated in

both ZR75-1shΔ40p53 and ZR75-1-shp53α, and mostly enriched in cell cycle-associated processes, indicating a lack of both isoforms to affect suppression of these genes. Nine genes (Figure 5.4, purple) were more down-regulated when Δ40p53 was knocked down and less down-regulated when p53α was knocked down.

MCF-7 and ZR75-1

When thinking about the sublines and the Δ40p53/p53α ratio, Δ40p53 level is highest in sublines where it has been overexpressed and in cases where p53α has been knocked down. In these sublines the Δ40p53/p53α ratio was increased compared to the corresponding control cells. Given this, hierarchical clustering was performed on the sublines where the ratio of Δ40p53/p53α was the highest (Including both MCF-7 and ZR-75-1) to determine whether there were any commonalities in the genes that were differentially regulated following DNA damage. Prior to DNA damage, the gene expression profiles of each of the cell lines was remarkably similar. However, there were 187 DEGs in at least one of the 6 sublines when comparing each of them after DOX-treatment (T) to before DOX-treatment (UT), and these genes are hierarchically clustered and shown in a colour scale ranging from green (lowest, down-regulated) and red (highest, up-regulated) in Figure 5.9. The SeqMonk cluster tool was used to filter out genes that were differentially regulated by either Δ40p53 overexpression or p53 knockdown following DOX treatment and this resulted in 73 DEGs which are shown by the white dashed rectangles in Figure 5.9 between these sublines and listed in Table 5.6 with significant log_2FC values indicated with bold characters. These resulting 73 DEGs were further used to perform GSE analysis and significant results are shown in Table 5.7. The most enriched GO Biological Processes are identical to those of the previous GSE analysis shown in Table 5.3 and Table 5.5 (performed on MCF7 and ZR sublines respectively) that DOX-down-regulated genes in either MCF-7 or ZR75-1 sublines are involved in regulation of multiple cell cycle phases, indicating a high Δ40p53/p53α ratio attenuates the sensitivity to DOX-treatment in these cells.

The above results showed a well-directed impact by DOX-treatment, and the down-regulated genes are mostly associated with cell cycle progression and cell division. Δ40p53 was a stronger transcriptional repressor than p53α in MCF-7 cells, whereas Δ40p53-knockdown had limited effect on DOX-induced genes in ZR75-1 cells.

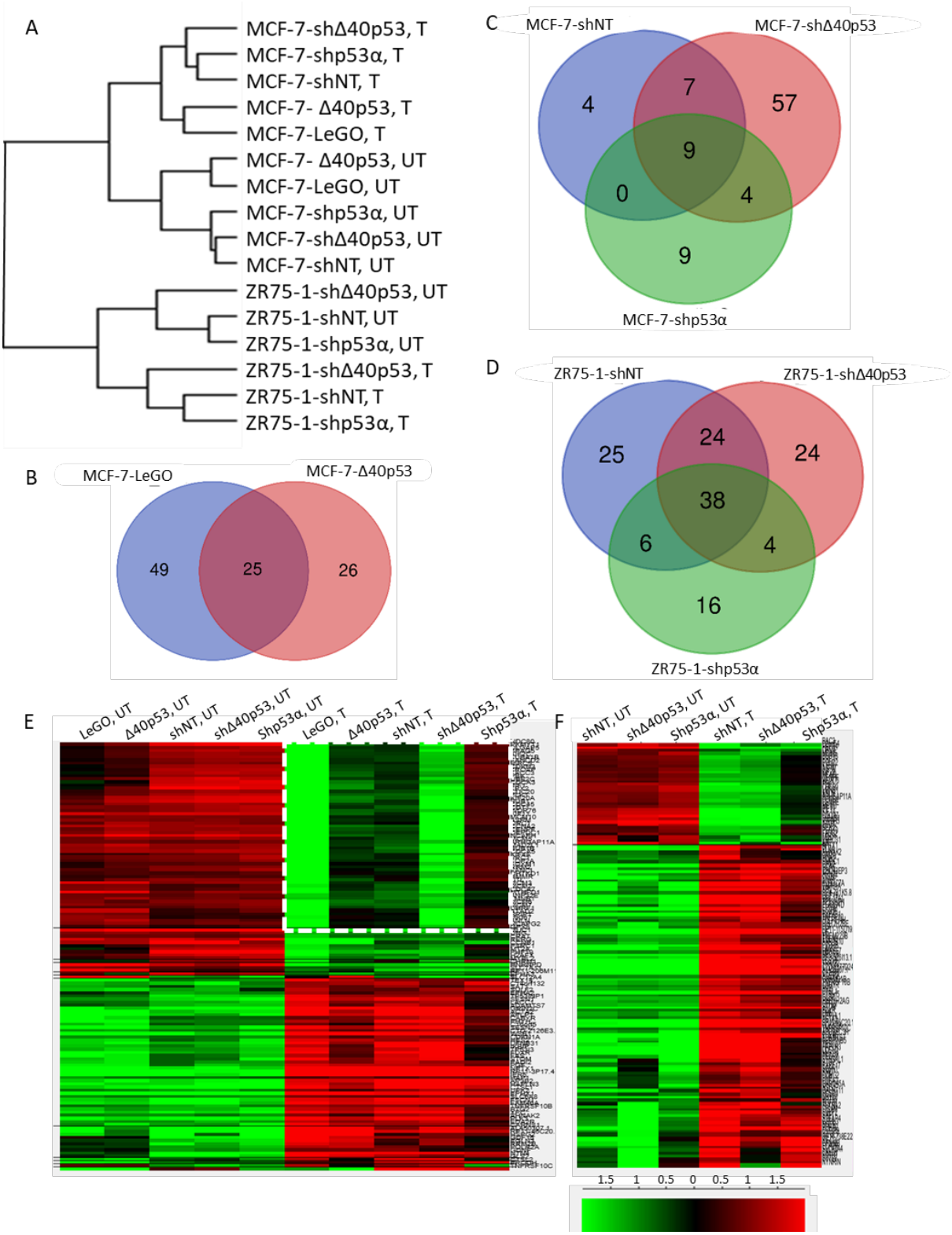

Figure 5.8 Overview of RNA-seq analysis of all p53 isoform sublines before (UT) and after DOX treatment (T). A, dendrogram of all sublines based on mRNA expression profiles showing the similarity among samples. Differentially expressed genes (DEGs) compared to the corresponding controls of MCF-7 (B, C) and ZR75-1 (D) were shown in Venn diagrams. 136 and 137 DEGs were found in at least one of the sublines before and after treatment in MCF-7 and ZR75-1 respectively. E and F, heatmaps of 136 genes of MCF-7 sublines (D) and 137 genes of ZR75-1 sublines (E). The expression of each gene was individually normalised and indicated on the right. The expression profiles of a cluster of genes that was associated with Δ40p53/p53α ratio and is highlighted with white dashes.

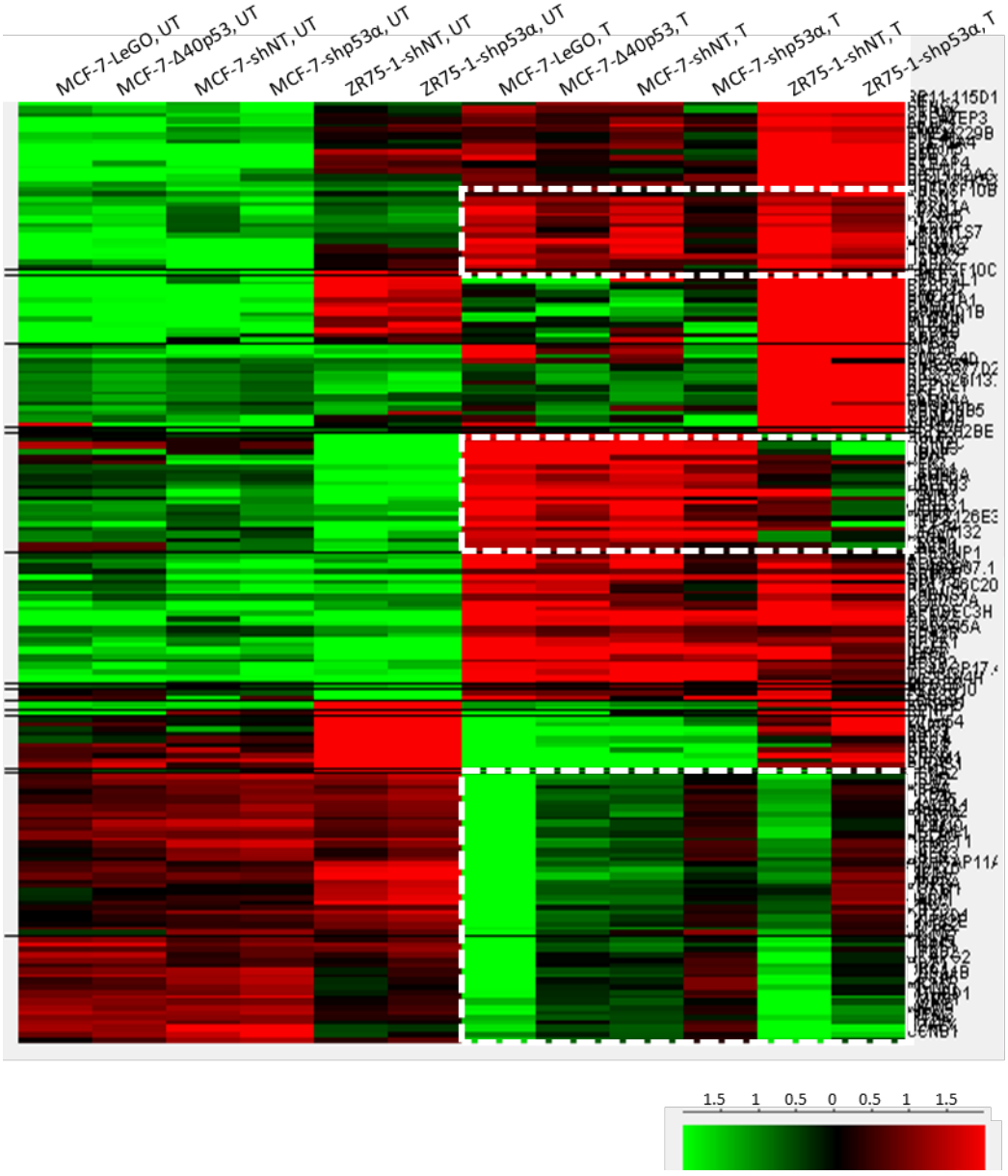

Figure 5.9 Hierarchical cluster of 187 differentially expressed genes in Δ40p53/p53α ratio high MCF-7 and ZR75-1 cells before (UT) and after (T) DOX-treatment. The differentially expressed gene present in at least one subline before (UT) and after DOX-treatment (T) were hierarchically clustered in a colour scale (lowest in green and highest in red). White dashes indicate the genes that are less induced or less reduced compared to the corresponding controls.

Table 5.2 136 differentially expressed genes in response to DOX in all MCF-7 sublines.

Probe	Description	Log_2FC by DOX-treatment				
		LeGO	Δ40p53	shNT	shΔ40p53	shp53α
ANLN	anillin, actin binding protein [Source:HGNC Symbol;Acc:14082]	-3.91	-1.38	-0.99	**-3.43**	-0.38
ANP32E	acidic (leucine-rich) nuclear phosphoprotein 32 family, member E [Source:HGNC Symbol;Acc:16673]	-2.49	**-1.92**	-1.73	-2.63	-1.08
ARHGAP11A	Rho GTPase activating protein 11A [Source:HGNC Symbol;Acc:15783]	-4.54	-1.98	-1.87	**-3.6**	-1.04
ASPM	asp (abnormal spindle) homolog, microcephaly associated (Drosophila) [Source:HGNC Symbol;Acc:19048]	-4.28	-1.63	-1.21	**-3.56**	-0.29
BIRC5	baculoviral IAP repeat containing 5 [Source:HGNC Symbol;Acc:593]	-3.33	-1	-1.6	**-2.73**	-0.48
BRIP1	BRCA1 interacting protein C-terminal helicase 1 [Source:HGNC Symbol;Acc:20473]	**-3.04**	-0.92	-0.34	-2.43	-0.16
BUB1	budding uninhibited by benzimidazoles 1 homolog (yeast) [Source:HGNC Symbol;Acc:1148]	**-4.19**	-1.69	-1.62	**-3.51**	-0.71
BUB1B	budding uninhibited by benzimidazoles 1 homolog beta (yeast) [Source:HGNC Symbol;Acc:1149]	-4.38	-1.75	-2.03	**-4.34**	-1.1
CCNA2	cyclin A2 [Source:HGNC Symbol;Acc:1578]	**-3.8**	-1.9	-1.72	**-3.31**	-0.9
CCNB1	cyclin B1 [Source:HGNC Symbol;Acc:1579]	-1.76	-1.36	-1.83	**-2.38**	-1.13
CDC20	cell division cycle 20 homolog (S. cerevisiae) [Source:HGNC Symbol;Acc:1723]	**-3.51**	-1.6	-2.07	**-3.27**	-1.15
CDC45	cell division cycle 45 homolog (S. cerevisiae) [Source:HGNC Symbol;Acc:1739]	**-4.6**	-1.22	-1.86	**-3.44**	-0.89
CDCA3	cell division cycle associated 3 [Source:HGNC Symbol;Acc:14624]	-3.38	-1.48	-2.05	**-3.47**	-1.12
CDCA5	cell division cycle associated 5 [Source:HGNC Symbol;Acc:14626]	**-3.17**	-0.86	-1.01	**-2.31**	-0.31
CDCA7	cell division cycle associated 7 [Source:HGNC Symbol;Acc:14628]	**-4.92**	-2.42	-1.72	-3.6	-1.63
CDKN3	cyclin-dependent kinase inhibitor 3 [Source:HGNC Symbol;Acc:1791]	-3.4	-0.94	-1.77	**-3.03**	-0.66
CDT1	chromatin licensing and DNA replication factor 1 [Source:HGNC Symbol;Acc:24576]	**-4.33**	-1.62	-1.7	-2.86	-0.92
CENPF	centromere protein F, 350/400kDa (mitosin) [Source:HGNC Symbol;Acc:1857]	**-4.42**	-1.95	-1.47	**-3.82**	-0.73
CHRM1	cholinergic receptor, muscarinic 1 [Source:HGNC Symbol;Acc:1950]	-4.79	**-4.19**	-3.04	-3.8	-4.13
CRAT	carnitine O-acetyltransferase [Source:HGNC Symbol;Acc:2342]	**-5.3**	**-3.41**	-2.84	-2.71	**-2.8**
DEPDC1	DEP domain containing 1 [Source:HGNC Symbol;Acc:22949]	**-6.4**	**-2.79**	-2.23	**-5.08**	-1.48
DHTKD1	dehydrogenase E1 and transketolase domain containing 1 [Source:HGNC Symbol;Acc:23537]	**-2.46**	-0.77	-0.6	-2.14	-0.09
DLGAP5	discs, large (Drosophila) homolog-associated protein 5 [Source:HGNC Symbol;Acc:16864]	-3.51	-1.11	-1.7	**-3.37**	-0.64
DTL	denticleless homolog (Drosophila) [Source:HGNC Symbol;Acc:30288]	**-6.07**	-2.05	-1.52	-3.62	-1.05
FANCD2	Fanconi anemia, complementation group D2 [Source:HGNC Symbol;Acc:3585]	**-2.79**	-0.77	-1.13	**-2.59**	-0.44
FANCI	Fanconi anemia, complementation group I [Source:HGNC Symbol;Acc:25568]	**-2.96**	-0.53	-0.7	-2.04	-0.15
FOXM1	forkhead box M1 [Source:HGNC Symbol;Acc:3818]	**-3.16**	-0.98	-1.24	**-2.9**	-0.41
GPX8	glutathione peroxidase 8 (putative) [Source:HGNC Symbol;Acc:33100]	-4.61	**-5.79**	-4.59	-4.78	-4.39

H2AFX	H2A histone family, member X [Source:HGNC Symbol;Acc:4739]	-1.92	-1.44	-2.26	-2.07	**-1.91**
HMMR	hyaluronan-mediated motility receptor (RHAMM) [Source:HGNC Symbol;Acc:5012]	-3.82	-1.61	-0.96	**-3.12**	-0.16
HNRNPD	heterogeneous nuclear ribonucleoprotein D (AU-rich element RNA binding protein 1, 37kDa) [Source:HGNC Symbol;Acc:5036]	-1.87	**-1.77**	-1.88	-1.9	**-1.88**
KIF11	kinesin family member 11 [Source:HGNC Symbol;Acc:6388]	-3.6	-1.3	-1.18	**-3.56**	-0.47
KIF20A	kinesin family member 20A [Source:HGNC Symbol;Acc:9787]	**-5.38**	**-2.4**	-2.02	**-4.35**	-1.36
KIF2C	kinesin family member 2C [Source:HGNC Symbol;Acc:6393]	**-3.28**	-1.06	-1.69	**-2.75**	-0.74
KIF4A	kinesin family member 4A [Source:HGNC Symbol;Acc:13339]	**-4.11**	-1.35	-1.17	-3.29	-0.57

LMNB1	lamin B1 [Source:HGNC Symbol;Acc:6637]	**-3.17**	-1.6	-1.72	**-2.74**	-1.14
MAD2L1	MAD2 mitotic arrest deficient-like 1 (yeast) [Source:HGNC Symbol;Acc:6763]	**-4.45**	-1.52	-2.05	-3.38	-0.85
MCM10	minichromosome maintenance complex component 10 [Source:HGNC Symbol;Acc:18043]	**-4.45**	-1.41	-1.15	-3.16	-0.34
MCM2	minichromosome maintenance complex component 2 [Source:HGNC Symbol;Acc:6944]	**-3.06**	-1.4	-1.17	**-2.43**	-0.75
MCM3	minichromosome maintenance complex component 3 [Source:HGNC Symbol;Acc:6945]	**-2.79**	-1.24	-1.26	-2.22	-0.63
MCM5	minichromosome maintenance complex component 5 [Source:HGNC Symbol;Acc:6948]	**-3.09**	-1.29	-1.39	-2.3	-0.82
MCM6	minichromosome maintenance complex component 6 [Source:HGNC Symbol;Acc:6949]	**-3.47**	-1.75	-1.7	**-2.4**	-1.15
MCM7	minichromosome maintenance complex component 7 [Source:HGNC Symbol;Acc:6950]	**-2.84**	-1.23	-1.44	**-2.23**	-0.78
MKI67	antigen identified by monoclonal antibody Ki-67 [Source:HGNC Symbol;Acc:7107]	**-4.25**	-1.47	-0.83	**-3.46**	-0.22
MT2A	metallothionein 2A [Source:HGNC Symbol;Acc:7406]	**-3.08**	-1.68	**-3.61**	**-3.7**	**-2.31**
MTHFD1	methylenetetrahydrofolate dehydrogenase (NADP+ dependent) 1, methenyltetrahydrofolate cyclohydrolase, formyltetrahydrofolate synthetase [Source:HGNC Symbol;Acc:7432]	**-2.52**	-1.38	-1.55	-2.27	-1.03
MUC1	mucin 1, cell surface associated [Source:HGNC Symbol;Acc:7508]	-2.43	**-2.23**	-2.21	-2.32	-1.83
MYBL2	v-myb myeloblastosis viral oncogene homolog (avian)-like 2 [Source:HGNC Symbol;Acc:7548]	**-2.5**	-0.15	-0.86	**-2.43**	-0.02
NCAPG2	non-SMC condensin II complex, subunit G2 [Source:HGNC Symbol;Acc:21904]	**-2.66**	-0.64	-0.47	-1.99	-0.01
NCAPH	non-SMC condensin I complex, subunit H [Source:HGNC Symbol;Acc:1112]	-4.16	-1.4	-1.67	**-3.55**	-0.71
NDC80	NDC80 homolog, kinetochore complex component (S. cerevisiae) [Source:HGNC Symbol;Acc:16909]	**-5.46**	-1.78	-2.19	**-4.2**	-1.14
ORC1	origin recognition complex, subunit 1 [Source:HGNC Symbol;Acc:8487]	-4.89	**-2.41**	-1.89	-3.58	-1.02
PBK	PDZ binding kinase [Source:HGNC Symbol;Acc:18282]	**-5.3**	-1.4	-1.79	**-3.45**	-0.87
PHF19	PHD finger protein 19 [Source:HGNC Symbol;Acc:24566]	-3.57	-1.83	-2.52	**-3.3**	-1.63
PIF1	PIF1 5'-to-3' DNA helicase homolog (S. cerevisiae) [Source:HGNC Symbol;Acc:26220]	-3.43	-2.03	-2.37	**-4.79**	-1.14
PKMYT1	protein kinase, membrane associated tyrosine/threonine 1 [Source:HGNC Symbol;Acc:29650]	**-3.11**	-0.89	-1.38	**-2.74**	-0.69

PLK1	polo-like kinase 1 [Source:HGNC Symbol;Acc:9077]	**-4.15**	**-2.4**	-2.28	**-4.15**	-1.66
PRC1	protein regulator of cytokinesis 1 [Source:HGNC Symbol;Acc:9341]	**-3.25**	-1.16	-1.23	**-2.83**	-0.62
PSRC1	proline/serine-rich coiled-coil 1 [Source:HGNC Symbol;Acc:24472]	-1.52	-1.16	-2.16	**-2.91**	-1.15
RERG	RAS-like, estrogen-regulated, growth inhibitor [Source:HGNC Symbol;Acc:15980]	-4.27	**-3.84**	-2.55	-2.89	-2.63
RP11-206M11.7	No description	-1.39	-0.94	**-3.03**	-2.39	-2.31
RRM2	ribonucleotide reductase M2 [Source:HGNC Symbol;Acc:10452]	**-4.06**	-0.65	-1.44	**-3.14**	-0.52
SLC7A11	solute carrier family 7 (anionic amino acid transporter light chain, xc- system), member 11 [Source:HGNC Symbol;Acc:11059]	-3.46	**-3.3**	-2.18	-2.86	-2.36
SPAG5	sperm associated antigen 5 [Source:HGNC Symbol;Acc:13452]	-3.16	-1.14	-1.54	**-2.78**	-0.62
TACC3	transforming, acidic coiled-coil containing protein 3 [Source:HGNC Symbol;Acc:11524]	**-3.28**	-1.09	-1.46	-2.44	-0.5
TOP2A	topoisomerase (DNA) II alpha 170kDa [Source:HGNC Symbol;Acc:11989]	**-2.68**	-0.68	-0.67	-2.33	-0.13
TPX2	TPX2, microtubule-associated, homolog (Xenopus laevis) [Source:HGNC Symbol;Acc:1249]	-3.16	-1.3	-1.64	**-3.1**	-0.8
TROAP	trophinin associated protein (tastin) [Source:HGNC Symbol;Acc:12327]	-3.05	-1.13	-1.66	**-2.82**	-0.72
TUBA1B	tubulin, alpha 1b [Source:HGNC Symbol;Acc:18809]	**-2.86**	-0.76	-1.48	**-2.63**	-0.46
UBE2C	ubiquitin-conjugating enzyme E2C [Source:HGNC Symbol;Acc:15937]	-3.02	-1.03	-2.07	**-2.91**	-1.01
UHRF1	ubiquitin-like with PHD and ring finger domains 1 [Source:HGNC Symbol;Acc:12556]	**-4.34**	-1.48	-0.64	-3.25	-0.37
UNG	uracil-DNA glycosylase [Source:HGNC Symbol;Acc:12572]	-2.45	**-1.71**	-1.65	-1.69	-1.26

WDR76	WD repeat domain 76 [Source:HGNC Symbol;Acc:25773]	**-6.02**	-2.18	-1.98	**-5.22**	-1.02
ATAD2	ATPase family, AAA domain containing 2 [Source:HGNC Symbol;Acc:30123]	**-3.11**	-1	-0.36	**-2.35**	0.11
EPHA3	EPH receptor A3 [Source:HGNC Symbol;Acc:3387]	-2.26	**-1.73**	0.25	-1.19	-0.56
PRODH	proline dehydrogenase (oxidase) 1 [Source:HGNC Symbol;Acc:9453]	0.69	-0.69	2.27	**3.16**	-0.13
TNFRSF10C	tumor necrosis factor receptor superfamily, member 10c, decoy without an intracellular domain [Source:HGNC Symbol;Acc:11906]	1.63	-0.42	**4.18**	3.02	2.83
ACTA2	actin, alpha 2, smooth muscle, aorta [Source:HGNC Symbol;Acc:130]	**5.88**	**5.22**	**4.08**	**4.43**	**3.14**
ADAMTS7	ADAM metallopeptidase with thrombospondin type 1 motif, 7 [Source:HGNC Symbol;Acc:223]	**6.84**	**4.47**	**6.59**	**6.12**	4.72
AHNAK2	AHNAK nucleoprotein 2 [Source:HGNC Symbol;Acc:20125]	**4.62**	3.16	**5.52**	**5.29**	2.65
AL450307.1	Uncharacterized proteincDNA FLJ46300 fis, clone TESTI4035989 [Source:UniProtKB/TrEMBL;Acc:Q6ZRK0]	**8.99**	**6.4**	5.9	**6.68**	5.48
AP3B2	adaptor-related protein complex 3, beta 2 subunit [Source:HGNC Symbol;Acc:567]	3.95	2.86	4.14	**4.67**	**4.42**
APLP1	amyloid beta (A4) precursor-like protein 1 [Source:HGNC Symbol;Acc:597]	2.77	**2.62**	1.96	2.54	1.43
BTG2	BTG family, member 2 [Source:HGNC Symbol;Acc:1131]	**3.9**	**3**	**4.14**	**4.16**	**3.24**

C14orf132	chromosome 14 open reading frame 132 [Source:HGNC Symbol;Acc:20346]	2.54	1.86	1.65	1.82	**2.19**
C16orf5	chromosome 16 open reading frame 5 [Source:HGNC Symbol;Acc:13234]	**5.23**	3.73	3.41	3.79	2.86
CABYR	calcium binding tyrosine-(Y)-phosphorylation regulated [Source:HGNC Symbol;Acc:15569]	**4.19**	3.1	3.01	3.13	1.69
CARNS1	carnosine synthase 1 [Source:HGNC Symbol;Acc:29268]	4.96	**3.97**	3.32	3.78	3.82
CDKN1A	cyclin-dependent kinase inhibitor 1A (p21, Cip1) [Source:HGNC Symbol;Acc:1784]	**3.39**	**3.2**	1.92	**2.5**	**2.24**
CTD-2126E3.1	No description	6	**5.4**	4.47	**5.07**	3.35
CTSL1	cathepsin L1 [Source:HGNC Symbol;Acc:2537]	1.97	1.44	2.2	**2.68**	**1.88**
CTSL2	cathepsin L2 [Source:HGNC Symbol;Acc:2538]	2.65	2.14	2.35	2.18	**2.37**
DFNB31	deafness, autosomal recessive 31 [Source:HGNC Symbol;Acc:16361]	**3.06**	2.14	**2.95**	**3.27**	1.93
EDA2R	ectodysplasin A2 receptor [Source:HGNC Symbol;Acc:17756]	3.35	**3.32**	2.47	2.45	2.54
EGLN3	egl nine homolog 3 (C. elegans) [Source:HGNC Symbol;Acc:14661]	1.98	**1.93**	2.38	**2.54**	2.09
EPHA2	EPH receptor A2 [Source:HGNC Symbol;Acc:3386]	**2.54**	**2.03**	**2.94**	**2.93**	1.98
EPHX1	epoxide hydrolase 1, microsomal (xenobiotic) [Source:HGNC Symbol;Acc:3401]	2.01	1.64	1.8	2.18	**2.11**
FAM46A	family with sequence similarity 46, member A [Source:HGNC Symbol;Acc:18345]	2.09	**2**	2.45	2.35	1.76
FAS	Fas (TNF receptor superfamily, member 6) [Source:HGNC Symbol;Acc:11920]	**3.55**	**2.77**	2.45	2.7	2.43
FDXR	ferredoxin reductase [Source:HGNC Symbol;Acc:3642]	**3.47**	**2.41**	2.36	**3.29**	1.82
FSCN1	fascin homolog 1, actin-bundling protein (Strongylocentrotus purpuratus) [Source:HGNC Symbol;Acc:11148]	**3.75**	**3.33**	**4.02**	**4.33**	**3.17**
GDF15	growth differentiation factor 15 [Source:HGNC Symbol;Acc:30142]	2.4	**2.19**	1.9	**2.92**	1.71
GDNF	glial cell derived neurotrophic factor [Source:HGNC Symbol;Acc:4232]	3.12	2.63	**5.92**	**5.28**	**5.15**
GLS2	glutaminase 2 (liver, mitochondrial) [Source:HGNC Symbol;Acc:29570]	**3.24**	2.43	2.54	**2.81**	1.17
GRIN2C	glutamate receptor, ionotropic, N-methyl D-aspartate 2C [Source:HGNC Symbol;Acc:4587]	4.82	**4.61**	**4.33**	**4.91**	2.89
HAP1	huntingtin-associated protein 1 [Source:HGNC Symbol;Acc:4812]	3.38	**3.84**	3.79	4.18	**4.67**
HAPLN3	hyaluronan and proteoglycan link protein 3 [Source:HGNC Symbol;Acc:21446]	4.1	3.33	5.12	**4.83**	3.65
HES2	hairy and enhancer of split 2 (Drosophila) [Source:HGNC Symbol;Acc:16005]	3.92	**4.1**	3.4	3.66	2.92
HSPG2	heparan sulfate proteoglycan 2 [Source:HGNC Symbol;Acc:5273]	1.92	1.57	**3.7**	2.82	2.39
IER5	immediate early response 5 [Source:HGNC Symbol;Acc:5393]	1.82	**1.79**	1.46	1.81	1.47
IKBIP	IKBKB interacting protein [Source:HGNC Symbol;Acc:26430]	**3.23**	**2.43**	2.7	**3.22**	1.56
LACC1	laccase (multicopper oxidoreductase) domain containing 1 [Source:HGNC Symbol;Acc:26789]	2.36	1.49	**2.98**	**2.81**	1.65
NPTX1	neuronal pentraxin I [Source:HGNC Symbol;Acc:7952]	5.51	**4.15**	4.49	4.32	3.96
NTN4	netrin 4 [Source:HGNC Symbol;Acc:13658]	3.23	2.38	**4.79**	3.98	2.97
PADI2	peptidyl arginine deiminase, type II [Source:HGNC Symbol;Acc:18341]	**3.6**	**3.36**	2.26	2.91	2.06

PGF	placental growth factor [Source:HGNC Symbol;Acc:8893]	**7.55**	**5.85**	3.75	5.24	3.53
PHYH	phytanoyl-CoA 2-hydroxylase [Source:HGNC Symbol;Acc:8940]	2.35	2.08	2.02	**2.49**	1.93
PLK3	polo-like kinase 3 [Source:HGNC Symbol;Acc:2154]	**2.78**	2.17	2.44	3.04	1.46
POLR2A	polymerase (RNA) II (DNA directed) polypeptide A, 220kDa [Source:HGNC Symbol;Acc:9187]	1.1	0.96	2.27	1.29	**1.72**
RP11-3P17.4	No description	**5.35**	**5.1**	4.76	4.43	4.42
RP11-46C20.1	No description	4.24	**4.35**	3.5	1.71	2.94
RRM2B	ribonucleotide reductase M2 B (TP53 inducible) [Source:HGNC Symbol;Acc:17296]	1.89	**1.97**	2.06	1.67	1.48
SAT1	spermidine/spermine N1-acetyltransferase 1 [Source:HGNC Symbol;Acc:10540]	**3.02**	**2.5**	1.88	2.61	1.77
SESN1	sestrin 1 [Source:HGNC Symbol;Acc:21595]	2.57	1.81	2.63	**2.68**	1.83
SESN2	sestrin 2 [Source:HGNC Symbol;Acc:20746]	2.66	**2.07**	2.14	2.28	1.61
SLC12A4	solute carrier family 12 (potassium/chloride transporters), member 4 [Source:HGNC Symbol;Acc:10913]	**4.57**	**3.56**	1.84	1.9	1.9
SLC6A8	solute carrier family 6 (neurotransmitter transporter, creatine), member 8 [Source:HGNC Symbol;Acc:11055]	**3.38**	**3.09**	**4.11**	**4.34**	**3.45**
STOM	stomatin [Source:HGNC Symbol;Acc:3383]	**2.96**	**2.77**	2.35	**2.37**	**2.16**
SULF2	sulfatase 2 [Source:HGNC Symbol;Acc:20392]	1.6	1	2.34	**2.25**	1.21
TEX14	testis expressed 14 [Source:HGNC Symbol;Acc:11737]	2.64	**2.52**	3.09	3	**2.77**
TNFRSF10B	tumor necrosis factor receptor superfamily, member 10b [Source:HGNC Symbol;Acc:11905]	**3.06**	**2.46**	**3.17**	**3.04**	2.49
TP53I3	tumor protein p53 inducible protein 3 [Source:HGNC Symbol;Acc:19373]	**4.74**	**2.95**	**3.51**	**4.23**	1.53
TP53INP1	tumor protein p53 inducible nuclear protein 1 [Source:HGNC Symbol;Acc:18022]	**3.46**	**2.61**	**3.54**	**3.49**	**2.82**
UPK2	uroplakin 2 [Source:HGNC Symbol;Acc:12579]	**4.69**	**3.96**	**4.2**	**4.97**	**3.98**
WSB1	WD repeat and SOCS box containing 1 [Source:HGNC Symbol;Acc:19221]	**2.41**	1.81	2.07	1.89	1.53
XPC	xeroderma pigmentosum, complementation group C [Source:HGNC Symbol;Acc:12816]	2.08	1.59	2.45	**2.31**	1.62

Up-regulated and down-regulated DEGs in all sublines after DOX-treatment are shaded in orange and blue. Significant DEGs of each subline are indicated with the $\log_2$FC values in bold characters.

Table 5.3 GESA results of the 136 DEGs in MCF-7 sublines.

GO Biological Process Term	Adjusted P-value	Odds Ratio	Combined Score	Genes
136 DEG				
mitotic cell cycle phase transition (GO:0044772)	4.11E-12	12.59	437.42	CDT1;PLK3;CDKN1A;MCM7;UBE2C;PLK1;MCM10;PKMYT1;FOXM1;CCNA2;CCNB1;CDC45;ORC1;MCM3;TACC3;MCM5;MCM6;MCM2;CDKN3

cell cycle G1/S phase transition (GO:0044843)	1.54E-10	20.56	625.65	CDT1;PLK3;CDKN1A;MCM7;MCM10;CCNA2;CDC45;ORC1;MCM3;MCM5;MCM6;MCM2;CDKN3
G1/S transition of mitotic cell cycle (GO:0000082)	5.86E-10	18.04	517.56	PLK3;CDT1;CDKN1A;RRM2;MCM7;MCM10;CDC45;ORC1;MCM3;MCM5;MCM6;MCM2;CDKN3
mitotic sister chromatid segregation (GO:0000070)	1.29E-08	19.49	493.35	CCNB1;PSRC1;SPAG5;PRC1;CDCA5;PLK1;TEX14;KIF2C;DLGAP5;NCAPH;NDC80
DNA metabolic process (GO:0006259)	4.77E-07	7.47	160.48	TOP2A;PIF1;BTG2;MCM7;UHRF1;XPC;MCM10;UNG;BRIP1;CDC45;ORC1;FANCD2;MCM3;MCM5;MCM6;MCM2
DNA replication (GO:0006260)	8.58E-06	12.15	223.77	PIF1;BRIP1;CDC45;ORC1;MCM7;MCM3;MCM10;MCM5;MCM6;MCM2
regulation of mitotic cell cycle (GO:0007346)	1.34E-05	9.74	173.58	TPX2;CCNB1;BTG2;PSRC1;PLK1;TACC3;BIRC5;XPC;MKI67;PKMYT1;MAD2L1
mitotic nuclear division (GO:0140014)	2.42E-05	15.69	266.17	TPX2;SPAG5;UBE2C;PLK1;BIRC5;MYBL2;KIF11;NDC80
mitotic spindle organization (GO:0007052)	2.73E-05	15.69	266.17	TPX2;CCNB1;PRC1;KIF4A;BIRC5;MYBL2;KIF11;NDC80
regulation of mitotic cell cycle phase transition (GO:1901990)	2.87E-05	8.74	145.97	CDC20;ANLN;TPX2;CCNB1;CENPF;UBE2C;PLK1;BUB1B;XPC;HMMR;MAD2L1
mitotic spindle checkpoint (GO:0071174)	3.07E-05	43.25	707.76	CENPF;PLK1;BUB1B;TEX14;BUB1
mitotic spindle assembly checkpoint (GO:0007094)	3.33E-05	43.25	707.76	CENPF;PLK1;BUB1B;TEX14;BUB1
spindle assembly checkpoint (GO:0071173)	3.63E-05	43.25	707.76	CENPF;PLK1;BUB1B;TEX14;BUB1
regulation of cell cycle process (GO:0010564)	7.16E-05	12.93	199.65	PLK3;SPAG5;PRC1;PLK1;KIF20A;MKI67;FOXM1;PKMYT1
positive regulation of mitotic cell cycle phase transition (GO:1901992)	1.11E-04	21.52	321.36	CCNB1;CDC45;UBE2C;CDCA5;DTL;DLGAP5
cellular response to DNA damage stimulus (GO:0006974)	1.33E-04	5.79	85.12	TOP2A;PLK3;CDKN1A;BTG2;MCM7;H2AFX;XPC;MCM10;UNG;BRIP1;FANCD2;DTL;EPHA2
mitotic metaphase plate congression (GO:0007080)	1.52E-04	20.05	290.74	CDT1;CCNB1;PSRC1;CDCA5;KIF2C;NDC80
metaphase plate congression (GO:0051310)	1.64E-04	19.61	281.59	CCNB1;CENPF;PSRC1;CDCA5;KIF2C;NDC80
DNA damage response, signal transduction by p53 class mediator (GO:0030330)	4.17E-04	12.40	165.88	PLK3;BTG2;CDKN1A;MUC1;CCNB1;SESN2;FOXM1
regulation of mitotic cell cycle spindle assembly checkpoint (GO:0090266)	4.96E-04	42.02	552.60	CDT1;CCNB1;NDC80;MAD2L1
regulation of ubiquitin protein ligase activity (GO:1904666)	1.20E-03	19.87	242.80	CDC20;CCNB1;UBE2C;PLK1;MAD2L1
regulation of ubiquitin-protein ligase activity involved in mitotic cell cycle (GO:0051439)	2.40E-03	12.09	138.72	CDC20;CCNB1;UBE2C;PLK1;BUB1B;MAD2L1

regulation of cell proliferation (GO:0042127)	2.59E-03	3.37	38.32	CDKN1A;BTG2;EGLN3;CHRM1;CDCA7;TNFRSF10C;TNFRSF10B;FOXM1;PGF;RERG;GDNF;PRC1;TP53INP1;BIRC5;FAS;IER5;CDKN3
microtubule cytoskeleton organization involved in mitosis (GO:1902850)	2.82E-03	16.34	183.51	CCNB1;KIF4A;TACC3;KIF11;NDC80
positive regulation of ubiquitin-protein ligase activity involved in regulation of mitotic cell cycle transition (GO:0051437)	2.88E-03	11.46	127.97	CDC20;CCNB1;UBE2C;PLK1;BUB1B;MAD2L1
mitotic spindle assembly (GO:0090307)	3.23E-03	15.64	172.31	TPX2;KIF4A;BIRC5;MYBL2;KIF11
anaphase-promoting complex-dependent catabolic process (GO:0031145)	3.33E-03	11.03	120.75	CDC20;CCNB1;UBE2C;PLK1;BUB1B;MAD2L1
DNA replication initiation (GO:0006270)	3.94E-03	23.53	251.13	CDC45;ORC1;MCM10;MCM2
positive regulation of ubiquitin protein ligase activity (GO:1904668)	3.96E-03	10.63	114.13	CDC20;CCNB1;UBE2C;PLK1;BUB1B;MAD2L1
regulation of chromosome organization (GO:0033044)	4.08E-03	23.53	251.13	PIF1;CDT1;HNRNPD;MKI67
G2/M transition of mitotic cell cycle (GO:0000086)	4.30E-03	8.11	85.54	CCNA2;PLK3;CCNB1;CDKN1A;PLK1;PKMYT1;FOXM1
cell cycle G2/M phase transition (GO:0044839)	4.38E-03	8.04	84.47	CCNA2;PLK3;CCNB1;CDKN1A;PLK1;PKMYT1;FOXM1
positive regulation of protein ubiquitination involved in ubiquitin-dependent protein catabolic process (GO:2000060)	4.70E-03	10.03	104.30	CDC20;CCNB1;UBE2C;PLK1;BUB1B;MAD2L1
regulation of transcription involved in G1/S transition of mitotic cell cycle (GO:0000083)	4.77E-03	21.79	225.63	CDT1;CDC45;RRM2;ORC1
regulation of apoptotic process (GO:0042981)	0.01	3.06	31.04	TOP2A;PLK3;EGLN3;GLS2;GDF15;PLK1;TNFRSF10C;TNFRSF10B;TP53I3;GDNF;TP53INP1;ANP32E;BIRC5;FAS;EPHA3;EPHA2;MAD2L1
cellular macromolecule biosynthetic process (GO:0034645)	0.01	4.40	44.08	PIF1;BRIP1;CDC45;ORC1;MCM7;POLR2A;MCM3;MCM10;MCM5;MCM6;MCM2
regulation of chromosome segregation (GO:0051983)	0.01	19.61	194.64	SPAG5;KIF2C;MKI67;BUB1
regulation of chromatin silencing (GO:0031935)	0.01	40.11	398.21	CDC45;UHRF1;ATAD2
attachment of mitotic spindle microtubules to kinetochore (GO:0051315)	0.01	36.76	354.63	CDT1;KIF2C;NDC80
kinetochore organization (GO:0051383)	0.01	36.76	354.63	CDT1;CENPF;NDC80
DNA damage response, signal transduction by p53 class mediator resulting in cell cycle arrest (GO:0006977)	0.01	11.67	111.80	PLK3;BTG2;CDKN1A;MUC1;CCNB1

sister chromatid segregation (GO:0000819)	0.01	17.83	170.08	TOP2A;SPAG5;PLK1;NDC80
signal transduction involved in mitotic G1 DNA damage checkpoint (GO:0072431)	0.01	11.49	109.18	PLK3;BTG2;CDKN1A;MUC1;CCNB1
establishment of chromosome localization (GO:0051303)	0.01	33.94	318.62	CENPF;KIF2C;NDC80
positive regulation of cellular protein localization (GO:1903829)	0.01	10.97	101.88	CDT1;PLK3;SESN2;PLK1;NDC80
regulation of programmed cell death (GO:0043067)	0.01	4.92	45.55	TP53I3;GLS2;GDF15;TP53INP1;TNFRSF10C;ANP32E;TNFRSF10B;BIRC5;FAS

regulation of mitotic spindle organization (GO:0060236)	0.01	16.34	150.21	TPX2;PSRC1;PLK1;TACC3
regulation of cyclin-dependent protein serine/threonine kinase activity (GO:0000079)	0.01	10.81	99.61	CDKN1A;PSRC1;PLK1;PKMYT1;CDKN3
regulation of cell cycle (GO:0051726)	0.01	5.45	49.30	CCNB1;CENPF;PLK1;BIRC5;MYBL2;PKMYT1;FOXM1;DTL
regulation of mitotic metaphase/anaphase transition (GO:0030071)	0.01	29.41	262.77	UBE2C;PLK1;DLGAP5
regulation of exit from mitosis (GO:0007096)	0.01	29.41	262.77	ANLN;UBE2C;CDCA5
regulation of mitotic sister chromatid separation (GO:0010965)	0.01	29.41	262.77	UBE2C;PLK1;TACC3
negative regulation of ubiquitin-protein ligase activity involved in mitotic cell cycle (GO:0051436)	0.01	10.21	91.29	CDC20;CCNB1;UBE2C;BUB1B;MAD2L1
cellular response to amino acid starvation (GO:0034198)	0.01	14.71	129.04	CDKN1A;SESN1;SESN2;FAS
negative regulation of ubiquitin protein ligase activity (GO:1904667)	0.02	9.43	80.70	CDC20;CCNB1;UBE2C;BUB1B;MAD2L1
regulation of spindle organization (GO:0090224)	0.02	24.51	205.02	TPX2;PSRC1;TACC3
positive regulation of cell cycle arrest (GO:0071158)	0.02	8.86	73.26	PLK3;BTG2;CDKN1A;MUC1;CCNB1
regulation of mitotic nuclear division (GO:0007088)	0.03	8.65	70.57	ANLN;PLK1;KIF11;MKI67;PKMYT1
chromosome condensation (GO:0030261)	0.04	19.18	146.07	TOP2A;CDCA5;NCAPH
regulation of G2/M transition of mitotic cell cycle (GO:0010389)	0.05	5.88	43.96	TPX2;CCNB1;CENPF;PLK1;HMMR;DTL
73 DOX-down-regulated genes				
mitotic cell cycle phase transition (GO:0044772)	1.65E-14	20.98	844.87	CDT1;MCM7;UBE2C;PLK1;MCM10;FOXM1;PKMYT1;CCNA2;CCNB1;CDC45;ORC1;MCM3;TACC3;MCM5;MCM6;MCM2;CDKN3
cell cycle G1/S phase transition (GO:0044843)	8.56E-11	32.41	1005.40	CCNA2;CDT1;CDC45;MCM7;ORC1;MCM3;MCM10;MCM5;MCM6;MCM2;CDKN3

G1/S transition of mitotic cell cycle (GO:0000082)	2.51E-10	28.43	840.01	CDT1;CDC45;RRM2;MCM7;ORC1;MCM3;MCM10;MCM5;MCM6;MCM2;CDKN3
mitotic sister chromatid segregation (GO:0000070)	5.55E-10	33.01	939.54	CCNB1;PSRC1;SPAG5;PRC1;CDCA5;PLK1;KIF2C;DLGAP5;NCAPH;NDC80
DNA metabolic process (GO:0006259)	7.09E-09	12.18	312.85	TOP2A;PIF1;MCM7;UHRF1;MCM10;UNG;BRIP1;CDC45;ORC1;FANCD2;MCM3;MCM5;MCM6;MCM2
DNA replication (GO:0006260)	1.73E-08	22.64	557.47	PIF1;BRIP1;CDC45;MCM7;ORC1;MCM3;MCM10;MCM5;MCM6;MCM2
mitotic spindle organization (GO:0007052)	1.88E-07	29.22	641.33	TPX2;CCNB1;PRC1;KIF4A;BIRC5;MYBL2;KIF11;NDC80
mitotic nuclear division (GO:0140014)	2.15E-07	29.22	641.33	TPX2;SPAG5;UBE2C;PLK1;BIRC5;MYBL2;KIF11;NDC80
regulation of mitotic cell cycle phase transition (GO:1901990)	7.64E-07	14.81	302.48	CDC20;ANLN;TPX2;CCNB1;CENPF;UBE2C;PLK1;BUB1B;HMMR;MAD2L1
positive regulation of mitotic cell cycle phase transition (GO:1901992)	3.98E-06	40.09	748.56	CCNB1;CDC45;UBE2C;CDCA5;DTL;DLGAP5

regulation of mitotic cell cycle (GO:0007346)	4.30E-06	14.85	274.76	TPX2;CCNB1;PSRC1;PLK1;TACC3;BIRC5;MKI67;PKMYT1;MAD2L1
mitotic metaphase plate congression (GO:0007080)	5.16E-06	37.36	680.99	CDT1;CCNB1;PSRC1;CDCA5;KIF2C;NDC80
metaphase plate congression (GO:0051310)	5.48E-06	36.53	660.74	CCNB1;CENPF;PSRC1;CDCA5;KIF2C;NDC80
regulation of cell cycle process (GO:0010564)	1.49E-05	21.07	358.60	SPAG5;PRC1;PLK1;KIF20A;MKI67;FOXM1;PKMYT1
regulation of mitotic cell cycle spindle assembly checkpoint (GO:0090266)	5.41E-05	78.28	1225.39	CDT1;CCNB1;NDC80;MAD2L1
regulation of ubiquitin protein ligase activity (GO:1904666)	7.15E-05	37.02	566.84	CDC20;CCNB1;UBE2C;PLK1;MAD2L1
regulation of ubiquitin-protein ligase activity involved in mitotic cell cycle (GO:0051439)	8.08E-05	22.52	340.66	CDC20;CCNB1;UBE2C;PLK1;BUB1B;MAD2L1
mitotic spindle checkpoint (GO:0071174)	9.11E-05	64.46	953.84	CENPF;PLK1;BUB1B;BUB1
mitotic spindle assembly checkpoint (GO:0007094)	9.57E-05	64.46	953.84	CENPF;PLK1;BUB1B;BUB1
spindle assembly checkpoint (GO:0071173)	1.01E-04	64.46	953.84	CENPF;PLK1;BUB1B;BUB1
positive regulation of ubiquitin-protein ligase activity involved in regulation of mitotic cell cycle transition (GO:0051437)	1.05E-04	21.35	316.14	CDC20;CCNB1;UBE2C;PLK1;BUB1B;MAD2L1
anaphase-promoting complex-dependent catabolic process (GO:0031145)	1.08E-04	20.55	299.59	CDC20;CCNB1;UBE2C;PLK1;BUB1B;MAD2L1

positive regulation of ubiquitin protein ligase activity (GO:1904668)	1.29E-04	19.81	284.42	CDC20;CCNB1;UBE2C;PLK1;BUB1B;MAD2L1
microtubule cytoskeleton organization involved in mitosis (GO:1902850)	1.31E-04	30.44	435.38	CCNB1;KIF4A;TACC3;KIF11;NDC80
mitotic spindle assembly (GO:0090307)	1.57E-04	29.15	410.39	TPX2;KIF4A;BIRC5;MYBL2;KIF11
positive regulation of protein ubiquitination involved in ubiquitin-dependent protein catabolic process (GO:2000060)	1.61E-04	18.68	261.77	CDC20;CCNB1;UBE2C;PLK1;BUB1B;MAD2L1
cellular macromolecule biosynthetic process (GO:0034645)	1.65E-04	7.44	103.86	PIF1;BRIP1;CDC45;MCM7;ORC1;MCM3;MCM10;MCM5;MCM6;MCM2
regulation of cell cycle (GO:0051726)	2.18E-04	10.15	138.37	CCNB1;CENPF;PLK1;BIRC5;MYBL2;FOXM1;PKMYT1;DTL
DNA replication initiation (GO:0006270)	3.32E-04	43.84	576.35	CDC45;ORC1;MCM10;MCM2
regulation of chromosome organization (GO:0033044)	3.43E-04	43.84	576.35	PIF1;CDT1;HNRNPD;MKI67
regulation of transcription involved in G1/S transition of mitotic cell cycle (GO:0000083)	4.43E-04	40.59	520.59	CDT1;CDC45;RRM2;ORC1
regulation of chromosome segregation (GO:0051983)	6.64E-04	36.53	452.56	SPAG5;KIF2C;MKI67;BUB1
sister chromatid segregation (GO:0000819)	9.54E-04	33.21	398.38	TOP2A;SPAG5;PLK1;NDC80
negative regulation of ubiquitin-protein ligase activity involved in mitotic cell cycle (GO:0051436)	9.79E-04	19.03	227.18	CDC20;CCNB1;UBE2C;BUB1B;MAD2L1
regulation of mitotic spindle organization (GO:0060236)	1.28E-03	30.44	354.34	TPX2;PSRC1;PLK1;TACC3
attachment of mitotic spindle microtubules to kinetochore (GO:0051315)	1.35E-03	68.49	788.40	CDT1;KIF2C;NDC80
negative regulation of ubiquitin protein ligase activity (GO:1904667)	1.37E-03	17.56	202.78	CDC20;CCNB1;UBE2C;BUB1B;MAD2L1
kinetochore organization (GO:0051383)	1.38E-03	68.49	788.40	CDT1;CENPF;NDC80
establishment of chromosome localization (GO:0051303)	1.70E-03	63.22	711.33	CENPF;KIF2C;NDC80
regulation of mitotic nuclear division (GO:0007088)	1.88E-03	16.12	179.30	ANLN;PLK1;KIF11;MKI67;PKMYT1
regulation of G2/M transition of mitotic cell cycle (GO:0010389)	2.25E-03	10.96	119.66	TPX2;CCNB1;CENPF;PLK1;HMMR;DTL
regulation of mitotic metaphase/anaphase transition (GO:0030071)	2.39E-03	54.79	591.33	UBE2C;PLK1;DLGAP5
regulation of exit from mitosis (GO:0007096)	2.44E-03	54.79	591.33	ANLN;UBE2C;CDCA5
regulation of mitotic sister chromatid separation (GO:0010965)	2.50E-03	54.79	591.33	UBE2C;PLK1;TACC3

cellular response to DNA damage stimulus (GO:0006974)	3.03E-03	6.64	69.94	TOP2A;BRIP1;MCM7;FANCD2;H2AFX;MCM10;DTL;UNG
regulation of spindle organization (GO:0090224)	4.06E-03	45.66	466.46	TPX2;PSRC1;TACC3
DNA-dependent DNA replication (GO:0006261)	0.01	19.23	188.32	CDC45;ORC1;MCM10;MCM2
mitotic cytokinesis (GO:0000281)	0.01	18.26	175.21	ANLN;KIF4A;PLK1;KIF20A
chromosome condensation (GO:0030261)	0.01	35.74	337.84	TOP2A;CDCA5;NCAPH
G2/M transition of mitotic cell cycle (GO:0000086)	0.01	10.79	99.19	CCNA2;CCNB1;PLK1;FOXM1;PKMYT1
cell cycle G2/M phase transition (GO:0044839)	0.01	10.70	98.02	CCNA2;CCNB1;PLK1;FOXM1;PKMYT1
regulation of cyclin-dependent protein serine/threonine kinase activity (GO:0000079)	0.01	16.12	146.68	PSRC1;PLK1;PKMYT1;CDKN3
cytoskeleton-dependent cytokinesis (GO:0061640)	0.01	15.44	137.89	ANLN;KIF4A;PLK1;KIF20A
centromeric sister chromatid cohesion (GO:0070601)	0.02	91.32	780.02	BUB1B;BUB1
positive regulation of ubiquitin-protein transferase activity (GO:0051443)	0.02	25.68	216.97	CDC20;UBE2C;PLK1
spindle assembly (GO:0051225)	0.02	13.53	113.96	TPX2;BIRC5;MYBL2;KIF11
G2 DNA damage checkpoint (GO:0031572)	0.02	24.91	208.09	FANCI;PLK1;DTL
microtubule bundle formation (GO:0001578)	0.02	24.91	208.09	PSRC1;PLK1;KIF20A
regulation of cell cycle G2/M phase transition (GO:1902749)	0.02	12.89	106.21	TPX2;CENPF;PLK1;HMMR
positive regulation of mitotic cell cycle spindle assembly checkpoint (GO:0090267)	0.02	78.28	642.44	NDC80;MAD2L1
regulation of metaphase/anaphase transition of cell cycle (GO:1902099)	0.03	68.49	542.59	UBE2C;PLK1
positive regulation of spindle checkpoint (GO:0090232)	0.03	68.49	542.59	NDC80;MAD2L1
positive regulation of mitotic metaphase/anaphase transition (GO:0045842)	0.04	60.88	467.15	CDT1;DLGAP5
regulation of attachment of spindle microtubules to kinetochore (GO:0051988)	0.05	54.79	408.33	CCNB1;SPAG5
59 DOX-up-regulated genes				
cellular response to amino acid starvation (GO:0034198)	0.03	33.90	408.94	CDKN1A;SESN1;SESN2;FAS
positive regulation of autophagy (GO:0010508)	0.12	19.94	198.16	PLK3;SESN1;SESN2;TP53INP1
protein kinase B signaling (GO:0043491)	0.14	28.25	246.47	PLK3;CDKN1A;EPHA2
regulation of programmed cell death (GO:0043067)	0.14	7.56	67.16	TP53I3;GLS2;GDF15;TP53INP1;TNFRSF10B;FAS
response to leucine (GO:0043201)	0.16	75.33	610.08	SESN1;SESN2

regulation of apoptotic process (GO:0042981)	0.16	4.15	37.37	PLK3;EGLN3;TP53I3;GDNF;GLS2;GDF15;TP53INP1;TNFRSF10B;FAS;EPHA2
cellular response to leucine (GO:0071233)	0.17	75.33	610.08	SESN1;SESN2
cellular response to leucine starvation (GO:1990253)	0.18	67.80	534.07	SESN1;SESN2
DNA damage response, signal transduction by p53 class mediator (GO:0030330)	0.18	16.34	149.59	PLK3;CDKN1A;BTG2;SESN2
activation of cysteine-type endopeptidase activity involved in apoptotic signaling pathway (GO:0097296)	0.18	61.63	473.27	FAS;TNFRSF10B

Table 5.4 137 differentially expressed genes in response to DOX in all ZR75-1 sublines.

Probe	Description	Log_2FC by DOX-treatment		
		shNT	shΔ40p53	shp53α
ANLN	anillin, actin binding protein [Source:HGNC Symbol;Acc:14082]	**-2.53**	**-2.43**	-1.5
ARHGAP11A	Rho GTPase activating protein 11A [Source:HGNC Symbol;Acc:15783]	**-2.75**	-2.3	-1.48
ASPM	asp (abnormal spindle) homolog, microcephaly associated (Drosophila) [Source:HGNC Symbol;Acc:19048]	**-2.65**	**-2.13**	-1.15
ATAD2	ATPase family, AAA domain containing 2 [Source:HGNC Symbol;Acc:30123]	**-2.3**	**-2.02**	-0.71
BUB1B	budding uninhibited by benzimidazoles 1 homolog beta (yeast) [Source:HGNC Symbol;Acc:1149]	-2.16	**-2.11**	-0.95
C2orf54	chromosome 2 open reading frame 54 [Source:HGNC Symbol;Acc:26216]	**-5.12**	**-4.98**	**-4.41**
CCNB1	cyclin B1 [Source:HGNC Symbol;Acc:1579]	**-2.1**	-1.95	-1.27
CDC20	cell division cycle 20 homolog (S. cerevisiae) [Source:HGNC Symbol;Acc:1723]	**-2.82**	**-2.81**	-1.89
CDCA7	cell division cycle associated 7 [Source:HGNC Symbol;Acc:14628]	-3.32	**-3.95**	-1.69
CENPE	centromere protein E, 312kDa [Source:HGNC Symbol;Acc:1856]	-2.54	**-2.4**	-1.31
CENPF	centromere protein F, 350/400kDa (mitosin) [Source:HGNC Symbol;Acc:1857]	**-2**	-1.79	-0.92
DBN1	drebrin 1 [Source:HGNC Symbol;Acc:2695]	-2.17	-2.36	**-1.91**
DIRAS1	DIRAS family, GTP-binding RAS-like 1 [Source:HGNC Symbol;Acc:19127]	-5.07	-4.6	**-3.71**
FADS2	fatty acid desaturase 2 [Source:HGNC Symbol;Acc:3575]	**-1.96**	**-2.02**	**-1.96**
FGFR4	fibroblast growth factor receptor 4 [Source:HGNC Symbol;Acc:3691]	-1.82	**-2.09**	-1.63
IGFBP5	insulin-like growth factor binding protein 5 [Source:HGNC Symbol;Acc:5474]	**-2.54**	**-3.78**	**-1.71**
KIF11	kinesin family member 11 [Source:HGNC Symbol;Acc:6388]	**-2.17**	-1.92	-0.92
KIF1A	kinesin family member 1A [Source:HGNC Symbol;Acc:888]	**-3.74**	**-4.38**	**-2.98**
KIF23	kinesin family member 23 [Source:HGNC Symbol;Acc:6392]	**-1.99**	-1.95	-0.82
LMNB1	lamin B1 [Source:HGNC Symbol;Acc:6637]	-2.45	-2.29	**-1.63**
LRRC31	leucine rich repeat containing 31 [Source:HGNC Symbol;Acc:26261]	**-5.95**	**-3.63**	-3.4
MCM3	minichromosome maintenance complex component 3 [Source:HGNC Symbol;Acc:6945]	**-2.39**	**-2.26**	-0.97
MCM5	minichromosome maintenance complex component 5 [Source:HGNC Symbol;Acc:6948]	**-2.39**	**-2.31**	-1
MCM6	minichromosome maintenance complex component 6 [Source:HGNC Symbol;Acc:6949]	**-3.43**	**-3.52**	**-1.76**
MUC1	mucin 1, cell surface associated [Source:HGNC Symbol;Acc:7508]	**-2.42**	**-1.7**	-1.65
NEK2	NIMA (never in mitosis gene a)-related kinase 2 [Source:HGNC Symbol;Acc:7745]	-2.31	**-2.3**	-0.42
PEG10	paternally expressed 10 [Source:HGNC Symbol;Acc:14005]	-1.73	**-2.35**	-0.4
PIF1	PIF1 5'-to-3' DNA helicase homolog (S. cerevisiae) [Source:HGNC Symbol;Acc:26220]	-3.53	**-4.02**	-1.84

PLK1	polo-like kinase 1 [Source:HGNC Symbol;Acc:9077]	**-2.97**	**-2.94**	**-2.03**
POLD2	polymerase (DNA directed), delta 2, regulatory subunit 50kDa [Source:HGNC Symbol;Acc:9176]	-1.91	**-1.82**	-0.75
PRC1	protein regulator of cytokinesis 1 [Source:HGNC Symbol;Acc:9341]	**-2.12**	**-1.89**	-0.94
RAC3	ras-related C3 botulinum toxin substrate 3 (rho family, small GTP binding protein Rac3) [Source:HGNC Symbol;Acc:9803]	**-2.99**	**-2.65**	**-2.79**
WDR76	WD repeat domain 76 [Source:HGNC Symbol;Acc:25773]	**-3.36**	**-2.91**	-1.21
ACER2	alkaline ceramidase 2 [Source:HGNC Symbol;Acc:23675]	**3.8**	3.27	2.86
ACTA2	actin, alpha 2, smooth muscle, aorta [Source:HGNC Symbol;Acc:130]	**4.67**	**4.45**	**4.72**
ADAMTS7	ADAM metallopeptidase with thrombospondin type 1 motif, 7 [Source:HGNC Symbol;Acc:223]	**4.66**	**3.43**	2.36
AHNAK2	AHNAK nucleoprotein 2 [Source:HGNC Symbol;Acc:20125]	**3.08**	1.52	0.71
AKR1B10	aldo-keto reductase family 1, member B10 (aldose reductase) [Source:HGNC Symbol;Acc:382]	**7.46**	**7.12**	4.55
AL450307.1	Uncharacterized proteincDNA FLJ46300 fis, clone TESTI4035989 [Source:UniProtKB/TrEMBL;Acc:Q6ZRK0]	**8.89**	**7.12**	**7.18**
ANK1	ankyrin 1, erythrocytic [Source:HGNC Symbol;Acc:492]	**5.71**	**3.87**	**3.87**
APOBEC3H	apolipoprotein B mRNA editing enzyme, catalytic polypeptide-like 3H [Source:HGNC Symbol;Acc:24100]	4.83	4.88	**5.65**
ARNT2	aryl-hydrocarbon receptor nuclear translocator 2 [Source:HGNC Symbol;Acc:16876]	3.6	**4.89**	2.52
AXL	AXL receptor tyrosine kinase [Source:HGNC Symbol;Acc:905]	**5.9**	4.34	3
BMF	Bcl2 modifying factor [Source:HGNC Symbol;Acc:24132]	2.1	1.86	**2.11**
BTG2	BTG family, member 2 [Source:HGNC Symbol;Acc:1131]	**2.07**	1.68	**2.22**
C12orf5	chromosome 12 open reading frame 5 [Source:HGNC Symbol;Acc:1185]	**2.34**	**2.07**	**1.93**
C16orf5	chromosome 16 open reading frame 5 [Source:HGNC Symbol;Acc:13234]	**3.5**	**2.67**	**2.22**
C5orf4	chromosome 5 open reading frame 4 [Source:HGNC Symbol;Acc:1334]	5.74	**6.65**	4.01
CABYR	calcium binding tyrosine-(Y)-phosphorylation regulated [Source:HGNC Symbol;Acc:15569]	**2.9**	2.15	**2.21**
CALD1	caldesmon 1 [Source:HGNC Symbol;Acc:1441]	**4.01**	3.69	2.46
CCNG2	cyclin G2 [Source:HGNC Symbol;Acc:1593]	1.47	1.6	**1.68**
CDC42EP3	CDC42 effector protein (Rho GTPase binding) 3 [Source:HGNC Symbol;Acc:16943]	**3.74**	3.12	2.58
CDKN1A	cyclin-dependent kinase inhibitor 1A (p21, Cip1) [Source:HGNC Symbol;Acc:1784]	2.1	1.89	**2.15**
CECR1	cat eye syndrome chromosome region, candidate 1 [Source:HGNC Symbol;Acc:1839]	**3.32**	**2.23**	**3.05**
CLCA2	chloride channel accessory 2 [Source:HGNC Symbol;Acc:2016]	**3.2**	**2.26**	**2.39**
COL17A1	collagen, type XVII, alpha 1 [Source:HGNC Symbol;Acc:2194]	**5.12**	**4.5**	**3.9**
CTD-2377D24.6	No description	**7.85**	**6.21**	**6.14**
CTSL1	cathepsin L1 [Source:HGNC Symbol;Acc:2537]	**2.37**	1.95	1.59

CXCL17	chemokine (C-X-C motif) ligand 17 [Source:HGNC Symbol;Acc:19232]	**3.8**	**2.38**	**3.21**
CYFIP2	cytoplasmic FMR1 interacting protein 2 [Source:HGNC Symbol;Acc:13760]	1.81	**2.51**	1.07
CYP4B1	cytochrome P450, family 4, subfamily B, polypeptide 1 [Source:HGNC Symbol;Acc:2644]	2.28	**3.02**	1.66
DDB2	damage-specific DNA binding protein 2, 48kDa [Source:HGNC Symbol;Acc:2718]	1.49	1.29	**1.83**
EDA2R	ectodysplasin A2 receptor [Source:HGNC Symbol;Acc:17756]	3.19	4	**3.55**
EGLN3	egl nine homolog 3 (C. elegans) [Source:HGNC Symbol;Acc:14661]	**3**	**2.94**	1.97
EPHA2	EPH receptor A2 [Source:HGNC Symbol;Acc:3386]	**3.12**	2.58	1.59
EPHX1	epoxide hydrolase 1, microsomal (xenobiotic) [Source:HGNC Symbol;Acc:3401]	**2.16**	**2.23**	1.45
FAM84A	family with sequence similarity 84, member A [Source:HGNC Symbol;Acc:20743]	**4.93**	**3.57**	**3.21**
FDXR	ferredoxin reductase [Source:HGNC Symbol;Acc:3642]	**3.16**	**2.43**	**2.13**
FLNA	filamin A, alpha [Source:HGNC Symbol;Acc:3754]	**2.19**	1.34	0.43
GADD45A	growth arrest and DNA-damage-inducible, alpha [Source:HGNC Symbol;Acc:4095]	1.6	1.28	**2.16**
GALNT11	No description	1.72	**2.11**	0.92
GDF15	growth differentiation factor 15 [Source:HGNC Symbol;Acc:30142]	**4.22**	**3.9**	**3.58**
GDNF	glial cell derived neurotrophic factor [Source:HGNC Symbol;Acc:4232]	5.43	**6.21**	**6.11**
GLS2	glutaminase 2 (liver, mitochondrial) [Source:HGNC Symbol;Acc:29570]	**3.2**	2.23	2.06
GM2A	GM2 ganglioside activator [Source:HGNC Symbol;Acc:4367]	**2.8**	**2.16**	1.02

GPNMB	glycoprotein (transmembrane) nmb [Source:HGNC Symbol;Acc:4462]	**2.34**	**2.32**	**2.11**
GPR87	G protein-coupled receptor 87 [Source:HGNC Symbol;Acc:4538]	**5.01**	**5.31**	**4.37**
GPX2	glutathione peroxidase 2 (gastrointestinal) [Source:HGNC Symbol;Acc:4554]	2.48	2.61	**2.3**
GRAMD1B	GRAM domain containing 1B [Source:HGNC Symbol;Acc:29214]	**3.22**	2.62	2.55
GRHL3	grainyhead-like 3 (Drosophila) [Source:HGNC Symbol;Acc:25839]	**3.09**	2.99	2.23
HAPLN3	hyaluronan and proteoglycan link protein 3 [Source:HGNC Symbol;Acc:21446]	**6.8**	5.41	2.76
HEPHL1	hephaestin-like 1 [Source:HGNC Symbol;Acc:30477]	**7.67**	**7.49**	4.95
HIST1H2AG	histone cluster 1, H2ag [Source:HGNC Symbol;Acc:4737]	**3.02**	**3.04**	**2.48**
HIST1H4H	histone cluster 1, H4h [Source:HGNC Symbol;Acc:4788]	**2.72**	**3.21**	**2.35**
HIST2H2BE	histone cluster 2, H2be [Source:HGNC Symbol;Acc:4760]	2.85	**3.12**	**2.08**
IGFBP7	insulin-like growth factor binding protein 7 [Source:HGNC Symbol;Acc:5476]	4.56	**6.23**	2.27
ITGAM	integrin, alpha M (complement component 3 receptor 3 subunit) [Source:HGNC Symbol;Acc:6149]	2.82	**6.42**	2.06
ITGB6	integrin, beta 6 [Source:HGNC Symbol;Acc:6161]	1.8	**2.73**	1.63

KIFC3	kinesin family member C3 [Source:HGNC Symbol;Acc:6326]	**4.25**	**4.58**	2.56
KLHDC7A	kelch domain containing 7A [Source:HGNC Symbol;Acc:26791]	**3.62**	2.49	**2.88**
KMO	kynurenine 3-monooxygenase (kynurenine 3-hydroxylase) [Source:HGNC Symbol;Acc:6381]	1.76	1.79	**1.86**
KRT15	keratin 15 [Source:HGNC Symbol;Acc:6421]	1.8	**4.31**	0.91
KRT80	keratin 80 [Source:HGNC Symbol;Acc:27056]	1.93	2.28	**1.46**
LCE1B	late cornified envelope 1B [Source:HGNC Symbol;Acc:16611]	**9.07**	**8.35**	**6.49**
LCE1C	late cornified envelope 1C [Source:HGNC Symbol;Acc:29464]	**6.78**	5.08	2.61
LIF	leukemia inhibitory factor (cholinergic differentiation factor) [Source:HGNC Symbol;Acc:6596]	**2.9**	2.56	**2.52**
LIMK2	LIM domain kinase 2 [Source:HGNC Symbol;Acc:6614]	**2.47**	**2.24**	1.63
MFGE8	milk fat globule-EGF factor 8 protein [Source:HGNC Symbol;Acc:7036]	**4**	**3.26**	**2.55**
MUC19	mucin 19, oligomeric [Source:HGNC Symbol;Acc:14362]	**3.09**	**3.35**	**2.79**
NGFR	nerve growth factor receptor [Source:HGNC Symbol;Acc:7809]	**5.88**	**6.35**	3.17
NPTX1	neuronal pentraxin I [Source:HGNC Symbol;Acc:7952]	**6.66**	3.54	3.88
NR1D1	nuclear receptor subfamily 1, group D, member 1 [Source:HGNC Symbol;Acc:7962]	1.28	1.13	**2.37**
NSG1	Neuron-specific protein family member 1 [Source:UniProtKB/Swiss-Prot;Acc:P42857]	**6.34**	3.45	0.68
NYNRIN	NYN domain and retroviral integrase containing [Source:HGNC Symbol;Acc:20165]	**3.45**	2.39	1.66
PDE4C	phosphodiesterase 4C, cAMP-specific [Source:HGNC Symbol;Acc:8782]	**5.29**	**3.67**	2.6
PGF	placental growth factor [Source:HGNC Symbol;Acc:8893]	**6.57**	5.47	**5.45**
PLA2G4D	phospholipase A2, group IVD (cytosolic) [Source:HGNC Symbol;Acc:30038]	**6.59**	**6.54**	3.91
PLXNA2	plexin A2 [Source:HGNC Symbol;Acc:9100]	2.11	**3.37**	1.25
PML	promyelocytic leukemia [Source:HGNC Symbol;Acc:9113]	**2.46**	1.88	1.55
PTPRB	protein tyrosine phosphatase, receptor type, B [Source:HGNC Symbol;Acc:9665]	**4.55**	4.16	2.4
RCSD1	RCSD domain containing 1 [Source:HGNC Symbol;Acc:28310]	4.15	**7.82**	2.62
RIC3	resistance to inhibitors of cholinesterase 3 homolog (C. elegans) [Source:HGNC Symbol;Acc:30338]	**6.92**	5.58	5.56
RNASE7	ribonuclease, RNase A family, 7 [Source:HGNC Symbol;Acc:19278]	**7.22**	**6.67**	4.46
RP11-115D19.1	No description	**5.61**	**5.45**	**5.48**
RP11-46C20.1	No description	**6.01**	**5.16**	**5.95**
RP11-738E22.2	No description	4.53	**6.14**	2.31
RP3-326I13.1	No description	**7.47**	**6.6**	5.42
RP4-781K5.8	No description	4.5	**4.23**	**3.76**
SAT1	spermidine/spermine N1-acetyltransferase 1 [Source:HGNC Symbol;Acc:10540]	**2.92**	**4.02**	**2.55**

SERPINB5	serpin peptidase inhibitor, clade B (ovalbumin), member 5 [Source:HGNC Symbol;Acc:8949]	**4.59**	**3.95**	2.54
SESN1	sestrin 1 [Source:HGNC Symbol;Acc:21595]	2.22	**2.04**	2.02
SLC12A4	solute carrier family 12 (potassium/chloride transporters), member 4 [Source:HGNC Symbol;Acc:10913]	**2.47**	**2.52**	**1.75**
SMOC1	SPARC related modular calcium binding 1 [Source:HGNC Symbol;Acc:20318]	3.95	**4.72**	**3.65**
ST6GAL1	ST6 beta-galactosamide alpha-2,6-sialyltranferase 1 [Source:HGNC Symbol;Acc:10860]	1.64	1.47	**1.74**
STEAP4	STEAP family member 4 [Source:HGNC Symbol;Acc:21923]	**3.2**	**3.93**	**2.64**
STOM	stomatin [Source:HGNC Symbol;Acc:3383]	1.97	1.81	**1.65**
SULF2	sulfatase 2 [Source:HGNC Symbol;Acc:20392]	**3.89**	**4.65**	**2.81**
SYTL2	synaptotagmin-like 2 [Source:HGNC Symbol;Acc:15585]	1.89	**3.14**	1.12
TGFBI	transforming growth factor, beta-induced, 68kDa [Source:HGNC Symbol;Acc:11771]	4.47	**6.73**	2.07
TMEM229B	transmembrane protein 229B [Source:HGNC Symbol;Acc:20130]	**2.37**	**2.08**	**2.02**
TNFRSF10B	tumor necrosis factor receptor superfamily, member 10b [Source:HGNC Symbol;Acc:11905]	**2.39**	1.85	**1.87**
TNFRSF10C	tumor necrosis factor receptor superfamily, member 10c, decoy without an intracellular domain [Source:HGNC Symbol;Acc:11906]	**3.17**	**2.37**	**2.9**
TNFSF10	tumor necrosis factor (ligand) superfamily, member 10 [Source:HGNC Symbol;Acc:11925]	2.42	**2.33**	1.53
TP53I3	tumor protein p53 inducible protein 3 [Source:HGNC Symbol;Acc:19373]	**5.37**	**4.67**	**2.48**
TP53INP1	tumor protein p53 inducible nuclear protein 1 [Source:HGNC Symbol;Acc:18022]	**2.34**	**2.24**	**2.32**
TRIM22	tripartite motif containing 22 [Source:HGNC Symbol;Acc:16379]	**6.29**	**5.71**	**4.76**
XPC	xeroderma pigmentosum, complementation group C [Source:HGNC Symbol;Acc:12816]	**2.21**	1.84	1.67

Up-regulated and down-regulated DEGs in all sublines after DOX-treatment are shaded in orange and blue. Significant DEGs of each subline are indicated with the $\log_2$FC values in bold characters.

Table 5.5 GSEA results of 137 DEGs in ZR75-1 sublines.

GO Biological Process Term	Adjusted P -value	Odds Ratio	Combined Score	Genes
137 DEGs				
regulation of mitotic cell cycle phase transition (GO:1901990)	0.01	7.10	86.29	CDC20;ANLN;CENPE;CCNB1;CENPF;PLK1;BUB1B ;NEK2;XPC
signal transduction involved in mitotic G1 DNA damage checkpoint (GO:0072431)	0.01	13.69	167.03	BTG2;CDKN1A;MUC1;CCNB1;GADD45A;PML
regulation of cell proliferation (GO:0042127)	0.01	3.35	37.71	NGFR;CDKN1A;BTG2;EGLN3;CDCA7;TNFRSF10C; LIF;TNFRSF10B;PGF;PML;ACER2;GDNF;GPNMB; PRC1;TP53INP1;IGFBP7;FGFR4
mitotic spindle organization (GO:0007052)	0.02	11.68	131.72	CENPE;CCNB1;PRC1;FLNA;KIF23;KIF11

positive regulation of cell cycle arrest (GO:0071158)	0.02	10.55	112.86	BTG2;CDKN1A;MUC1;CCNB1;GADD45A;PML
positive regulation of protein phosphorylation (GO:0001934)	0.02	4.24	44.48	NGFR;CENPE;CDKN1A;GPNMB;GDF15;AXL;PLK1;TNFRSF10C;LIF;TNFRSF10B;FGFR4;EPHA2
DNA damage response, signal transduction by p53 class mediator (GO:0030330)	0.02	10.55	112.86	BTG2;CDKN1A;MUC1;CCNB1;GADD45A;PML
DNA damage response, signal transduction by p53 class mediator resulting in cell cycle arrest (GO:0006977)	0.02	13.90	170.98	BTG2;CDKN1A;MUC1;CCNB1;GADD45A;PML
regulation of apoptotic process (GO:0042981)	0.02	3.04	30.53	NGFR;EGLN3;GADD45A;GLS2;GDF15;PLK1;TNFRSF10C;TNFRSF10B;TP53I3;GDNF;AXL;TP53INP1;TNFSF10;FLNA;BMF;FGFR4;EPHA2
regulation of MAPK cascade (GO:0043408)	0.04	5.72	53.80	NGFR;GDF15;AXL;TNFRSF10C;LIF;TNFRSF10B;FGFR4;EPHA2
33 DOX-down-regulated genes				
regulation of mitotic cell cycle phase transition (GO:1901990)	2.68E-06	26.21	560.02	CDC20;ANLN;CENPE;CCNB1;CENPF;PLK1;BUB1B;NEK2
mitotic spindle organization (GO:0007052)	3.61E-04	40.40	637.18	CENPE;CCNB1;PRC1;KIF23;KIF11
mitotic sister chromatid segregation (GO:0000070)	4.01E-04	36.51	557.12	CENPE;CCNB1;PRC1;PLK1;KIF23
DNA replication (GO:0006260)	1.58E-03	25.04	335.09	PIF1;POLD2;MCM3;MCM5;MCM6
mitotic spindle checkpoint (GO:0071174)	1.75E-03	106.95	1369.82	CENPF;PLK1;BUB1B
mitotic cell cycle phase transition (GO:0044772)	1.92E-03	16.38	219.58	CCNB1;PLK1;MCM3;NEK2;MCM5;MCM6
mitotic spindle assembly checkpoint (GO:0007094)	2.00E-03	106.95	1369.82	CENPF;PLK1;BUB1B
spindle assembly checkpoint (GO:0071173)	2.33E-03	106.95	1369.82	CENPF;PLK1;BUB1B
regulation of ubiquitin-protein ligase activity involved in mitotic cell cycle (GO:0051439)	3.50E-03	33.21	398.38	CDC20;CCNB1;PLK1;BUB1B
positive regulation of ubiquitin-protein ligase activity involved in regulation of mitotic cell cycle transition (GO:0051437)	3.90E-03	31.48	370.97	CDC20;CCNB1;PLK1;BUB1B
anaphase-promoting complex-dependent catabolic process (GO:0031145)	4.12E-03	30.30	352.44	CDC20;CCNB1;PLK1;BUB1B
positive regulation of ubiquitin protein ligase activity (GO:1904668)	4.38E-03	29.21	335.42	CDC20;CCNB1;PLK1;BUB1B
regulation of mitotic nuclear division (GO:0007088)	4.44E-03	28.52	324.83	ANLN;PLK1;NEK2;KIF11

positive regulation of protein ubiquitination involved in ubiquitindependent protein catabolic process (GO:2000060)	4.73E-03	27.55	309.96	CDC20;CCNB1;PLK1;BUB1B
regulation of ubiquitin protein ligase activity (GO:1904666)	0.01	49.14	510.78	CDC20;CCNB1;PLK1
microtubule cytoskeleton organization involved in mitosis (GO:1902850)	0.02	40.40	396.00	CENPE;CCNB1;KIF11
metaphase plate congression (GO:0051310)	0.02	40.40	396.00	CENPE;CCNB1;CENPF
kinetochore assembly (GO:0051382)	0.02	151.52	1442.23	CENPE;CENPF
regulation of metaphase/anaphase transition of cell cycle (GO:1902099)	0.02	151.52	1442.23	CENPE;PLK1
regulation of G2/M transition of mitotic cell cycle (GO:0010389)	0.03	16.16	148.06	CCNB1;CENPF;PLK1;NEK2
regulation of attachment of spindle microtubules to kinetochore (GO:0051988)	0.03	121.21	1096.52	CCNB1;NEK2
mitotic cytokinesis (GO:0000281)	0.03	30.30	270.84	ANLN;PLK1;KIF23
regulation of mitotic centrosome separation (GO:0046602)	0.03	110.19	974.84	NEK2;KIF11
DNA metabolic process (GO:0006259)	0.03	9.62	84.38	PIF1;POLD2;MCM3;MCM5;MCM6
mitotic spindle elongation (GO:0000022)	0.03	110.19	974.84	PRC1;KIF23
kinetochore organization (GO:0051383)	0.03	101.01	875.29	CENPE;CENPF
establishment of chromosome localization (GO:0051303)	0.04	93.24	792.48	CENPE;CENPF
cytoskeleton-dependent cytokinesis (GO:0061640)	0.04	25.61	216.06	ANLN;PLK1;KIF23
negative regulation of ubiquitin-protein ligase activity involved in mitotic cell cycle (GO:0051436)	0.04	25.25	212.01	CDC20;CCNB1;BUB1B
regulation of cytokinesis (GO:0032465)	0.04	23.31	190.19	PRC1;PLK1;KIF23
regulation of mitotic metaphase/anaphase transition (GO:0030071)	0.05	80.81	662.96	CENPE;PLK1
negative regulation of ubiquitin protein ligase activity (GO:1904667)	0.05	23.31	190.19	CDC20;CCNB1;BUB1B
regulation of mitotic sister chromatid separation (GO:0010965)	0.05	80.81	662.96	CENPE;PLK1
retrograde vesicle-mediated transport, Golgi to ER (GO:0006890)	0.05	22.45	180.64	CENPE;KIF23;KIF11
cellular macromolecule biosynthetic process (GO:0034645)	0.05	8.23	66.30	PIF1;POLD2;MCM3;MCM5;MCM6
104 DOX-upregulated genes				
positive regulation of intracellular signal transduction (GO:1902533)	0.07	4.41	44.56	NGFR;AXL;TNFSF10;TNFRSF10C;LIF;TNFRSF10B;FLNA;BMF;TRIM22;EDA2R;EPHA2
regulation of cell proliferation (GO:0042127)	0.08	3.63	37.90	NGFR;CDKN1A;BTG2;EGLN3;TNFRSF10C;LIF;TNFRSF10B;PGF;PML;ACER2;GDNF;GPNMB;TP53INP1;IGFBP7

activation of cysteine-type endopeptidase activity involved in apoptotic process (GO:0006919)	0.08	12.02	116.67	ACER2;NGFR;EGLN3;TNFSF10;TNFRSF10B
regulation of MAPK cascade (GO:0043408)	0.10	6.60	61.09	NGFR;GDF15;AXL;TNFRSF10C;LIF;TNFRSF10B;EPHA2
regulation of apoptotic process (GO:0042981)	0.10	3.54	38.15	NGFR;EGLN3;GADD45A;GLS2;GDF15;TNFRSF10C;TNFRSF10B;TP53I3;GDNF;AXL;TP53INP1;TNFSF10;FLNA;BMF;EPHA2
signal transduction involved in mitotic G1 DNA damage checkpoint (GO:0072431)	0.18	12.02	95.82	BTG2;CDKN1A;GADD45A;PML
apoptotic process (GO:0006915)	0.18	5.80	49.10	CYFIP2;NGFR;EGLN3;GADD45A;TNFRSF10B;BMF;NSG1
DNA damage response, signal transduction by p53 class mediator resulting in cell cycle arrest (GO:0006977)	0.18	12.21	98.08	BTG2;CDKN1A;GADD45A;PML
positive regulation of protein phosphorylation (GO:0001934)	0.19	4.19	33.92	NGFR;CDKN1A;GPNMB;GDF15;AXL;TNFRSF10C;LIF;TNFRSF10B;EPHA2
positive regulation of cysteine-type endopeptidase activity involved in apoptotic process (GO:0043280)	0.20	8.74	71.70	ACER2;NGFR;EGLN3;TNFSF10;TNFRSF10B

Table 5.6 73 DEGs less regulated after DOX-treatment by Δ40p53-overexpression and p53α-knockdown in MCF-7 cells and by p53α-knockdown in ZR75-1 cells.

		Log$_2$FC by DOX-treatment					
		MCF-7				ZR75-1	
Probe	Description	LeGO	Δ40p53	shNT	shp53α	shNT	shp53α
ANLN	anillin, actin binding protein [Source:HGNC Symbol;Acc:14082]	**-3.91**	-1.38	-0.99	-0.38	**-2.53**	-1.50
ANP32E	acidic (leucine-rich) nuclear phosphoprotein 32 family, member E [Source:HGNC Symbol;Acc:16673]	**-2.49**	**-1.92**	-1.73	-1.08	-1.69	-0.79
ARHGAP11A	Rho GTPase activating protein 11A [Source:HGNC Symbol;Acc:15783]	-4.54	-1.98	-1.87	-1.04	**-2.75**	-1.48
ASPM	asp (abnormal spindle) homolog, microcephaly associated (Drosophila) [Source:HGNC Symbol;Acc:19048]	-4.28	-1.63	-1.21	-0.29	**-2.65**	-1.15
ATAD2	ATPase family, AAA domain containing 2 [Source:HGNC Symbol;Acc:30123]	**-3.11**	-1.00	-0.36	0.11	**-2.30**	-0.71
BUB1	budding uninhibited by benzimidazoles 1 homolog (yeast) [Source:HGNC Symbol;Acc:1148]	**-4.19**	-1.69	-1.62	-0.71	-2.34	-1.09
CCNA2	cyclin A2 [Source:HGNC Symbol;Acc:1578]	**-3.80**	-1.90	-1.72	-0.90	-2.26	-1.23
CCNB1	cyclin B1 [Source:HGNC Symbol;Acc:1579]	-1.76	-1.36	-1.83	-1.13	**-2.10**	-1.27
CDC20	cell division cycle 20 homolog (S. cerevisiae) [Source:HGNC Symbol;Acc:1723]	**-3.51**	-1.60	-2.07	-1.15	**-2.82**	-1.89
CDC45	cell division cycle 45 homolog (S. cerevisiae) [Source:HGNC Symbol;Acc:1739]	**-4.60**	-1.22	-1.86	-0.89	-2.24	-0.87
CDCA7	cell division cycle associated 7 [Source:HGNC Symbol;Acc:14628]	**-4.92**	-2.42	-1.72	-1.63	-3.32	-1.69
DEPDC1	DEP domain containing 1 [Source:HGNC Symbol;Acc:22949]	**-6.40**	**-2.79**	-2.23	-1.48	-2.53	-1.19
DHTKD1	dehydrogenase E1 and transketolase domain containing 1 [Source:HGNC Symbol;Acc:23537]	**-2.46**	-0.77	-0.60	-0.09	-1.65	-0.70
FANCD2	Fanconi anemia, complementation group D2 [Source:HGNC Symbol;Acc:3585]	**-2.79**	-0.77	-1.13	-0.44	-1.75	-0.68
FOXM1	forkhead box M1 [Source:HGNC Symbol;Acc:3818]	**-3.16**	-0.98	-1.24	-0.41	-1.97	-0.92
H2AFX	H2A histone family, member X [Source:HGNC Symbol;Acc:4739]	-1.92	-1.44	-2.26	**-1.91**	-1.92	-1.68
KIF11	kinesin family member 11 [Source:HGNC Symbol;Acc:6388]	-3.60	-1.30	-1.18	-0.47	**-2.17**	-0.92
KIF20A	kinesin family member 20A [Source:HGNC Symbol;Acc:9787]	**-5.38**	**-2.40**	-2.02	-1.36	-2.16	-1.22
KIF23	kinesin family member 23 [Source:HGNC Symbol;Acc:6392]	-2.77	-1.07	-0.80	-0.19	**-1.99**	-0.82
KIF4A	kinesin family member 4A [Source:HGNC Symbol;Acc:13339]	**-4.11**	-1.35	-1.17	-0.57	-2.28	-1.01
LMNB1	lamin B1 [Source:HGNC Symbol;Acc:6637]	**-3.17**	-1.60	-1.72	-1.14	-2.45	**-1.63**
MAD2L1	MAD2 mitotic arrest deficient-like 1 (yeast) [Source:HGNC Symbol;Acc:6763]	**-4.45**	-1.52	-2.05	-0.85	-1.88	-0.84
MCM10	minichromosome maintenance complex component 10 [Source:HGNC Symbol;Acc:18043]	**-4.45**	-1.41	-1.15	-0.34	-2.21	-0.61
MCM2	minichromosome maintenance complex component 2 [Source:HGNC Symbol;Acc:6944]	**-3.06**	-1.40	-1.17	-0.75	-2.00	-0.84

MCM3	minichromosome maintenance complex component 3 [Source:HGNC Symbol;Acc:6945]	**-2.79**	-1.24	-1.26	-0.63	**-2.39**	-0.97
MCM5	minichromosome maintenance complex component 5 [Source:HGNC Symbol;Acc:6948]	**-3.09**	-1.29	-1.39	-0.82	**-2.39**	-1.00
MCM6	minichromosome maintenance complex component 6 [Source:HGNC Symbol;Acc:6949]	**-3.47**	-1.75	-1.70	-1.15	**-3.43**	-1.76
MKI67	antigen identified by monoclonal antibody Ki-67 [Source:HGNC Symbol;Acc:7107]	**-4.25**	-1.47	-0.83	-0.22	-1.72	-0.59
MT2A	metallothionein 2A [Source:HGNC Symbol;Acc:7406]	**-3.08**	-1.68	**-3.61**	**-2.31**	-3.24	-1.55
MTHFD1	methylenetetrahydrofolate dehydrogenase (NADP+ dependent) 1, methenyltetrahydrofolate cyclohydrolase, formyltetrahydrofolate synthetase [Source:HGNC Symbol;Acc:7432]	**-2.52**	-1.38	-1.55	-1.03	-2.10	-0.99

NCAPG2	non-SMC condensin II complex, subunit G2 [Source:HGNC Symbol;Acc:21904]	**-2.66**	-0.64	-0.47	-0.01	-1.59	-0.65
PBK	PDZ binding kinase [Source:HGNC Symbol;Acc:18282]	**-5.30**	-1.40	-1.79	-0.87	-1.89	-0.82
PLK1	polo-like kinase 1 [Source:HGNC Symbol;Acc:9077]	**-4.15**	**-2.40**	-2.28	-1.66	**-2.97**	**-2.03**
PRC1	protein regulator of cytokinesis 1 [Source:HGNC Symbol;Acc:9341]	**-3.25**	-1.16	-1.23	-0.62	**-2.12**	-0.94
TACC3	transforming, acidic coiled-coil containing protein 3 [Source:HGNC Symbol;Acc:11524]	**-3.28**	-1.09	-1.46	-0.50	-1.14	-0.61
TOP2A	topoisomerase (DNA) II alpha 170kDa [Source:HGNC Symbol;Acc:11989]	**-2.68**	-0.68	-0.67	-0.13	-1.59	-0.78
TPX2	TPX2, microtubule-associated, homolog (Xenopus laevis) [Source:HGNC Symbol;Acc:1249]	**-3.16**	-1.30	-1.64	-0.80	-1.86	-0.66
TUBA1B	tubulin, alpha 1b [Source:HGNC Symbol;Acc:18809]	**-2.86**	-0.76	-1.48	-0.46	-1.64	-0.62
UHRF1	ubiquitin-like with PHD and ring finger domains 1 [Source:HGNC Symbol;Acc:12556]	**-4.34**	-1.48	-0.64	-0.37	-2.90	-1.15
UNG	uracil-DNA glycosylase [Source:HGNC Symbol;Acc:12572]	-2.45	**-1.71**	-1.65	-1.26	-1.99	-1.24
WDR76	WD repeat domain 76 [Source:HGNC Symbol;Acc:25773]	**-6.02**	-2.18	-1.98	-1.02	**-3.36**	-1.21
ADAMTS7	ADAM metallopeptidase with thrombospondin type 1 motif, 7 [Source:HGNC Symbol;Acc:223]	**6.84**	**4.47**	**6.59**	4.72	**4.66**	2.36
AHNAK2	AHNAK nucleoprotein 2 [Source:HGNC Symbol;Acc:20125]	**4.62**	3.16	**5.52**	2.65	**3.08**	0.71
BTG2	BTG family, member 2 [Source:HGNC Symbol;Acc:1131]	**3.90**	**3.00**	**4.14**	**3.24**	**2.07**	**2.22**
C12orf5	chromosome 12 open reading frame 5 [Source:HGNC Symbol;Acc:1185]	2.47	2.11	1.63	1.15	**2.34**	**1.93**
CABYR	calcium binding tyrosine-(Y)-phosphorylation regulated [Source:HGNC Symbol;Acc:15569]	**4.19**	3.10	3.01	1.69	**2.90**	**2.21**
CDKN1A	cyclin-dependent kinase inhibitor 1A (p21, Cip1) [Source:HGNC Symbol;Acc:1784]	**3.39**	**3.20**	1.92	**2.24**	2.10	**2.15**
CTSL1	cathepsin L1 [Source:HGNC Symbol;Acc:2537]	1.97	1.44	2.20	**1.88**	**2.37**	1.59
DFNB31	deafness, autosomal recessive 31 [Source:HGNC Symbol;Acc:16361]	**3.06**	2.14	**2.95**	1.93	2.32	1.29
EGLN3	egl nine homolog 3 (C. elegans) [Source:HGNC Symbol;Acc:14661]	1.98	**1.93**	2.38	2.09	**3.00**	1.97
EPHA2	EPH receptor A2 [Source:HGNC Symbol;Acc:3386]	**2.54**	**2.03**	**2.94**	1.98	**3.12**	1.59
FAM46A	family with sequence similarity 46, member A [Source:HGNC Symbol;Acc:18345]	2.09	**2.00**	2.45	1.76	1.57	1.62

FAS	Fas (TNF receptor superfamily, member 6) [Source:HGNC Symbol;Acc:11920]	**3.55**	**2.77**	**2.45**	**2.43**	**2.58**	**2.28**
FDXR	ferredoxin reductase [Source:HGNC Symbol;Acc:3642]	**3.47**	**2.41**	2.36	1.82	**3.16**	**2.13**
FSCN1	fascin homolog 1, actin-bundling protein (Strongylocentrotus purpuratus) [Source:HGNC Symbol;Acc:11148]	**3.75**	**3.33**	**4.02**	**3.17**	3.73	0.75
GDNF	glial cell derived neurotrophic factor [Source:HGNC Symbol;Acc:4232]	3.12	2.63	**5.92**	**5.15**	5.43	**6.11**
GLS2	glutaminase 2 (liver, mitochondrial) [Source:HGNC Symbol;Acc:29570]	**3.24**	2.43	2.54	1.17	**3.20**	2.06
GRHL3	grainyhead-like 3 (Drosophila) [Source:HGNC Symbol;Acc:25839]	1.66	1.27	2.39	1.19	**3.09**	2.23
GRIN2C	glutamate receptor, ionotropic, N-methyl D-aspartate 2C [Source:HGNC Symbol;Acc:4587]	4.82	**4.61**	**4.33**	2.89	3.64	1.18
HAPLN3	hyaluronan and proteoglycan link protein 3 [Source:HGNC Symbol;Acc:21446]	4.10	3.33	5.12	3.65	**6.80**	2.76
HIST2H2BE	histone cluster 2, H2be [Source:HGNC Symbol;Acc:4760]	1.82	1.14	1.62	1.24	2.85	**2.08**
IKBIP	IKBKB interacting protein [Source:HGNC Symbol;Acc:26430]	**3.23**	**2.43**	2.70	1.56	2.12	0.71
KIFC3	kinesin family member C3 [Source:HGNC Symbol;Acc:6326]	1.84	1.69	1.79	1.32	**4.25**	2.56
KRT80	keratin 80 [Source:HGNC Symbol;Acc:27056]	0.74	0.78	0.87	0.82	1.93	**1.46**
PLK3	polo-like kinase 3 [Source:HGNC Symbol;Acc:2154]	**2.78**	2.17	2.44	1.46	3.71	2.49
SESN2	sestrin 2 [Source:HGNC Symbol;Acc:20746]	2.66	**2.07**	2.14	1.61	1.80	1.55
SLC6A8	solute carrier family 6 (neurotransmitter transporter, creatine), member 8 [Source:HGNC Symbol;Acc:11055]	**3.38**	**3.09**	**4.11**	**3.45**	1.44	0.75
SULF2	sulfatase 2 [Source:HGNC Symbol;Acc:20392]	1.60	1.00	2.34	1.21	**3.89**	**2.81**
TEX14	testis expressed 14 [Source:HGNC Symbol;Acc:11737]	2.64	**2.52**	3.09	**2.77**	1.40	1.19
TNFRSF10B	tumor necrosis factor receptor superfamily, member 10b [Source:HGNC Symbol;Acc:11905]	**3.06**	**2.46**	**3.17**	**2.49**	**2.39**	**1.87**
UPK2	uroplakin 2 [Source:HGNC Symbol;Acc:12579]	4.69	**3.96**	4.20	3.98	6.10	4.50
WSB1	WD repeat and SOCS box containing 1 [Source:HGNC Symbol;Acc:19221]	**2.41**	1.81	2.07	1.53	1.19	0.96
XPC	xeroderma pigmentosum, complementation group C [Source:HGNC Symbol;Acc:12816]	2.08	1.59	2.45	1.62	**2.21**	1.67

Up-regulated and down-regulated DEGs in all sublines after DOX-treatment are shaded in orange and blue. Significant DEGs of each subline are indicated with the $\log_2$FC values in bold characters.

Table 5.7 GSEA results of 73 DEGs less regulated after DOX-treatment by Δ40p53-overexpression and p53α-knockdown in MCF-7 cells and by p53α-knockdown in ZR75-1 cells.

GO Biological Process Term	Adjusted P-value	Odds Ratio	Combined Score	Genes
mitotic cell cycle phase transition (GO:0044772)	6.68E-09	16.04	438.98	PLK3;CDKN1A;PLK1;MCM10;FOXM1;CCNA2;CCNB1;CDC45;MCM3;TACC3;MCM5;MCM6;MCM2
cell cycle G1/S phase transition (GO:0044843)	1.33E-07	26.51	627.83	CCNA2;PLK3;CDKN1A;CDC45;MCM3;MCM10;MCM5;MCM6;MCM2
DNA metabolic process (GO:0006259)	2.51E-06	10.44	212.25	TOP2A;BTG2;CDC45;FANCD2;UHRF1;MCM3;MCM10;MCM5;XPC;MCM6;MCM2;UNG
G1/S transition of mitotic cell cycle (GO:0000082)	6.14E-06	20.68	396.01	PLK3;CDKN1A;CDC45;MCM3;MCM10;MCM5;MCM6;MCM2
regulation of mitotic cell cycle (GO:0007346)	1.65E-04	13.20	206.47	TPX2;BTG2;CCNB1;PLK1;TACC3;XPC;MKI67;MAD2L1
cellular response to DNA damage stimulus (GO:0006974)	2.35E-04	8.30	124.08	TOP2A;PLK3;BTG2;CDKN1A;FANCD2;H2AFX;MCM10;XPC;EPHA2;UNG
mitotic spindle organization (GO:0007052)	2.69E-04	21.92	328.02	TPX2;CCNB1;PRC1;KIF4A;KIF23;KIF11
DNA damage response, signal transduction by p53 class mediator (GO:0030330)	3.70E-04	19.81	284.42	PLK3;BTG2;CDKN1A;CCNB1;SESN2;FOXM1
regulation of cell cycle process (GO:0010564)	5.67E-04	18.06	249.56	PLK3;PRC1;PLK1;KIF20A;FOXM1;MKI67
mitotic cytokinesis (GO:0000281)	0.001	22.83	293.32	ANLN;KIF4A;PLK1;KIF23;KIF20A
DNA replication (GO:0006260)	0.002	13.59	165.05	CDC45;MCM3;MCM10;MCM5;MCM6;MCM2
mitotic spindle elongation (GO:0000022)	0.002	74.72	881.37	PRC1;KIF4A;KIF23
regulation of mitotic cell cycle phase transition (GO:1901990)	0.002	10.37	126.46	CDC20;ANLN;TPX2;CCNB1;PLK1;XPC;MAD2L1
cytoskeleton-dependent cytokinesis (GO:0061640)	0.002	19.29	231.71	ANLN;KIF4A;PLK1;KIF23;KIF20A
regulation of chromatin silencing (GO:0031935)	0.002	74.72	881.37	CDC45;UHRF1;ATAD2
cell cycle G2/M phase transition (GO:0044839)	0.002	12.84	151.86	CCNA2;PLK3;CDKN1A;CCNB1;PLK1;FOXM1
G2/M transition of mitotic cell cycle (GO:0000086)	0.003	12.94	153.64	CCNA2;PLK3;CDKN1A;CCNB1;PLK1;FOXM1
regulation of ubiquitin protein ligase activity (GO:1904666)	0.003	29.62	341.46	CDC20;CCNB1;PLK1;MAD2L1
regulation of cytokinesis (GO:0032465)	0.003	17.56	202.78	PLK3;PRC1;PLK1;KIF23;KIF20A
mitotic sister chromatid segregation (GO:0000070)	0.003	16.50	185.54	CCNB1;PRC1;PLK1;KIF23;TEX14
microtubule cytoskeleton organization involved in mitosis (GO:1902850)	0.005	24.35	261.48	CCNB1;KIF4A;TACC3;KIF11
mitotic spindle assembly (GO:0090307)	0.006	23.32	246.28	TPX2;KIF4A;KIF23;KIF11
mitotic spindle checkpoint (GO:0071174)	0.006	48.35	502.59	PLK1;TEX14;BUB1

mitotic spindle assembly checkpoint (GO:0007094)	0.006	48.35	502.59	PLK1;TEX14;BUB1
spindle assembly checkpoint (GO:0071173)	0.007	48.35	502.59	PLK1;TEX14;BUB1
DNA damage response, signal transduction by p53 class mediator resulting in cell cycle arrest (GO:0006977)	0.016	17.40	163.53	PLK3;BTG2;CDKN1A;CCNB1
signal transduction involved in mitotic G1 DNA damage checkpoint (GO:0072431)	0.017	17.12	159.91	PLK3;BTG2;CDKN1A;CCNB1
DNA replication initiation (GO:0006270)	0.018	32.88	302.39	CDC45;MCM10;MCM2
regulation of cell division (GO:0051302)	0.018	16.60	153.07	PLK3;PRC1;PLK1;KIF20A
regulation of ubiquitin-protein ligase activity involved in mitotic cell cycle (GO:0051439)	0.025	15.01	132.49	CDC20;CCNB1;PLK1;MAD2L1
regulation of apoptotic process (GO:0042981)	0.028	3.69	32.01	TOP2A;PLK3;EGLN3;GDNF;GLS2;PLK1;ANP32E;TNFRSF10B;FAS;EPHA2;MAD2L1
positive regulation of ubiquitin-protein ligase activity involved in regulation of mitotic cell cycle transition (GO:0051437)	0.029	14.23	122.66	CDC20;CCNB1;PLK1;MAD2L1
response to ionizing radiation (GO:0010212)	0.029	14.05	120.39	IKBIP;CDKN1A;FANCD2;H2AFX
anaphase-promoting complex-dependent catabolic process (GO:0031145)	0.031	13.70	116.04	CDC20;CCNB1;PLK1;MAD2L1
positive regulation of ubiquitin protein ligase activity (GO:1904668)	0.034	13.20	109.97	CDC20;CCNB1;PLK1;MAD2L1
positive regulation of cell cycle arrest (GO:0071158)	0.035	13.20	109.97	PLK3;BTG2;CDKN1A;CCNB1
regulation of mitotic nuclear division (GO:0007088)	0.036	12.89	106.21	ANLN;PLK1;KIF11;MKI67
protein kinase B signaling (GO:0043491)	0.039	22.83	184.79	PLK3;CDKN1A;EPHA2
regulation of mitotic spindle organization (GO:0060236)	0.04	22.83	184.79	TPX2;PLK1;TACC3
positive regulation of protein ubiquitination involved in ubiquitin-dependent protein catabolic process (GO:2000060)	0.04	12.45	100.93	CDC20;CCNB1;PLK1;MAD2L1
protein-DNA complex assembly (GO:0065004)	0.045	11.91	94.52	H2AFX;ANP32E;XPC;HIST2H2BE

5.5 Discussion

The tumour suppressor p53 is critical to maintain the DNA integrity and response to stress stimuli. In this Chapter, the influence of altered Δ40p53 and p53α levels on the DNA-damage response in our breast cancer cell line models was investigated. Two common chemotherapeutic drugs cisplatin (CDDP) and doxorubicin (DOX) were utilised, both of which have been demonstrated to induce p53dependent responses regarding DNA-repair, cell cycle arrest and apoptosis.

At the basal level prior to treatment, cells were mostly in the G1 phase in all sublines, including the isoform-altered and control sublines (Figure 5.1). The outcome of p53 activation includes G1 cell cycle arrest (309), but our results showed that at the basal level there was very little difference in cell cycle distribution between the sublines and these results were largely expected given the minimal effect of either isoform knockdown on proliferation in Chapter 3 and the fact that either p53α or the Δ40p53 isoform need to be activated to induce cell cycle arrest. Although p53 expression was increased following Δ40p53 overexpression, this did not necessarily result in its activation and hence, we would not expect to see an increase in G1 arrest.

After DNA-damaging treatment, there was a general trend of a decreased G1 population and a sequential increase in the S and G2 population (Figure 5.2-5.4).

CDDP is a cell cycle non-specific drug that induces cell cycle arrest at all phases, but G1-arrest has been shown not to be preferred in p53-defective tumours, where instead, G2 and S arrest was favoured (310). Others have reported that MCF-7 cells do not undergo G1 arrest in response to CDDP even though this cell line contains wt p53 (311).

DOX is a cell cycle specific drug, which mostly inhibits DNA synthesis, and therefore induces cell cycle arrest at S and G2 phases (307). Indeed, we observed G2 arrest following 24 hours of treatment. We also observed a significant increase in S-phase following 24 hours treatment, which has been observed in other studies, where a decrease in the S-phase population is observed at later time points (~72 hours), but an increase is observed at earlier time points (~24 hours) (312).

In response to CDDP, G2 arrest was observed in shNT cells, but this was significantly inhibited by knockdown of Δ40p53 and enhanced by knockdown of p53α when compared to shNT cells in both MCF-7 and ZR75-1, highlighting the opposing roles played by these two p53 isoforms on this cell cycle checkpoint. In response to DOX, similar results were observed. Knockdown of Δ40p53 inhibited G2 arrest. Δ40p53-overexpression enhanced G2, whilst p53α knockdown also enhanced G2. Hence, when Δ40p53 is more highly expressed than p53α, G2 arrest is promoted, very much highlighting alternative roles for these two isoforms. There have been reports of differential regulatory roles of these two

isoforms following endoplasmic reticulum stress, where it has been shown that G1 arrest was governed by p53α, while G2 was governed by Δ40p53 (160). In addition, a study using vector transfection of p53-null H1299 cells has shown that the expression of growth arrest and DNA damage GADD45 (mediating G2 *(103)*) was down-regulated in cells transfected with p53α and was slightly upregulated in cells transfected with Δ40p53 compared to cells transfected with the vector generating both isoforms, further confirming a role for Δ40p53 in control of the G2 checkpoint (313). Knocking down endogenous p53 isoform expression in the context of breast cancer cell lines has not been done previously, and we also confirmed this with the Δ40p53-overexpression model, corroborating a ratio of Δ40p53/p53α being the decisive factor regulating G2 arrest.

Δ40p53-overexpression inhibited apoptosis in response to CDDP and DOX whilst Δ40p53-knockdown enhanced apoptosis in response to these agents in MCF-7 cells. In contrast, p53α-knockdown had limited effect on apoptosis when compared to MCF-7-shNT cells. This suggests that Δ40p53 is the primary isoform responsible for inhibition of apoptosis following DNA damage in this cell line. Those findings are consistent with studies showing Δ40p53 impaired the function of p53 in suppressing tumour growth in H1299 cells and fibroblasts (14, 16), though other studies showed a tumour suppressing function of Δ40p53-overexpression in melanoma cells and hepatocellular carcinoma cells (209, 314). Overexpression models have previously shown that high ratio of Δ40p53 to p53α result in increased formation of heterotetramers, leading to two main consequences. Firstly, heterotetramers composed of both Δ40p53 and p53α do not inactivate p53, instead, the repertoire of target genes regulated by p53 is altered (207). This is due to the fact that the second TAD is still present in Δ40p53. Secondly, Δ40p53 has a high propensity to form aggregates and this is likely to contribute to misfolded-p53 aggregates in cancer cells (315). These two effects contribute to the loss of the traditional p53-induced apoptosis and to increased survival.

We showed that DNA damage was concomitant with induction of p53 protein in MCF-7-LeGO and shNT cells. The induction of p53 by both DNA damaging agents was enhanced in shΔ40p53 cells.

Conversely, p53 was constitutively highly expressed in Δ40p53-overexpression cells and could not be induced further following DNA damage. These results suggest that endogenously, Δ40p53 suppresses post-translational stabilisation/activation of p53. This was further exemplified by the real-time PCR results which demonstrated a significant enhancement of p53-dependent pro-apoptotic target genes compared to shNT cells, when Δ40p53 was knocked down. In contrast, both Δ40p53- and p53α-knockdown inhibited apoptosis induction by the DNA damaging agents in ZR75-1 cells, suggesting that Δ40p53 has a similar function to p53α in this cell line. This has been reported by others as well using overexpression models as described above (209, 314). In addition, expression of Δ40p53 in H1299 cells

lead to increased expression of BAX (of which Δ40p53 has a higher affinity to (208)) and other p53dependent apoptotic genes (313). These results show that the Δ40p53 has the ability to induce apoptosis, but this may be cell context dependent.

Given the discrepancies in the apoptosis results between the Δ40p53-shRNA-transduced ZR75-1 cells and MCF-7 cells, RNA-seq was performed on DOX-treated cells to identify the molecular changes that were responsible for these differences. Clustering showed high levels of separation between cell lines and between treatments (Figure 5.8A).

All differentially expressed genes (DEGs) in MCF-7 or ZR75-1 cells were hierarchically clustered. The down-regulated genes were mostly involved in control over cell cycle progression and the upregulated genes were mostly associated with apoptosis (Table 4.3 and 4.5), in agreement with the current literature investigating DOX (316, 317). In MCF-7 cells particularly, several genes were identified to be differentially suppressed by altering the ratio of Δ40p53/p53α. A critical gene *CCNB1* in cell cycle progression from G2 to M was less down-regulated by DOX-treatment when this ratio was high, and more down-regulated when this ratio was low, implying a positive correlation between G2 arrest and Δ40p53/p53α ratio, and this was in agreement with our cell cycle analysis. CCNB1 is commonly overexpressed in breast cancers and was reported to be a prognostic marker of metastatic ER+ breast cancers (318). Indeed, in our cell lines, the *CCNB1* mRNA expression was relatively abundant (log_2RPM > 7), and it was down-regulated after DOX-treatment in MCF-7 sublines. Similar to this, mitotic checkpoint serine/threonine-protein kinases BUB1 and BUB1B, essential for spindle assembly (319), as well as serine/threonine-protein kinase PLK1, essential for correct centromere localization (320), were differentially down-regulated following the alteration of Δ40p53/p53α ratio. The inhibition of these genes prevents the entry into mitosis phase, and therefore resulted in increased G2 arrest. Several DNA replication licensing factors such as MCM2, 3, 5, 6, 7 and 10 exhibited the same regulation pattern as above, which are necessary for DNA replication at S phase. These MCM proteins promote cell proliferation (321) and have been reported to be associated with multiple cancer types including breast cancer (318, 320). Inhibition of MCM2 resulted in S phase arrest in MCF7 cells after DOX treatment (Figure 5.4), which has also been reported in fibroblasts (322). However in ZR75-1 cells, in spite of global inhibition of gene expression in cell cycle progression, knockdown of Δ40p53 resulted in few differentially inhibited genes governing cell cycle arrest. For example, there was hardly any change in *MCM3, MCM5* and *MCM6* expressions (log_2FC ~0.1 to shNT cells after DOXtreatment), same with *CCNB1* and *PLK1*. The three most significantly down-regulated genes by Δ40p53-knockdown after DOX-treatment were *CDCA7, IGFBP5* and *KIF1A.* The first two are associated with cell proliferation and the last was reported to be associated with DNA repair capacity in breast cancers (323). These DOX-down-regulated genes cannot explain the increased G2 arrest in ZR75-1 cells.

The DOX-up-regulated genes in MCF-7 cells were associated with p53-mediated apoptosis through differentially induced genes expressions of *TP53I3, TP53INP1* and *BTG2* (324-326). BTG2, not only induces apoptosis, but is also reported to induce G2 arrest via CD32 (326). Interestingly, the DOX-upregulated genes in ZR75-1 cells, *BTG2* as well as another G2 arrest-associated gene *GADD45,* were differentially regulated following isoform knockdown, where Δ40p53-knockdown resulted in less induction of both genes, and p53α-knockdown resulted in more induction of both genes (Table 5.4). These results showed that after DOX-treatment in MCF-7 cells, cell cycle arrest was achieved mainly by inhibiting cell cycle progression gene expression; whilst in ZR75-1 cells, this was achieved by activation of cell cycle arrest genes. This illustrates further the difference between different cell lines, but also illustrates that the p53 directed DNA-damage response to the same DNA-damaging agent occurs through various pathways depending on the cellular context.

In ZR75-1 cells, in addition, several growth factors were differentially induced after DOX-treatment. For example, *GDNF* and *IGFBP7*, promoting glioma invasive growth and breast cancer (327, 328) were more up-regulated when knocking down Δ40p53. Moreover, p53-inducible proteins such as TP53I3 and TP53INP1 were not necessarily up-regulated by knockdown of Δ40p53. These factors may counteract one another and neutralize the final outcome induced by DOX, and this may explain why no difference regarding apoptosis was observed in isoform knocked down ZR75-1 cells.

In MCF-7 cells, the Δ40p53/p53 ratio was clearly associated with DOX-inhibited genes (Figure 5.8E). This shows that a high Δ40p53/p53α ratio led to less inhibition of the cell cycle progression. A low Δ40p53/p53α ratio had little impact on ZR75-1 cells but knockdown of p53α had more impact on these DEGs, where they were shown to be less down-regulated and less up-regulated. The same trend was observed when Δ40p53 was overexpressed and p53α was knocked down in MCF-7 cells. After analysis, the genes following this trend belonged to three distinct clusters: one down-regulated cluster where high Δ40p53/p53α inhibited the suppression of these genes in the cluster and two clusters where high Δ40p53/p53α ratio inhibited the induction of these genes within the clusters. These genes were enriched in almost the same categories as the enriched GO categories of the down-regulated genes. Notably, several tumour suppressing genes were still up-regulated, such as *BTG2, CDKN1A and TNFRSF10B,* which was expected because endogenous p53α was knocked down rather than knocked out completely. Even though these genes were up-regulated, the scale of up-regulation was less, suggesting p53α had the dominant control over tumour suppressor genes.

To sum up, our results showed a high ratio of Δ40p53/p53 was negatively associated with inhibition of cell cycle progression following DNA damage, or in other words, lifted the inhibition on cell division. This is not ideal for DNA-repair and replication error correction, and therefore may possibly lead to

genomic instability and accumulated mutations. Additionally, in some cellular contexts, inhibiting the expression of Δ40p53 (such as in MCF-7 cells) resulted in enhanced apoptosis, suggesting a therapeutic benefit of co-administration of siRNA/shRNA to Δ40p53 with DNA-damaging chemotherapies used in breast cancer treatment.

Chapter 6
General Discussion

Chapter 6 Discussion

6.1 Overview

Breast cancer is the most commonly diagnosed female malignancy and the 2nd leading cause of cancerrelated mortalities (1). Breast cancers can be divided into different histological subclasses depending primarily on the positivity of three receptors (ER, PR and HER2) (2), the molecular classification is rather complicated and continuously being updated as knowledge increases. Generally, most breast cancer cases are ER+ (60-80%) (3), and most breast cancers have wild-type *TP53* (9, 10). The *TP53* gene is the most frequently mutated gene in all solid cancers due to its critical role in modulating DNArepair, cell cycle arrest and apoptosis (89, 90). It is regarded as the guardian of the genome and reacts to all types of cytosolic and environmental signals that may lead to abnormalities in the genome (89, 90). The p53 protein acts as a transcription factor in its tetrameric form and activates or suppresses various target genes depending on the stress and cell type (96, 97). Cancer cells commonly contain *TP53* mutations, thus accumulating errors that contribute to genomic instability, and more severely, mutant p53 may act as an oncogene and stimulate tumour progression (137). *TP53* mutations are present in around a quarter of all breast cancer cases and p53 dysregulated genes are a better predictor of outcome and therapeutic responses in breast cancers (11, 12), implying a compromised p53 function by mechanisms other than mutation.

The discovery of p53 isoforms have offered a new perspective in looking at the function of p53. The N-terminally or C-terminally truncated p53 isoforms selectively retain different functional domains of the typical full-length p53 (p53α) (13). Numerous studies over the past decade have linked the

significance of p53 isoforms to cancer and p53 isoforms can serve as independent prognostic markers for patient survival and chemo-responses (13-16). The focus of this thesis is on the N-terminally truncated isoform Δ40p53. Δ40p53 lacks the first 40 amino acids and arises from alternative splicing or alternative initiation of translation. The truncated domain is the first transactivation domain (TAD 1) (14), which has been reported to be essential in transactivating some p53 target genes. However, the second TAD which is retained by Δ40p53 has also been shown to preserve its transactivation abilities on a number of p53 target genes (14, 16), but deciphering which target genes Δ40p53 is capable of regulating is still an area of intense investigation. Δ40p53 is C-terminally intact, and therefore is able to form a homotetramer on its own, or a heterotetramer with p53α (14, 16, 159, 160). Δ40p53 has been reported to have canonical p53-like tumour-suppressor activity but also, lacks the ability to transactivate specific p53-target genes and perform typical p53 functions, and is largely thought to act as an inhibitor of the full-length p53 protein when overexpressed (14, 16). However, there are a lack of studies of the function of endogenous Δ40p53 in breast cancer.

Our laboratory focuses on the relationship between Δ40p53 and breast cancers and have previously revealed a negative link with Δ40p53:p53 expression levels and disease-free survival. Δ40p53 is expressed at a higher level than the other p53 isoforms and is expressed at a higher level in breast tumours when compared to the adjacent normal tissues (17). The negative association between a high Δ40p53/p53α ratio and disease-free survival suggests a potential role for Δ40p53 in breast cancer progression and treatment responses (18).

TP53 status has recently been associated with metastasis-associated processes such as epithelial mesenchymal transition (EMT) and cell mobility, which is relatively under-studied compared with its role in DNA-repair and apoptosis (112, 117). The invasive outgrowth of the tumour is the primary cause of cancer-related deaths, when cancer cells have lost connection to the primary sites, acquired the ability to navigate through other tissue types, escape from the immune system surveillance and adapt to a foreign environment (6, 7). EMT is believed to be a prerequisite for breast cancer metastasis. Breast cancer cells originate commonly from the epithelial cells, which separate the lumen and the stroma like a barrier. In normal conditions, tight cell-cell connections prevent movement of epithelial cells, and upon tumorigenesis, loss of epithelial phenotype accompanied by diminishing E-cadherin and a gain of mesenchymal phenotype and molecular markers, the epithelial cells gradually lose polarity and cell-cell connections (113). Multiple metastatic processes are reported to be directly or indirectly regulated by p53. Given the previous finding of Δ40p53:p53 relationship with patient disease-free survival, we hypothesized a role for Δ40p53 in EMT, cell migration and invasion. An understanding of how Δ40p53 and p53α interplay in the regulation of tumour progression is currently unknown, therefore we performed functional assays and molecular characterization approaches

including RNA-seq and DNA-methylation to define the distinct targets regulated by these isoforms in breast cancer.

One of the major challenges in increasing breast cancer survival is to improve the treatment response. DNA-damaging agents are used to activate p53 in cancer cells in order to trigger p53-mediated apoptosis, but resistance to DNA-damaging agents including cisplatin occurs in breast cancer cases (305) and therefore, a better understanding of the mechanisms that can enhance the DNA damage response in breast cancer is needed. Even though wt p53 is present in the majority of breast cancers and activation of p53 can be observed upon administration of DNA-damaging agents, knowledge is still lacking in understanding the role that Δ40p53 has in the response to DNA-damaging therapies used in breast cancer treatment.

The scope of this thesis is to investigate the function of Δ40p53 in processes that enable tumour progression including EMT and the response to DNA-damage. An appropriate model needed to be established with endogenously altered □40p53 and p53□ isoform levels. Two breast cancer cell lines (ER+ and wt p53) were chosen to specifically knockdown Δ40p53 or p53α and examine the functional and molecular consequences.

The aims of the studies described in this thesis were:

4. To investigate the functional role of Δ40p53 in breast cancer including the regulation of gene expression, proliferation, cell migration, invasion and EMT;
5. To characterise the epigenetic changes associated with altered Δ40p53 expression;
6. To investigate the role of Δ40p53 in the response to DNA-damaging agents.

This thesis has provided breast cancer cell line models with stably altered Δ40p53 and p53α expression levels, which can be easily used for other functional assays and provide repeatable and consistent results. By researching metastasis-associated functional assays accompanied by molecular characterisation, the mediators of these responses were identified. This thesis has provided novel information of p53 isoform-associated DNA-methylation and p53 isoform-associated DNA-damage responses, which may be applicable to the study of other isoforms and may provide novel insight into the molecular mechanisms governing DNA-damaging treatment responses and resistance in breast cancer.

6.2 Δ40p53 differentially affects EMT re-programming in breast cancer cell lines

The primary goal of the studies described in Chapter 3 was to unveil the link between Δ40p53 and EMT. This is based on our previous publications outlining a negative association between Δ40p53 and

patient survival (17, 18), from which we hypothesized that Δ40p53 may be a negative regulator of EMT-related biological processes leading to a higher metastatic potential.

Gene expression arrays performed on ER+ and ER- breast cancers and grouped based on their relative Δ40p53 mRNA level showed differentially expressed genes were identified between Δ40p53 high and Δ40p53 low samples in ER+ breast cancers but not in ER- breast cancers (Figure 3.1). The differentially expressed genes were mostly enriched in immune-associated processes, but there were also a number of candidates that were significantly associated with cytoskeletal components and ECM connections, indicating a role for Δ40p53 in cell mobility. We also observed that tumour-suppressor genes and immune-stimulating factors were up-regulated. In fact, we found from our RNA-seq and whole genome methylation analysis of breast cancer cell lines that the link between Δ40p53 and immune responses may be underestimated, which will be discussed shortly below.

To determine the functional consequences of alterations in the Δ40p53/p53α ratio in breast cancer, cell proliferation and migration/invasion were evaluated in Chapter 3 of this thesis. Δ40p53overexpression (pre-established MCF-7 cell model, stably overexpressing Δ40p53) inhibited cell proliferation and mobility with a restrained cell migratory front (Figure 3.4A and Figure 3.5A-E). This may due to stronger cell-cell connections mediated by enhanced E-cadherin expression and decreased expression of E-cadherin suppressors (Figure 3.7 and 3.8). Δ40p53 was overexpressed and p53α mRNA (Table 3.3) and protein (Figure 3.2) expression was also enhanced, suggesting a role for Δ40p53 to stabilize p53α, potentially by forming a heterotetramer thus attenuating HDM2-mediated degradation (159). In addition, Δ40p53 has been reported to retain tumour suppressor function under stress due to the presence of the second transactivation domain (206). As such, Δ40p53-overexpression at the basal level was similar to the function of p53α. The overexpression of Δ40p53 resulted in the transcriptional regulation of a number of unique genes as demonstrated from the RNA-seq analysis, which were mostly associated with immune responses through up-regulating multiple cytokineassociated proteins. Interferon/interleukin have been used in immunotherapy treatment of cancer and they work by boosting the innate immune responses (329). Several PARP family members were up-regulated, indicating activated DNA repair. PARP inhibitors in conjunction with genotoxic drugs have been trialed in cancer treatment, and the principle of this is to increase the genomic instability for the immune system to attack the cancer cells (330). Perhaps PARP inhibitors will sensitize cells which overexpress Δ40p53 to the immune system. We also observed an increased expression of *ZEB1* (Figure 3.8G) and *SOX2* (Table 3.3) at the mRNA level, both of which are associated with increased cancer stem cell potential (331, 332). Cancer stem cells mostly grow slowly, while the differentiated progenitor cells replicate faster (333), which may partly explain the reduced proliferation when Δ40p53 was overexpressed (Figure 3.4A).

In contrast, isoform-knockdown in MCF-7 cells was associated with increased cell proliferation and loss of p53α was the dominant factor contributing to cell growth. The role for p53 in suppressing cell growth has been well-studied in the context of DNA repair under stress and in cancer cell models (103), and the p53 isoform Δ133p53 has been found to have mutant p53-like function due to partially loss of DBD (136, 334), demonstrating the regulation of p53 isoforms on the canonical function of the fulllength p53. The fact that Δ40p53-knockdown did not inhibit, but rather moderately enhanced proliferation suggests that Δ40p53 retains tumour suppressive activity in part at the basal level, consistent with the tumour suppressor function observed when Δ40p53 was overexpressed in this cell line. The function of Δ40p53 in cell mobility has never been examined, but p53 has been revealed to regulate EMT and cell migration and invasion, mostly indirectly via other cofactors. Loss and mutation of p53 fails to maintain E-cadherin expression (112, 117) and contributes to increased metastasis in multiple cell types as well as breast cancers (104-107). This was consistent with our results, where we showed increased cell mobility when p53α was knocked down in both MCF-7 and ZR75-1 cells. In MCF7 cells, this was accompanied by decreased expression of the epithelial marker E-cadherin and increased expression of the mesenchymal marker vimentin, demonstrating the significance of p53 in regulating E-cadherin expression. This was not observed following □40p53 knockdown, suggesting that this isoform is partly defective in this ability. RNA-seq analysis showed that genes associated with increased proliferation potential and decreased tumour suppression were differentially expressed following p53α-knockdown, supporting the functional assays. Taken together, these results suggest that loss of p53α in MCF-7 enhanced cancer cell tumorigenecity as expected, and that □40p53 was at least partly defective in these functions, when compared to p53.

Knockdown of p53α in ZR75-1 did not alter proliferation in our hands, but it did significantly enhance migration and invasion, as mentioned above. Knockdown of □40p53 had no effect on proliferation either, but led to an aggregated morphology and decreased cell mobility. Curiously, knockdown of either isoform resulted in high levels of E-cadherin and low levels of vimentin. Re-expression of Ecadherin in metastatic cancer cells while occupying distal sites has been reported in breast cancers using a mouse model (245). This observation may be associated with Δ40p53 or other p53 family members. For instance, loss of p73 was found to promote EMT and down-regulate E-cadherin in MCF10A cells (335), and ZR75-1 are known to express p73 and p73 isoforms (336).

Following knockdown of either isoform in ZR75-1 cells, a number of tumour-asssociated genes and tumour suppressing genes were differentially expressed in the RNA-seq analysis, suggesting that in ZR75-1 cells, p53 was depleted in most of the canonical functions at the basal level. However, isoformknockdown led to a higher numbers of DEGs compared to those of MCF-7 cells, indicating p53 was involved in other biological processes. Unique genes differentially expressed following

Δ40p53knockdown in ZR75-1 cells were enriched in membrane trafficking and adhesion, which was expected from the morphological change. Even though Δ40p53-knockdown led to the highest number of DEGs in this cell line in the RNA-seq analysis, these DEGs were involved in a number of diverse functions with no consistent gene ontologies, indicating Δ40p53 in ZR75-1 cells was of great importance at the basal level where a range of functions were likely to be affected. Unique genes regulated by p53αknockdown were enriched in xenobiotic substance metabolism and carbon metabolism in cancers, showing that loss of p53α mainly affected metabolic processes in ZR75-1 cells. Indeed, p53 affects pathways that mediate metabolic homeostasis and adapt cells to stress and loss or mutation of p53 can result in gain of function, contributing to tumour progression (337). For instance, PIK3/AKT signaling is activated in cancer cells, leading to increased glycolysis, serving as a power source (338); and p53 suppresses this signaling pathway by activating PTEN (339). Δ40p53, in addition, has been associated with PIK3 and IGF signaling, maintaining the embryonic pluripotency (211), Xenobiotic metabolism is closely related to drug resistance. Oxidative stress and reactive oxygen species from metabolizing xenobiotic substances activate p53, and loss of p53 is therefore unable to prevent inflammatory injuries (340). This has been observed in breast cancer cell lines with mutant p53 (341).

Inconsistent results from these MCF-7 and ZR75-1-derived sublines may result from differences in the expression of other endogenous regulators. For example, HDM2 expression level was reported to be higher in ZR75-1 cells than MCF-7 cells (342), and thus suppresses p53 function in this cell line. Δ40p53 is HDM2-insensitive and therefore, may have taken over the function of p53 to a greater extent in these cells when compared to MCF-7 cells; this may be the reason why Δ40p53-knockdown has affected more genes in our RNA-seq analysis. In contrast, a role for Δ40p53 in immunity was evident from both the cell line models and in the breast cancer specimens, which is an area that there has been very few studies in and needs to be examined in order to provide therapeutic strategies. A number of studies have demonstrated a role for Δ133p53 (N-terminus deletion encompassing both TADs) in inflammation. The study by Braithwaite and colleagues using mouse models showed that Δ122p53 (counterpart of Δ133p53 in humans) was pro-inflammatory and led to increased expression of pro-inflammatory cytokines (242). Our study on Δ40p53 adds to this field, showing a strong link between Δ40p53 and immunogenic responses. This has increased the complexity of the function of Δ40p53 in breast cancer, yet meanwhile provides new perspective in targeting breast cancers with a high Δ40p53 expression level.

In these studies, we examined two breast cancer cell lines and this is not necessarily representative of all breast cancer cases and subtypes. Even in our gene expression analysis of the ER+ breast cancer samples, outliers that didn't follow high or low Δ40p53 grouping did exist. A limitation of our cohort

study is the sample size. A much larger cohort is needed to account for all possible aspects that may be affected by altered Δ40p53 level. It is worthy to mention that we showed Δ40p53 expression level to be the highest in TNBC samples, of which mutant p53 was very frequently mutated (10, 17). The purpose of the current studies was to define the function of Δ40p53 in a wt p53 setting, but the role of Δ40p53 in the context of mutant p53 is not known, which needs to be further investigated. In addition, other breast cancer cell lines, including those from different breast cancer subtypes and with mutant p53 could be added to our studies for further EMT-associated functional and molecular analysis, and our custom shRNA will be a very useful tool for this.

6.3 Δ40p53 can regulate DNA methylation

In Chapter 4, the role of p53 and 40p53 in the regulation of methylation was investigated. p53, as the guardian of the genome, is undisputable in maintaining genome integrity by promoting DNA repair and the response to various stressors; furthermore, as discussed in Chapter 1 (Section 1.3.1.5), the function of p53 in epigenetic regulation is an emerging area. As reviewed by Levine, A.J. and colleagues (124), most studies are focused on p53 and epigenetic modifications in stem cells, since stem cells give rise to multiple lineages, which require a large amount of control over epigenetic modifications without altering the genomic information. Epigenetic changes in breast cancer are mostly studied in TNBC cases, which present the highest p53 mutation rate (11, 12, 343), suggesting a less stable epigenome upon p53 loss. The reprogramming factors such as NANOG and SOX2, when added to mouse fibroblast, can alter the DNA methylation signatures to generate iPS (297), and iPS, when differentiating into other progenitor cells, undergo re-established DNA methylation (296). Δ40p53 is highly expressed in mouse embryonic cells maintaining pluripotency, and is down-regulated when differentiation occurs accompanied by down-regulation of the reprogramming factor NANOG (211), and this is a good indicator of a role for Δ40p53 in epigenetic modifications.

Our results support this theory. The number of DMPs were isoform-dependent and cell linedependent. Most DMPs occurred in the gene body and intergenic regions (IGR), which account for the scale of gene expression/splicing variant generation and enhancer occupation respectively (263, 264, 268-270) (Table 4.1). These results indicate that p53 and isoform alteration-mediated DNA methylation predominantly affected the extent of gene expression, rather than direct regulation of the promoters.

DMR analysis showed that the number of DMPs cannot predict the number of DMRs in the current analysis (Table 4.2). DMRs are better predictors of gene regulation than DMPs (274, 275). Multiple DMR analysis vignettes have been developed to identify DMRs in Illumina EPIC BeadChip data, including Bumphunter, DMRcate and the Probe lasso method used in this thesis (236, 260, 274). In addition, DMR identification can be variable depending on the criteria such as minimum DMP within

a DMR and scaling factors defining DMR length and distance between two DMRs. A supplementary method to this is bisulfite-sequencing (344), which uses next-generation sequencing to map the bisulfite-converted DNA to the human genome,, the geographical landscape of DNA methylation is therefore may be better presented.

Our results showed that loss of p53 isoforms are a stronger influencing factor than Δ40p53overexpression toward DNA methylation and subsequent gene expression regulation. AML patients with mutant p53 respond better to demethylation drugs than patients with wt p53 (129), supporting the surveillance of wt p53 over DNA methylation, and our result showing knockdown of p53α contributing to the highest number of DMRs agrees with this. However, p53α-knockdown in ZR75-1 cells did not shown the same extent of control over DNA methylation. p53 may have been suppressed by a high expression level of HDM2 in ZR75-1 cells (342) and our studies in Chapter 3 showed that Δ40p53 functioned similarly to p53α in these cells. Because Δ40p53 cannot be regulated by HDM2, it is possible that in ZR75-1 cells, Δ40p53 is a more active p53 isoform than the full-length p53α, therefore loss of Δ40p53 affected more regional methylation than loss of p53α. Hence, the less predominant impact of p53α-knockdown in these cells may be explained by these observations.

In contrast to the basal level RNA-seq results in Chapter 3, where we showed little overlap between DEGs of isoform-knockdown within MCF-7/ZR75-1 cells, or DEGs in MCF-7 and ZR75-1 cells when a particular isoform was knocked down; we showed a larger overlap between isoform-mediated regional methylation. Indeed, GSEA analysis provided more insights into the potential roles of the genes affected by DMRs, and overall, a large body of transcription factors binding sites were enriched regardless of cell line and isoform status, suggesting that both isoforms are critical in regulating the transactivation of genes. Of note, these affected genes were transcription factors that bind to certain consensus DNA motifs, indicating that p53 and its isoforms execute their functions through the epigenetic regulation of multiple cofactors and other transcription factors. As Sullivan and colleagues reviewed in 2018 (345), p53 is a direct transcriptional activator, but not a direct repressor, and this is realized by recruiting different sets of co-factors. The impact of p53 and its isoforms on methylation also supports this theory, and adding p53-directed methylation to the complexity of the p53 network. In addition, isoform-mediated methylation is associated with multiple inflammatory factors, and this has also been reflected from the gene expression arrays in breast tumours and basal RNA-seq results in breast cancer cell lines in Chapter 3, showing the critical and novel role of Δ40p53 in immune responses, which has previously only been demonstrated for the Δ133p53 isoform (203).

We identified a cytoband region affect by all isoform alterations, chr6p21, which is pathogenic in lymphoid, thymic and ovarian malignancies (281-283). We showed that the aberrant methylation signatures occurred at this region in breast cancer cell lines and that this was associated with p53

isoforms. Genes located in this region include for example, *TNF* and *LTA*, both of which are proinflammatory cytokines promoting carcinogenesis (284, 285), but can also exert an anti-tumour impact by inducing cell death (346). A relationship between p53 and TNF proteins has been established (291), but a link between Δ40p53 and TNF proteins is yet to be investigated. A role for Δ40p53 in inflammatory processes is supported by our analysis of both gene expression and DNA methylation, particularly associated with TNF-associated signalling.

Distinct difference between MCF-7 and ZR75-1 were observed as well, further suggesting that the function of Δ40p53 is context dependent. In MCF-7 cells, isoform-knockdown commonly affected transcription factors that bind to consensus sequences or that were involved in designated pathways such as NF-κB (Table 4.3); whereas in ZR75-1 cells, isoform-knockdown additionally affected a number of micro-RNAs. The expression of micro-RNAs can be controlled by p53 (122) to indirectly regulate downstream targets (p53 induces miR-34a to maintain E-cadherin expression (118)). Relating back to the RNA-seq at the basal level, the difference when Δ40p53 was knocked down between MCF-7 and ZR75-1 cells results from various sources. These evident differences between simply two cell lines exemplified the complexity of breast cancers.

The results in Chapters 3 and 4 showed cell line dependent effects and thus additional wt p53/ER+ breast cancer cell lines are required to validate the findings. A further limitation of this study is that only breast cancer cell lines were used, therefore the methylation changes can only be compared to the vector transduced control sublines, which were also cancer cell lines. Therefore, we are not able to predict isoform-associated methylation involved in tumorigenesis, and a comparison with normal cells is required for this. This could be done by using the normal-like breast cell line MCF10A cells as mentioned above, investigating whether isoform-loss contributes to a cancer-like phenotype. This could also be done by using the HMT-3522 cell line (347), which can transform into malignant cells, and this would provide more information regarding isoform-mediated transition to malignancy.

6.4 The Δ40p53/p53α ratio governs G2 arrest and mediates apoptosis following DNAdamage

Given that canonical p53 functions mainly when cells are under stress through opposing DNAreplication error and cell cycle progression as well as inducing apoptosis (89, 90), and that p53 in MCF7 and ZR75-1 cells is known to be responsive to DNA-damage (342), we sought to investigate the effect of altering the Δ40p53/p53α ratio, following the administration of DNA-damaging agents. In Chapter 5, two drugs, Cisplatin and Doxorubicin, were used to induce DNA-damage in MCF-7 and ZR75-1 derived sublines, following which cell cycle, apoptosis and RNA-seq experiments were performed. In

our hands, physiologically relevant doses were used and there were few apoptotic cells within the first 24 hours of drug treatment. Figure 5.5 showed that differences in apoptosis started to emerge at 24 hours post treatment of either drug, and that this is also the time point when apoptosis in most cells initiated. The major events in the first 24 hours post treatment were likely to be associated with cell cycle arrest.

We revealed that the Δ40p53/p53α ratio governed the cell cycle arrest in response to CDDP/DOX, particularly at G2 in both MCF-7 and ZR75-1. The high Δ40p53/p53α ratio achieved by Δ40p53overexpression or p53α-knockdown was associated with significantly increased G2 arrest (with the exception of CDDP-treated Δ40p53-overexpressing MCF-7 cells), whereas the low Δ40p53/p53α ratio achieved by Δ40p53-knockdown failed to induced G2 arrest. Others have shown that p53α and Δ40p53 separately control G1 arrest and G2 arrest respectively in response to endoplasmic reticulum stress (160). Δ40p53 cannot transactivate p21 due to the loss of TAD1 (16), but the remaining TAD2 retains the ability to transactivate multiple p53-targets including 14-3-3σ (160). 14-3-3σ is a p53 effector that can induce p53-dependent G2 arrest (348). During stress, Δ40p53 has been shown to sequentially induce 14-3-3σ-mediated G2 arrest (349). Our findings here support this, and further suggest that the Δ40p53/p53α ratio is positively associated with G2 arrest.

Extended drug treatment (more than 24 hours) led to apoptosis in MCF-7 cells, where Δ40p53overexpressing cells were less responsive to drug treatment and Δ40p53-knockdown cells were sensitized to drug treatment (Figure 5.5). This suggests that the DNA-damage induced by CDDP/DOX led to breast cancer cell death after cell cycle modulation in the first 24 hours. Both MCF-7 and ZR751 are classified as luminal A breast cancer cell lines (350, 351). The classification was reported by Subik *et al*, based on immunohistochemical staining against ERα, PR and HER2: MCF-7 cells showed more positive ERα and PR staining than ZR75-1 cells and the former also a higher Ki67 index than that of ZR75-1 cells (90% vs. 80%) (350). *TP53* mutations are rare in ER-positive tumours (12% and 29% in luminal A and B respectively), but are common in ER-negative intrinsic subtypes (72% and 80% in HER2-enriched and basal-like respectively) (3). The use of endocrine therapies to treat ER-positive breast cancer is well established. Endocrine therapies inhibit estrogen signalling, either by impeding the transcriptional activity of ER (Tamoxifen, Raloxifene) or diminishing estrogen synthesis (aromatase inhibitors such as Anastrozole, Letrozole and Exemestane), thereby blocking estrogen-induced proliferation (352, 353). Whether Δ40p53 inhibition could further sensitise ER+ cells to these agents is unknown. Addtionally, it is not known whether Δ40p53 would have the same function in other breast cancer subtypes, such as TNBC, which predominantly, contain mutated *TP53*.

As 24-hour post DOX-treatment was a good indicator of the transition from cell cycle arrest to apoptosis, RNA-seq was performed on cells harvested from this time-point. The ratio of Δ40p53/p53α

was negatively associated with DOX-down-regulated genes in MCF-7 cells (Figure 5.8E), and GSEA showed that these genes were mostly enriched in cell cycle progression affecting all phases. Increased G2 arrest associated with a high Δ40p53/p53α ratio was achieved by stronger inhibition of G2-M transition factors such as *CCNB1* (318) and stronger inhibition of factors governing sister chromatid segregation such as MCM proteins (319-321). When Δ40p53/p53α ratio was low, G2 arrest was decreased, while apoptotic processes were switched on by up-regulation of p53 and pro-apoptotic genes *BAX, PUMA* and *NOXA* (Figure 5.6). This is the fundamental reason for using DNA-damage drugs in the clinic (305-307). Even though ZR75-1 cells arrested in G2 exhibited the same trend according to Δ40p53/p53α ratio as shown in MCF-7 cells after DOX-treatment, the ratio-associated pattern in the hierarchical cluster diagram was not seen (Figure 5.3). The DEG list provided some explanations. As mentioned in the discussion in Chapter 5, *BTG2* and *GADD45* were less up-regulated when Δ40p53 was knocked down in ZR75-1 cells, both of which contribute to G2 arrest (103, 326). Cell cycle arrest can be essential for cancer cells to adapt to the environment. For example, colon cancer cells entered p21-induced cell cycle arrest after γ radiation, but were able to regrow, whereas checkpoint deficient cells proceeded to apoptosis (354). These results showed that cell growth arrest and apoptosis are intimately related and governed by the central role of p53 and the Δ40p53 isoform.

The two cell lines used in this thesis were breast cancer cell lines, in which mutations are already present. For instance, the Catalogue Of Somatic Mutation in Cancer database lists 42 entries of MCF7 cell line (some subjected to drug exposures) and the top mutant genes reported include *ERBB4, PIK3CA* and *GATA3* (355). These genes are common mutations in hormone-positive breast cancers and are associated with tumour growth (150). Transduction of shRNA, as used in this thesis, may introduce further mutations into the transformed cell lines. Although we did not specifically investigate mutations arising by this procedure, all transduced sublines were considered relative to the shNT or vector control cell lines. Hence, the biological effects are most likely due to the knockdown or overexpression of p53 and the Δ40p53 isoform rather than mutations that may have been introduced through the transduction process. This could also be further investigated in future studies.

6.5 Future directions

In this thesis, we primarily invesitagted the N-terminally truncated Δ40p53 isoform and its expression at the mRNA and protein levels were validated using real-time quantitative PCR and western blot at the basal level. Other isoforms were not examined, for the reason that our previous study showed the mRNA expression level of Δ40p53 in a panel of breast cancer cell lines including MCF-7 were significantly higher than the other isoforms including p53β, p53γ and Δ133p53 (17). Other p53

isoforms in the established cell line models could be further investigated to reveal the dynamic change of the p53 isoforms in these cells, and this may explain the inconsistent responses between MCF-7 and ZR75-1 cells. The mRNA levels of the p53 isoforms are relatively easy to detect by qPCR, but it will not be possible to examine the protein level via western blotting without specific antibodies for each of the isoforms. The KJCA40 antibody detects isoforms with the first 40 amino acid truncation including α, β and γ forms. Although the latter two forms are rare, we cannot rule out the possibility of their existence within these cell lines. This is also true for the Δ133p53 isoforms when using western blotting. Specific antibodies for the p53 isoforms are needed in order to progress this field further. Alternatively, targeted mass spectrometry may be used to investigate protein expression level of p53 isoforms, the principle of which is to detect the the ions fragmented from the specific peptide (356).

There is a need to investigate the heterogeneity of Δ40p53 expression in both MCF-7 and ZR75-1 cells, as both may not express this isoform in all cells at all times, thus contributing to the variable results. This could be done by performing immunofluorescent staining to investigate the presence and localization of Δ40p53 as well as its co-localization with p53α. Given the results that MCF-7 and ZR751 cells presented similar changes at the molecular level after DOX-treatment, it may be worthwhile to include different stress types. It is very likely that the response of Δ40p53 will depend on the type and severity of DNA damage inflicted, hence, determining which DNA-damaging agents are affected by its expression is crucial. There is also a need to include more breast cancer cell lines in this analysis. MCF7 and ZR75-1 cell lines are appropriate cell line models to use given the aims of this study, but they are not representative of all breast cancer cases, and this also reflects the complexity of breast cancer and its treatment. It is important to note that there are few commercially available breast cancer cell lines with wt p53. A potential solution for this may be culturing primary patient-derived cells.

In addition to the fact that both MCF-7 and ZR75-1 cells express wt p53 as well as ERα, they are both classified as luminal A breast cancer cell lines (350, 351) and are responsive to ER-antagonists as described in Section 6.4. A further direction hereby is by using an ER-antagonist such as tamoxifen (357) to treat these cells and investigate the response while Δ40p53 level was altered.

This study has identified quite a few molecular markers that were differentially regulated by the Δ40p53/p53α ratio and that could be used as molecular markers predicting responses to DNAdamaging drugs. These markers could also be investigated in other cancer types that have low *TP53* mutations, for example, melanoma and prostate cancers. In addition, drugs targeting or enhancing the corresponding markers to augment p53 function could be designed accordingly. Our results have clearly outlined a role for Δ40p53 in immune responses, which has never been examined previously, for this particular p53 isoform. However, whether Δ40p53 exerts an impact on tumour growth or tumour prevention is hard to interpret at the current stage. We have shown that Δ40p53

alteration affects both gene expression and epigenetic modifications, and that the affected genes have both a negative and positive influence on tumorigenesis and/or metastasis. Future studies could focus on these aspects based on the findings of this thesis.

Additionally, studies are lacking regarding Δ40p53 in different subtypes of breast cancers. We have previously reported that the relative mRNA expression level of Δ40p53 was higher in TNBC specimens and cell lines (MDA-MB-231 and MDA-MB-468), but the T-47D cell line (mutant p53/ER+) also expressed a higher Δ40p53 expression level (17). This indicates that the generation of the Δ40p53 isoform may be closely associated with the *TP53* mutation status and/or the hormone receptor status. There is a need to examine Δ40p53 expression level in regards to different molecular subtypes in breast cancers. Estrogen is the main mitogen for the majority of breast cancers, and a growing body of work has shown interaction between ERα and p53, such as loss of p53 expression is concomitant with loss of ERα expression level at the mRNA and protein levels, and vice versa (358). As mentioned in the introduction (Section 1.5.3), p53 isoforms have fundamental regulatory function on the functionality of full-length p53, and thus it can be speculated that Δ40p53, as the mostly highly expressed p53 isoform in breast cancers, has a critical role in the crosstalk between the p53 pathway and ERα pathway. Further studies can be designed to unveil this link. This can be realised by including the tamoxifen-resistant MCF-7 cells (359, 360), which can provide key information on the potential role of Δ40p53 in treatment resistance.

Finally, a major outcome of the work presented in this thesis was that inhibition of endogenous □40p53 expression resulted in enhanced apoptosis following DNA-damaging therapies, suggesting that it acts as an inhibitor of p53□ in certain cellular contexts. More than 19,000 new cases of breast cancer are diagnosed annually in Australia and treatment resistance occurs in approximately a quarter of patients. Almost all cytotoxic therapies used in breast cancer activate the p53 pathway and our results suggest that cases with high levels of □40p53 may not be as responsive to such therapies, when compared to those patients with low levels of this protein. It is possible that a predictive test could be developed to analyse the p53 isoform ratio to determine the likelihood of a particular patient responding to DNA-damaging therapies or whether other treatments may be more beneficial. In this way treatments will be tailored to the patient, providing a better chance of successful responses to therapy. A long-term goal of this project is to develop an inhibitor of Δ40p53 that could be used to treat breast cancer in combination with DNA-damaging therapies. The major challenge will be to develop delivery approaches for Δ40p53 siRNA/shRNA in breast cancer, as the methods used in the laboratory may not be feasible in patients. There are many siRNA-based cancer therapeutics that are in phase I clinical trials and that have proved to have low toxicity and to effectively inhibit their targets and tumour growth (361), so it is possible that an si-therapeutic could be developed to inhibit to

□40p53. Furthermore, an alternative strategy to negate the effects of high □40p53 expression is to increase the levels of full-length p53 and therefore tip the full-length p53 to □40p53 ratio in favour of p53. In order to do this, Nutlin 3a (an HMDM2 antagonist) could be used to inhibit MDM-2-mediated ubiquitination of full-length p53 and prevent its degradation (362). □40p53 lacks the MDM-2 binding domain and cannot be stabilised by Nutlin 3a.

6.6 Conclusions

The aim of the work described in this thesis was to investigate the functional relevance of Δ40p53 in breast cancer. This was done by establishment of stable isoform-altered breast cancer cell line models, performing a series of functional assays on EMT, cell mobility and response to DNA-damaging agents, and the analysis of the associated molecular changes and epigenetic modifications. The results described in this thesis showed the role of Δ40p53 in cancer cell invasiveness is limited and contextdependent and this may involve multi-level modulation, including gene expression through direct transcriptional activation, as well as epigenetic modifications on transcription factors and microRNAs. More importantly, we proposed that a high ratio of Δ40p53/p53α was associated with enhanced G2 arrest and attenuated apoptosis, providing insights into future treatment strategies. This work has also highlighted the heterogeneity of the common luminal A breast cancer subtype and how changes in critical tumor suppressor genes, particularly p53 isoforms, can alter their cellular function.

This thesis has also further provided a novel understanding of the functional role played by Δ40p53 in breast cancers and has further emphasized the potential clinical relevance between Δ40p53 and breast cancer, in particular, it has provided a critical implication for its expression in the response to DNA-damaging therapies. While the focus of this thesis has been on □40p53, it is recognized that a multi-protein system of p53 and isoforms is accountable for cell fate determination (188) and that we cannot study any of the isoforms in isolation- they are all likely to affect the expression and functionality of each other. Looking forward, more functions are likely to be discovered in the p53 isoform field and eventually provide a better understanding of their role in cancer studies.

References

1. Australian Cancer Incidence and Mortality (ACIM) books (AIHW) [Available from: http://www.aihw.gov.au/acim-books/.
2. Macias H, Hinck L. Mammary gland development. Wiley Interdiscip Rev Dev Biol. 2012;1(4):533-57.
3. Eroles P, Bosch A, Perez-Fidalgo JA, Lluch A. Molecular biology in breast cancer: intrinsic subtypes and signaling pathways. Cancer Treat Rev. 2012;38(6):698-707.
4. Bernstein L, Lacey JV, Jr. Receptors, associations, and risk factor differences by breast cancer subtypes: positive or negative? J Natl Cancer Inst. 2011;103(6):451-3.
5. Incidence and Incidence Rates Metastatic Breast Cancer Network [Available from: http://mbcn.org/incidence-and-incidence-rates/.
6. Lu J, Steeg PS, Price JE, Krishnamurthy S, Mani SA, Reuben J, et al. Breast Cancer Metastasis: Challenges and Opportunities. Cancer Research. 2009;69(12):4951-3.
7. Weigelt B, Peterse JL, van 't Veer LJ. Breast cancer metastasis: markers and models. Nat Rev Cancer. 2005;5(8):591-602.
8. Lane DP. Cancer. p53, guardian of the genome. Nature. 1992;358(6381):15-6.
9. Olivier M, Langerød A, Carrieri P, Bergh J, Klaar S, Eyfjord J, et al. The clinical value of somatic TP53 gene mutations in 1,794 patients with breast cancer. Clin Cancer Res. 2006;12.
10. The Cancer Genome Atlas N. Comprehensive molecular portraits of human breast tumours. Nature. 2012;490:61.
11. Miller LD, Smeds J, George J, Vega VB, Vergara L, Ploner A, et al. An expression signature for p53 status in human breast cancer predicts mutation status, transcriptional effects, and patient survival. Proc Natl Acad Sci USA. 2005;102(38):13550-5.
12. Coutant C, Rouzier R, Qi Y, Lehmann-Che J, Bianchini G, Iwamoto T, et al. Distinct p53 gene signatures are needed to predict prognosis and response to chemotherapy in ER-positive and ERnegative breast cancers. Clin Cancer Res. 2011;17(8):2591-601.
13. Bourdon J-C, Fernandes K, Murray-Zmijewski F, Liu G, Diot A, Xirodimas DP, et al. p53 isoforms can regulate p53 transcriptional activity. Genes & Development. 2005;19(18):2122-37.
14. Ghosh A, Stewart D, Matlashewski G. Regulation of Human p53 Activity and Cell Localization by Alternative Splicing. Molecular and Cellular Biology. 2004;24(18):7987-97.
15. Marcel V, Perrier S, Aoubala M, Ageorges S, Groves MJ, Diot A, et al. Delta160p53 is a novel N-terminal p53 isoform encoded by Delta133p53 transcript. FEBS Lett. 2010;584(21):4463-8.
16. Courtois S, Verhaegh G, North S, Luciani MG, Lassus P, Hibner U, et al. DeltaN-p53, a natural isoform of p53 lacking the first transactivation domain, counteracts growth suppression by wild-type p53. Oncogene. 2002;21(44):6722-8.
17. Avery-Kiejda KA, Morten B, Wong-Brown MW, Mathe A, Scott RJ. The relative mRNA expression of p53 isoforms in breast cancer is associated with clinical features and outcome. Carcinogenesis. 2014;35(3):586-96.
18. Morten BC, Wong-Brown MW, Scott RJ, Avery-Kiejda KA. The presence of the intron 3 16 bp duplication polymorphism of p53 (rs17878362) in breast cancer is associated with a low Delta40p53:p53 ratio and better outcome. Carcinogenesis. 2016;37(1):81-6.
19. Australian Institute of Health and Welfare (AIHW) 2015. Australian Cancer Incidence and Mortality (ACIM) books: Breast cancer. Canberra: AIHW. <http://www.aihw.gov.au/acim-books> [Available from: http://www.aihw.gov.au/acim-books/.
20. Breast cancer in Australia: an overview (AIHW) [Available from: http://www.aihw.gov.au/publication-detail/?id=10737423008.
21. Polyak K. Breast cancer: origins and evolution. The Journal of Clinical Investigation. 2007;117(11):3155-63.

22. Cancer in Australia 2017 [Available from: https://www.aihw.gov.au/reports/cancer/cancerin-australia-2017/formats.
23. Cancer in Australia: an overview 2012 (AIHW) [Available from: http://www.aihw.gov.au/publication-detail/?id=60129542359.
24. Pandya S, Moore RG. Breast development and anatomy. Clin Obstet Gynecol. 2011;54(1):91-5.
25. Nounou MI, ElAmrawy F, Ahmed N, Abdelraouf K, Goda S, Syed-Sha-Qhattal H. Breast Cancer: Conventional Diagnosis and Treatment Modalities and Recent Patents and Technologies. Breast Cancer : Basic and Clinical Research. 2015;9(Suppl 2):17-34.
26. Seltenrich N. Institutes in the Lead: Identifying Environmental Factors in Breast Cancer. Environ Health Perspect. 2016;124(11):A199-A205.
27. Ford D, Easton DF. The genetics of breast and ovarian cancer. Br J Cancer. 1995;72(4):80512.
28. Easton D, Ford D, Peto J. Inherited susceptibility to breast cancer. Cancer Surv. 1993;18:95113.
29. de Jong MM, Nolte IM, te Meerman GJ, van der Graaf WT, Oosterwijk JC, Kleibeuker JH, et al. Genes other than BRCA1 and BRCA2 involved in breast cancer susceptibility. J Med Genet. 2002;39(4):225-42.
30. Russo IH, Russo J. Mammary gland neoplasia in long-term rodent studies. Environ Health Perspect. 1996;104(9):938-67.
31. Vorherr H. The Breast: Morphology, Physiology, and Lactation: Academic Press; 1974.
32. Brook CGD, Marshall NJ. Essential Endocrinology: Wiley; 2001.
33. Pietras RJ, Arboleda J, Reese DM, Wongvipat N, Pegram MD, Ramos L, et al. HER-2 tyrosine kinase pathway targets estrogen receptor and promotes hormone-independent growth in human breast cancer cells. Oncogene. 1995;10(12):2435-46.
34. Marquez DC, Chen HW, Curran EM, Welshons WV, Pietras RJ. Estrogen receptors in membrane lipid rafts and signal transduction in breast cancer. Mol Cell Endocrinol. 2006;246(12):91-100.
35. Couse JF, Korach KS. Estrogen receptor null mice: what have we learned and where will they lead us? Endocr Rev. 1999;20(3):358-417.
36. Heldring N, Pike A, Andersson S, Matthews J, Cheng G, Hartman J, et al. Estrogen receptors: how do they signal and what are their targets. Physiol Rev. 2007;87(3):905-31.
37. Wetendorf M, DeMayo FJ. The progesterone receptor regulates implantation, decidualization, and glandular development via a complex paracrine signaling network. Mol Cell Endocrinol. 2012;357(1-2):108-18.
38. Evans RM. The steroid and thyroid hormone receptor superfamily. Science. 1988;240(4854):889-95.
39. Giangrande PH, McDonnell DP. The A and B isoforms of the human progesterone receptor: two functionally different transcription factors encoded by a single gene. Recent Prog Horm Res. 1999;54:291-313; discussion -4.
40. Lange CA, Yee D. Progesterone and breast cancer. Womens Health (Lond Engl). 2008;4(2):151-62.
41. Koutras AK, Evans TR. The epidermal growth factor receptor family in breast cancer. Onco Targets Ther. 2008;1:5-19.
42. Yarden Y, Sliwkowski MX. Untangling the ErbB signalling network. Nat Rev Mol Cell Biol. 2001;2(2):127-37.

43. Pinhel I, Hills M, Drury S, Salter J, Sumo G, A'Hern R, et al. ER and HER2 expression are positively correlated in HER2 non-overexpressing breast cancer. Breast Cancer Res. 2012;14(2):R46.
44. Arpino G, Wiechmann L, Osborne CK, Schiff R. Crosstalk between the estrogen receptor and the HER tyrosine kinase receptor family: molecular mechanism and clinical implications for endocrine therapy resistance. Endocr Rev. 2008;29(2):217-33.
45. Chacon RD, Costanzo MV. Triple-negative breast cancer. Breast Cancer Res. 2010;12 Suppl 2:S3.
46. Sonnenblick A, Fumagalli D, Sotiriou C, Piccart M. Is the differentiation into molecular subtypes of breast cancer important for staging, local and systemic therapy, and follow up? Cancer Treatment Reviews. 2014;40(9):1089-95.
47. Goals fo Treatment fro Metastatic Breast Cancer Living Beyond Breast Cancer [Available from: https://www.lbbc.org/learn/types-breast-cancer/metastatic-breast-cancer/treatments-andresearch-metastatic-breast-cance-5.
48. Harbeck N, Sotlar K, Wuerstlein R, Doisneau-Sixou S. Molecular and protein markers for clinical decision making in breast cancer: Today and tomorrow. Cancer Treatment Reviews.
2014;40(3):434-44.
49. Prat A, Parker JS, Karginova O, Fan C, Livasy C, Herschkowitz JI, et al. Phenotypic and molecular characterization of the claudin-low intrinsic subtype of breast cancer. Breast Cancer Res.
2010;12(5):R68.
50. JCI - Identification of human triple-negative breast cancer subtypes and preclinical models for selection of targeted therapies [Available from: http://www.jci.org/articles/view/45014/pdf.
51. Chiang AC, Massague J. Molecular basis of metastasis. N Engl J Med. 2008;359(26):2814-23. 52. Pereira B, Chin S-F, Rueda OM, Vollan H-KM, Provenzano E, Bardwell HA, et al. The somatic mutation profiles of 2,433 breast cancers refine their genomic and transcriptomic landscapes.
Nature Communications. 2016;7:11479.
53. Kalluri R, Weinberg RA. The basics of epithelial-mesenchymal transition. J Clin Invest. 2009;119(6):1420-8.
54. Powell E, Piwnica-Worms D, Piwnica-Worms H. Contribution of p53 to metastasis. Cancer Discov. 2014;4(4):405-14.
55. Valastyan S, Weinberg RA. Tumor metastasis: molecular insights and evolving paradigms. Cell. 2011;147(2):275-92.
56. Hu M, Yao J, Carroll DK, Weremowicz S, Chen H, Carrasco D, et al. Regulation of in situ to invasive breast carcinoma transition. Cancer Cell. 2008;13(5):394-406.
57. Lewis CE, Pollard JW. Distinct role of macrophages in different tumor microenvironments. Cancer Res. 2006;66(2):605-12.
58. Joyce JA. Therapeutic targeting of the tumor microenvironment. Cancer Cell. 2005;7(6):51320.
59. Tak W. Mak MES. The Immune Response: Basic and Clinical Principles2006.
60. Nagarsheth N, Wicha MS, Zou W. Chemokines in the cancer microenvironment and their relevance in cancer immunotherapy. Nat Rev Immunol. 2017;17(9):559-72.
61. Friedl P, Wolf K. Tumour-cell invasion and migration: diversity and escape mechanisms. Nat Rev Cancer. 2003;3(5):362-74.
62. Enterline HT, Coman DR. The ameboid motility of human and animal neoplastic cells. Cancer. 1950;3(6):1033-8.

63. Condeelis J, Jones J, Segall JE. Chemotaxis of metastatic tumor cells: clues to mechanisms from the Dictyostelium paradigm. Cancer Metastasis Rev. 1992;11(1):55-68.
64. Rintoul RC, Sethi T. The role of extracellular matrix in small-cell lung cancer. Lancet Oncol. 2001;2(7):437-42.
65. Friedl P, Entschladen F, Conrad C, Niggemann B, Zanker KS. CD4+ T lymphocytes migrating in three-dimensional collagen lattices lack focal adhesions and utilize beta1 integrin-independent strategies for polarization, interaction with collagen fibers and locomotion. Eur J Immunol.
1998;28(8):2331-43.
66. Friedl P, Zanker KS, Brocker EB. Cell migration strategies in 3-D extracellular matrix: differences in morphology, cell matrix interactions, and integrin function. Microsc Res Tech.
1998;43(5):369-78.
67. Wolf K, Mazo I, Leung H, Engelke K, von Andrian UH, Deryugina EI, et al. Compensation mechanism in tumor cell migration: mesenchymal-amoeboid transition after blocking of pericellular proteolysis. J Cell Biol. 2003;160(2):267-77.
68. Tester AM, Ruangpanit N, Anderson RL, Thompson EW. MMP-9 secretion and MMP-2 activation distinguish invasive and metastatic sublines of a mouse mammary carcinoma system showing epithelial-mesenchymal transition traits. Clin Exp Metastasis. 2000;18(7):553-60.
69. Nabeshima K, Inoue T, Shimao Y, Okada Y, Itoh Y, Seiki M, et al. Front-cell-specific expression of membrane-type 1 matrix metalloproteinase and gelatinase A during cohort migration of colon carcinoma cells induced by hepatocyte growth factor/scatter factor. Cancer Res. 2000;60(13):3364-
9.
70. Friedl P, Noble PB, Walton PA, Laird DW, Chauvin PJ, Tabah RJ, et al. Migration of coordinated cell clusters in mesenchymal and epithelial cancer explants in vitro. Cancer Res.
1995;55(20):4557-60.
71. Bell CD, Waizbard E. Variability of cell size in primary and metastatic human breast carcinoma. Invasion Metastasis. 1986;6(1):11-20.
72. Nabeshima K, Inoue T, Shimao Y, Kataoka H, Koono M. Cohort migration of carcinoma cells: differentiated colorectal carcinoma cells move as coherent cell clusters or sheets. Histol Histopathol.
1999;14(4):1183-97.
73. Doherty MR, Smigiel JM, Junk DJ, Jackson MW. Cancer Stem Cell Plasticity Drives Therapeutic Resistance. Cancers (Basel). 2016;8(1).
74. Lu Z, Jiang G, Blume-Jensen P, Hunter T. Epidermal growth factor-induced tumor cell invasion and metastasis initiated by dephosphorylation and downregulation of focal adhesion kinase. Mol Cell Biol. 2001;21(12):4016-31.
75. Lamouille S, Derynck R. Cell size and invasion in TGF-beta-induced epithelial to mesenchymal transition is regulated by activation of the mTOR pathway. J Cell Biol. 2007;178(3):437-51.
76. Minchenko A, Bauer T, Salceda S, Caro J. Hypoxic stimulation of vascular endothelial growth factor expression in vitro and in vivo. Laboratory investigation; a journal of technical methods and pathology. 1994;71(3):374-9.
77. Romon R, Adriaenssens E, Lagadec C, Germain E, Hondermarck H, Le Bourhis X. Nerve growth factor promotes breast cancer angiogenesis by activating multiple pathways. Mol Cancer.
2010;9:157.

78. Wang WC, Zhang XF, Peng J, Li XF, Wang AL, Bie YQ, et al. Survival Mechanisms and Influence Factors of Circulating Tumor Cells. Biomed Res Int. 2018;2018:6304701.
79. Kennecke H, Yerushalmi R, Woods R, Cheang MC, Voduc D, Speers CH, et al. Metastatic behavior of breast cancer subtypes. J Clin Oncol. 2010;28(20):3271-7.
80. Soni A, Ren Z, Hameed O, Chanda D, Morgan CJ, Siegal GP, et al. Breast cancer subtypes predispose the site of distant metastases. Am J Clin Pathol. 2015;143(4):471-8.
81. Wang H, Zhang C, Zhang J, Kong L, Zhu H, Yu J. The prognosis analysis of different metastasis pattern in patients with different breast cancer subtypes: a SEER based study. Oncotarget. 2017;8(16):26368-79.
82. Wu SG, Sun JY, Yang LC, Tang LY, Wang X, Chen XT, et al. Patterns of distant metastasis in Chinese women according to breast cancer subtypes. Oncotarget. 2016;7(30):47975-84.
83. Brook N, Brook E, Dharmarajan A, Dass CR, Chan A. Breast cancer bone metastases: pathogenesis and therapeutic targets. Int J Biochem Cell Biol. 2018;96:63-78.
84. Breastcancer.org. https://www.breastcancer.org/symptoms/types/recur_metast/metastic/bone [updated 2018.
85. Braun S, Vogl FD, Naume B, Janni W, Osborne MP, Coombes RC, et al. A pooled analysis of bone marrow micrometastasis in breast cancer. N Engl J Med. 2005;353(8):793-802.
86. Janni W, Vogl FD, Wiedswang G, Synnestvedt M, Fehm T, Juckstock J, et al. Persistence of disseminated tumor cells in the bone marrow of breast cancer patients predicts increased risk for relapse--a European pooled analysis. Clin Cancer Res. 2011;17(9):2967-76.
87. Chambers AF, Naumov GN, Vantyghem SA, Tuck AB. Molecular biology of breast cancer metastasis. Clinical implications of experimental studies on metastatic inefficiency. Breast Cancer Res. 2000;2(6):400-7.
88. Bourdon J-C. p53 and its isoforms in cancer. British Journal of Cancer. 2007;97(3):277-82.
89. Ozaki T, Nakagawara A. Role of p53 in Cell Death and Human. Cancers. 2011;3(1):994-1013.
90. Avery-Kiejda KA, Zhang XD, Adams LJ, Scott RJ, Vojtesek B, Lane DP, et al. Small Molecular Weight Variants of p53 Are Expressed in Human Melanoma Cells and Are Induced by the DNADamaging Agent Cisplatin. Clinical Cancer Research. 2008;14(6):1659-68.
91. Alarcon-Vargas D, Ronai Z. p53-Mdm2--the affair that never ends. Carcinogenesis. 2002;23(4):541-7.
92. Meek DW. Regulation of the p53 response and its relationship to cancer. Biochemical Journal. 2015;469(3):325-46.
93. Junttila MR, Evan GI. p53--a Jack of all trades but master of none. Nat Rev Cancer. 2009;9(11):821-9.
94. Jacobs JJ, Keblusek P, Robanus-Maandag E, Kristel P, Lingbeek M, Nederlof PM, et al. Senescence bypass screen identifies TBX2, which represses Cdkn2a (p19(ARF)) and is amplified in a subset of human breast cancers. Nat Genet. 2000;26(3):291-9.
95. Ozenne P, Eymin B, Brambilla E, Gazzeri S. The ARF tumor suppressor: structure, functions and status in cancer. Int J Cancer. 2010;127(10):2239-47.
96. Shi D, Gu W. Dual Roles of MDM2 in the Regulation of p53: Ubiquitination Dependent and Ubiquitination Independent Mechanisms of MDM2 Repression of p53 Activity. Genes Cancer. 2012;3(3-4):240-8.
97. Levine AJ. p53, the Cellular Gatekeeper for Growth and Division. Cell. 1997;88(3):323-31.
98. Pflaum J, Schlosser S, Müller M. p53 Family and Cellular Stress Responses in Cancer. Frontiers in Oncology. 2014;4.
99. Williams AB, Schumacher B. p53 in the DNA-Damage-Repair Process. Cold Spring Harb Perspect Med. 2016;6(5).

100. Taylor WR, Stark GR. Regulation of the G2/M transition by p53. Oncogene. 2001;20(15):1803-15.
101. Speidel D. Transcription-independent p53 apoptosis: an alternative route to death. Trends Cell Biol. 2010;20(1):14-24.
102. Feng Z. p53 regulation of the IGF-1/AKT/mTOR pathways and the endosomal compartment. Cold Spring Harb Perspect Biol. 2010;2(2):a001057.
103. Levine AJ, Hu W, Feng Z. The P53 pathway: what questions remain to be explored? Cell Death Differ. 2006;13(6):1027-36.
104. Wang S-P, Wang W-L, Chang Y-L, Wu C-T, Chao Y-C, Kao S-H, et al. p53 controls cancer cell invasion by inducing the MDM2-mediated degradation of Slug. Nat Cell Biol. 2009;11(6):694-704. 105. D'Assoro AB, Busby R, Acu ID, Quatraro C, Reinholz MM, Farrugia DJ, et al. Impaired p53 function leads to centrosome amplification, acquired ERalpha phenotypic heterogeneity and distant metastases in breast cancer MCF-7 xenografts. Oncogene. 2008;27(28):3901-11.
106. Xia M, Land H. Tumor suppressor p53 restricts Ras stimulation of RhoA and cancer cell motility. Nat Struct Mol Biol. 2007;14(3):215-23.
107. Sablina AA, Chumakov PM, Kopnin BP. Tumor suppressor p53 and its homologue p73alpha affect cell migration. J Biol Chem. 2003;278(30):27362-71.
108. Toschi E, Rota R, Antonini A, Melillo G, Capogrossi MC. Wild-type p53 gene transfer inhibits invasion and reduces matrix metalloproteinase-2 levels in p53-mutated human melanoma cells. J Invest Dermatol. 2000;114(6):1188-94.
109. Bishop AL, Hall A. Rho GTPases and their effector proteins. Biochem J. 2000;348 Pt 2:241-55.
110. Etienne-Manneville S, Hall A. Rho GTPases in cell biology. Nature. 2002;420(6916):629-35.
111. Guo F, Zheng Y. Rho family GTPases cooperate with p53 deletion to promote primary mouse embryonic fibroblast cell invasion. Oncogene. 2004;23(33):5577-85.
112. Lamouille S, Xu J, Derynck R. Molecular mechanisms of epithelial–mesenchymal transition. Nat Rev Mol Cell Biol. 2014;15(3):178-96.
113. Christofori G, Semb H. The role of the cell-adhesion molecule E-cadherin as a tumoursuppressor gene. Trends Biochem Sci. 1999;24(2):73-6.
114. Valcourt U, Kowanetz M, Niimi H, Heldin CH, Moustakas A. TGF-beta and the Smad signaling pathway support transcriptomic reprogramming during epithelial-mesenchymal cell transition. Mol Biol Cell. 2005;16(4):1987-2002.
115. Zavadil J, Cermak L, Soto-Nieves N, Bottinger EP. Integration of TGF-beta/Smad and Jagged1/Notch signalling in epithelial-to-mesenchymal transition. Embo j. 2004;23(5):1155-65. 116. Wu Y, Zhou BP. New insights of epithelial-mesenchymal transition in cancer metastasis. Acta Biochim Biophys Sin (Shanghai). 2008;40(7):643-50.
117. Peinado H, Olmeda D, Cano A. Snail, Zeb and bHLH factors in tumour progression: an alliance against the epithelial phenotype? Nat Rev Cancer. 2007;7(6):415-28.
118. Siemens H, Jackstadt R, Hunten S, Kaller M, Menssen A, Gotz U, et al. miR-34 and SNAIL form a double-negative feedback loop to regulate epithelial-mesenchymal transitions. Cell Cycle. 2011;10(24):4256-71.
119. Jung CH, Kim J, Park JK, Hwang SG, Moon SK, Kim WJ, et al. Mdm2 increases cellular invasiveness by binding to and stabilizing the Slug mRNA. Cancer Lett. 2013;335(2):270-7. 120. Shiota M, Izumi H, Onitsuka T, Miyamoto N, Kashiwagi E, Kidani A, et al. Twist and p53 reciprocally regulate target genes via direct interaction. Oncogene. 2008;27(42):5543-53.
121. Vaziri H, Dessain SK, Ng Eaton E, Imai SI, Frye RA, Pandita TK, et al. hSIR2(SIRT1) functions as an NAD-dependent p53 deacetylase. Cell. 2001;107(2):149-59.

122. Yamakuchi M, Lowenstein CJ. MiR-34, SIRT1 and p53: the feedback loop. Cell Cycle. 2009;8(5):712-5.
123. Xu J, Zhu W, Xu W, Yao W, Zhang B, Xu Y, et al. Up-regulation of MBD1 promotes pancreatic cancer cell epithelial-mesenchymal transition and invasion by epigenetic down-regulation of Ecadherin. Current molecular medicine. 2013;13(3):387-400.
124. Levine AJ, Berger SL. The interplay between epigenetic changes and the p53 protein in stem cells. Genes Dev. 2017;31(12):1195-201.
125. Huang J, Perez-Burgos L, Placek BJ, Sengupta R, Richter M, Dorsey JA, et al. Repression of p53 activity by Smyd2-mediated methylation. Nature. 2006;444(7119):629-32.
126. Shi X, Kachirskaia I, Yamaguchi H, West LE, Wen H, Wang EW, et al. Modulation of p53 function by SET8-mediated methylation at lysine 382. Mol Cell. 2007;27(4):636-46.
127. Noguchi H, Miyagi-Shiohira C, Nakashima Y. Induced Tissue-Specific Stem Cells and Epigenetic Memory in Induced Pluripotent Stem Cells. International journal of molecular sciences. 2018;19(4).
128. Hong H, Takahashi K, Ichisaka T, Aoi T, Kanagawa O, Nakagawa M, et al. Suppression of induced pluripotent stem cell generation by the p53-p21 pathway. Nature. 2009;460(7259):1132-5. 129. Welch JS, Petti AA, Miller CA, Fronick CC, O'Laughlin M, Fulton RS, et al. TP53 and Decitabine in Acute Myeloid Leukemia and Myelodysplastic Syndromes. N Engl J Med. 2016;375(21):2023-36. 130. Goll MG, Bestor TH. Eukaryotic cytosine methyltransferases. Annu Rev Biochem. 2005;74:481-514.
131. Peterson EJ, Bogler O, Taylor SM. p53-mediated repression of DNA methyltransferase 1 expression by specific DNA binding. Cancer Res. 2003;63(20):6579-82.
132. Lin RK, Wu CY, Chang JW, Juan LJ, Hsu HS, Chen CY, et al. Dysregulation of p53/Sp1 control leads to DNA methyltransferase-1 overexpression in lung cancer. Cancer Res. 2010;70(14):5807-17.
133. Surget S, Khoury MP, Bourdon J-C. Uncovering the role of p53 splice variants in human malignancy: a clinical perspective. OncoTargets and therapy. 2013;7:57-68.
134. Strano S, Dell'Orso S, Di Agostino S, Fontemaggi G, Sacchi A, Blandino G. Mutant p53: an oncogenic transcription factor. Oncogene. 2007;26(15):2212-9.
135. Marcel V, Hainaut P. p53 isoforms - a conspiracy to kidnap p53 tumor suppressor activity? Cell Mol Life Sci. 2009;66(3):391-406.
136. Vieler M, Sanyal S. p53 Isoforms and Their Implications in Cancer. Cancers (Basel). 2018;10(9).
137. Freed-Pastor WA, Prives C. Mutant p53: one name, many proteins. Genes Dev. 2012;26(12):1268-86.
138. Oren M, Rotter V. Mutant p53 gain-of-function in cancer. Cold Spring Harb Perspect Biol. 2010;2(2):a001107.
139. Will K, Warnecke G, Wiesmuller L, Deppert W. Specific interaction of mutant p53 with regions of matrix attachment region DNA elements (MARs) with a high potential for base-unpairing. Proc Natl Acad Sci U S A. 1998;95(23):13681-6.
140. IARC TP53 Database.
141. Kress M, May E, Cassingena R, May P. Simian virus 40-transformed cells express new species of proteins precipitable by anti-simian virus 40 tumor serum. J Virol. 1979;31(2):472-83.
142. Mietz JA, Unger T, Huibregtse JM, Howley PM. The transcriptional transactivation function of wild-type p53 is inhibited by SV40 large T-antigen and by HPV-16 E6 oncoprotein. EMBO J. 1992;11(13):5013-20.
143. Pipas JM. SV40: Cell transformation and tumorigenesis. Virology. 2009;384(2):294-303.

144. Michael D, Oren M. The p53 and Mdm2 families in cancer. Curr Opin Genet Dev. 2002;12(1):53-9.
145. Wu H, Pomeroy SL, Ferreira M, Teider N, Mariani J, Nakayama KI, et al. UBE4B promotes Hdm2-mediated degradation of the tumor suppressor p53. Nat Med. 2011;17(3):347-55.
146. Dillon LM, Miller TW. Therapeutic targeting of cancers with loss of PTEN function. Curr Drug Targets. 2014;15(1):65-79.
147. Dai C, Gu W. p53 post-translational modification: deregulated in tumorigenesis. Trends Mol Med. 2010;16(11):528-36.
148. O'Brate A, Giannakakou P. The importance of p53 location: nuclear or cytoplasmic zip code? Drug Resist Updat. 2003;6(6):313-22.
149. Bosari S, Viale G, Roncalli M, Graziani D, Borsani G, Lee AK, et al. p53 gene mutations, p53 protein accumulation and compartmentalization in colorectal adenocarcinoma. Am J Pathol. 1995;147(3):790-8.
150. The Cancer Genome Atlas Network. Comprehensive molecular portraits of human breast tumours. Nature. 2012;490(7418):61-70.
151. Soussi T, Leroy B, Taschner PE. Recommendations for analyzing and reporting TP53 gene variants in the high-throughput sequencing era. Human mutation. 2014;35(6):766-78.
152. Murray-Zmijewski F, Lane DP, Bourdon JC. p53/p63/p73 isoforms: an orchestra of isoforms to harmonise cell differentiation and response to stress. Cell Death Differ. 2006;13(6):962-72.
153. Aoubala M, Murray-Zmijewski F, Khoury MP, Fernandes K, Perrier S, Bernard H, et al. p53 directly transactivates Delta133p53alpha, regulating cell fate outcome in response to DNA damage.
Cell Death Differ. 2011;18(2):248-58.
154. Rohaly G, Chemnitz J, Dehde S, Nunez AM, Heukeshoven J, Deppert W, et al. A novel human p53 isoform is an essential element of the ATR-intra-S phase checkpoint. Cell. 2005;122(1):21-32.
155. Gorrini C. Discovery of a p53 variant that controls metastasis. Proc Natl Acad Sci U S A. 2014;111(32):11576-7.
156. McLure KG, Lee PW. How p53 binds DNA as a tetramer. EMBO J. 1998;17(12):3342-50. 157. Rodriguez MS, Desterro JM, Lain S, Lane DP, Hay RT. Multiple C-terminal lysine residues target p53 for ubiquitin-proteasome-mediated degradation. Mol Cell Biol. 2000;20(22):8458-67. 158. Graupner V, Schulze-Osthoff K, Essmann F, Janicke RU. Functional characterization of p53beta and p53gamma, two isoforms of the tumor suppressor p53. Cell Cycle. 2009;8(8):1238-48. 159. Hafsi H, Santos-Silva D, Courtois-Cox S, Hainaut P. Effects of Delta40p53, an isoform of p53 lacking the N-terminus, on transactivation capacity of the tumor suppressor protein p53. BMC Cancer. 2013;13:134.
160. Bourougaa K, Naski N, Boularan C, Mlynarczyk C, Candeias MM, Marullo S, et al. Endoplasmic reticulum stress induces G2 cell-cycle arrest via mRNA translation of the p53 isoform p53/47. Mol Cell. 2010;38(1):78-88.
161. Chan WM, Poon RY. The p53 Isoform Deltap53 lacks intrinsic transcriptional activity and reveals the critical role of nuclear import in dominant-negative activity. Cancer Res. 2007;67(5):1959-69.
162. Khoury MP, Bourdon JC. p53 Isoforms: An Intracellular Microprocessor? Genes Cancer. 2011;2(4):453-65.
163. Milicevic Z, Bajic V, Zivkovic L, Kasapovic J, Andjelkovic U, Spremo-Potparevic B. Identification of p53 and its isoforms in human breast carcinoma cells. ScientificWorldJournal. 2014;2014:618698.

164. Senturk S, Yao Z, Camiolo M, Stiles B, Rathod T, Walsh AM, et al. p53Psi is a transcriptionally inactive p53 isoform able to reprogram cells toward a metastatic-like state. Proc Natl Acad Sci U S A.
2014;111(32):E3287-96.
165. Bode AM, Dong Z. Post-translational modification of p53 in tumorigenesis. Nat Rev Cancer. 2004;4(10):793-805.
166. Johannes G, Carter MS, Eisen MB, Brown PO, Sarnow P. Identification of eukaryotic mRNAs that are translated at reduced cap binding complex eIF4F concentrations using a cDNA microarray.
Proc Natl Acad Sci U S A. 1999;96(23):13118-23.
167. Ray PS, Grover R, Das S. Two internal ribosome entry sites mediate the translation of p53 isoforms. EMBO Rep. 2006;7(4):404-10.
168. Yang DQ, Halaby MJ, Zhang Y. The identification of an internal ribosomal entry site in the 5'untranslated region of p53 mRNA provides a novel mechanism for the regulation of its translation following DNA damage. Oncogene. 2006;25(33):4613-9.
169. Candeias MM, Powell DJ, Roubalova E, Apcher S, Bourougaa K, Vojtesek B, et al. Expression of p53 and p53/47 are controlled by alternative mechanisms of messenger RNA translation initiation. Oncogene. 2006;25(52):6936-47.
170. Marcel V, Tran PL, Sagne C, Martel-Planche G, Vaslin L, Teulade-Fichou MP, et al. Gquadruplex structures in TP53 intron 3: role in alternative splicing and in production of p53 mRNA isoforms. Carcinogenesis. 2011;32(3):271-8.
171. Lazar V, Hazard F, Bertin F, Janin N, Bellet D, Bressac B. Simple sequence repeat polymorphism within the p53 gene. Oncogene. 1993;8(6):1703-5.
172. Sagne C, Marcel V, Amadou A, Hainaut P, Olivier M, Hall J. A meta-analysis of cancer risk associated with the TP53 intron 3 duplication polymorphism (rs17878362): geographic and tumorspecific effects. Cell Death Dis. 2013;4:e492.
173. Sagne C, Marcel V, Bota M, Martel-Planche G, Nobrega A, Palmero EI, et al. Age at cancer onset in germline TP53 mutation carriers: association with polymorphisms in predicted Gquadruplex structures. Carcinogenesis. 2014;35(4):807-15.
174. Perriaud L, Marcel V, Sagne C, Favaudon V, Guedin A, De Rache A, et al. Impact of Gquadruplex structures and intronic polymorphisms rs17878362 and rs1642785 on basal and ionizing radiation-induced expression of alternative p53 transcripts. Carcinogenesis. 2014;35(12):2706-15. 175. Solomon H, Brauning B, Fainer I, Ben-Nissan G, Rabani S, Goldfinger N, et al. Posttranslational regulation of p53 function through 20S proteasome-mediated cleavage. Cell Death Differ. 2017;24(12):2187-98.
176. Chen J, Ng SM, Chang C, Zhang Z, Bourdon JC, Lane DP, et al. p53 isoform delta113p53 is a p53 target gene that antagonizes p53 apoptotic activity via BclxL activation in zebrafish. Genes Dev.
2009;23(3):278-90.
177. Marcel V, Vijayakumar V, Fernandez-Cuesta L, Hafsi H, Sagne C, Hautefeuille A, et al. p53 regulates the transcription of its Delta133p53 isoform through specific response elements contained within the TP53 P2 internal promoter. Oncogene. 2010;29(18):2691-700.

178. Marcel V, Petit I, Murray-Zmijewski F, Goullet de Rugy T, Fernandes K, Meuray V, et al. Diverse p63 and p73 isoforms regulate Delta133p53 expression through modulation of the internal TP53 promoter activity. Cell Death Differ. 2012;19(5):816-26.
179. Moore HC, Jordan LB, Bray SE, Baker L, Quinlan PR, Purdie CA, et al. The RNA helicase p68 modulates expression and function of the Delta133 isoform(s) of p53, and is inversely associated with Delta133p53 expression in breast cancer. Oncogene. 2010;29(49):6475-84.
180. Chen J, Ruan H, Ng SM, Gao C, Soo HM, Wu W, et al. Loss of function of def selectively upregulates Delta113p53 expression to arrest expansion growth of digestive organs in zebrafish. Genes Dev. 2005;19(23):2900-11.
181. Shi H, Tao T, Huang D, Ou Z, Chen J, Peng J. A naturally occurring 4-bp deletion in the intron 4 of p53 creates a spectrum of novel p53 isoforms with anti-apoptosis function. Nucleic Acids Res. 2015;43(2):1035-43.
182. Wei J, Noto J, Zaika E, Romero-Gallo J, Correa P, El-Rifai W, et al. Pathogenic bacterium Helicobacter pylori alters the expression profile of p53 protein isoforms and p53 response to cellular stresses. Proc Natl Acad Sci U S A. 2012;109(38):E2543-50.
183. Candeias MM, Hagiwara M, Matsuda M. Cancer-specific mutations in p53 induce the translation of Delta160p53 promoting tumorigenesis. EMBO Rep. 2016;17(11):1542-51.
184. Tang Y, Horikawa I, Ajiro M, Robles AI, Fujita K, Mondal AM, et al. Downregulation of splicing factor SRSF3 induces p53beta, an alternatively spliced isoform of p53 that promotes cellular senescence. Oncogene. 2013;32(22):2792-8.
185. Marcel V, Fernandes K, Terrier O, Lane DP, Bourdon JC. Modulation of p53beta and p53gamma expression by regulating the alternative splicing of TP53 gene modifies cellular response. Cell Death Differ. 2014;21(9):1377-87.
186. Chen J, Crutchley J, Zhang D, Owzar K, Kastan MB. Identification of a DNA Damage-Induced Alternative Splicing Pathway That Regulates p53 and Cellular Senescence Markers. Cancer Discov. 2017;7(7):766-81.
187. Cowen LE, Tang Y. Identification of nonsense-mediated mRNA decay pathway as a critical regulator of p53 isoform beta. Sci Rep. 2017;7(1):17535.
188. Hayman L, Chaudhry WR, Revin VV, Zhelev N, Bourdon JC. What is the potential of p53 isoforms as a predictive biomarker in the treatment of cancer? Expert review of molecular diagnostics. 2018.
189. Goldschneider D, Horvilleur E, Plassa LF, Guillaud-Bataille M, Million K, Wittmer-Dupret E, et al. Expression of C-terminal deleted p53 isoforms in neuroblastoma. Nucleic Acids Res. 2006;34(19):5603-12.
190. Fujita K, Mondal AM, Horikawa I, Nguyen GH, Kumamoto K, Sohn JJ, et al. p53 isoforms, Δ133p53 and p53β, are endogenous regulators of replicative cellular senescence. Nature cell biology. 2009;11(9):1135-42.
191. Anensen N, Hjelle SM, Van Belle W, Haaland I, Silden E, Bourdon JC, et al. Correlation analysis of p53 protein isoforms with NPM1/FLT3 mutations and therapy response in acute myeloid leukemia. Oncogene. 2012;31(12):1533-45.
192. Avery-Kiejda KA, Zhang XD, Adams LJ, Scott RJ, Vojtesek B, Lane DP, et al. Small molecular weight variants of p53 are expressed in human melanoma cells and are induced by the DNAdamaging agent cisplatin. Clin Cancer Res. 2008;14.
193. Silden E, Hjelle SM, Wergeland L, Sulen A, Andresen V, Bourdon JC, et al. Expression of TP53 isoforms p53beta or p53gamma enhances chemosensitivity in TP53(null) cell lines. PLoS One. 2013;8(2):e56276.
194. Song W, Huo SW, Lu JJ, Liu Z, Fang XL, Jin XB, et al. Expression of p53 isoforms in renal cell carcinoma. Chin Med J (Engl). 2009;122(8):921-6.

195. Hofstetter G, Berger A, Fiegl H, Slade N, Zoric A, Holzer B, et al. Alternative splicing of p53 and p73: the novel p53 splice variant p53delta is an independent prognostic marker in ovarian cancer. Oncogene. 2010;29(13):1997-2004.

196. Boldrup L, Bourdon JC, Coates PJ, Sjostrom B, Nylander K. Expression of p53 isoforms in squamous cell carcinoma of the head and neck. Eur J Cancer. 2007;43.
197. Takahashi R, Giannini C, Sarkaria JN, Schroeder M, Rogers J, Mastroeni D, et al. p53 isoform profiling in glioblastoma and injured brain. Oncogene. 2013;32(26):3165-74.
198. Bourdon J-C, Khoury MP, Diot A, Baker L, Fernandes K, Aoubala M, et al. p53 mutant breast cancer patients expressing p53γ have as good a prognosis as wild-type p53 breast cancer patients. Breast Cancer Research. 2011;13(1):1-10.
199. Anensen N, Oyan AM, Bourdon JC, Kalland KH, Bruserud O, Gjertsen BT. A distinct p53 protein isoform signature reflects the onset of induction chemotherapy for acute myeloid leukemia. Clin Cancer Res. 2006;12(13):3985-92.
200. Bernard H, Garmy-Susini B, Ainaoui N, Van Den Berghe L, Peurichard A, Javerzat S, et al. The p53 isoform, Delta133p53alpha, stimulates angiogenesis and tumour progression. Oncogene. 2013;32(17):2150-60.
201. Rangel LP, Costa DC, Vieira TC, Silva JL. The aggregation of mutant p53 produces prion-like properties in cancer. Prion. 2014;8(1):75-84.
202. Chen J, Ng SM, Chang C, Zhang Z, Bourdon JC, Lane DP, et al. p53 isoform Δ113p53 is a p53 target gene that antagonizes p53 apoptotic activity via BclxL activation in zebrafish. Genes Dev. 2009;23.
203. Roth I, Campbell H, Rubio C, Vennin C, Wilson M, Wiles A, et al. The Delta133p53 isoform and its mouse analogue Delta122p53 promote invasion and metastasis involving pro-inflammatory molecules interleukin-6 and CCL2. Oncogene. 2016;35(38):4981-9.
204. Fujita K, Mondal AM, Horikawa I, Nguyen GH, Kumamoto K, Sohn JJ, et al. p53 isoforms Delta133p53 and p53beta are endogenous regulators of replicative cellular senescence. Nat Cell Biol. 2009;11(9):1135-42.
205. Arsic N, Gadea G, Lagerqvist EL, Busson M, Cahuzac N, Brock C, et al. The p53 isoform Delta133p53beta promotes cancer stem cell potential. Stem Cell Reports. 2015;4(4):531-40. 206. Takahashi R, Markovic SN, Scrable HJ. Dominant effects of Δ40p53 on p53 function and melanoma cell fate. Journal of Investigative Dermatology. 2014;134(3):791-800.
207. Ohki R, Kawase T, Ohta T, Ichikawa H, Taya Y. Dissecting functional roles of p53 N-terminal transactivation domains by microarray expression analysis. Cancer science. 2007;98(2):189-200. 208. Jiang D, Brady CA, Johnson TM, Lee EY, Park EJ, Scott MP, et al. Full p53 transcriptional activation potential is dispensable for tumor suppression in diverse lineages. Proc Natl Acad Sci U S A. 2011;108(41):17123-8.
209. Ota A, Nakao H, Sawada Y, Karnan S, Wahiduzzaman M, Inoue T, et al. Delta40p53alpha suppresses tumor cell proliferation and induces cellular senescence in hepatocellular carcinoma cells. J Cell Sci. 2017;130(3):614-25.
210. Maier B, Gluba W, Bernier B, Turner T, Mohammad K, Guise T, et al. Modulation of mammalian life span by the short isoform of p53. Genes Dev. 2004;18(3):306-19.
211. Ungewitter E, Scrable H. Delta40p53 controls the switch from pluripotency to differentiation by regulating IGF signaling in ESCs. Genes Dev. 2010;24(21):2408-19.
212. Pehar M, O'Riordan KJ, Burns-Cusato M, Andrzejewski ME, del Alcazar CG, Burger C, et al. Altered longevity-assurance activity of p53:p44 in the mouse causes memory loss, neurodegeneration and premature death. Aging Cell. 2010;9(2):174-90.

213. Davidson WR, Kari C, Ren Q, Daroczi B, Dicker AP, Rodeck U. Differential regulation of p53 function by the N-terminal DeltaNp53 and Delta113p53 isoforms in zebrafish embryos. BMC Dev Biol. 2010;10:102.
214. Derry WB, Putzke AP, Rothman JH. Caenorhabditis elegans p53: role in apoptosis, meiosis, and stress resistance. Science. 2001;294(5542):591-5.
215. Jin S, Martinek S, Joo WS, Wortman JR, Mirkovic N, Sali A, et al. Identification and characterization of a p53 homologue in Drosophila melanogaster. Proc Natl Acad Sci U S A. 2000;97(13):7301-6.
216. Ollmann M, Young LM, Di Como CJ, Karim F, Belvin M, Robertson S, et al. Drosophila p53 is a structural and functional homolog of the tumor suppressor p53. Cell. 2000;101(1):91-101.
217. Jain AK, Barton MC. p53: emerging roles in stem cells, development and beyond.
Development (Cambridge, England). 2018;145(8).
218. Hofstetter G, Berger A, Berger R, Zoric A, Braicu EI, Reimer D, et al. The N-terminally truncated p53 isoform Delta40p53 influences prognosis in mucinous ovarian cancer. International journal of gynecological cancer : official journal of the International Gynecological Cancer Society.
2012;22(3):372-9.
219. Bourdon JC, Fernandes K, Murray-Zmijewski F, Liu G, Diot A, Xirodimas DP, et al. p53 isoforms can regulate p53 transcriptional activity. Genes Dev. 2005;19.
220. Gadea G, Arsic N, Fernandes K, Diot A, Joruiz SM, Abdallah S, et al. TP53 drives invasion through expression of its Delta133p53beta variant. Elife. 2016;5.
221. Baumbusch LO, Myhre S, Langerod A, Bergamaschi A, Geisler SB, Lonning PE, et al. Expression of full-length p53 and its isoform Deltap53 in breast carcinomas in relation to mutation status and clinical parameters. Mol Cancer. 2006;5:47.
222. Mehta S, Tsai P, Lasham A, Campbell H, Reddel R, Braithwaite A, et al. A Study of TP53 RNA Splicing Illustrates Pitfalls of RNA-seq Methodology. Cancer Res. 2016;76(24):7151-9.
223. ATCC breast cancer cell lines [Available from: https://www.atcc.org/products/all/.
224. Database IT. TP53 mutation status of human cell-lines [Available from:
http://p53.iarc.fr/CellLines.aspx.
225. Mathe A, Wong-Brown M, Morten B, Forbes JF, Braye SG, Avery-Kiejda KA, et al. Novel genes associated with lymph node metastasis in triple negative breast cancer. Sci Rep. 2015;5:15832.
226. Rao DD, Vorhies JS, Senzer N, Nemunaitis J. siRNA vs. shRNA: similarities and differences.
Adv Drug Deliv Rev. 2009;61(9):746-59.
227. Real-Time qRT-PCR: NCBI; [Available from: https://www.ncbi.nlm.nih.gov/probe/docs/techqpcr/.
228. Morten BC, Scott RJ, Avery-Kiejda KA. Comparison of the QuantiGene 2.0 Assay and RealTime RT-PCR in the Detection of p53 Isoform mRNA Expression in Formalin-Fixed Paraffin-Embedded Tissues- A Preliminary Study. PLoS One. 2016;11(11):e0165930.
229. Livak KJ, Schmittgen TD. Analysis of relative gene expression data using real-time quantitative PCR and the 2(-Delta Delta C(T)) Method. Methods. 2001;25(4):402-8.
230. Bradford MM. A rapid and sensitive method for the quantitation of microgram quantities of protein utilizing the principle of protein-dye binding. Anal Biochem. 1976;72:248-54. 231. Laemmli UK. Cleavage of structural proteins during the assembly of the head of bacteriophage T4. Nature. 1970;227(5259):680-5.
232. Protocolplace. Gelatin Zymography Tutorial 5: Quantifying MMP Activity with Image J and Normalizing Samples [Available from: https://www.youtube.com/watch?v=K8aCPblvfCw.
233. Au - Zhang X, Au - Morten BC, Au - Scott RJ, Au - Avery-Kiejda KA. A Simple
Migration/Invasion Workflow Using an Automated Live-cell Imager. JoVE. 2019(144):e59042.

234. Shaw LM. Tumor cell invasion assays. Methods Mol Biol. 2005;294:97-105.
235. Yuan Tian TJM, Amy P Webster, Zhen Yang, Stephan Beck, Andrew Feber, and Andrew E Teschendorff. The Chip Analysis Methylation Pipeline Bioconductor2019 [Available from: https://bioconductor.org/packages/release/bioc/vignettes/ChAMP/inst/doc/ChAMP.html#sectiondifferential-methylation-probes.
236. Peters TJ, Buckley MJ, Statham AL, Pidsley R, Samaras K, R VL, et al. De novo identification of differentially methylated regions in the human genome. Epigenetics Chromatin. 2015;8:6.
237. Khatri P, Draghici S, Ostermeier GC, Krawetz SA. Profiling gene expression using ontoexpress. Genomics. 2002;79(2):266-70.
238. Chen EY, Tan CM, Kou Y, Duan Q, Wang Z, Meirelles GV, et al. Enrichr: interactive and collaborative HTML5 gene list enrichment analysis tool. BMC Bioinformatics. 2013;14:128.
239. Kuleshov MV, Jones MR, Rouillard AD, Fernandez NF, Duan Q, Wang Z, et al. Enrichr: a comprehensive gene set enrichment analysis web server 2016 update. Nucleic Acids Res. 2016;44(W1):W90-7.
240. Morten BC, Scott RJ, Avery-Kiejda KA. Comparison of Three Different Methods for Determining Cell Proliferation in Breast Cancer Cell Lines. J Vis Exp. 2016(115).
241. Institute B. GSEA User Guide [Available from: https://software.broadinstitute.org/gsea/doc/GSEAUserGuideFrame.html.
242. Slatter TL, Hung N, Campbell H, Rubio C, Mehta R, Renshaw P, et al. Hyperproliferation, cancer, and inflammation in mice expressing a Delta133p53-like isoform. Blood. 2011;117(19):516677.
243. Terrier O, Marcel V, Cartet G, Lane DP, Lina B, Rosa-Calatrava M, et al. Influenza A viruses control expression of proviral human p53 isoforms p53beta and Delta133p53alpha. J Virol. 2012;86(16):8452-60.
244. Chaffer CL, Marjanovic ND, Lee T, Bell G, Kleer CG, Reinhardt F, et al. Poised chromatin at the ZEB1 promoter enables breast cancer cell plasticity and enhances tumorigenicity. Cell. 2013;154(1):61-74.
245. Palen K, Weber J, Dwinell MB, Johnson BD, Ramchandran R, Gershan JA. E-cadherin reexpression shows in vivo evidence for mesenchymal to epithelial transition in clonal metastatic breast tumor cells. Oncotarget. 2016;7(28):43363-75.
246. Lin YC, Lee YC, Li LH, Cheng CJ, Yang RB. Tumor suppressor SCUBE2 inhibits breast-cancer cell migration and invasion through the reversal of epithelial-mesenchymal transition. J Cell Sci. 2014;127(Pt 1):85-100.
247. Mu Y, Lou J, Srivastava M, Zhao B, Feng XH, Liu T, et al. SLFN11 inhibits checkpoint maintenance and homologous recombination repair. EMBO Rep. 2016;17(1):94-109.
248. Busby M, Hallett MT, Plante I. The Complex Subtype-Dependent Role of Connexin 43 (GJA1) in Breast Cancer. International journal of molecular sciences. 2018;19(3).
249. Prest SJ, May FE, Westley BR. The estrogen-regulated protein, TFF1, stimulates migration of human breast cancer cells. FASEB J. 2002;16(6):592-4.
250. Basu NK, Kole L, Basu M, McDonagh AF, Owens IS. Targeted inhibition of glucuronidation markedly improves drug efficacy in mice - a model. Biochem Biophys Res Commun. 2007;360(1):713.
251. Taverna SD, Li H, Ruthenburg AJ, Allis CD, Patel DJ. How chromatin-binding modules interpret histone modifications: lessons from professional pocket pickers. Nat Struct Mol Biol. 2007;14(11):1025-40.
252. Jeffrey Craig NCW. Epigenetics: A Reference Manual. Horizon Scientific Press2011.
253. Dodge JE, Ramsahoye BH, Wo ZG, Okano M, Li E. De novo methylation of MMLV provirus in embryonic stem cells: CpG versus non-CpG methylation. Gene. 2002;289(1-2):41-8.

254. Anderson JL, Lutz JR, Gilbert EM, Sorensen SG, Yanowitz FG, Menlove RL, et al. A randomized trial of low-dose beta-blockade therapy for idiopathic dilated cardiomyopathy. Am J Cardiol.
1985;55(4):471-5.
255. Lister R, Mukamel EA, Nery JR, Urich M, Puddifoot CA, Johnson ND, et al. Global epigenomic reconfiguration during mammalian brain development. Science. 2013;341(6146):1237905. 256.
Tost J. DNA methylation: an introduction to the biology and the disease-associated changes of a promising biomarker. Mol Biotechnol. 2010;44(1):71-81.
257. Gonzalo S. Epigenetic alterations in aging. J Appl Physiol (1985). 2010;109(2):586-97. 258.
Smyth GK. Linear models and empirical bayes methods for assessing differential expression in microarray experiments. Stat Appl Genet Mol Biol. 2004;3:Article3.
259. Wettenhall JM, Smyth GK. limmaGUI: a graphical user interface for linear modeling of microarray data. Bioinformatics. 2004;20(18):3705-6.
260. Butcher LM, Beck S. Probe Lasso: a novel method to rope in differentially methylated regions with 450K DNA methylation data. Methods. 2015;72:21-8.
261. Mootha VK, Lindgren CM, Eriksson KF, Subramanian A, Sihag S, Lehar J, et al. PGC-1alpharesponsive genes involved in oxidative phosphorylation are coordinately downregulated in human diabetes. Nat Genet. 2003;34(3):267-73.
262. Subramanian A, Tamayo P, Mootha VK, Mukherjee S, Ebert BL, Gillette MA, et al. Gene set enrichment analysis: a knowledge-based approach for interpreting genome-wide expression profiles.
Proc Natl Acad Sci U S A. 2005;102(43):15545-50.
263. Lev Maor G, Yearim A, Ast G. The alternative role of DNA methylation in splicing regulation.
Trends Genet. 2015;31(5):274-80.
264. Dixon G, Liao Y, Bay LK, Matz MV. Role of gene body methylation in acclimatization and adaptation in a basal metazoan. Proc Natl Acad Sci U S A. 2018;115(52):13342-6.
265. Teissandier A, Bourc'his D. Gene body DNA methylation conspires with H3K36me3 to preclude aberrant transcription. Embo j. 2017;36(11):1471-3.
266. Wang YA, Kamarova Y, Shen KC, Jiang Z, Hahn MJ, Wang Y, et al. DNA methyltransferase-3a interacts with p53 and represses p53-mediated gene expression. Cancer Biol Ther. 2005;4(10):113843.
267. Tovy A, Spiro A, McCarthy R, Shipony Z, Aylon Y, Allton K, et al. p53 is essential for DNA methylation homeostasis in naive embryonic stem cells, and its loss promotes clonal heterogeneity.
Genes Dev. 2017;31(10):959-72.
268. Godbout R, Ingram R, Tilghman SM. Multiple regulatory elements in the intergenic region between the alpha-fetoprotein and albumin genes. Mol Cell Biol. 1986;6(2):477-87.
269. Zerucha T, Stuhmer T, Hatch G, Park BK, Long Q, Yu G, et al. A highly conserved enhancer in the Dlx5/Dlx6 intergenic region is the site of cross-regulatory interactions between Dlx genes in the embryonic forebrain. J Neurosci. 2000;20(2):709-21.
270. Shin HY, Hennighausen L, Yoo KH. STAT5-Driven Enhancers Tightly Control Temporal Expression of Mammary-Specific Genes. J Mammary Gland Biol Neoplasia. 2019;24(1):61-71.
271. Sammons MA, Zhu J, Drake AM, Berger SL. TP53 engagement with the genome occurs in distinct local chromatin environments via pioneer factor activity. Genome Res. 2015;25(2):179-88. 272. Mundt HM, Stremmel W, Melino G, Krammer PH, Schilling T, Muller M. Dominant negative (DeltaN) p63alpha induces drug resistance in hepatocellular carcinoma by interference with apoptosis signaling pathways. Biochem Biophys Res Commun. 2010;396(2):335-41.
273. Song Y, van den Berg PR, Markoulaki S, Soldner F, Dall'Agnese A, Henninger JE, et al.

Dynamic Enhancer DNA Methylation as Basis for Transcriptional and Cellular Heterogeneity of ESCs. Mol Cell. 2019;75(5):905-20.e6.

274. Gomez L, Odom GJ, Young JI, Martin ER, Liu L, Chen X, et al. coMethDMR: accurate identification of co-methylated and differentially methylated regions in epigenome-wide association studies with continuous phenotypes. Nucleic Acids Res. 2019;47(17):e98.
275. Irizarry RA, Ladd-Acosta C, Wen B, Wu Z, Montano C, Onyango P, et al. The human colon cancer methylome shows similar hypo- and hypermethylation at conserved tissue-specific CpG island shores. Nat Genet. 2009;41(2):178-86.
276. Yan DW, Li DW, Yang YX, Xia J, Wang XL, Zhou CZ, et al. Ubiquitin D is correlated with colon cancer progression and predicts recurrence for stage II-III disease after curative surgery. Br J Cancer.

2010;103(7):961-9.

277. Heiskala M, Leidenius M, Joensuu K, Heikkila P. High expression of CCL2 in tumor cells and abundant infiltration with CD14 positive macrophages predict early relapse in breast cancer. Virchows Arch. 2019;474(1):3-12.
278. Tang X, Asano M, O'Reilly A, Farquhar A, Yang Y, Amar S. p53 is an important regulator of CCL2 gene expression. Current molecular medicine. 2012;12(8):929-43.
279. Xing M, Usadel H, Cohen Y, Tokumaru Y, Guo Z, Westra WB, et al. Methylation of the thyroid-stimulating hormone receptor gene in epithelial thyroid tumors: a marker of malignancy and a cause of gene silencing. Cancer Res. 2003;63(9):2316-21. 280. Human Mutation. 2002. p. 607.
281. Vijai J, Kirchhoff T, Schrader KA, Brown J, Dutra-Clarke AV, Manschreck C, et al. Susceptibility loci associated with specific and shared subtypes of lymphoid malignancies. PLoS Genet.

2013;9(1):e1003220.

282. Lee Y, Park S, Lee SH, Lee H. Characterization of genetic aberrations in a single case of metastatic thymic adenocarcinoma. BMC Cancer. 2017;17(1):330.
283. Wang C, Cicek MS, Charbonneau B, Kalli KR, Armasu SM, Larson MC, et al. Tumor hypomethylation at 6p21.3 associates with longer time to recurrence of high-grade serous epithelial ovarian cancer. Cancer Res. 2014;74(11):3084-91.
284. Aggarwal BB. Signalling pathways of the TNF superfamily: a double-edged sword. Nat Rev Immunol. 2003;3(9):745-56.
285. Wajant H, Pfizenmaier K, Scheurich P. Tumor necrosis factor signaling. Cell Death Differ.

2003;10(1):45-65.

286. Hu J, Nakano H, Sakurai H, Colburn NH. Insufficient p65 phosphorylation at S536 specifically contributes to the lack of NF-kappaB activation and transformation in resistant JB6 cells.

Carcinogenesis. 2004;25(10):1991-2003.

287. Suzukawa K, Weber TJ, Colburn NH. AP-1, NF-kappa-B, and ERK activation thresholds for promotion of neoplastic transformation in the mouse epidermal JB6 model. Environ Health Perspect.

2002;110(9):865-70.

288. Yang H, Bocchetta M, Kroczynska B, Elmishad AG, Chen Y, Liu Z, et al. TNF-alpha inhibits asbestos-induced cytotoxicity via a NF-kappaB-dependent pathway, a possible mechanism for asbestos-induced oncogenesis. Proc Natl Acad Sci U S A. 2006;103(27):10397-402.
289. Ho SY, Wang YJ, Chen HL, Chen CH, Chang CJ, Wang PJ, et al. Increased risk of developing hepatocellular carcinoma associated with carriage of the TNF2 allele of the -308 tumor necrosis factor-alpha promoter gene. Cancer Causes Control. 2004;15(7):657-63.
290. Gaudet MM, Egan KM, Lissowska J, Newcomb PA, Brinton LA, Titus-Ernstoff L, et al. Genetic variation in tumor necrosis factor and lymphotoxin-alpha (TNF-LTA) and breast cancer risk. Hum Genet. 2007;121(3-4):483-90.

291. Rokhlin OW, Gudkov AV, Kwek S, Glover RA, Gewies AS, Cohen MB. p53 is involved in tumor necrosis factor-alpha-induced apoptosis in the human prostatic carcinoma cell line LNCaP. Oncogene. 2000;19(15):1959-68.
292. Di Minin G, Bellazzo A, Dal Ferro M, Chiaruttini G, Nuzzo S, Bicciato S, et al. Mutant p53 reprograms TNF signaling in cancer cells through interaction with the tumor suppressor DAB2IP. Mol Cell. 2014;56(5):617-29.
293. Hsia HC, Schwarzbauer JE. Meet the tenascins: multifunctional and mysterious. J Biol Chem. 2005;280(29):26641-4.
294. Tucker RP, Chiquet-Ehrismann R. The regulation of tenascin expression by tissue microenvironments. Biochim Biophys Acta. 2009;1793(5):888-92.
295. Roos L, van Dongen J, Bell CG, Burri A, Deloukas P, Boomsma DI, et al. Integrative DNA methylome analysis of pan-cancer biomarkers in cancer discordant monozygotic twin-pairs. Clin Epigenetics. 2016;8:7.
296. Nishino K, Toyoda M, Yamazaki-Inoue M, Fukawatase Y, Chikazawa E, Sakaguchi H, et al. DNA methylation dynamics in human induced pluripotent stem cells over time. PLoS Genet. 2011;7(5):e1002085.
297. Yi L, Lu C, Hu W, Sun Y, Levine AJ. Multiple roles of p53-related pathways in somatic cell reprogramming and stem cell differentiation. Cancer Res. 2012;72(21):5635-45.
298. Zhang ZN, Chung SK, Xu Z, Xu Y. Oct4 maintains the pluripotency of human embryonic stem cells by inactivating p53 through Sirt1-mediated deacetylation. Stem Cells. 2014;32(1):157-65. 299. Lee DF, Su J, Ang YS, Carvajal-Vergara X, Mulero-Navarro S, Pereira CF, et al. Regulation of embryonic and induced pluripotency by aurora kinase-p53 signaling. Cell Stem Cell. 2012;11(2):17994.
300. Sengelaub CA, Navrazhina K, Ross JB, Halberg N, Tavazoie SF. PTPRN2 and PLCbeta1 promote metastatic breast cancer cell migration through PI(4,5)P2-dependent actin remodeling. Embo j. 2016;35(1):62-76.
301. Morishita H, Yagi T. Protocadherin family: diversity, structure, and function. Curr Opin Cell Biol. 2007;19(5):584-92.
302. Jain AK, Allton K, Iacovino M, Mahen E, Milczarek RJ, Zwaka TP, et al. p53 regulates cell cycle and microRNAs to promote differentiation of human embryonic stem cells. PLoS Biol. 2012;10(2):e1001268.
303. Shiozawa T, Iyama S, Toshima S, Sakata A, Usui S, Minami Y, et al. Dimethylarginine dimethylaminohydrolase 2 promotes tumor angiogenesis in lung adenocarcinoma. Virchows Arch. 2016;468(2):179-90.
304. Vousden KH, Lane DP. p53 in health and disease. Nat Rev Mol Cell Biol. 2007;8(4):275-83. 305. Florea AM, Busselberg D. Cisplatin as an anti-tumor drug: cellular mechanisms of activity, drug resistance and induced side effects. Cancers (Basel). 2011;3(1):1351-71.
306. Dasari S, Tchounwou PB. Cisplatin in cancer therapy: molecular mechanisms of action. Eur J Pharmacol. 2014;740:364-78.
307. Patel AG, Kaufmann SH. How does doxorubicin work? Elife. 2012;1:e00387.
308. al SAe. Seqmonk_Babraham Bioinformatics [Available from: https://www.bioinformatics.babraham.ac.uk/projects/seqmonk/.
309. Chen J. The Cell-Cycle Arrest and Apoptotic Functions of p53 in Tumor Initiation and Progression. Cold Spring Harb Perspect Med. 2016;6(3):a026104.
310. Eastman A, Kohn EA, Brown MK, Rathman J, Livingstone M, Blank DH, et al. A novel indolocarbazole, ICP-1, abrogates DNA damage-induced cell cycle arrest and enhances cytotoxicity: similarities and differences to the cell cycle checkpoint abrogator UCN-01. Mol Cancer Ther. 2002;1(12):1067-78.

311. Fan S, Smith ML, Rivet DJ, 2nd, Duba D, Zhan Q, Kohn KW, et al. Disruption of p53 function sensitizes breast cancer MCF-7 cells to cisplatin and pentoxifylline. Cancer Res. 1995;55(8):1649-54. 312. Shin HJ, Kwon HK, Lee JH, Gui X, Achek A, Kim JH, et al. Doxorubicin-induced necrosis is mediated by poly-(ADP-ribose) polymerase 1 (PARP1) but is independent of p53. Sci Rep.
2015;5:15798.
313. Powell DJ, Hrstka R, Candeias M, Bourougaa K, Vojtesek B, Fahraeus R. Stress-dependent changes in the properties of p53 complexes by the alternative translation product p53/47. Cell Cycle. 2008;7(7):950-9.
314. Takahashi R, Markovic SN, Scrable HJ. Dominant effects of Delta40p53 on p53 function and melanoma cell fate. J Invest Dermatol. 2014;134(3):791-800.
315. Melo Dos Santos N, de Oliveira GAP, Ramos Rocha M, Pedrote MM, Diniz da Silva Ferretti G, Pereira Rangel L, et al. Loss of the p53 transactivation domain results in high amyloid aggregation of the Delta40p53 isoform in endometrial carcinoma cells. J Biol Chem. 2019;294(24):9430-9. 316. Lupertz R, Watjen W, Kahl R, Chovolou Y. Dose- and time-dependent effects of doxorubicin on cytotoxicity, cell cycle and apoptotic cell death in human colon cancer cells. Toxicology.
2010;271(3):115-21.
317. Denard B, Lee C, Ye J. Doxorubicin blocks proliferation of cancer cells through proteolytic activation of CREB3L1. Elife. 2012;1:e00090.
318. Ding K, Li W, Zou Z, Zou X, Wang C. CCNB1 is a prognostic biomarker for ER+ breast cancer.
Med Hypotheses. 2014;83(3):359-64.
319. Bolanos-Garcia VM, Blundell TL. BUB1 and BUBR1: multifaceted kinases of the cell cycle.
Trends Biochem Sci. 2011;36(3):141-50.
320. Lee KS, Oh DY, Kang YH, Park JE. Self-regulated mechanism of Plk1 localization to kinetochores: lessons from the Plk1-PBIP1 interaction. Cell Div. 2008;3:4.
321. Bochman ML, Schwacha A. The Mcm complex: unwinding the mechanism of a replicative helicase. Microbiol Mol Biol Rev. 2009;73(4):652-83.
322. Borel F, Lacroix FB, Margolis RL. Prolonged arrest of mammalian cells at the G1/S boundary results in permanent S phase stasis. J Cell Sci. 2002;115(Pt 14):2829-38.
323. Guerrero-Preston R, Hadar T, Ostrow KL, Soudry E, Echenique M, Ili-Gangas C, et al. Differential promoter methylation of kinesin family member 1a in plasma is associated with breast cancer and DNA repair capacity. Oncol Rep. 2014;32(2):505-12.
324. Lee JH, Kang Y, Khare V, Jin ZY, Kang MY, Yoon Y, et al. The p53-inducible gene 3 (PIG3) contributes to early cellular response to DNA damage. Oncogene. 2010;29(10):1431-50.
325. Shahbazi J, Lock R, Liu T. Tumor Protein 53-Induced Nuclear Protein 1 Enhances p53 Function and Represses Tumorigenesis. Front Genet. 2013;4:80.
326. Rouault JP, Falette N, Guehenneux F, Guillot C, Rimokh R, Wang Q, et al. Identification of BTG2, an antiproliferative p53-dependent component of the DNA damage cellular response pathway. Nat Genet. 1996;14(4):482-6.
327. Zhang BL, Dong FL, Guo TW, Gu XH, Huang LY, Gao DS. MiRNAs Mediate GDNF-Induced Proliferation and Migration of Glioma Cells. Cell Physiol Biochem. 2017;44(5):1923-38.
328. Amemiya Y, Yang W, Benatar T, Nofech-Mozes S, Yee A, Kahn H, et al. Insulin like growth factor binding protein-7 reduces growth of human breast cancer cells and xenografted tumors.
Breast Cancer Res Treat. 2011;126(2):373-84.
329. Maus MV. Immunology: T-cell tweaks to target tumours. Nature. 2017;543(7643):48-9. 330. Yelamos J, Farres J, Llacuna L, Ampurdanes C, Martin-Caballero J. PARP-1 and PARP-2: New players in tumour development. Am J Cancer Res. 2011;1(3):328-46.

331. Zhou C, Jiang H, Zhang Z, Zhang G, Wang H, Zhang Q, et al. ZEB1 confers stem cell-like properties in breast cancer by targeting neurogenin-3. Oncotarget. 2017;8(33):54388-401.
332. Leis O, Eguiara A, Lopez-Arribillaga E, Alberdi MJ, Hernandez-Garcia S, Elorriaga K, et al. Sox2 expression in breast tumours and activation in breast cancer stem cells. Oncogene. 2012;31(11):1354-65.
333. Rahman M JH, Akhtar N, Rahman K, Islam R, Asaduzzaman S. STEM CELL AND CANCER STEM CELL: A Tale of Two Cells. Progress in Stem Cell. 2016.
334. Fujita K, Mondal AM, Horikawa I, Nguyen GH, Kumamoto K, Sohn JJ, et al. p53 isoforms Δ133p53 and p53β are endogenous regulators of replicative cellular senescence. Nat Cell Biol. 2009;11.
335. Zhang Y, Yan W, Jung YS, Chen X. Mammary epithelial cell polarity is regulated differentially by p73 isoforms via epithelial-to-mesenchymal transition. J Biol Chem. 2012;287(21):17746-53. 336. Alsafadi S, Tourpin S, Bessoltane N, Salome-Desnoulez S, Vassal G, Andre F, et al. Nuclear localization of the caspase-3-cleaved form of p73 in anoikis. Oncotarget. 2016;7(11):12331-43. 337. Liu J, Zhang C, Hu W, Feng Z. Tumor suppressor p53 and metabolism. J Mol Cell Biol. 2019;11(4):284-92.
338. Feng Z, Levine AJ. The regulation of energy metabolism and the IGF-1/mTOR pathways by the p53 protein. Trends Cell Biol. 2010;20(7):427-34.
339. Stambolic V, MacPherson D, Sas D, Lin Y, Snow B, Jang Y, et al. Regulation of PTEN transcription by p53. Mol Cell. 2001;8(2):317-25.
340. Nantasanti S, Toussaint MJ, Youssef SA, Tooten PC, de Bruin A. Rb and p53 Liver Functions Are Essential for Xenobiotic Metabolism and Tumor Suppression. PLoS One. 2016;11(3):e0150064.
341. Aas T, Borresen AL, Geisler S, Smith-Sorensen B, Johnsen H, Varhaug JE, et al. Specific P53 mutations are associated with de novo resistance to doxorubicin in breast cancer patients. Nat Med. 1996;2(7):811-4.
342. Troester MA, Herschkowitz JI, Oh DS, He X, Hoadley KA, Barbier CS, et al. Gene expression patterns associated with p53 status in breast cancer. BMC Cancer. 2006;6:276.
343. Mathe A, Wong-Brown M, Locke WJ, Stirzaker C, Braye SG, Forbes JF, et al. DNA methylation profile of triple negative breast cancer-specific genes comparing lymph node positive patients to lymph node negative patients. Sci Rep. 2016;6:33435.
344. Huh I, Wu X, Park T, Yi SV. Detecting differential DNA methylation from sequencing of bisulfite converted DNA of diverse species. Brief Bioinform. 2019;20(1):33-46.
345. Sullivan KD, Galbraith MD, Andrysik Z, Espinosa JM. Mechanisms of transcriptional regulation by p53. Cell Death Differ. 2018;25(1):133-43.
346. Wang X, Ju W, Renouard J, Aden J, Belinsky SA, Lin Y. 17-allylamino-17demethoxygeldanamycin synergistically potentiates tumor necrosis factor-induced lung cancer cell death by blocking the nuclear factor-kappaB pathway. Cancer Res. 2006;66(2):1089-95. 347. Rizki A, Weaver VM, Lee SY, Rozenberg GI, Chin K, Myers CA, et al. A human breast cell model of preinvasive to invasive transition. Cancer Res. 2008;68(5):1378-87.
348. Benzinger A, Muster N, Koch HB, Yates JR, 3rd, Hermeking H. Targeted proteomic analysis of 14-3-3 sigma, a p53 effector commonly silenced in cancer. Mol Cell Proteomics. 2005;4(6):785-95.
349. Grover R, Candeias MM, Fahraeus R, Das S. p53 and little brother p53/47: linking IRES activities with protein functions. Oncogene. 2009;28(30):2766-72.
350. Subik K, Lee JF, Baxter L, Strzepek T, Costello D, Crowley P, et al. The Expression Patterns of ER, PR, HER2, CK5/6, EGFR, Ki-67 and AR by Immunohistochemical Analysis in Breast Cancer Cell Lines. Breast Cancer (Auckl). 2010;4:35-41.
351. Narayanan R, Dalton JT. Androgen Receptor: A Complex Therapeutic Target for Breast Cancer. Cancers (Basel). 2016;8(12).

352. Fabian CJ. The what, why and how of aromatase inhibitors: hormonal agents for treatment and prevention of breast cancer. Int J Clin Pract. 2007;61(12):2051-63.
353. de Cremoux P, Dieras V, Poupon MF, Magdelenat H, Sigal-Zafrani B, Fourquet A, et al. [Tamoxifen and aromatase inhibitors in the treatment of breast cancer in menopausal women: pharmacological and clinical aspects]. Bull Cancer. 2004;91(12):917-27.
354. Waldman T, Zhang Y, Dillehay L, Yu J, Kinzler K, Vogelstein B, et al. Cell-cycle arrest versus cell death in cancer therapy. Nat Med. 1997;3(9):1034-6.
355. Somatic mutations in MCF-7 breast cancer cell lines. Catalogue Of Somatic Muations in Cancer [Available from: https://cancer.sanger.ac.uk/cosmic/search?q=MCF-7.
356. Liebler DC, Zimmerman LJ. Targeted quantitation of proteins by mass spectrometry. Biochemistry. 2013;52(22):3797-806.
357. Effects of chemotherapy and hormonal therapy for early breast cancer on recurrence and 15-year survival: an overview of the randomised trials. Lancet. 2005;365(9472):1687-717.
358. Angeloni SV, Martin MB, Garcia-Morales P, Castro-Galache MD, Ferragut JA, Saceda M. Regulation of estrogen receptor-alpha expression by the tumor suppressor gene p53 in MCF-7 cells. J Endocrinol. 2004;180(3):497-504.
359. Knowlden JM, Hutcheson IR, Jones HE, Madden T, Gee JM, Harper ME, et al. Elevated levels of epidermal growth factor receptor/c-erbB2 heterodimers mediate an autocrine growth regulatory pathway in tamoxifen-resistant MCF-7 cells. Endocrinology. 2003;144(3):1032-44.
360. Zhou C, Zhong Q, Rhodes LV, Townley I, Bratton MR, Zhang Q, et al. Proteomic analysis of acquired tamoxifen resistance in MCF-7 cells reveals expression signatures associated with enhanced migration. Breast Cancer Res. 2012;14(2):R45.
361. Resnier P, Montier T, Mathieu V, Benoit JP, Passirani C. A review of the current status of siRNA nanomedicines in the treatment of cancer. Biomaterials. 2013;34(27):6429-43.
362. Kojima K, Konopleva M, McQueen T, O'Brien S, Plunkett W, Andreeff M. Mdm2 inhibitor Nutlin-3a induces p53-mediated apoptosis by transcription-dependent and transcriptionindependent mechanisms and may overcome Atm-mediated resistance to fludarabine in chronic lymphocytic leukemia. Blood. 2006;108(3):993-1000.

Appendices

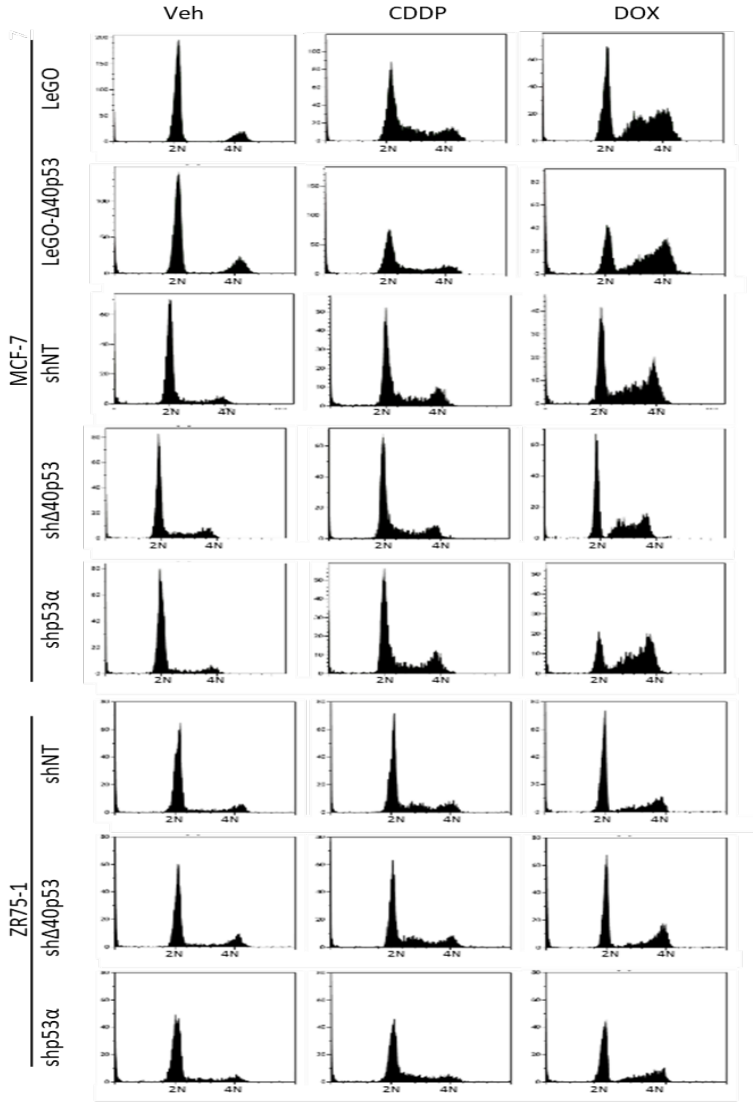

Appendix 1 PI staining histogram of all sublines before and after CDDP and DOX treatments using flow cytometry. Y-axis, cell count; x-axis, DNA content (2N for G1 phase or 4N for G2 phase). Events detected by the flow cytometer before 2N were dead cells.

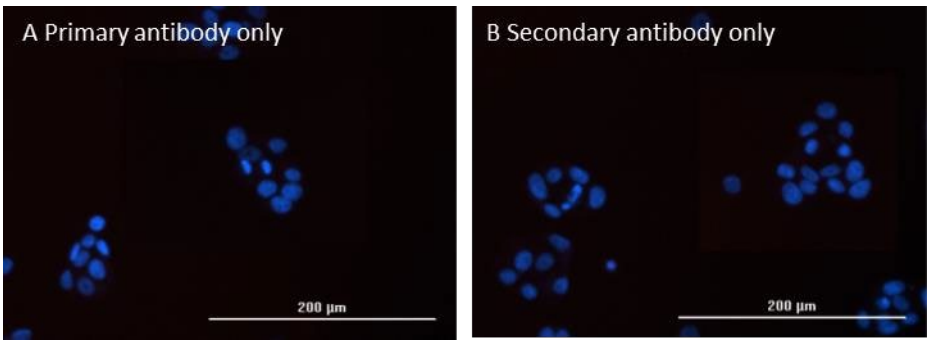

Appendix 2 Negative controls (primary antibody only (A) and secondary antibody only (B) of immunofluorescent staining against E-cadherin. Images were taken by Cytation 3 using a 10x objective. Blue: DAPI staining of nuclei.

Appendix 3 Full table of GSEA pathways when isoform levels were altered in MCF-7 cells.

MCF-7Δ40p53 vs. MCF-7-LeGO	MCF-7shΔ40p53 vs. MCF-7shNT	MCF-7shp53α vs. MCF-7 shNT	Description	MCF-7-Δ40p53 vs. MCF-7-LeGO		MCF-7-shΔ40p53 vs. MCF-7-shNT		MCF-7-shp53α vs. MCF-7 shNT	
				p	Genes	*p*	Genes	*p*	Genes
BRIDEAU_IMPRINTED_GENES	BRIDEAU_IMPRINTED_GENES	BRIDEAU_IMPRINTED_GENES		6.17E-03	ATP10A; SLC22A18; PEG10; SGCE; GNAS	2.80E-02	SLC38A4; SLC22A18; PEG10; SGCE; GNAS	3.81E-02	HTR2A; SLC22A18; PEG10; SGCE; GNAS
chr6p21	**chr6p21**	**chr6p21**		1.82E-18	RXRB; HLA-DRA; PPT2; MAS1L; TRIM15; TRIM10; SLC44A4; NEU1; DPCR1; SYNGAP1; HLA-DMB; GPSM3; VARS; PRRT1; NOTCH4; COL11A2; PBX2; RNF39; TRIM40; PSMB9; LTA; TNF; TNXB	6.72E-15	ZNF192P1; DDAH2; HLADRA; PPT2; DAXX; EGFL8; TRIM10; C2; HSD17B8; HLA-J; UBD; HCG4; GPSM3; VARS; FKBPL; CFB; GPX5; COL11A2; PBX2; TRIM38; ATF6B; LTA; BTNL2; TNF; TNXB	9.13E-19	ZNF192P1; DDAH2; HLADRA; PPT2; LY6G5C; DAXX; MAS1L; ZBTB9; SKIV2L; TRIM15; TRIM10; C2; HSD17B8; PPP1R10; HLA-J; HLA-DMB; UBD; GPSM3; FKBPL; CFB; NOTCH4; GPX5; COL11A2; OR2H1; PLA2G7; PBX2; ATF6B; LTA; DDR1; TNF; TAP2; TNXB
GGGAGGRR_V$MAZ_Q6	GGGAGGRR_V$MAZ_Q6	GGGAGGRR_V$MAZ_Q6	Genes with 3'UTR containing motif GGGAGGRR which matches annotation for MAZ: MYC-associated zinc finger protein (purine-binding transcription factor)	2.07E-03	MARK2; SCNN1A; KEL; SHC1; FLI1; PPT2; GNAS; ZIC4; LGALS1; LTBR; RNF39; TNXB; PPP2R2B; FGF5; PRSS8; KLC2; FSTL5; RXRB; EGFLAM; SLC7A8; SLC6A12; TREX1; COL11A2; PBX2	2.93E-02	AMPH; CCR7; CBFA2T3; FLI1; DDAH2; PPT2; GNAS; CREM; ZIC4; BDNF; AKAP12; MITF; PAK6; TNXB; MAPK3; FGF5; DAXX; LMO3; KLC2; TUG1; CHST8; ST3GAL1; SYNE1; MARCKS; ZMYND8; HSD17B8; SLC7A8; COL11A2; PBX2; ATF6B; LDB3	4.59E-03	CCR7; KEL; CRMP1; F13A1; FLI1; DDAH2; PPT2; MAPT; GNAS; CREM; ZIC4; ESR1; TSHR; SNCA; BMP7; NOS1; RBFOX1; SLITRK3; PAK6; CALD1; TNXB; DAXX; PLA2G7; KLC2; TUG1; CHST8; EGFLAM; MARCKS; ZBTB9; HSD17B8; PPP1R10; ELAVL4; SLC7A8; PITX2; TREX1; COL11A2; CLDN16; PBX2; PHYHIP; ATF6B; LDB3

	AACTTT_UNKNOWN	AACTTT_UNKNOWN		.	.	3.17E-02	ZFP36L2; GABRA1; CBFA2T3; TNF; ARPP21; FLI1; GNAS; CREM; RPS6KA2; AFF3; ZIC4; ADCY2; BDNF; MITF; NEUROD1; SDPR; MAPK3; LMO3; NTM; EYA4; CHST8; ST3GAL1; SYNE1; ZNF804B; C1QTNF7; CREB5; SLC6A1	1.86E-04	LRRC2; GPR133; ZFP36L2; GABRA1; ALX4; TNF; FLI1; GNAS; CREM; RPS6KA2; ZEB2; AFF3; ZIC4; ESR1; TSHR; ADCY2; SNCA; NOS1; RBFOX1; NEUROD1; SLITRK3; SDPR; CALD1; SLC24A4; CHN2; NOVA1; EYA4; CHST8; EGFLAM; ZNF804B; ZBTB9; ELAVL4; HTR2A; PDE4B; TRIM2; C1QTNF7; CREB5; PITX2; PHYHIP; CCDC80
	CATTGTYY_V$SOX9_B1	CATTGTYY_V$SOX9_B1	Genes with 3'UTR containing motif CATTGTYY which matches annotation for SOX9: SRY (sex determining region Y)-box 9 (campomelic dysplasia, autosomal sexreversal)	.	.	4.51E-02	FLI1; DDAH2; MAPK3; GJC2; MARCKS; MITF; ZMYND8; LMO3; CHST8; LOC84931	4.30E-02	FLI1; DDAH2; MGAT5B; CRMP1; EGFLAM; TREX1; SFRP1; MARCKS; TRIM2; CHST8; CALD1
	CTTTGA_V$LEF1_Q2	CTTTGA_V$LEF1_Q2	Genes with 3'UTR containing motif CTTTGA which matches annotation for LEF1: lymphoid enhancer-binding factor 1	.	.	5.48E-04	NTF3; ELF5; CFB; EIF4EBP3; STRA6; CASP8; LOC84931; CCR7; DLX5; ARPP21; CREM; SLC7A8; AFF3; ZIC4; C1QTNF7; CREB5; LAMA3; MITF; COL11A2; NEUROD1; PBX2; BEST3; PCDHGA4; SDPR; TNXB	8.84E-03	CFB; STRA6; CASP8; CCR7; DLX5; SLC24A4; CHN2; EGFLAM; CREM; ELAVL4; SLC7A8; ZEB2; AFF3; ZIC4; TRIM2; C1QTNF7; CREB5; PITX2; BMP7; COL11A2; NEUROD1; PBX2; PHYHIP; CPS1; SDPR; TNXB
	MODULE_84	MODULE_84	Immune (humoral) and inflammatory response.	.	.	1.76E-02	SLC16A3; SYNE1; NUPR1; TNXB; MAN2B1; C2; GPSM3; LMO3; SLC22A18AS; UBD; TNF; HLA-DRA; SLC7A8; LAMA3	3.74E-05	SLC16A3; DARC; F13A1; IGFBP3; APOE; NUPR1; TNXB; MAN2B1; ARHGDIB; C2; GPSM3; CD8A; SLC22A18AS; UBD;

									TNFAIP8; PDE4B; TNF; HLADRA; SLC7A8; PLA2G7; CPVL
	POTTI_CYTOXAN_SENSITIVITY	POTTI_CYTOXAN_SENSITIVITY		.	.	2.80E-02	SGCE; AKAP12; MARCKS; PEG10	3.12E-02	SGCE; CALD1; MARCKS; PEG10
	TAATTA_V$CHX10_01	TAATTA_V$CHX10_01	Genes with 3'UTR containing motif TAATTA which matches annotation for VSX1: visual system homeobox 1 homolog, CHX10-like (zebrafish)	.	.	7.23E-03	LMO3; ADARB2; CYFIP2; CHST8; ARPP21; MARCKS; GNAS; CLRN1; AFF3; ZIC4; CREB5; BDNF; MITF; COL11A2; NEUROD1; PBX2; BEST3; SLC6A5	2.10E-04	FOXF2; ARHGDIB; BAIAP2L2; NOVA1; CYFIP2; CHST8; EGFLAM; MARCKS; GNAS; ZBTB9; ELAVL4; CLRN1; ZEB2; AFF3; ZIC4; CREB5; PITX2; SFRP1; COL11A2; RBFOX1; NEUROD1; PBX2; SLITRK3; CALD1
	TGATTTRY_V$GFI1_01	TGATTTRY_V$GFI1_01	Genes having at least one occurence of the highly conserved motif M94 TGATTTRY sites. The motif matches transcription factor binding site V$GFI1_01 (v7.4 TRANSFAC).	.	.	4.34E-02	BDNF; CLRN1; GABRA1; ZIC4; PAK6; SDPR; C1QTNF7; CREB5; SLC6A5	3.37E-04	SNCA; PITX2; LRRC2; ELAVL4; CLRN1; CCDC80; NOVA1; GABRA1; ZIC4; PAK6; SDPR; ESR1; C1QTNF7; CREB5
	V$AFP1_Q6	V$AFP1_Q6	Genes with 3'UTR containing motif ATTAAYTRCAC which matches annotation for ZHX2: transcription factor ZHX2	.	.	2.68E-02	BDNF; FLI1; ZMYND8; CFB; AFF3; FOXP1; ZIC4; SDPR; CREB5	2.05E-03	FLI1; FOXF2; CFB; RBFOX1; ZEB2; ARHGDIB; AFF3; ZIC4; SDPR; ESR1; CALD1; CREB5

	V$CEBPDELTA_Q6	V$CEBPDELTA_Q6	Genes with 3'UTR containing motif MATTKCNTMAYY which matches annotation for CEBPD: CCAAT/enhancer binding protein (C/EBP), delta	.	.	7.56E-04	BDNF; FLI1; MARCKS; MITF; CFB; NEUROD1; LMO3; FOXP1; PAK6; SDPR; CREB5	4.60E-03	FLI1; MARCKS; CFB; PPP1R10; RBFOX1; NEUROD1; ZEB2; CPS1; PAK6; SDPR; CREB5
	V$COMP1_01	V$COMP1_01	Genes with 3'UTR containing motif NVTNWTGATTGACNACAAVARRBN which matches annotation for MYOG: myogenin (myogenic factor 4)	.	.	9.22E-03	FLI1; ZIC4; DLX5; MITF; DAXX; ZMYND8; CREB5	4.76E-02	FLI1; ZIC4; DLX5; DAXX; CALD1; CREB5
	V$NFKAPPAB_01	V$NFKAPPAB_01	Genes having at least one occurence of the transcription factor binding site V$NFKAPPAB_01 (v7.4 TRANSFAC)	.	.	2.68E-02	BDNF; RND1; COL11A2; RIN2; ZFP36L2; LTA; MSC; UBD; TNF	1.94E-02	FGF1; COL11A2; RIN2; ZBTB9; ZFP36L2; LTA; MSC; DDR1; UBD; TNF
			in the regions spanning up to 4 kb around their transcription starting sites.						
	V$NKX61_01	V$NKX61_01		.	.	2.00E-02	FLI1; MARCKS; COL11A2; CLRN1; LMO3; ZIC4; SDPR; C1QTNF7; CREB5	1.39E-02	FLI1; MARCKS; COL11A2; RBFOX1; CLRN1; SLITRK3; ZIC4; SDPR; C1QTNF7; CREB5
	V$PAX4_02	V$PAX4_02	Genes with 3'UTR containing motif NAAWAATTANS which matches annotation for PAX4: paired box gene 4	.	.	2.00E-02	MARCKS; MITF; ZMYND8; ZFP36L2; FOXP1; ZIC4; CYFIP2; SDPR; SLC6A5	1.40E-02	BAIAP2L2; PITX2; MARCKS; ZFP36L2; PPP1R10; RBFOX1; SLITRK3; ZIC4; CYFIP2; SDPR

	YCATTAA_UNKNOWN	YCATTAA_UNKNOWN		.	.	2.80E-02	FLI1; FGF5; CLRN1; LMO3; ZIC4; C1QTNF7; CREB5; MITF; PBX2; GABRA1; PCDHGB7; NTM; CHST8	4.59E-03	FLI1; MGAT5B; PPP1R10; ELAVL4; CLRN1; ARHGDIB; ZIC4; C1QTNF7; CREB5; PITX2; NOS1; RBFOX1; PBX2; NOVA1; GABRA1; CPS1; CHST8
CERVERA_SDHB_TARGETS_1_DN		CERVERA_SDHB_TARGETS_1_DN	Genes turned off in Hep3B cells (hepatocellular carcinoma, HCC) upon knockdown of SDHB [GeneID=6390] by RNAi.	1.45E-02	ITPR2; EYA4; PEG10; TMC8	.	.	8.88E-03	ITPR2; PLA2G7; EYA4; PEG10; CPS1
KEGG_TYPE_I_DIABETES_MELLITUS		KEGG_TYPE_I_DIABETES_MELLITUS		1.62E-02	LTA; TNF; HLA-DMB; HLADRA	.	.	1.23E-02	LTA; TNF; PTPRN2; HLADMB; HLA-DRA
MIKKELSEN_MCV6_LCP_WITH_H3K4ME3		MIKKELSEN_MCV6_LCP_WITH_H3K4ME3	Genes with lowCpG-density promoters (LCP) bearing the trimethylation mark at H3K4 (H3K4me3) in MCV6 cells (embryonic fibroblasts trapped in a differentiated state).	1.72E-02	TREX1; NOTCH4; MARK2; TRIM40; GPSM3; ACY3	.	.	4.76E-02	TREX1; NOTCH4; GCNT3; ZFP57; GPSM3; ARHGDIB; ACY3

ATATGCA.MIR448	ATATGCA.MIR-448			1.41E-04	PCDHGA6; PCDHGA5; PCDHGA4; PCDHGA3; PCDHGA2; PCDHGA1; PCDHGB1; PCDHGB3; PCDHGB2	3.26E-14	NTF3; PCDHGA12; PCDHGA10; PCDHGA11; PCDHGA9; PCDHGA8; PCDHGA7; PCDHGA6; PCDHGA5; PCDHGA4; PCDHGA3; PCDHGA2; PCDHGA1; PCDHGB1; PCDHGB7; PCDHGB6; PCDHGB3; PCDHGB2; PCDHGB5; PCDHGB4	.	.
chr5q31	chr5q31			1.43E-06	PPP2R2B; TIFAB; PCDHGA6; PCDHGA5; PCDHGA4; PCDHGA3; PCDHGA2; PCDHGA1; PCDHGB1; PCDHGB3; PCDHGB2	4.46E-15	EIF4EBP3; PCDHGA12; PCDHGA10; PCDHGA11; ANKHD1-EIF4EBP3; PCDHGA9; PCDHGA8; PCDHGA7; PCDHGA6; PCDHGA5; PCDHGA4; PCDHGA3; PCDHGA2; PCDHGA1; PCDHGB1; PCDHGB7; PCDHGB6; PCDHGB3; PCDHGB2; PCDHGB5; PCDHGB4	.	.
GGGACCA.MIR-133A.MIR-133B	GGGACCA.MIR-133A.MIR-133B			9.89E-06	SLC7A8; PCDHGA6; PCDHGA5; PCDHGA4; PCDHGA3; PCDHGA2; PCDHGA1; PCDHGB1; PCDHGB3; PCDHGB2	2.19E-14	SLC7A8; PCDHGA12; PCDHGA10; PCDHGA11; PCDHGA9; PCDHGA8; PCDHGA7; PCDHGA6; PCDHGA5; PCDHGA4; PCDHGA3; PCDHGA2; PCDHGA1; PCDHGB1; PCDHGB7; PCDHGB6; PCDHGB3; PCDHGB2; PCDHGB5; PCDHGB4	.	.
TCCAGAG.MIR518C	TCCAGAG.MIR-518C			9.89E-06	PCDHGA6; PCDHGA5; PCDHGA4; PCDHGA3; PCDHGA2; PCDHGA1; PCDHGB1; PCDHGB3; PCDHGB2	2.01E-16	PCDHGA12; PCDHGA10; PCDHGA11; RND1; PCDHGA9; PCDHGA8; PCDHGA7; PCDHGA6; PCDHGA5; PCDHGA4; PCDHGA3; PCDHGA2; PCDHGA1; PCDHGB1; PCDHGB7; PCDHGB6;	.	.

							PCDHGB3; PCDHGB2; PCDHGB5; PCDHGB4		
CELL_FATE_COMMITMENT				1.56E-02	POU6F2; TRIM15; NOTCH4	.	.	.	.
chr6q23				2.98E-02	SNORD100; SNORA33; EYA4; RPS12	.	.	.	.
MODULE_543			nnexin, MHCII, and lectins.	1.62E-02	HLA-DRA; HLA-DMB; LGALS1	.	.	.	.
V$AR_03			Genes having at least one occurence of the transcription factor binding site V$AR_03 (v7.4 TRANSFAC) in the regions spanning up to 4 kb around their transcription starting sites.	4.04E-02	SLC7A8; RAB1B; FSTL5; SCNN1A	.	.	.	.
	ACEVEDO_LIVER_CANCER_WITH_H3K27ME3_DN			.	.	1.10E-05	PCDHGB7; PCDHGB5; PCDHGB6; PCDHGA10; PCDHGA8; LAMA3; PCDHGA9; PCDHGB4; PCDHGA6; PCDHGB3; PCDHGA11; PCDHGA7	.	.
	CAGTATT.MIR-200B.MIR200C.MIR429			.	.	2.80E-02	FLI1; NTF3; MARCKS; RPS6KA2; CREB5; ADCY2; TMCC1; XKR6; AFF3; SLC6A1; SLC38A4; ARPP21	.	.
	CHIARADONNA_NEOPLASTIC_TRANSFORMATION_KRAS_DN			.	.	2.68E-02	FOXP1; GUK1; AKAP12; MAN2B1; NUPR1; TNXB; SLC38A4	.	.

	FIGUEROA_AML_METHYLATION_CLUSTER_3_UP			.	.	3.42E-02	PCDHGB7; PCDHGA11; PCDHGA8; PCDHGA5; PCDHGB4; RECQL5; ZNF264	.	.
	KEGG_MELANOGENESIS			.	.	2.80E-02	EDNRB; ADCY2; GNAS; WNT16; MAPK3; MITF	.	.
	MIKKELSEN_MCV6_ICP_WITH_H3K27ME3		Genes with intermediateCpG-density promoters (ICP) bearing the trimethylation mark at H3K27 (H3K27me3) in MCV6 cells (embryonic fibroblasts trapped in a differentiated state).	.	.	4.55E-02	PAK6; TNF; KCNJ5; COL11A2; ADM2	.	.
	SCHAEFFER_PROSTATE_DEVELOPMENT_AND_CANCER_BOX1_DN			.	.	2.30E-02	AFF3; ZMYND8; SDPR	.	.
	TGTTTGY_V$HNF3_Q6		Genes with 3'UTR containing motif TGTTTGY which matches annotation for FOXA1: forkhead box A1	.	.	7.60E-03	MAPK3; ELF5; LRRC17; CFB; AFF3; ZIC4; LOC84931; ADARB2; CREB5; MITF; NEUROD1; SLC6A1; SLC38A4; TUG1; FOXP1; BEST3; ARPP21	.	.
	TRANSC_FACT			.	.	2.37E-02	WIZ; LMO3; MSC; AFF3; TNXB; DLX5; ELF5; EYA4; ZNF264; ZIC4; KCNJ5; MITF; ZFP36L2; CREM; FOXP1; NEUROD1; TRIM10; PBX2; FLI1; TRIM38; CBFA2T3; CREB5	.	.

	V$AP1_Q2_01		Genes with 3'UTR containing motif TGACTCANNSKN which matches annotation for JUN: v-jun sarcoma virus 17 oncogene homolog (avian)	.	.	2.93E-02	FLI1; LAMA3; MITF; CLRN1; COBL; PAK6; LDB3; TNXB; SLC6A5	.	.
	V$GFI1_01		Genes with 3'UTR containing motif NNNNNNNAAATCACWGYNNNNNNN which matches annotation for GFI1: growth factor independent 1	.	.	2.80E-02	BDNF; CCR7; LAMA3; CREM; CLRN1; LMO3; ZIC4; C1QTNF7; CREB5	.	.
	V$HFH8_01		Genes having at least one occurence of the transcription factor binding site V$HFH8_01 (v7.4 TRANSFAC) in the regions spanning up to 4 kb around their transcription starting sites.	.	.	2.68E-02	FLI1; GDPD3; NTF3; MARCKS; ZMYND8; LTA; TNF; CREB5	.	.
	V$NFKB_Q6_01		Genes having at least one occurence of the transcription factor binding site V$NFKB_Q6_01 (v7.4 TRANSFAC) in the regions spanning up to 4 kb around their transcription starting sites.	.	.	2.15E-02	BDNF; RND1; MITF; RIN2; ANKHD1-EIF4EBP3; ZIC4; LTA; MSC; UBD	.	.

	WGTTNNNNNAAA_UNKNOWN			.	.	2.68E-02	FLI1; NTF3; ZMYND8; CLRN1; LMO3; C1QTNF7; ADARB2; CREB5; BDNF; CCR7; MITF; RIN2; ARPP21	.	.
	YAATNRNNNYNATT_UNKNOWN			.	.	2.80E-02	LMO3; BDNF; ELF5; CREM; CREB5; CLRN1	.	.
		ACEVEDO_METHYLATED_IN_LIVER_CANCER_DN		.	.	.	.	3.62E-02	ARMC3; EGFLAM; TNF; CCDC80; MTNR1A; RBFOX1; LTA; ARHGAP25; F13A1; SLC24A4; TNP1; PHYHIP; TIAM2; FGF1; PTPRN2; APOE; SDPR; GIMAP7
		ANATOMICAL_STRUCTURE_DEVELOPMENT		.	.	.	.	4.21E-02	FGF1; TRIM15; MOG; APOE; KEL; CRMP1; DLX5; EYA4; IGFBP3; FLI1; MAPT; SNCA; ADORA1; TWIST1; PITX2; TAGLN3; SFRP1; NOTCH4; SGCE; PTN; SPRR1A
		APOPTOSIS_GO		.	.	.	.	3.12E-02	DDAH2; DAXX; TNFAIP8; CASP8; SNCA; ADORA1; APOE; SFRP1; BIK; CYFIP2; LTA; TNF; IGFBP3
		ARGGGTTAA_UNKNOWN		.	.	.	.	5.99E-03	FLI1; CRMP1; CCDC80; SFRP1; SLC24A4; ESR1; PPP1R10; NEUROD1
		ATGCAGT.MIR217		.	.	.	.	4.76E-02	SLITRK3; NOVA1; RIN2; RBFOX1; CHN2; NEUROD1
		AZARE_NEOPLASTIC_TRANSFORMATION_BY_STAT3_DN		.	.	.	.	2.06E-02	SFRP1; ARHGAP25; FLI1; CPS1; CALD1; ARHGDIB; NUPR1

		BENPORATH_EED_TARGETS	Set 'Eed targets': genes identified by ChIP on chip as targets of the Polycomb protein EED [GeneID=8726] in human embryonic stem cells.	.	.	.	.	1.72E-02	CHST8; DLX5; FLI1; PLA2G7; MAPT; TWIST1; NEUROD1; FLRT2; FOXF2; ALX4; EYA4; SFRP1; ZEB2; SLITRK3; PPP1R10; ZIC4; IGFBP3; PITX2; CHN2; MSC; CD8A; SLC24A4; SLC6A3
		BENPORATH_ES_WITH_H3K27ME3	Set 'H3K27 bound': genes posessing the trimethylated H3K27 (H3K27me3) mark in their promoters in human embryonic stem cells, as identified by ChIP on chip.	.	.	.	.	2.47E-04	NEUROD1; MAPT; SFRP1; ZIC4; ESR1; FLRT2; SLC6A3; MSC; RPS6KA2; SLC24A4; EYA4; CD8A; FOXF2; EGFLAM; CRMP1; ALX4; PITX2; PTPRN2; NGF; TWIST1; IGFBP3; FLI1; CHST8; SLITRK3; CSMD2; CHN2; ZEB2; DLX5; CACNB4
		BENPORATH_SUZ12_TARGETS	Set 'Suz12 targets': genes identified by ChIP on chip as targets of the Polycomb protein SUZ12 [GeneID=23512] in human embryonic stem cells.	.	.	.	.	4.59E-03	NGF; ZEB2; CRMP1; SFRP1; KCNJ5; ALX4; SLC24A4; GNAS; CACNB4; CD8A; FLI1; NEUROD1; CADM3; MAPT; NOS1; MSC; CHST8; ZIC4; EGFLAM; PITX2; SLC6A3; MGAT5B; FLRT2; SLITRK3
		BOQUEST_STEM_CELL_UP		.	.	.	.	8.88E-03	TWIST1; PEG10; IGFBP3; NOVA1; APOE; CFB; TNXB; LRRC17; FLRT2; MSC; SGCE

		CAGGTG_V$E12_Q6	Genes with 3'UTR containing motif CAGGTG which matches annotation for TCF3: Transcription factor 3 (E2A immunoglobulin enhancer binding factors E12/E47)	.	.	.	.	1.90E-02	TRIM15; CRMP1; ALX4; DDR1; DDAH2; PPT2; MAPT; GNAS; TMEM105; ZEB2; AFF3; ZIC4; MTNR1A; ESR1; SNCA; BMP7; NOS1; ITPR2; NEUROD1; SLITRK3; PAK6; SDPR; LTA; FGF1; STRA6; PLA2G6; MSC; EYA4; CHST8; NGF; MGAT5B; LY6G5C; ELAVL4; SLC7A8; PDE4B; GCNT3; SFRP1; COL11A2; PHYHIP; LDB3; GHDC
		CELL_DEVELOPMENT		.	.	.	.	2.07E-02	DDAH2; DAXX; MAPT; TNP1; TNFAIP8; CASP8; SNCA; ADORA1; APOE; SFRP1; BMP7; BIK; CYFIP2; LTA; TNF; IGFBP3
		CHEN_METABOLIC_SYNDROM_NETWORK		.	.	.	.	4.79E-02	MSC; ARHGDIB; TREX1; UBD; ARMC3; SPRR1A; MAN2B1; IFI27L2; DDAH2; GPSM3; RASA3; TNFAIP8; RIN2; TNF; F13A1; FSCN1; CCRL2; SLC7A8; CCDC80; PLA2G7; ARHGAP25; RPS6KA2; HLA-DMB
		DAVICIONI_RHABDOMYOSARCOMA_PAX_FOXO1_FUSION_DN		.	.	.	.	3.89E-02	IGFBP3; ZFP36L2; MARCKS
		EGFR1		.	.	.	.	3.97E-02	IGFBP3; TRIM2; SPOCD1; PEG10; NOS1; MAPT; ESR1; ZFP36L2; PPP1R10
		FULCHER_INFLAMMATORY_RESPONSE_LECTIN_VS_LPS_DN		.	.	.	.	3.62E-02	IFI27L2; RBFOX1; F13A1; HLA-DMB; C2; NUPR1; CFB; MARCKS; ZFP36L2; CHN2; DDAH2; ZEB2; RIN2

		GATAAGR_V$GATA_C	Genes with 3'UTR containing motif GATAAGR. Motif does not match any known transcription factor	.	.	.	.	1.86E-02	FLI1; PITX2; PPT2; TRIM15; TRIM10; ELAVL4; SLC7A8; CCDC80; ARHGDIB; TNXB; CREB5
		GAURNIER_PSMD4_TARGETS		.	.	.	.	4.76E-02	HLA-DMB; HLA-DRA; C2; TNF; CCR7
		GNF2_DNM1	Neighborhood of DNM1 dynamin 1 in the GNF2 expression compendium	.	.	.	.	4.36E-02	MAPT; PHYHIP; TAGLN3; GABRA1; RBFOX1
		HELLER_SILENCED_BY_METHYLATION_UP		.	.	.	.	2.74E-02	FSCN1; HLA-DMB; DDAH2; HLA-DRA; APOE; UBD; CFB; IGFBP3; GCNT3; CCR7
		KAAB_HEART_ATRIUM_VS_VENTRICLE_UP		.	.	.	.	1.94E-02	NUPR1; ADORA1; FLRT2; RPL3; DDR1; PDE4B; ZFP36L2; SLC22A18; SFRP1; SGCE
		KAYO_CALORIE_RESTRICTION_MUSCLE_DN		.	.	.	.	2.25E-02	TNP1; ADCY2; TUG1; ATF6B; CREM; DDR1
		LIM_MAMMARY_LUMINAL_MATURE_DN		.	.	.	.	3.62E-02	IGFBP3; APOE; SFRP1; CALD1; TIAM2; RASA3
		MALIK_REPRESSED_BY_ESTROGEN	Genes consistently and robustly repressed by estradiol [PubChem=5757] in MCF7 cells (breast cancer); this reperession was prevented by fulvestrant [PubChem=3478439].	.	.	.	.	2.74E-02	BMP7; BIK; RPRM

		MCLACHLAN_DENTAL_CARIES_DN		.	.	.	.	3.74E-05	CYFIP2; HLA-DRA; TNFAIP8; ARHGDIB; DARC; PEG10; MAN2B1; CFB; F13A1; APOE; CPVL; PLA2G7; TRIM2; HLA-DMB
		MCLACHLAN_DENTAL_CARIES_UP		.	.	.	.	4.77E-03	APOE; ARHGDIB; F13A1; HLA-DRA; DARC; MAN2B1; TNFAIP8; PLA2G7; CPVL; CFB; HLA-DMB
		MEISSNER_NPC_HCP_WITH_H3K4ME2_AND_H3K27ME3	Genes with highCpG-density promoters (HCP) bearing histone H3 dimethylation mark at K4 (H3K4me2) and trimethylation mark at K27 (H3K27me3) in neural precursor cells (NPC).	.	.	.	.	2.06E-02	BIK; SFRP1; DLX5; CADM3; AFF3; FLI1; GNAS; PTPRN2; FAM155A; FOXF2; EGFLAM; MSC
		MIKKELSEN_ES_ICP_WITH_H3K27ME3		.	.	.	.	4.81E-02	ZIC4; PLEKHG4; TNF; ZEB2
		MODULE_1	Ovary genes.	.	.	.	.	2.28E-02	CALD1; PEG10; SGCE; DARC; SFRP1; F13A1; IGFBP3; APOE; NUPR1; DBN1; TNXB; MAN2B1
		MODULE_100	Genes in the cancer module 100.	.	.	.	.	2.56E-06	PEG10; SGCE; SFRP1; IGFBP3; APOE; NUPR1; DBN1; PTN; TRIM2; CLDN10; PTPRN2; TAGLN3; SLC22A18AS; MAPT; CRMP1; CHN2; ELAVL4; NOVA1; PHYHIP; PDE4B; EDNRB; TNF; SLC6A3

		MODULE_11	Genes in the cancer **module 11**	.	.	.	.	3.74E-05	PEG10; SGCE; SFRP1; APOE; NUPR1; DBN1; PTN; TRIM2; CLDN10; PTPRN2; TAGLN3; SLC22A18AS; MAPT; CRMP1; CHN2; ELAVL4; NOVA1; PHYHIP; PDE4B; EDNRB; TNF
		MODULE_117	Signaling	.	.	.	.	9.62E-03	CADM3; ARHGDIB; CLDN10; CFB; ADORA1; BIK; NGF; PBX2; PLA2G7; CPVL; LTA; CACNB4; SLC6A3; DLX5; PLA2G6; NEUROD1; CREB5; RASA3; SLITRK3
		MODULE_118	cell line expressed genes.	.	.	.	.	1.94E-02	SLC16A3; CALD1; PEG10; SGCE; DARC; DBN1; PPT2; ARHGDIB; GPSM3; SLC22A18AS; PDE4B; TNF; BIK
		MODULE_12	Spinal cord (neurodevelopment) genes	.	.	.	.	7.55E-04	PEG10; SGCE; DARC; SFRP1; IGFBP3; APOE; NUPR1; DBN1; PTN; TRIM2; FGF1; CRMP1; NOVA1; PDE4B; EDNRB
		MODULE_137	CNS genes	.	.	.	.	2.56E-06	PEG10; SGCE; SFRP1; IGFBP3; APOE; NUPR1; DBN1; PTN; TRIM2; CLDN10; PTPRN2; TAGLN3; SLC22A18AS; MAPT; CRMP1; CHN2; ELAVL4; NOVA1; PHYHIP; PDE4B; EDNRB; TNF; SLC6A3
		MODULE_2	DRG (dorsal root ganglia) genes	.	.	.	.	2.84E-02	SGCE; DARC; SFRP1; IGFBP3; APOE; NUPR1; TNXB; PTN; TRIM2; CADM3; PPT2; FGF1
		MODULE_220	Developmental processes	.	.	.	.	1.48E-02	CALD1; APOE; PTN; FGF1; ARHGDIB; CD8A; ADORA1; CRMP1; EDNRB; NGF; DLX5; ZEB2

		MODULE_23	Liver genes - metabolism and xenobiotics	.	.	.	.	3.10E-02	IGFBP3; APOE; NUPR1; TNXB; MAN2B1; C2; CFB; ITIH1; SLC22A18AS; HTR2A; NOVA1; TNF; ESR1; CPS1; SLC22A18
		MODULE_41	Genes in the cancer **module 41**.	.	.	.	.	2.99E-02	DARC; PPT2; GPSM3; CD8A; ITIH1; TAGLN3; TRIM10; SLC22A18AS; HTR2A; PHYHIP; TNP1; ATF6B; TRIM15; ESR1; MSC
		MODULE_44	Thymus genes	.	.	.	.	1.16E-02	DARC; F13A1; IGFBP3; APOE; NUPR1; ARHGDIB; C2; GPSM3; CD8A; UBD; TNFAIP8; CPVL
		MODULE_45	Whole blood genes	.	.	.	.	3.35E-02	SLC16A3; F13A1; TNXB; MAN2B1; ARHGDIB; C2; GPSM3; CD8A; SLC22A18AS; HTR2A; TNFAIP8; PDE4B; TNF; CPVL; ARHGAP25
		MODULE_55	Genes in the cancer **module 55**	.	.	.	.	1.89E-02	PEG10; SGCE; DARC; SFRP1; IGFBP3; APOE; NUPR1; TNXB; PTN; C2; CLDN10; CFB; PTPRN2; ITIH1; SLC22A18AS; PHYHIP; TRIM15; ESR1; CPS1; SLC7A8
		MODULE_6	Trachea genes	.	.	.	.	4.36E-02	SGCE; DARC; SFRP1; IGFBP3; NUPR1; TNXB; TRIM2; C2; CLDN10; CFB; PTPRN2; DDR1
		MODULE_66	Genes in the cancer **module 66**	.	.	.	.	2.60E-06	PEG10; SGCE; SFRP1; IGFBP3; APOE; NUPR1; DBN1; PTN; TRIM2; CLDN10; PTPRN2; TAGLN3; SLC22A18AS; MAPT; CRMP1; CHN2; ELAVL4; NOVA1; PHYHIP; PDE4B; EDNRB; TNF; SLC6A3

		MODULE_88	Heart, liver, kidney and pancreas metabolic and xenobiotic response genes	.	.	.	.	9.59E-03	PEG10; SGCE; DARC; SFRP1; IGFBP3; APOE; NUPR1; TNXB; PTN; C2; GPSM3; CLDN10; CFB; PTPRN2; ITIH1; SLC22A18AS; PHYHIP; TRIM15; ESR1; CPS1; SLC7A8
		MOREAUX_MULTIPLE_MYELOMA_BY_TACI_UP		.	.	.	.	7.55E-04	TNF; HLA-DMB; MSC; PBX2; SLC6A13; DDAH2; COL11A2; BIK; FOXF2; STRA6; NOS1; CLDN10; DDR1; INF2; FLRT2; SNCA
		MULTICELLULAR_ORGANISMAL_DEVELOPMENT		.	.	.	.	4.79E-02	FGF1; TRIM15; ARHGDIB; MOG; APOE; KEL; CRMP1; DLX5; IGFBP3; FLI1; MAPT; SNCA; ADORA1; PITX2; TWIST1; TAGLN3; NOTCH4; SGCE; AFF3; PTN; SPRR1A
		PLASMA_MEMBRANE		.	.	.	.	1.94E-02	HLA-DRA; CACNB4; PTPRN2; CADM3; CCR7; KEL; SLC16A3; SLC22A18; GABRA1; DDR1; KCNJ5; MAPT; GNAS; RASA3; HTR2A; SLC7A8; MTNR1A; CCRL2; TSHR; ADORA1; NOTCH4; EDNRB; SGCE; CLDN16; CLDN10; ITPR2; SLC6A3; DARC
		PROGRAMMED_CELL_DEATH		.	.	.	.	3.15E-02	DDAH2; DAXX; TNFAIP8; CASP8; SNCA; ADORA1; APOE; SFRP1; BIK; CYFIP2; LTA; TNF; IGFBP3
		QI_HYPOXIA_TARGETS_OF_HIF1A_AND_FOXA2		.	.	.	.	4.21E-02	FSCN1; SLC16A3; NGF; ZFP57

		REACTOME_INITIAL_TRIGGERING_OF_COMPLEMENT		.	.	.	.	3.10E-02	CRP; CFB; C2
		REGULATION_OF_APOPTOSIS		.	.	.	.	4.21E-02	SNCA; ADORA1; APOE; DDAH2; SFRP1; DAXX; BIK; TNFAIP8; LTA; TNF; IGFBP3
		REGULATION_OF_DEVELOPMENTAL_PROCESS		.	.	.	.	3.62E-02	DDAH2; DAXX; MAPT; TNFAIP8; SNCA; ADORA1; APOE; SFRP1; NOTCH4; BIK; LTA; TNF; IGFBP3
		REGULATION_OF_PROGRAMMED_CELL_DEATH		.	.	.	.	4.25E-02	SNCA; ADORA1; APOE; DDAH2; SFRP1; DAXX; BIK; TNFAIP8; LTA; TNF; IGFBP3
		RPS14_DN.V1_UP	Genes upregulated in CD34+ hematopoietic progenitor cells after knockdown of RPS14 [GeneID=6208] by RNAi.	.	.	.	.	4.56E-02	PLA2G7; CYFIP2; HLA-DMB; CACNB4; MARCKS; ARHGAP25; RIN2; F13A1
		RTTTNNNYTGGM_UNKNOWN		.	.	.	.	1.40E-02	F13A1; CCDC80; NOVA1; ZIC4; ESR1; CALD1; NGF; CREB5
		RYTTCCTG_V$ETS2_B	Genes with 3'UTR containing motif RYTTCCTG which matches annotation for ETS2: v-ets erythroblastosis virus E26 oncogene homolog 2 (avian)	.	.	.	.	1.16E-02	ARHGDIB; CASP8; CRMP1; DLX5; RIN2; CHN2; ACY3; EGFLAM; CREM; ZBTB9; RASA3; ELAVL4; ZEB2; ZIC4; PITX2; GCNT3; TREX1; NOTCH4; BMP7; NOS1; ITPR2; CCDC80; SDPR; CALD1
		SCHAEFFER_PROSTATE_DEVELOPMENT_12HR_DN		.	.	.	.	2.74E-02	RASA3; SFRP1; TAGLN3; ELAVL4; CRMP1

		SCHUETZ_BREAST_CANCER_DUCTAL_INVASIVE_UP		.	.	.	.	4.12E-02	HLA-DMB; CALD1; HLA-DRA; FLI1; TWIST1; APOE; SLC16A3; CPVL; IGFBP3; LRRC17; ZEB2
		SHEPARD_BMYB_MORPHOLINO_DN		.	.	.	.	4.36E-02	SLC6A13; CFB; SFRP1; STRA6; APOE; TNXB; CPVL; ELAVL4
		SMID_BREAST_CANCER_LUMINAL_B_DN		.	.	.	.	4.21E-02	HLA-DRA; TRIM2; SFRP1; IGFBP3; CCR7; ARHGAP25; FSCN1; TNFAIP8; DARC; CSGALNACT1; CALD1; ADCY2; PTN; DLX5
		SMID_BREAST_CANCER_NORMAL_LIKE_UP		.	.	.	.	1.90E-02	TNXB; SFRP1; DARC; ARHGAP25; F13A1; TNFAIP8; PTN; FLI1; CD8A; HLA-DRA; CSGALNACT1; CPVL; CCR7; FLRT2
		SNF5_DN.V1_DN	Genes downregulated in MEF cells (embryonic fibroblasts) with knockout of SNF5 [GeneID=65 98] gene.	.	.	.	.	1.90E-02	SNCA; CCR7; RPS6KA2; ESR1; CRMP1; SLC16A3; CSGALNACT1; CACNB4
		ST_ADRENERGIC		.	.	.	.	3.62E-02	ITPR2; PITX2; KCNJ5; CFB
		ST_G_ALPHA_I_PATHWAY	G alpha i Pathway	.	.	.	.	3.78E-02	ITPR2; PITX2; KCNJ5; CFB
		ST_MYOCYTE_AD_PATHWAY		.	.	.	.	2.06E-02	ITPR2; PITX2; KCNJ5; CFB
		TARTE_PLASMA_CELL_VS_PLASMABLAST_UP		.	.	.	.	3.12E-02	CFB; TNP1; GABRA1; FSCN1; SPRR1A; APOE; ATF6B; NOTCH4; PBX2; DDR1; CCR7; SNCA

		TGGAAA_V$NFAT_Q4_01	Genes with 3'UTR containing motif TGGAAA which matches annotation for NFAT	.	.	.	.	4.59E-03	FOXF2; LRRC2; UBD; TNF; FLI1; PPT2; GNAS; CREM; ZEB2; AFF3; ZIC4; ESR1; ADCY2; TWIST1; NOS1; RBFOX1; SLITRK3; CALD1; TNXB; DBN1; RIN2; CYFIP2; NGF; IGFBP3; EGFLAM; PPP1R10; ELAVL4; SLC7A8; PDE4B; TNFAIP8; CREB5; ADORA1; PITX2; TREX1; CCDC80; LDB3
		TTGTTT_V$FOXO4_01	Genes with 3'UTR containing motif TTGTTT which matches annotation for MLLT7: myeloid/lymphoid or mixed-lineage leukemia (trithorax homolog, Drosophila); translocated to, 7	.	.	.	.	1.40E-02	LRRC17; CRMP1; BIK; CADM3; GABRA1; FLI1; GNAS; CREM; ZEB2; AFF3; ZIC4; TSHR; TWIST1; RBFOX1; PAK6; PTN; TNXB; RAB1B; CHN2; NOVA1; TUG1; MSC; CHST8; EGFLAM; MARCKS; ZBTB9; PPP1R10; ELAVL4; C1QTNF7; CREB5; ADORA1; PITX2; TREX1; CCDC80; CPS1; CPVL
		V$ALPHACP1_01	Genes having at least one occurence of the transcription factor binding site V$ALPHACP1_01 (v7.4 TRANSFAC) in the regions spanning up to 4 kb around their transcription starting sites.	.	.	.	.	2.07E-02	SNCA; SFRP1; PPP1R10; ELAVL4; CLRN1; ZEB2; ATF6B; TUG1; AFF3; CALD1

		V$CEBP_01	Genes with 3'UTR containing motif NNTKTGGWNANNN which matches annotation for CEBPA: CCAAT/enhancer binding protein (C/EBP), alpha	.	.	.	.	4.76E-02	FLI1; SLC24A4; CLDN16; ZBTB9; RBFOX1; NEUROD1; SLITRK3; ZEB2; TNF
		V$CP2_01	Genes with 3'UTR containing motif GCHCDAMCCAG which matches annotation for TFCP2: transcription factor CP2	.	.	.	.	4.79E-02	CRMP1; COL11A2; GNAS; ZBTB9; STRA6; DDR1; CALD1; NGF; TNXB
		V$FOXD3_01	Genes with 3'UTR containing motif NAWTGTTTRTTT which matches annotation for FOXD3: forkhead box D3	.	.	.	.	4.93E-03	TWIST1; MARCKS; RBFOX1; CHN2; SLITRK3; ZEB2; NOVA1; AFF3; CALD1; CREB5
		V$GATA1_03	Genes with 3'UTR containing motif ANGNDGATAANNGN which matches annotation for GATA1: GATA binding protein 1 (globin transcription factor 1)	.	.	.	.	3.71E-02	SNCA; PITX2; TWIST1; EGFLAM; ELAVL4; ZEB2; CCDC80; TNXB; CREB5

		V$GATA1_04	Genes with 3'UTR containing motif ANGNDGATAANN GN which matches annotation for GATA1: GATA binding protein 1 (globin transcription factor 1)	.	.	.	.	1.72E-02	FLI1; PITX2; TWIST1; EGFLAM; GPX5; CCDC80; EYA4; CALD1; TNXB; CREB5
		V$GATA1_05	Genes with 3'UTR containing motif ANGNDGATAANN GN which matches annotation for GATA1: GATA binding protein 1 (globin transcription factor 1)	.	.	.	.	3.07E-02	FLI1; TWIST1; PITX2; KEL; SFRP1; BMP7; ELAVL4; CCDC80; SDPR; CREB5
		V$GATA3_01	Genes with 3'UTR containing motif NNGATARNG which matches annotation for GATA3: GATA binding protein 3	.	.	.	.	3.62E-02	SNCA; FLI1; APOE; TRIM15; TRIM10; ELAVL4; ESR1; TNXB; CREB5
		V$IRF7_01	Genes with 3'UTR containing motif TNSGAAWNCGAA ANTNNN which matches annotation for IRF7: interferon regulatory factor 7	.	.	.	.	1.90E-02	FLI1; PITX2; COL11A2; FLRT2; NOS1; PPP1R10; RBFOX1; ESR1; CHST8; CALD1

		V$LHX3_01	Genes with 3'UTR containing motif AATTAATTAA which matches annotation for LHX3: LIM homeobox 3	.	.	.	.	2.92E-02	PITX2; MARCKS; SLC24A4; CFB; RBFOX1; CHN2; CLRN1; ZEB2; NOVA1
		V$MEIS1AHOXA9_01	Genes having at least one occurence of the transcription factor binding site V$MEIS1AHOXA9_01 (v7.4 TRANSFAC) in the regions spanning up to 4 kb around their transcription starting sites.	.	.	.	.	4.79E-02	NOVA1; TAGLN3; PPP1R10; CREB5; ELAVL4; CHN2
		V$NKX62_Q2	Genes with 3'UTR containing motif NWADTAAWTANN which matches annotation for NKX6-2: NK6	.	.	.	.	3.78E-02	TWIST1; MARCKS; COL11A2; ELAVL4; RBFOX1; ZIC4; CYFIP2; SDPR; CALD1
			transcription factor related, locus 2 (Drosophila)						
		WOO_LIVER_CANCER_RECURRENCE_UP		.	.	.	.	4.21E-02	DBN1; CSGALNACT1; MARCKS; ZEB2; DDR1; IGFBP3
		YOSHIMURA_MAPK8_TARGETS_UP		.	.	.	.	9.20E-04	CACNB4; CFB; MTNR1A; GPX5; PDE4B; GNAS; ELAVL4; DBN1; SPRR1A; DLX5; SNCA; SKIV2L; KCNJ5; NOS1; MARCKS; TSHR; APOE; NGF; DDR1; TNF; PPT2; SLC6A13; MAPT; CD8A; TAP2; BMP7; TNP1; HTR2A; IGFBP3; LTA; CRP

Common pathways are indicated by colours: yellow, present in all MCF-7 sublines with alteration of isoforms; green, present in MCF-7 cells with Δ40p53/p53α-knockdown; blue, present in MCF-7 with Δ40p53-overexpression and p53α-knockdown; purple, present in MCF-7 with Δ40p53-overexpression and p53α-knockdown. Pathways enriched in ZR75-1 cells are indicated with red bold italic characters with associated genes of each contrast listed in cells below with grey shading. Adjusted *p*-value and associated genes are listed.

Appendix 4 Full table of GSEA pathways when isoform levels were altered in ZR75-1 cells.

ZR75-1-shΔ40p53 vs. ZR75-1-shNT	**ZR75-1-shp53α vs. ZR75-1 shNT**	**Description**	**ZR75-1-shΔ40p53 vs. ZR75-1-shNT**		**ZR75-1-shp53α vs. ZR75-1 shNT**	
			p	**Genes**	***p***	**Genes**
AAGCACA.MIR-218	AAGCACA.MIR-218		3.47E-08	LMO3 PCDHA10 PCDHA11 PCDHA12 PCDHA13 FRMD4A GNAO1 PCDHA6 PCDHA7 PCDHA8 PCDHA9 PCDHA2 PCDHA3 PCDHA4 PCDHA5 PCDHA1 PCDHAC2 PCDHAC1 CHST8	6.65E-09	FAM5C PCDHA10 PCDHA11 PCDHA12 PCDHA13 GNAO1 PCDHA6 PCDHA7 PCDHA8 PCDHA9 PCDHA2 PCDHA3 PCDHA4 PCDHA5 PCDHA1 CSMD3 PCDHAC2 PCDHAC1 CHST8
ACCAATC.MIR-509	**ACCAATC.MIR-509**		9.24E-18	PCDHA6 PCDHA7 PCDHA8 PCDHA9 PCDHA2 PCDHA3 PCDHA4 PCDHA5 PCDHA1 PCDHAC2 PCDHAC1 PCDHA10 PCDHA11 PCDHA12 PCDHA13	4.58E-18	PCDHA6 PCDHA7 PCDHA8 PCDHA9 PCDHA2 PCDHA3 PCDHA4 PCDHA5 PCDHA1 PCDHAC2 PCDHAC1 PCDHA10 PCDHA11 PCDHA12 PCDHA13
AGCACTT.MIR93.MIR-302A.MIR302B.MIR-302C.MIR-302D.MIR-372.MIR-373.MIR-520E.MIR520A.MIR-526B.MIR-520B.MIR-520C.MIR-520D	AGCACTT.MIR93.MIR-302A.MIR-302B.MIR302C.MIR-302D.MIR-372.MIR-373.MIR-520E.MIR-520A.MIR-526B.MIR-520B.MIR520C.MIR-520D		3.29E-10	PCDHA6 PCDHA7 PCDHA8 PCDHA9 PCDHA2 PCDHA3 PCDHA4 PCDHA5 PCDHA1 EDNRB NEUROD1 LMO3 PCDHAC2 PCDHAC1 PCDHA10 PCDHA11 PCDHA12 PCDHA13 ESR1 FRMD4A	2.86E-08	PCDHA6 PCDHA7 PCDHA8 PCDHA9 PCDHA2 PCDHA3 PCDHA4 PCDHA5 PCDHA1 EDNRB PCDHAC2 PCDHAC1 PCDHA10 PCDHA11 PCDHA12 PCDHA13 ESR1
AGGGCAG.MIR-18A	AGGGCAG.MIR-18A		1.71E-12	PCDHAC2 PCDHAC1 PCDHA10 PCDHA11 PCDHA12 PCDHA13 PCDHA6 PCDHA7 PCDHA8 PCDHA9 PCDHA2 PCDHA3 PCDHA4 PCDHA5 PCDHA1 ESR1	5.64E-13	PCDHAC2 PCDHAC1 PCDHA10 PCDHA11 PCDHA12 PCDHA13 PCDHA6 PCDHA7 PCDHA8 PCDHA9 PCDHA2 PCDHA3 PCDHA4 PCDHA5 PCDHA1 ESR1
ANATOMICAL_STRUCTURE_DEVELOPMENT	ANATOMICAL_STRUCTURE_DEVELOPMENT		1.80E-03	TRIM15 IGF2 PCDHA10 PCDHA11 PCDHA6 PCDHA7 PCDHA8 PCDHA2 PCDHA3 PCDHA4 PCDHA5 PCDHA1 PCDHAC2 PCDHAC1 FOXP2 CMKLR1 TWIST1 LAMA3 NOTCH4 CDSN SGCE	3.54E-05	IGF2 PCDHA10 PCDHA11 DLX5 PCDHA6 PCDHA7 PCDHA8 PCDHA2 PCDHA3 PCDHA4 PCDHA5 PCDHA1 KCNIP2 SEMA3B PCDHAC2 PCDHAC1 FOXP2 SIX1 BDNF TWIST1 LAMB3 SFRP1 PARD6B
ATGTAGC.MIR221.MIR-222	ATGTAGC.MIR221.MIR-222		3.80E-13	PCDHAC2 TMCC1 PCDHAC1 PCDHA10 PCDHA11 PCDHA12 PCDHA13 PCDHA6 PCDHA7 PCDHA8 PCDHA9 PCDHA2 PCDHA3 PCDHA4 PCDHA5 PCDHA1 ESR1	1.09E-12	PCDHAC2 PCDHAC1 PCDHA10 PCDHA11 PCDHA12 PCDHA13 PCDHA6 PCDHA7 PCDHA8 PCDHA9 PCDHA2 PCDHA3 PCDHA4 PCDHA5 PCDHA1 ESR1

ATTCTTT.MIR-186	ATTCTTT.MIR-186		3.46E-10	PCDHA6 PCDHA7 PCDHA8 PCDHA9 PCDHA2 PCDHA3 PCDHA4 PCDHA5 PCDHA1 RBFOX1 CAST PCDHAC2 PCDHAC1 PCDHA10 PCDHA11 PCDHA12 PCDHA13 FRMD4A	6.65E-09	PCDHA6 PCDHA7 PCDHA8 PCDHA9 PCDHA2 PCDHA3 PCDHA4 PCDHA5 PCDHA1 CAST PCDHAC2 PCDHAC1 PCDHA10 PCDHA11 PCDHA12 PCDHA13
CACTTTG.MIR-520G.MIR-520H	CACTTTG.MIR-520G.MIR-520H		5.87E-09	PCDHA6 PCDHA7 PCDHA8 PCDHA9 PCDHA2 PCDHA3 PCDHA4 PCDHA5 PCDHA1 FLRT2 PCDHAC2 PCDHAC1 PCDHA10 PCDHA11 PCDHA12 PCDHA13	1.70E-10	MACF1 PCDHA6 PCDHA7 PCDHA8 PCDHA9 PCDHA2 PCDHA3 PCDHA4 PCDHA5 PCDHA1 CSMD3 PCDHAC2 PCDHAC1 PCDHA10 PCDHA11 PCDHA12 PCDHA13
CAGCACT.MIR-512-3P	CAGCACT.MIR-5123P		1.37E-12	PCDHAC2 PCDHAC1 PCDHA10 PCDHA11 PCDHA12 PCDHA13 PCDHA6 PCDHA7 PCDHA8 PCDHA9 PCDHA2 PCDHA3 PCDHA4 PCDHA5 PCDHA1 FRMD4A PPFIA2	4.45E-13	SYT8 PCDHAC2 PCDHAC1 PCDHA10 PCDHA11 PCDHA12 PCDHA13 PCDHA6 PCDHA7 PCDHA8 PCDHA9 PCDHA2 PCDHA3 PCDHA4 PCDHA5 PCDHA1 TRIM2

CAGCTTT.MIR-320	CAGCTTT.MIR-320		1.15E-09	PCDHA6 PCDHA7 PCDHA8 PCDHA9 PCDHA2 PCDHA3 PCDHA4 PCDHA5 PCDHA1 RBFOX1 LMO3 PCDHAC2 PCDHAC1 PCDHA10 PCDHA11 PCDHA12 PCDHA13	2.88E-09	PCDHA6 PCDHA7 PCDHA8 PCDHA9 PCDHA2 PCDHA3 PCDHA4 PCDHA5 PCDHA1 PCDHAC2 PCDHAC1 PCDHA10 PCDHA11 PCDHA12 PCDHA13 CALD1
chr5q31	chr5q31		6.24E-12	PCDHA6 PCDHA7 PCDHA8 PCDHA9 PCDHA2 PCDHA3 PCDHA4 PCDHA5 PCDHA1 DNAJC18 BRD8 PCDHAC2 PCDHAC1 PCDHA10 PCDHA11 PCDHA12 PCDHA13 REEP2	2.09E-11	PCDHA6 PCDHA7 PCDHA8 PCDHA9 PCDHA2 PCDHA3 PCDHA4 PCDHA5 PCDHA1 DNAJC18 PCDHAC2 PCDHAC1 PCDHA10 PCDHA11 PCDHA12 PCDHA13 REEP2
chr6p21	**chr6p21**		4.51E-29	DDAH2 RXRB HLA-DRA PPT2 EGFL8 TRIM15 TRIM10 DOM3Z C2 SLC44A4 RGL2 HLA-J HLA-E NEU1 STK19 EHMT2 ZNF311 SYNGAP1 GABBR1 UBD GPSM3 PRRT1 CFB PSORS1C1 NOTCH4 CDSN GPX5 ZBTB22 OR2H1 PLA2G7 RNF39 TAPBP TRIM31 PSMB8 LTA TNF TNXB	1.61E-14	DDAH2 HLA-DRA PPT2 GTF2H4 EGFL8 TRIM10 TRIM26 SLC44A4 RGL2 HLA-J NEU1 EHMT2 ZNF311 SYNGAP1 VARS2 UBD PRRT1 PSORS1C2 PSORS1C1 COL11A2 OR2H1 LTA TNF TNXB
GCACTTT.MIR-17-5P.MIR-20A.MIR106A.MIR-106B.MIR-20B.MIR-519D	GCACTTT.MIR-175P.MIR-20A.MIR-106A.MIR-106B.MIR-20B.MIR-519D		6.21E-05	LMO3 PCDHA10 PCDHA11 PCDHA12 PCDHA13 FRMD4A TMCC1 PCDHA6 PCDHA7 PCDHA8 PCDHA9 PCDHA2 PCDHA3 PCDHA4 PCDHA5 PCDHA1 PCDHAC2 PCDHAC1	7.53E-05	PCDHA10 PCDHA11 PCDHA12 PCDHA13 PCDHA6 PCDHA7 PCDHA8 PCDHA9 PCDHA2 PCDHA3 PCDHA4 PCDHA5 PCDHA1 PCDHAC2 PCDHAC1 PARD6B CALD1
GGTGTGT.MIR-329	GGTGTGT.MIR-329		2.40E-13	BLCAP PCDHAC2 PCDHAC1 PCDHA10 PCDHA11 PCDHA12 PCDHA13 PCDHA6 PCDHA7 PCDHA8 PCDHA9 PCDHA2 PCDHA3 PCDHA4 PCDHA5 PCDHA1	7.92E-13	PCDHAC2 PCDHAC1 PCDHA10 PCDHA11 PCDHA12 PCDHA13 PCDHA6 PCDHA7 PCDHA8 PCDHA9 PCDHA2 PCDHA3 PCDHA4 PCDHA5 PCDHA1
GTATTAT.MIR-369-3P	GTATTAT.MIR-3693P		1.04E-09	PCDHA6 PCDHA7 PCDHA8 PCDHA9 PCDHA2 PCDHA3 PCDHA4 PCDHA5 PCDHA1 PCDHAC2 PCDHAC1 PCDHA10 PCDHA11 PCDHA12 PCDHA13 SULF1	2.88E-09	PCDHA6 PCDHA7 PCDHA8 PCDHA9 PCDHA2 PCDHA3 PCDHA4 PCDHA5 PCDHA1 PCDHAC2 PCDHAC1 PCDHA10 PCDHA11 PCDHA12 PCDHA13

GTGCCTT.MIR-506	GTGCCTT.MIR-506		3.67E-05	LMO3 PCDHA10 PCDHA11 PCDHA12 PCDHA13 GALNT9 GRID1 PCDHA6 PCDHA7 PCDHA8 PCDHA9 PCDHA2 PCDHA3 PCDHA4 PCDHA5 PCDHA1 EDNRB SEPT9 PCDHAC2 PCDHAC1	8.03E-06	PCDHA10 PCDHA11 PCDHA12 PCDHA13 DLX5 PCDHA6 PCDHA7 PCDHA8 PCDHA9 PCDHA2 PCDHA3 PCDHA4 PCDHA5 PCDHA1 EDNRB SBNO2 SEPT9 PCDHAC2 PCDHAC1 FAM134B
GTTTGTT.MIR-495	GTTTGTT.MIR-495		9.02E-08	PCDHA6 PCDHA7 PCDHA8 PCDHA9 PCDHA2 PCDHA3 PCDHA4 PCDHA5 PCDHA1 PCDHAC2 PCDHAC1 PCDHA10 PCDHA11 PCDHA12 PCDHA13	2.91E-10	BDNF PCDHA6 PCDHA7 PCDHA8 PCDHA9 PCDHA2 PCDHA3 PCDHA4 PCDHA5 PCDHA1 PCDHAC2 PCDHAC1 PCDHA10 PCDHA11 PCDHA12 PCDHA13 NTM
INTEGRAL_TO_PLASMA_MEMBRANE	INTEGRAL_TO_PLASMA_MEMBRANE		3.52E-04	PTPRN2 PCDHA10 PCDHA11 GABBR1 PCDHA6 PCDHA7 PCDHA8 PCDHA2 PCDHA3 PCDHA4 PCDHA5 PCDHA1 PCDHAC2 PCDHAC1 GABRA1 CMKLR1 TSHR NOTCH4 EDNRB SGCE ABCC3 IFNGR2	3.37E-02	PTPRN2 PCDHA10 PCDHA11 PCDHA6 PCDHA7 PCDHA8 PCDHA2 PCDHA3 PCDHA4 PCDHA5 PCDHA1 PCDHAC2 PCDHAC1 KCNJ1 CCRL2 TSHR EDNRB
INTRINSIC_TO_PLASMA_MEMBRANE	INTRINSIC_TO_PLASMA_MEMBRANE		4.28E-04	PTPRN2 PCDHA10 PCDHA11 GABBR1 PCDHA6 PCDHA7 PCDHA8 PCDHA2 PCDHA3 PCDHA4 PCDHA5 PCDHA1 PCDHAC2 PCDHAC1 GABRA1 CMKLR1 TSHR NOTCH4 EDNRB SGCE ABCC3 IFNGR2	3.73E-02	PTPRN2 PCDHA10 PCDHA11 PCDHA6 PCDHA7 PCDHA8 PCDHA2 PCDHA3 PCDHA4 PCDHA5 PCDHA1 PCDHAC2 PCDHAC1 KCNJ1 CCRL2 TSHR EDNRB

KEGG_TYPE_I_DIABETES_MELLITUS	KEGG_TYPE_I_DIABETES_MELLITUS		2.66E-03	LTA TNF PTPRN2 HLA-E HLA-DRA	3.38E-02	LTA TNF PTPRN2 HLA-DRA
MIKKELSEN_ES_HCP_WITH_H3K27ME3	MIKKELSEN_ES_HCP_WITH_H3K27ME3	Genes with high-CpG-density promoters (HCP) bearing histone H3 K27 trimethylation mark (H327me3) in embryonic stem cells (ES).	3.54E-02	HOXA3 PCDHA3 PCDHA10 PCDHA2	1.75E-03	HOXA3 PCDHA3 NTM PCDHA10 PCDHA2
MIKKELSEN_IPS_WITH_HCP_H3K27ME3	MIKKELSEN_IPS_WITH_HCP_H3K27ME3	Genes with high-CpG-density promoters (HCP) bearing the tri-methylation mark at H3K27 (H3K27me3) in MCV8.1 (induced pluripotent cells, iPS).	1.80E-03	PCDHA11 IGF2 HOXA3 PCDHA4 PCDHA13 PRRT1 PCDHA2	8.96E-05	PCDHA11 NTM IGF2 HOXA3 PCDHA4 PCDHA13 PRRT1 PCDHA2
MIKKELSEN_MEF_HCP_WITH_H3_UNMETHYLATED	MIKKELSEN_MEF_HCP_WITH_H3_UNMETHYLATED	Genes with high-CpG-density promoters (HCP) with unmethylated histone H3 in MEF cells (embryonic fibroblast).	4.42E-07	PCDHA4 PCDHA10 HOXA3 ZNF516 PCDHA7 RBFOX1 PCDHA1 PCDHAC1 PCDHA2 PCDHA9 PCDHA5 PCDHA6 PCDHA3	1.45E-07	PCDHA4 TMC8 PCDHA10 HOXA3 ZNF516 PCDHA7 PCDHA1 PCDHAC1 PCDHA2 PCDHA9 PCDHA5 PCDHA6 PCDHA3

MULTICELLULAR_ORGANISMAL_DEVELOPMENT	MULTICELLULAR_ORGANISMAL_DEVELOPMENT		2.15E-05	EGFL8 TRIM15 IGF2 LMO1 PCDHA10 PCDHA11 PCDHA6 PCDHA7 PCDHA8 PCDHA2 PCDHA3 PCDHA4 PCDHA5 PCDHA1 PCDHAC2 PCDHAC1 FOXP2 CMKLR1 TWIST1 LAMA3 NOTCH4 TBX21 CDSN SGCE CRABP1	5.21E-05	EGFL8 IGF2 PCDHA10 PCDHA11 DLX5 PCDHA6 PCDHA7 PCDHA8 PCDHA2 PCDHA3 PCDHA4 PCDHA5 PCDHA1 KCNIP2 SEMA3B PCDHAC2 PCDHAC1 FOXP2 SIX1 BDNF TWIST1 LAMB3 PARD6B
NERVOUS_SYSTEM_DEVELOPMENT	NERVOUS_SYSTEM_DEVELOPMENT		7.03E-04	PCDHA10 PCDHA11 PCDHA6 PCDHA7 PCDHA8 PCDHA2 PCDHA3 PCDHA4 PCDHA5 PCDHA1 PCDHAC2 PCDHAC1 FOXP2	1.79E-08	PCDHA10 PCDHA11 BDNF DLX5 PCDHA6 PCDHA7 PCDHA8 PCDHA2 PCDHA3 PCDHA4 PCDHA5 PCDHA1 KCNIP2 SEMA3B PCDHAC2 PCDHAC1 PARD6B FOXP2
SYSTEM_DEVELOPMENT	SYSTEM_DEVELOPMENT		1.80E-04	TRIM15 IGF2 PCDHA10 PCDHA11 PCDHA6 PCDHA7 PCDHA8 PCDHA2 PCDHA3 PCDHA4 PCDHA5 PCDHA1 PCDHAC2 PCDHAC1 FOXP2 CMKLR1 TWIST1 LAMA3 NOTCH4 CDSN SGCE	8.72E-06	IGF2 PCDHA10 PCDHA11 DLX5 PCDHA6 PCDHA7 PCDHA8 PCDHA2 PCDHA3 PCDHA4 PCDHA5 PCDHA1 KCNIP2 SEMA3B PCDHAC2 PCDHAC1 FOXP2 SIX1 BDNF TWIST1 LAMB3 PARD6B
TAATAAT.MIR-126	TAATAAT.MIR-126		2.19E-09	PCDHA6 PCDHA7 PCDHA8 PCDHA9 PCDHA2 PCDHA3 PCDHA4 PCDHA5 PCDHA1 FLRT2 PCDHAC2 PCDHAC1 PCDHA10 PCDHA11 PCDHA12 PCDHA13	6.33E-09	PCDHA6 PCDHA7 PCDHA8 PCDHA9 PCDHA2 PCDHA3 PCDHA4 PCDHA5 PCDHA1 PCDHAC2 PCDHAC1 PCDHA10 PCDHA11 PCDHA12 PCDHA13
TCTCTCC.MIR-185	TCTCTCC.MIR-185		1.09E-12	PCDHAC2 PCDHAC1 PCDHA10 PCDHA11 PCDHA12 PCDHA13 SYNGAP1 PCDHA6 PCDHA7 PCDHA8 PCDHA9 PCDHA2 PCDHA3 PCDHA4 PCDHA5 PCDHA1	1.61E-14	PCDHAC2 PCDHAC1 PCDHA10 PCDHA11 PCDHA12 LRFN5 PCDHA13 SYNGAP1 PCDHA6 PCDHA7 PCDHA8 PCDHA9 PCDHA2 PCDHA3 PCDHA4 PCDHA5 PCDHA1
TGAATGT.MIR181A.MIR-181B.MIR-181C.MIR-181D	TGAATGT.MIR181A.MIR-181B.MIR181C.MIR-181D		8.56E-08	LMO1 LMO3 PCDHA10 PCDHA11 PCDHA12 PCDHA13 ESR1 TMCC1 PCDHA6 PCDHA7 PCDHA8 PCDHA9 PCDHA2 PCDHA3 PCDHA4 PCDHA5 PCDHA1 PCDHAC2 PCDHAC1 GABRA1	6.62E-07	PCDHA10 PCDHA11 PCDHA12 PCDHA13 TRIM2 ESR1 PCDHA6 PCDHA7 PCDHA8 PCDHA9 PCDHA2 PCDHA3 PCDHA4 PCDHA5 PCDHA1 PCDHAC2 PCDHAC1 CBFA2T3
TGCACTT.MIR519C.MIR-519B.MIR-519A	TGCACTT.MIR-519C.MIR519B.MIR-519A		5.81E-06	PCDHA10 PCDHA11 PCDHA12 PCDHA13 BLCAP PCDHA6 PCDHA7 PCDHA8 PCDHA9 PCDHA2	2.86E-08	PCDHA10 PCDHA11 PCDHA12 PCDHA13 PCDHA6 PCDHA7 PCDHA8 PCDHA9 PCDHA2 PCDHA3
				PCDHA3 PCDHA4 PCDHA5 PCDHA1 PCDHAC2 PCDHAC1 HOXA3		PCDHA4 PCDHA5 PCDHA1 PCDHAC2 PCDHAC1 HOXA3 PARD6B ARHGAP24 CALD1
TGCTGCT.MIR15A.MIR-16.MIR-15B.MIR-195.MIR424.MIR-497	TGCTGCT.MIR15A.MIR-16.MIR-15B.MIR-195.MIR424.MIR-497		4.42E-07	STOX2 PCDHA10 PCDHA11 PCDHA12 STK19 PCDHA13 GABBR1 TMCC1 PCDHA6 PCDHA7 PCDHA8 PCDHA9 PCDHA2 PCDHA3 PCDHA4 PCDHA5 PCDHA1 KLC2 PCDHAC2 PCDHAC1 HOXA3	2.77E-09	MAPK3 STOX2 PCDHA10 PCDHA11 PCDHA12 PCDHA13 TRIM2 GRAMD3 SYT8 BDNF PCDHA6 PCDHA7 PCDHA8 PCDHA9 PCDHA2 PCDHA3 PCDHA4 PCDHA5 PCDHA1 PCDHAC2 PCDHAC1 HOXA3 CBFA2T3

TGCTTTG.MIR-330	TGCTTTG.MIR-330		6.30E-09	GRID1 PCDHA6 PCDHA7 PCDHA8 PCDHA9 PCDHA2 PCDHA3 PCDHA4 PCDHA5 PCDHA1 PCDHAC2 PCDHAC1 PCDHA10 PCDHA11 PCDHA12 PCDHA13 ESR1 GNAO1	1.84E-09	PCDHA6 PCDHA7 PCDHA8 PCDHA9 PCDHA2 PCDHA3 PCDHA4 PCDHA5 PCDHA1 KCNIP2 PCDHAC2 PCDHAC1 PCDHA10 PCDHA11 PCDHA12 PCDHA13 ESR1 GNAO1
TGGTGCT.MIR-29A.MIR-29B.MIR-29C	TGGTGCT.MIR29A.MIR-29B.MIR29C		3.65E-05	DGKD PCDHA10 PCDHA11 PCDHA12 PCDHA13 PCDHA6 PCDHA7 PCDHA8 PCDHA9 PCDHA2 PCDHA3 PCDHA4 PCDHA5 PCDHA1 RNF39 PCDHAC2 PCDHAC1	1.52E-06	PCDHA10 PCDHA11 PCDHA12 PCDHA13 SYT8 PCDHA6 PCDHA7 PCDHA8 PCDHA9 PCDHA2 PCDHA3 PCDHA4 PCDHA5 PCDHA1 KCNIP2 XKR4 PCDHAC2 PCDHAC1
TTTGCAC.MIR19A.MIR-19B	TTTGCAC.MIR19A.MIR-19B		2.25E-07	PCDHA10 PCDHA11 PCDHA12 PCDHA13 ESR1 BLCAP PCDHA6 PCDHA7 PCDHA8 PCDHA9 PCDHA2 PCDHA3 PCDHA4 PCDHA5 PCDHA1 NEUROD1 CAST PCDHAC2 PCDHAC1 SULF1	2.71E-07	ATP10A PCDHA10 PCDHA11 PCDHA12 PCDHA13 ESR1 MACF1 PCDHA6 PCDHA7 PCDHA8 PCDHA9 PCDHA2 PCDHA3 PCDHA4 PCDHA5 PCDHA1 CAST PCDHAC2 PCDHAC1
INTEGRAL_TO_MEMBRANE			1.44E-03	RER1 PTPRN2 PCDHA10 PCDHA11 GABBR1 PCDHA6 PCDHA7 PCDHA8 PCDHA2 PCDHA3 PCDHA4 PCDHA5 PCDHA1 SLC22A18 TAPBP PCDHAC2 PCDHAC1 GABRA1 CMKLR1 TSHR NOTCH4 EDNRB SGCE ABCC3 IFNGR2	.	.
INTRINSIC_TO_MEMBRANE			1.76E-03	RER1 PTPRN2 PCDHA10 PCDHA11 GABBR1 PCDHA6 PCDHA7 PCDHA8 PCDHA2 PCDHA3 PCDHA4 PCDHA5 PCDHA1 SLC22A18 TAPBP PCDHAC2 PCDHAC1 GABRA1 CMKLR1 TSHR NOTCH4 EDNRB SGCE ABCC3 IFNGR2	.	.
MEMBRANE			9.07E-03	HLA-DRA PTPRN2 GABBR1 PCDHA6 PCDHA7 PCDHA8 PCDHA2 PCDHA3 PCDHA4 PCDHA5 PCDHA1 TAPBP GABRA1 TSHR IFNGR2 RER1 PCDHA10 PCDHA11 SLC22A18 PCDHAC2 PCDHAC1 CMKLR1 DGKD OSTBETA NNT NOTCH4 EDNRB SGCE CLDN10 ABCC3	.	.
MEMBRANE_PART			7.26E-03	PTPRN2 GABBR1 PCDHA6 PCDHA7 PCDHA8 PCDHA2 PCDHA3 PCDHA4 PCDHA5 PCDHA1 TAPBP GABRA1 TSHR IFNGR2 RER1 PCDHA10 PCDHA11 SLC22A18 PCDHAC2 PCDHAC1 CMKLR1 NNT NOTCH4 EDNRB SGCE CLDN10 ABCC3	.	.
MODULE_11		Genes in the cancer **module 11**	1.85E-02	PEG10 SGCE GABBR1 CRABP1 LMO3 CLDN10 PTPRN2 SLC22A18AS GNAO1 SORBS2 ABAT EDNRB TNF	.	.

MODULE_118		cell line expressed genes	2.47E-02	PEG10 SGCE CRABP1 IGF2 FADS1 PPT2 GPSM3 SLC22A18AS TNF PSMB8 BIK	.	.

MODULE_55		Genes in the cancer **module 55**.	1.42E-02	PEG10 SGCE TNXB CRABP1 IGF2 FADS1 C2 CLDN10 CFB PTPRN2 SLC22A18AS SORBS2 ABAT TRIM15 ESR1 ABCC3 TCN2	.	.
MODULE_84		mmune (humoral) and inflammatory response	1.96E-02	TNXB CRABP1 FADS1 C2 GPSM3 LMO3 SLC22A18AS STAT4 UBD TNF HLA-DRA PLA2G7 LAMA3	.	.
MODULE_88		Heart, liver, kidney and pancreas metabolic and xenobiotic response genes.	4.80E-03	PEG10 SGCE TNXB CRABP1 IGF2 FADS1 C2 GPSM3 CLDN10 CFB PTPRN2 SLC22A18AS SORBS2 ABAT TRIM15 ESR1 ABCC3 TCN2	.	.
PLASMA_MEMBRANE			5.16E-04	HLA-DRA PTPRN2 PCDHA10 PCDHA11 GABBR1 PCDHA6 PCDHA7 PCDHA8 PCDHA2 PCDHA3 PCDHA4 PCDHA5 PCDHA1 SLC22A18 PCDHAC2 PCDHAC1 GABRA1 CMKLR1 DGKD TSHR OSTBETA NOTCH4 EDNRB SGCE CLDN10 ABCC3 IFNGR2	.	.
PLASMA_MEMBRANE_PART			1.40E-03	PTPRN2 PCDHA10 PCDHA11 GABBR1 PCDHA6 PCDHA7 PCDHA8 PCDHA2 PCDHA3 PCDHA4 PCDHA5 PCDHA1 PCDHAC2 PCDHAC1 GABRA1 CMKLR1 TSHR NOTCH4 EDNRB SGCE CLDN10 ABCC3 IFNGR2	.	.
RTAAACA_V$FREAC2_01		Genes with 3'UTR containing motif RTAAACA which matches annotation for FOXF2: forkhead box F2	1.41E-03	BRD8 LMO3 LOC84931 BLCAP PCDHA4 KLC2 BIK FOXP2 SULF1 RXRB PPT2 ZBTB22 FRMD4A GNAO1 NNT NOTCH4 RBFOX1 NEUROD1 RNF39 HOXA3	.	.
V$HFH4_01		Genes with 3'UTR containing motif AWKTGTTTGTTTA which matches annotation for FOXJ1: forkhead box J1	1.20E-02	TWIST1 ZBTB22 PPFIA2 RBFOX1 LMO3 HOXA3 FOXP2 CHST8	.	.
V$POU3F2_01		Genes with 3'UTR containing motif ATGMATWWATTCAT which matches annotation for POU3F2: POU domain, class 3, transcription factor 2	1.51E-02	LMO3 TAPBP TWIST1 HOXA3 FOXP2 CLRN1	.	.
YCATTAA_UNKNOWN			4.92E-03	MGAT5B CLRN1 LMO1 LMO3 C1QTNF7 EXPH5 KCNIP4 RBFOX1 PCDHAC2 HOXA3 GABRA1 FOXP2 CHST8 SULF1	.	.
	ACOSTA_PROLIFERATION_INDEPENDENT_MYC_TARGETS_DN		.	.	1.51E-02	CBFA2T3 NEU1 ESR1 FADS1 CREM TNFAIP8

	BENPORATH_ES_WITH_H3K27ME3		.	.	1.51E-02	LRFN5 CSMD3 SIX1 KCNIP4 GNAO1 SFRP1 ESR1 HOXA3 CDH23 KCNIP2 PTPRN2 LOC84931 TWIST1 CHST8 PRRT1 DLX5 FAM5C SEMA3B GUCY1A3
	CAGGTG_V$E12_Q6	**Genes with 3'UTR containing motif CAGGTG which matches annotation for TCF3: Transcription factor 3 (E2A immunoglobulin enhancer binding factors E12/E47)**	.	.	3.15E-04	SDK1 IGF2 RGL2 PCDHA6 PCDHA1 SEMA3B CBFA2T3 ARHGAP24 DDAH2 PPT2 GUCY1A3 SIPA1 ESR1 PRDM16 GNAO1 BDNF PSORS1C2 HOXA3 LTA ELF5 STRA6 PCDHA10 EXPH5 KCNIP2 KCNIP4 PLA2G6 PEX10 CAST CHST8 TNNI2 SYT8 MACF1 SFRP1 SORBS2 COL11A2 LRFN5
	CATTGTYY_V$SOX9_B1	Genes with 3'UTR containing motif CATTGTYY which matches annotation for SOX9: SRY (sex determining region Y)box 9 (campomelic dysplasia, autosomal sex-reversal)	.	.	1.25E-04	DDAH2 MAPK3 TREX1 SFRP1 SORBS2 SIX1 HOXA3 FOXP2 TRIM2 CHST8 CALD1 LOC84931 GNAO1
	LEE_METASTASIS_AND_ALTERNATIVE_SPLICING_DN		.	.	4.15E-02	PCDHA12 PCDHAC2 PCDHA5 SEMA3B
	TGGAAA_V$NFAT_Q4_01		.	.	2.42E-03	RGL2 UBD PCDHA6 FOXP2 TNF FAM5C PPT2 CREM SIPA1 ESR1 GNAO1 BDNF TWIST1 LGALS1 HOXA3 CALD1 TNXB ELF5 PCDHA11 PCDHA13 KCNIP2 CAST C1RL KCNJ1 EHMT2 TNFAIP8 LAMB3 TREX1
	TURASHVILI_BREAST_DUCTAL_CARCINOMA_VS_DUCTAL_NORMAL_DN		.	.	5.93E-03	SORBS2 LAMB3 HOXA3 ELF5 SFRP1 ZNF542 TRIM2 GRAMD3
	TURASHVILI_BREAST_LOBULAR_CARCINOMA_VS_DUCTAL_NORMAL_DN		.	.	4.85E-02	ZNF542 LAMB3 ISM1 SFRP1 ELF5
	V$HNF6_Q6		.	.	3.66E-03	TWIST1 CAST SIX1 SIPA1 CSMD3 HOXA3 LTA TNF GNAO1
	V$OCT1_Q6	Genes having at least one occurence of the transcription factor binding site V$OCT1_Q6 (v7.4 TRANSFAC) in the regions spanning up to 4 kb around their transcription starting sites.	.	.	3.73E-02	BDNF COL11A2 STAT4 SIX1 CSMD3 HOXA3 FOXP2 FAM5C

Common pathways between Δ40p53 and p53α-knockdown are indicated in green. Pathways enriched in MCF-7 cells are indicated with red bold italic characters with associated genes of each contrast listed in cells below with grey shading. Adjusted *p*-value and associated genes are listed.